DESIGN HYDROLOGY FOR STREAM RESTORATION AND CHANNEL STABILITY AT STREAM CROSSINGS

FINAL REPORT

Prepared for
National Cooperative Highway Research Program (NCHRP) Project 24-40
Transportation Research Board
of the
The National Academies of Sciences, Engineering, and Medicine

Brian Bledsoe, Dan Baker, Peter Nelson, Tyler Rosburg, Joel Sholtes,
and Travis Stroth
Department of Civil and Environmental Engineering
Colorado State University
Fort Collins, Colorado

September 2016

ACKNOWLEDGMENT OF SPONSORSHIP

DISCLAIMER

DESIGN HYDROLOGY FOR STREAM RESTORATION AND CHANNEL STABILITY AT STREAM CROSSINGS

FINAL REPORT

Brian Bledsoe, Dan Baker, Peter Nelson, Tyler Rosburg, Joel Sholtes,
and Travis Stroth
Department of Civil and Environmental Engineering
Colorado State University
Fort Collins, Colorado

September 2016

CONTENTS

LIST OF FIGURES

LIST OF TABLES

AUTHOR ACKNOWLEDGMENTS

ABSTRACT

This report presents the results of a study focused on developing scientifically supported methods for defining design hydrology for stream crossings. Theoretical and empirical approaches were used to explore flow and sediment relationships for diverse rivers across the U.S. and Puerto Rico. Results indicate that the appropriate depth of design hydrology analysis differs by stream type. The discharge at which 50% of cumulative sediment yield occurs (Q_{s50}) is identified as a robust alternative to current design metrics. Several decision support / analysis tools were developed during the project to improve and facilitate design hydrology analyses. The tools include: (1) a decision tree with web-based hydrologic analysis tools for generating design hydrology metrics under existing and future land use scenarios, (2) a tool for relating channel response potential to an appropriate level of design analysis, (3) guidance on selection of analog reaches (also referred to as reference reaches) and performing rapid geomorphic assessments of channel instability in the field, and (4) a spreadsheet tool for computing analytical channel designs that account for the full spectrum of sediment transporting events. The hydrologic metrics and tools developed in this project provide a general framework and stronger physical basis for design hydrology at stream crossings.

SUMMARY

This project developed scientifically supported methods for defining the design hydrology for stream crossings along with developing tools for understanding how design hydrology might change with land use changes. The methods and tools developed in this study were influenced by a survey of state Department of Transportation (DOT) engineers aimed at understanding their design hydrology needs. DOT engineers requested guidance on when the bankfull flow / peak flow is an appropriate and effective metric for design, or when a simple versus more-complicated approach is needed. Some engineers requested software or guidance that could facilitate sediment transport analyses. This study fulfills both these needs, and developed design hydrology approaches and tools that are physically-based yet as straightforward and user-friendly as possible.

In the initial phase of the project, we explored relationships between the drivers of sediment yield in rivers and streams, namely the flow regime and physical properties of the sediment and channels, and the magnitude and frequency of sediment transport described by various metrics based on the sediment yield curve. Theoretical approaches were used to explore relationships based on flow, physical characteristics, and sediment yield metrics calculated from fine- and coarse-bed rivers across the continental U.S. and Puerto Rico. This work expands on previous studies by applying a consistent method of bed-material yield analysis across a wide range and a large number of river types.

Results indicate that the appropriate depth of design hydrology analysis differs by stream type. The magnitude and frequency of sediment transport in all river types is sensitive to the variability of the flow regime; however, sediment yield and effectiveness in fine- and coarse-bed rivers respond differently to flow variability. Sediment yield metrics in fine-bed, suspended-load dominated streams are more sensitive to flow variability, whereas coarse-bed streams are more sensitive to physical aspects of the channel and bed sediment size. Bed sediment grain size plays a dominant role in sediment yield in rivers, especially coarse-bed rivers. In fine-bed rivers, a larger range of discharges is responsible for sediment yield. This range of flow narrows as the grain size of the bed increases. In coarse-bed rivers, a narrower range of less frequent flows dominates sediment yield. The most effective discharge also increases in magnitude and decreases in frequency as grain size increases.

We also tested the predictive ability of several metrics in estimating bankfull discharge (Q_{bf}), an important channel design variable. The discharge at which 50% of cumulative sediment yield occurs (Q_{s50}) is identified as a robust alternative to current design metrics. When compared to other hydrologic metrics, Q_{s50} is the least biased estimator of channel bankfull dimensions and has the lowest mean absolute percent error and root mean square error (RMSE) for fine-bed stream sites. In coarse-bed streams the 1.5-yr annual maximum flood predicts bankfull discharge just as well as Q_{s50}, indicating that a sediment yield-based approach to channel design is especially important for fine-bed streams and rivers.

With respect to the effects of flow data resolution (15-minute versus daily) on design hydrology, results indicate that accurate computation of sediment yield metrics such as Q_{s50} will depend on flow data resolution for rivers that are fine-bedded or flashy (i.e., exhibiting rapid short-term variations in streamflow during runoff events). Sediment transport calculations performed at 39 bedload sites and 99 suspended-load sites using both daily-averaged and sub-daily discharge records suggest that the use of daily-averaged flow data is not always appropriate. Furthermore, a case study of urbanizing watersheds indicated that flashiness, and the flow frequency distribution, are substantially affected by land use change. Urbanization caused upward shifts in the magnitude of the entire flow duration curve (FDC) for nearly all urban watersheds. Streamflow in nearly all the study watersheds became significantly flashier as a result of land use change. Flashiness is strongly related to behavior of sediment yield curves,

especially fine-grained channels, and was therefore identified as an important determinant of the appropriate level of design hydrology analysis.

Five primary design support / analysis tools were developed during the course of this project. In developing these tools, the research team strived for user-friendly structures (e.g., decision tables, decision trees, and spreadsheet tools) based on our discussions on current practices with state DOTs. Field reconnaissance is a critical component of the recommended approach. The tools are summarized below:

(1) A decision tree with complementary web-based hydrologic analysis tools was developed to provide practical guidance on generating the flow duration curves required for the computation of robust design hydrology metrics such as Q_{s50}. The decision tree presents a series of questions regarding land use change, potential non-stationarity of the flow record, and the availability of stream gage data and sediment transport measurements, to provide a standardized approach for calculating Q_{s50}.

(2) Decision tables are provided for relating channel response potential to an appropriate level of design analysis guidance. The tables account for inherent stream response potential and whether or not an acceptable analog channel is available in answering the following questions: (1) What level of hydrologic analysis should be undertaken? (2) Is it necessary to perform sediment transport analysis, and if so, what type of analysis is needed? (3) What spatial domain (i.e., how far upstream and/or downstream from the project location) is recommended for conducting the analysis? The fundamental philosophy underlying this analysis decision table is that, as stream response potential increases, it becomes necessary to conduct a deeper analysis over a larger area of influence.

(3) A decision table was developed to guide selection of analog reaches (also referred to as reference reaches) that may provide an additional line of evidence in design hydrology analyses. The analogy method has sometimes been used recklessly in design as streams from different watersheds and even different physiographic regions with disparate hydrologic and sediment supply characteristics have been used to define channel geometry in dissimilar settings. This decision support tool helps users identify upstream analogs that are very similar in terms of key criteria including the valley setting, boundary conditions, and inflowing loads of water and sediment, and to define supply reaches for sediment continuity analysis.

(4) A tool that supports rapid geomorphic assessments (RGAs) of channel instability and susceptibility at stream crossings was developed. This overtly simple approach is not intended to supplant more comprehensive and rigorous methods, most notably HEC-20 (*Hydraulic Engineering Circular No. 20*, Lagasse et al. 2012). Instead, it is intended to complement more in-depth approaches by orienting the design hydrology designer to some key considerations during field reconnaissance early in the design hydrology process. To develop the simplified RGA, we reduced a large pool of potential indicators to four:

   i. current stability status – Channel Evolution Model (CEM, Schumm et al. (1984)) stage, braiding, alluvial fan;
   ii. dominant bed material / armoring potential;
   iii. distance to downstream hardpoint / grade control; and
   iv. bank strength.

High ratings of stream susceptibility based on these indicators trigger a deeper level of design hydrology analysis as defined by the decision table for design described under item 2. above, and underscore the need for a greater stability analysis using more rigorous and comprehensive tools such as HEC-20.

(5) The CSR Stable Channel Design Tool (CSR Tool) was developed to compute analytical channel designs based on the Capacity-Supply Ratio (CSR), a robust design hydrologic metric that accounts for the full spectrum of sediment transporting events. This spreadsheet-based tool

reflects the growing body of scientific literature, indicating that sediment transport analysis is necessary for designing most alluvial channels.

Although the design hydrology approach described herein is applicable to a wide range of stream types, further research is needed on design hydrology for supply-limited systems, braided rivers, alluvial fans, ephemeral systems (where the typical dominant flow often has a recurrence interval of 10 to 25 yrs), and other non-equilibrium situations. This includes situations where high sediment loads and infrastructure constraints necessitate the design of a non-alluvial channel with transport capacity exceeding supply.

The hydrologic metrics and tools developed in this project provide a general framework and stronger physical basis for design hydrology at stream crossings. This framework is summarized in a separate guidance document that provides a concise summary and step-by-step approach for performing the recommended design hydrology analyses.

Introduction

The ubiquitous effects of land use change on stream hydrologic and geomorphic processes present an ongoing challenge for hydrologic design at the interface of built and natural environments. Changes in sediment and water delivery resulting from urbanization and other watershed alterations induce channel adjustments and threaten infrastructure via a wide variety of mechanisms. The effects of these modified runoff and sediment yields have in many instances been further exacerbated by direct channel disturbances that increase flow energy, decrease roughness, and increase erosion potential on some part of the channel boundary. Engineers are well aware of these issues, but currently lack clear guidance and systematic approaches for developing road-crossing and stream-restoration designs that are relatively robust and sustainable in the face of evolving water and sediment delivery. Depending on watershed drainage systems, storage, and management practices, land use changes often amplify the magnitudes and durations of channel-forming discharges across particular ranges of the flow frequency distribution. Identifying and designing for these somewhat contextual increases and shifts in channel erosion potential are critical elements of minimizing the risk of alluvial channel instability.

More rigorous tools and guidance are needed to assist engineers in designing stable channels. We define 'stable' after Biedenharn et al. (1997): "*In summary, a stable river, from a geomorphic perspective, is one that has adjusted its width, depth, and slope such that there is no significant aggradation or degradation of the stream bed or significant planform changes (meandering to braided, etc.) within the engineering time frame (generally less than about 50 years)."* These tools and guidance are also needed to assist engineers in designing road crossings for continuity of water and sediment across the spectrum of flows that primarily control channel response within a particular hydroclimatic and geomorphic setting. A key challenge in the development of such tools and guidance is keeping the design process as practical and parsimonious as possible without oversimplifying the situations that present higher risks and, therefore, require more in-depth analysis. For example, the design hydrology required for sustainable design of a supply-limited, armored cobble-bed stream with a gaged snowmelt flow regime is significantly different on many levels from the design hydrology needed for a high-energy, labile sand-bed channel with an ungaged flashy flow regime. Accordingly, prescribing "one-size-fits-all" approaches across the diverse ranges of hydrologic data availability, channel types, uncertainty, and existing valley constraints encountered in practice will not be cost effective.

Significant resources are being applied by public and private road and rail organizations to design and construct restored streams in disturbed watersheds, as well as to provide for stable transportation crossings (bridges and culverts) of streams. Lacking in this effort is a scientifically supported method for defining the design hydrology for such efforts along with an understanding of how that design hydrology might change with land use changes. In this project, we aim to address this knowledge gap by providing a set of guidance and decision support tools that are based on the best available science yet tempered with practical experience. The decision support tools presented herein are intended to be flexible and efficient in guiding users to an appropriate combination of design tools and depth of analysis for design hydrology in a given hydrologic and geomorphic context.

Because changes in channel forms and stability reflect the temporal sequence and combined action of water and sediment flows, designs that do not include consideration of both hydrologic and sedimentation regimes are incomplete and may produce erroneous conclusions. Thus, additional complexity in

performing design hydrology analyses is unavoidable in some instances. For example, an "effective discharge" analysis allows the designer of a stream crossing to analytically assess how the inflowing sediment load from upstream compares to the transport capacity of the design reach over a potentially broad range of geomorphically effective flows that the channel must convey, *if* they examine a spectrum of influential flow events.

This document describes decision support tools that provide guidance on how to generate design hydrology using gage data (proximate or otherwise), mechanistic modeling, regional dimensionless flow duration curves (FDCs), or some combination of these to perform a design analysis. Basic limitations in the current U.S. Geological Survey (USGS) streamflow gaging network will continue to require designers to rely on predictions in ungaged basins in many instances because continuous streamflow gages are heavily biased toward relatively large streams and rivers: 95% of streams have less than 3% of the gages and over 93% of stream length is represented with less than 1/3 of the gages (Figure 1-1). With such large empirical data gaps, especially on small streams, it is essential that appropriate guidance be provided on generating the hydrologic inputs needed for design under changing land use in different hydroclimatic and geomorphic contexts. The procedures recommended in this study for establishing design hydrology are commensurate with available data, and the particular geomorphic and climatic setting of a stream, and the inherent response potential of the stream.
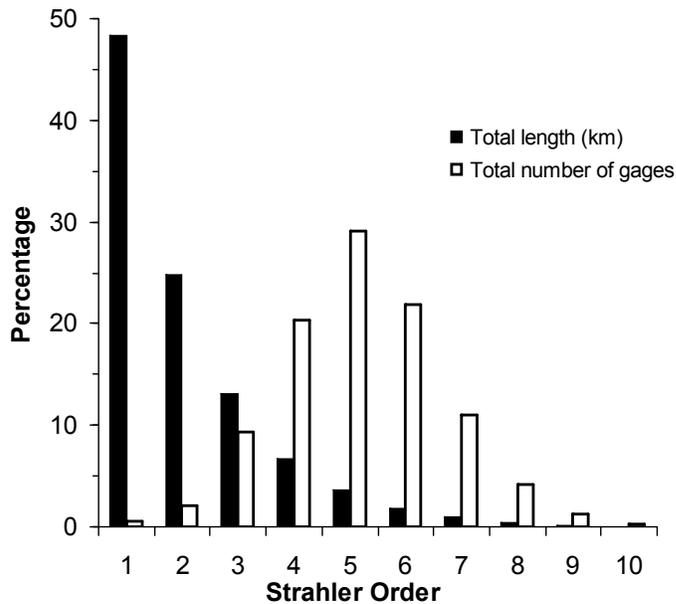
Figure 1-1. Percentage of USGS streamflow gages by stream length and Strahler stream order (Poff et al. 2006).

The decision and analysis tools developed in this project are also designed with "early off ramps" to simplify the design process. This means that in clear-cut or end-member cases, users can rapidly identify the needed design hydrology without getting bogged down in unnecessarily complex analyses that should be reserved for situations that involve high sediment loads outside the range of discharges typically considered "channel-forming," complex land use influences, susceptible channel types, and higher degrees of response potential (Figure 1-2). Users will be better positioned to balance tradeoffs between modeling complexity, costs, and uncertainty by rapidly identifying the appropriate tools for a given design, which will ultimately lead to more sustainable and cost-effective stream-crossings and restoration projects over the long term (Figure 1-3).

5

Increasing Channel Susceptibility

Figure 1-2. Severity of channel instability and risk to stream crossings increase with susceptibility of the channel setting and the extent of the amplification of the flow regime's erosivity.

Channel Erosion

Bank Failure

~$250,000 Highway Repair

Figure 1-3. Highway failures can occur across a gradient of stream settings, as seen by this ~$250,000 repair at a crossing with a cobble-bed channel draining ~2.6 km^2, adapted from Hawley et al. (2013).

1.1 Background

Current practice in stable channel design focuses on a single "dominant" discharge that is assumed to be the flow primarily responsible for performing work, transporting sediment, and shaping channel

geometry over a period of years. This flow is assumed to be a reasonable surrogate for the entire range and temporal sequence of channel-forming flows. The channel-forming discharge is typically identified through "bankfull" field indicators (a challenging task even in minimally-disturbed channels), recurrence interval analysis of peak flows (often extrapolated from gaged to ungaged sites), regional flood regression relationships, or a combination of these methods. Such an overall approach is problematic because it oversimplifies the physical controls on channel form and response, and frequently results in channel designs that are unstable. Specifically, most stable channel and stream-restoration designs are still not assessed for sediment continuity, even at a single presumed channel-forming discharge. Even analytical stable channel design techniques like the Copeland method (Thomas et al. 2002) in SAM (Hydraulic Design Package for Channels) and HEC-RAS (Hydrologic Engineering Centers River Analysis System) rely on a single design discharge and inflowing sediment load. Therefore, *there is an implicit and often dubious assumption that if sediment transport capacity is matched at the one presumed design discharge, it is sufficiently matched across the full spectrum of sediment transporting flows*. Unfortunately, this is frequently not the case because the channel geometry that minimizes differences between the cumulative sediment transport capacity of an upstream supply reach and a design reach is not the channel geometry indicated by examining only one design discharge. This issue is further complicated by land use changes interacting with different hydrologic regimes (e.g., snowmelt versus flashy, convective rainfall) to variably alter the frequency of flows competent to move sediment.

Effective discharge analysis has a strong physical basis and yields useful information even if a channel is unstable and lacks field indicators of an equilibrium form (Soar and Thorne 2011); however, designing a channel based on an effective discharge is not in itself a panacea. Channel designs based on a single discharge (effective or otherwise) can become unstable, even if there was an effort to match sediment capacity at that discharge. This is often due to a lack of sediment continuity at other ranges of discharge that were not considered in selecting the channel dimensions. In addition, many designers have been reluctant to perform effective discharge analysis because it requires a continuous flow series over a period of many years, and sometimes a flow series with a sub-daily time step for the flashy flow regimes typically encountered in urbanized watersheds and some climate regions. This has been an obstacle to wider acceptance of more rigorous channel design techniques, especially in ungaged basins. As such, designers have too often relied strictly on peak flow analysis and/or extrapolation of bankfull channel geometry from a location that may not be sufficiently comparable in terms of flow regime, sediment delivery, and watershed land use history. Lastly, effective discharge analyses are highly sensitive to the methods employed and there is uncertainty in all key aspects of effective discharge calculation (i.e., the flow frequency curve and sediment-discharge rating curve combine to produce uncertainty in the effectiveness curve). Although the U.S. Army Corps of Engineers (USACE) and others have made good progress in standardizing effective discharge analysis methods (and re-evaluating those methods is <u>not</u> the goal of this research), it is our experience that many designers still struggle with designing channels for sediment continuity. Therefore, there is a pressing need for decision support tools that help users conduct and interpret the full range of information provided by effective discharge analyses as part of an overall weight of evidence toward specifying hydrology for stable channel design.

1.2 Research Objectives and Tasks

The goal of this research is to develop scientifically supported methods for defining the design hydrology for stream crossings along with an understanding of how that design hydrology might change with land use changes. Steps employed in this study for achieving this goal included the following:

- Conducting a survey to understand the design hydrology needs of state Department of Transportation (DOT) engineers.
- Investigating flow metrics other than peak annual flood frequency curves for more consistent correlation with channel-forming processes (such as distribution of daily mean discharge, flow duration, key points on a FDC, etc.) across different geomorphic settings.

- Developing quantitative methods for estimating the impact of land use change on the design metric that is appropriate for design.
- Investigating the connection between land use change and modifications in channel-forming discharge, and consequently bankfull channel hydraulic geometry.

The project was composed of the following specific tasks:

Task 1 – Develop metrics describing effective discharge sediment yield curves.

Task 2 – Explore sensitivity of effective discharge analyses to climatic and analytical parameters.

Task 3 – Develop decision support tool for generating FDCs for use in effective discharge analysis.

Task 4 – Develop Soil and Water Assessment Tool (SWAT) interface to provide FDCs for ungaged sites at the national scale.

Task 5 – Develop software for effective discharge analysis and stable channel design.

Task 6 – Develop a decision support tool for identifying the upstream supply reach, geomorphic context, and inherent channel sensitivity.

Task 7 – Develop supporting guidance integrating the above tools for channel design.

Task 8 – Generate final project deliverables.

While the project was developed using the above task structure, it made sense to the project team to write this final report to be topically oriented. This ensures that the material is delivered in the way it will be used, as opposed to developed.

1.3 State-of-Design Discharge Practice and Survey

Another important goal of this project was to understand the needs of state DOT engineers and to develop tools that are likely to be adopted by end users. In early 2014, we invited state hydraulic engineers from 16 states representing all regions of the conterminous U.S. to participate in the survey described in the previous quarterly report. Ten states (California, Connecticut, Florida, Georgia, Minnesota, North Carolina, Oregon, Texas, Washington, and Wyoming; Figure 1-4) responded and agreed to respective phone interviews. The purpose of these interviews was to garner a better understanding of current practices used by state transportation engineers in designing geomorphic aspects of stream crossings, and to inform our envisioning of the final products that will emerge from this project. Each survey lasted approximately 30 minutes, and consisted of a discussion centered around four questions. These questions, and an overall summary of the responses, are provided below.
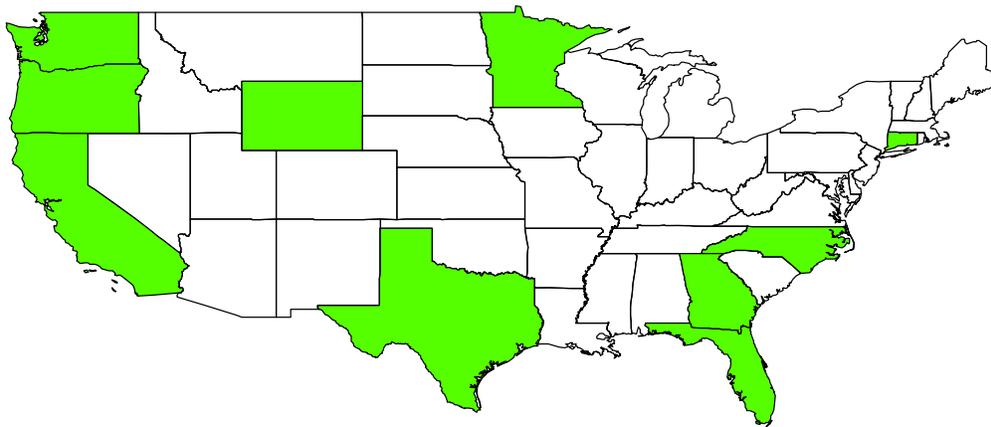
Figure 1-4. States participating in the survey of DOT hydraulic engineers.

Question 1: What hydrologic and hydraulic design variables / criteria besides peak annual flood frequency curves and erosive velocities / stresses does your organization use to design stable channels at stream crossings?

By far the most common approach is to use regional regression equations (generally USGS flood regressions for the state) to estimate peak flows for design discharges. For culverts, the annual peak, 2-yr flood, or estimated bankfull flow is typically used, while bridges are sized for flows ranging from the Q_{10} to the Q_{100} (10-yr to 100-yr recurrence interval, respectively) depending on the usage. For drainages smaller than a certain threshold, other peak flow methods were generally used such as the Natural Resources Conservation Service (NRCS) Curve Number Method and the Rational Method. Estimates of velocity or shear stress are generally not used, although occasionally these must be considered for fish passage or riprap sizing. Hydrologic models are rarely used to compute design discharges, with the notable exception of western Washington State, where long-duration, low-intensity precipitation has led to adoption of a continuous simulation model.

Question 2: What methods does your organization use to assess the impacts of future land use change on design hydrology at stream crossings?

Most states do not routinely take future land use changes into account when designing stream crossings. Occasionally, potential land use change is considered on a case-by-case basis, and in these circumstances it is generally accounted for by introducing anticipated changes in impervious cover into the USGS regression equations, or by adjusting the NRCS curve number for small basins.

Question 3: Aside from bridge scour calculations, are sediment transport analyses performed in the design of equilibrium channels at stream crossings? If so, please describe the circumstances and approach(es) utilized.

Although most of the surveyed states do some sort of bridge scour calculations, sediment transport calculations are rarely (and usually never) performed. Interviewees suggested that this was generally due to a lack of sediment transport expertise, and due to a lack of useful tools for this type of analysis. Additionally, it seemed that stable channel design approaches were often not considered due to the limited length of river or stream in the bridge- or stream-crossing right-of-way.

Question 4: In your opinion, what kinds of concepts, computations, and tools (software or otherwise) are needed to improve design hydrology for channel stability and restoration at stream crossings?

This question elicited a range of responses. Generally, it was suggested that case studies that provide the science that backs up design guidance would be beneficial. For instance, it would be useful to have guidance on when the bankfull flow / 2-yr flow is an appropriate and effective metric for design, or when a simple versus more-complicated approach is needed. Some engineers requested software or guidance that could facilitate sediment transport analyses. It was also suggested that a better understanding of how outliers affect the commonly-used peak flow analysis would be helpful.

1.4 Implications for Study as a Result of the Survey

Our discussions with practitioners at state DOT agencies helped guide subsequent work and influenced the products of this project. A consistent theme was having tools to help inform when simple approaches versus complex approaches were appropriate. To meet this end, we have developed:

- simple decision diagrams and flow charts to put this decision into the context of the hydrologic and geomorphic characteristics of the project site; and

- user-friendly tools with which to perform design hydrology analyses at a depth that is commensurate with the inherent susceptibility and response potential of different stream types and settings.

Another theme that emerged from the survey was that tools are unlikely to be used unless they are relatively simple and parsimonious. This is particularly true for analyses requiring any sort of sediment transport calculation, such as stable channel design, because sediment transport expertise at state agencies is uncommon. A major goal of the study is, therefore, to make tool usability a priority. As a result, these tools take the form of decision trees, straightforward spreadsheet-based software for stable channel design, and web-based interactive hydrologic analysis software. DOT engineers also expressed a desire for case studies highlighting the relevant science behind channel design. To this end, we studied the effects of land use change on temporal trends in FDC metrics, and the consequent implications for stable channel design. Finally, our survey encompassed diverse geographic regions that have different hydrologic regimes and channel types and, therefore, a variety of potential challenges for design or stream restoration. Although the tools developed in this project are not universally applicable, we have placed emphasis on developing guidance general enough to encompass a wide range of channel types and degrees of response potential, which in turn informs the recommended depth of design hydrology analysis.

1.5 Structure of the Report

The organization of this report is as follows. In Chapter 2, we develop the scientific basis for recommending straightforward hydrologic and sediment yield metrics for the design of stable channel geometry at stream crossings. Chapter 3 describes the development of a number of new web- and spreadsheet-based tools designed to be user-friendly and facilitate application of the novel hydrologic and sediment transport metrics developed in the preceding chapter. In Chapter 4, we describe three general types of decision support tools that inform the hydrologic design process through guidance on: (1) relating channel response potential to an appropriate level of design analysis guidance, (2) selection of analog reaches (also referred to as a reference reaches), and (3) rapid geomorphic assessments (RGAs) of channel instability and susceptibility at stream crossings. Given the overwhelming call for tool simplicity among DOT practitioners, Chapter 5 continues to document when certain simplified analyses are appropriate for design hydrology and provides case studies that address the following questions:
- In what situations are sub-daily streamflow data required in order to achieve a reasonable estimation of the sediment yield curve?
- How does watershed urbanization affect the FDC, and what are the possible implications for computing sediment yield metrics?

We then present guidance on estimating Q_{s50}, as well as worked examples using the tools developed as part of this project. Conclusions and suggestions for future research are provided in Chapter 6.

Four appendices are also provided. A summary of hydrologic and geomorphic data used in the research is provided in Appendix A with study sites categorized as coarse- versus fine-bed. Appendix B provides tutorials on using the eRAMS platform to perform a variety of hydrologic and watershed analyses that support the design hydrology process. A guidance document that provides a streamlined step-by-step description of the recommended design hydrology process and new design hydrology tools is provided in Appendix C. Finally, a reference manual summarizing the theoretical and methodological underpinnings of a new tool for performing design hydrology analyses and analytical channel design is provided in Appendix D.

Evaluation of Sediment Yield Techniques for Defining Design Discharge

In this chapter, we develop relatively simple hydrologic and sediment yield metrics for the design of stable channel geometry at stream crossings using the physically robust approach of magnitude-frequency analysis (MFA). Under Tasks 1 and 2, we developed and then tested the sensitivity of metrics based on effective discharge analysis, or what is henceforth referred to as MFA. MFA refers to the general procedure behind calculating the effective discharge (Q_{eff}), or the discharge that transports the most sediment in a channel on average, over time. It also refers more generally to calculating the sediment yield curve and quantifying how much sediment is transported by what frequency and magnitude of discharges over time. This is discussed in more detail in Section 2.2.

Section 2.1 introduces the sediment yield metrics, calculated from MFA, that are used for this analysis and provides a brief literature review about the relationships between sediment and flow properties and sediment yield magnitude and frequency. Section 2.2 first explores a theoretical examination of these relationships (Section 2.2.1) and then explores what empirical data have shown (Section 2.2.2). Under Section 2.2.2, we describe the data sources and methods, and the sites used throughout this portion of the study. We explore the ability of a new metric, the half-yield discharge (Q_{s50}) to predict bankfull discharge and compare its performance to Q_{eff} and hydrology-based bankfull predictors (Section 2.3). We end this chapter with a brief exploration of uncertainty in calculating sediment yield metrics for channel design (Section 2.4)

2.1 Defining Sediment Yield Metrics for Channel Design

An extensive literature review has identified dozens of MFA studies across a wide range of stream types defined by their flow regime (flashy to stable) and sediment transport mode (bedload to suspended-load dominated) in North America (Table 2-1). It has also revealed a variety of metrics in addition to those described in the original proposal (Table 2-2). We use the datasets referenced in these papers to assess the usefulness and descriptive power of the proposed sediment yield metrics in characterizing the discharge or range of discharges most responsible for maintaining equilibrium channel forms. These sediment yield metrics describe aspects of the effectiveness curve, such as the fraction of sediment transported above the effective discharge ($f+$) or the flow range straddling the effective discharge between which 50% of the total average sediment yield is transported under the sediment yield curve, *Qeff.spread*. Other sediment yield metrics relate specific discharges to aspects of the effectiveness curve, such as the discharge up to which all smaller discharges transport a cumulative 50% of the total average sediment yield (half-yield discharge), Q_{s50}.

Table 2-1. MFA studies and datasets used in the current study.

Reference	Type of Load	Reference	Type of Load
Andrews (1980)	Bed and suspended load	Mueller and Pitlick (2013)	Bed load
Andrews and Nankervis (1995)	Bed load	Nash (1994)	Suspended load
Ashmore and Day (1988)	Suspended load	Nolan et al. (1987)	Suspended load
Benson and Thomas (1966)	Suspended load	Pickup and Warner (1976)	Bed load
Biedenharn et al. (2000)	Bed-material load	Quader et al. (2008)	Bed-material load
Bunte et al. (2013)	Bed load	Sichingabula (1999)	Suspended load
Carling (1988)	Bed load	Simon et al. (2004)	Suspended load
Copeland et al. (2005)	Suspended load	Soar and Thorne (2001)	Bed-material load
Crowder and Knapp (2005)	Suspended load	Torizzo and Pitlick (2004)	Bed load
Doyle et al. (2007)	Bed load	Vogel et al. (2003)	Suspended load
Emmett and Wolman (2001)	Bed load	Webb and Walling (1982)	Suspended load
Hassan et al. (2014)	Bed-material load	Watson et al. (1997)	Bed-material load
Hey (1996)	Bed-material load	Whiting et al. (1999)	Bed load
Klonsky and Vogel (2011)	Suspended load	Wolman and Miller (1960)	Suspended load

Table 2-2. Flow, physical, and sediment yield metric definitions.

	Metric	Units	Description
Flow	yrs	[yrs]	number of years on flow record
	$mean$	[m^3/s]	mean of daily discharge
	cv	–	coefficient of variation of daily flow ($s / \bar{x}$)
	$skewness$	–	skewness of daily flow
	$spread$	–	(75th percentile flow – 25th percentile flow) / median flow
	$flash.RB$	–	daily flow Richards-Baker flashiness metric
	$Q1.5$	[m^3/s]	1.5-yr return interval flood
	$Q1.5.mean$	–	$Q_{1.5}$ normalized by the mean of the daily flows
	$Qeff$	[L^3/T]	effective discharge
Physical	$d50$	[mm]	average median diameter of the bed sediment
	$d84$	[mm]	84th percentile diameter of the bed sediment
	Qbf	[m^3/s]	bankfull discharge
	$tau.star$	–	dimensionless bed grain shear stress
	$w.d$	–	bankfull width-to-depth ratio
	$da.km2$	[km^2]	drainage area
Yield	$Q50.RI$	[yrs]	return interval of half-yield discharge (Q_{s50})
	$yield.spread$	–	($Q_{s75} – Q_{s25}$) / Q_{s50}
	$QS50.Q1.5$	–	half-yield discharge normalized by $Q_{1.5}$
	$Qeff.RI$	[yrs]	return interval of Q_{eff}
	$Qeff.spread$	–	similar to $yield.spread$, but centered on and normalized by Q_{eff}
	$Qeff.yield$	[%]	percent of cumulative sediment transport below Q_{eff}
	$f+$	[%]	percent of cumulative sediment transport above Q_{eff}
	$Qeff.Q1.5$	–	Q_{eff} normalized by the $Q_{1.5}$
	$β, beta$	–	sediment rating curve exponent

The return interval from the annual flood series and the percentile of the daily flow series can then be calculated for these discharge metrics to look for patterns in probability of occurrence for different stream types. If such patterns or correlations are found, then it may be possible to relate discharges significant in channel-forming processes based on MFA to more-easily calculate hydrologic metrics.

Datasets used in previous MFA studies fall into several categories: (1) only consider measured total suspended load (clay, silt, and sand), (2) only consider measured bedload (sand to large gravel, generally), and (3) model either bedload in coarse-bed streams (gravel- and cobble-dominated) or total load in fine-bed streams (sand-dominated) (as noted in Table 2-1). While many MFA studies have only considered total suspended load (e.g., Nash (1994), Vogel *et al.* (2003), and Ashmore and Day (1988)), which includes the silt and clay portion of the sediment load (wash load, < 0.0625 mm), others have argued that only the sediment found in appreciable amounts in the channel bed should be considered (bed-material load, ≥ 0.0625 mm) (Hey 1996; Soar and Thorne 2011). This is because the wash load tends to always be in transport and rarely settles into the bed, therefore, it tends to not play a formative role in channel morphology.

Previous MFA studies have focused on a few themes regarding the magnitude and frequency of sediment transport in rivers. Many seek to compare Q_{eff} with the bankfull discharge (Q_{bf}) the discharge that fills the channel just before spilling on the floodplain. The bankfull discharge in stable, quasi-equilibrium channels is an important channel design metric and is thought to be the channel-forming discharge in many cases (Wolman and Leopold 1957).

Some researchers have found a strong (e.g., 1:1) relationship between the bankfull discharge (Q_{bf}) and Q_{eff} (Andrews and Nankervis 1995; Andrews 1980; Hey 1996; Torizzo and Pitlick 2004), while others have found a wide range of variability in the $Q_{eff} - Q_{bf}$ relationship (Pickup and Warner 1976; Nolan et al. 1987; Soar and Thorne 2001). In a study of glaciated mountain streams in British Columbia, Hassan et al. (2014) attributed this variability in the $Q_{eff} - Q_{bf}$ relationship to characteristics of the bed material. In rivers with beds composed of sand and mobile gravel mixtures (un-armored, higher sediment loads), relatively frequent flows were most effective and $Q_{eff} < Q_{bf}$. Here, they ascribe Q_{eff} to a sediment continuity – channel maintenance flow rather than a channel-forming flow. In rivers with armored beds that were infrequently mobile, $Q_{eff} \geq Q_{bf}$ and Q_{eff} was more likely a channel-forming flow.

Another theme in this line of research attempts to relate MFA with some of the physical drivers of sediment transport, namely flow regime, sediment properties, as well as geomorphic setting (i.e., drainage area). The exponent of the sediment rating curve generated from bed-material load measurements, of the form $Q_s = \alpha Q^\beta$, is very influential in calculating the effective discharge value, as well as other MFA metrics such as Q_{s50} (Vogel et al. 2003; Barry et al. 2008; Bunte et al. 2013). For larger values of the exponent β, larger, less frequent discharges become more influential in overall sediment yields (Bunte et al. 2013; Hassan et al. 2014). Finally, previous work has found a connection between flow variability and MFA. As the flow in a river becomes more variable or flashy, larger flows and floods become relatively more frequent, and these more extreme events tend to dominate sediment yield overall. This was theorized by Wolman and Miller (1960), and has been demonstrated in fine-bed (Soar and Thorne 2001) and coarse-bed rivers (Bunte et al. 2013) separately. We propose a physical explanation for this in Section 2.2.1. All of these previous findings suggest that characterizing the flow regime well, especially in streams with highly variable or flashy flow regimes, becomes more important for predictions of stable channel form and sediment continuity.

It is often the case that an empirical sediment rating curve is not available for a particular stream due to a lack of sediment transport measurements required to construct one. However, because the exponent β tends to increase with the size of the coarser fraction of the bed material (Emmett and Wolman 2001; Barry et al. 2008) and tends to increase from sand-bed streams to coarse-bed streams, we can infer that MFA metrics may be more sensitive to estimates of the frequency of large infrequent flows in coarse-bed streams. We further explore this relationship in Section 2.2.

2.2 Exploring Sensitivity of Sediment Yield Metrics to Hydrologic and Physical Drivers

Here we consider the sensitivity of sediment yield to physical drivers across different types of rivers and the relationships with these metrics to other hydrologic metrics commonly used in channel design. To do this, we use theoretical MFA relationships to explore some of the underlying processes relating flow variability to sediment yield metrics. We also conduct MFA on a large sample of rivers and streams from across the country in which bed-material load data have been collected near stream gages. In the empirical analysis, we explore relationships between flow metrics, physical metrics (e.g., grain size), and sediment yield metrics (Table 2-2). Note that flow variability under this task is defined as a statistical property of the flow regime of a river. It is generally defined herein as the coefficient of variation (C_v) which is the ratio of the standard deviation of a flow record to its mean. When we discuss changes in flow variability, this generally refers to changes from one river to the next such as a snowmelt-fed river versus a convective precipitation-fed river. However, due to environmental change, flow variability may change within a river over time. Urbanization tends to increase flow variability, for example.

The fundamental output of MFA is the sediment yield curve (red curve in Figure 2-1), which is calculated as the product of the daily or sub-daily flow frequency distribution or histogram (blue curve in Figure 2-1) with the sediment transport relation (green curve in Figure 2-1). The flow distribution can be generated from nearby gage data with a reasonably long flow record (>10 yrs), preferably with hourly data if available. We explore other indirect methods for representing daily or sub-daily flow distributions for ungaged sites under Tasks 3 and 4 (Chapters 3 and 4). The sediment rating curve can either be generated directly from bed-material load measurements (bedload measurement in coarse-bed streams and suspended sand measurements in fine-bed streams) or by using a calibrated sediment transport model for a specific reach. See the U.S. Forest Service's website (USFS; http://www.stream.fs.fed.us/ publications/bags.html) for primers on bedload measurement and modeling, as well as a tool to do so. Other tools for modeling both bedload and suspended-load sediment transport are compiled and discussed in Chapters 3 and 4.
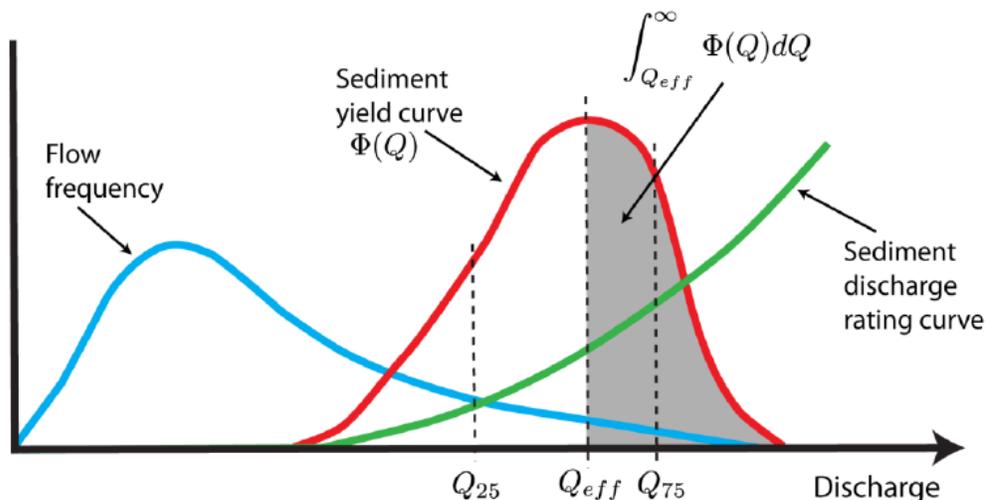
Figure 2-1. Representation of data, computations, and resulting metrics in sediment yield analysis. Blue curve is the flow frequency (as a probability density function in the general units of volume of water per time), the green curve is either a field data- or computational-based estimate of sediment transport (in units of sediment mass per volume of water), and finally, the red line is the product of the blue and green (in units of sediment mass) and summarize the sediment yield across all flows. Metrics derived from this red curve include the effective discharge (Q_{eff}) and half-load discharge metrics (Q_{s50}).

Flow frequency, as represented by a FDC is a graphical representation of the frequency, or the fraction of time that a discharge magnitude is equaled or exceeded. More specifically, FDCs and flow frequency curves both express the same information, the former as a cumulative distribution function (CDF) and the latter as a probability density function (PDF). Representation of the entire runoff hydrograph time series (typically daily runoff, but can be hourly, or even 15-minute) in a single curve makes the FDC a compact signature of streamflow variability. It is a valuable tool to understand precipitation-runoff responses in gaged watersheds, and to regionalize them to ungaged watersheds. FDCs are an essential part of effective discharge and channel stability analysis. At ungaged sites, and gaged sites with inadequate data (short record length and poor representation of land use changes), it is necessary to compute an estimated a FDC. FDCs can be estimated in ungaged basins using a variety of methods including regression methods (e.g., Hawley and Bledsoe (2011)), index methods (e.g., basin-area and regional scaling), continuous simulation modeling (e.g., Hydrologic Engineering Center Hydrologic Modeling System (HEC-HMS), Hydrologic Simulation Program Fortran (HSPF), Storm Water Management Model (SWMM), and SWAT), geostatistics, and methods that use short runoff records (Castellarin et al. 2012). Continuous simulation may be especially advantageous for areas undergoing rapid land use changes and with flashy flow regimes that require a shorter time step for adequate characterization of sediment transport potential. Novel tools developed in this study for generating FDCs are described below.

2.2.1 Theoretical MFA Study

We begin by exploring what theoretical approaches to MFA can tell us about relationships among flow regime, sediment transport properties, and channel form. While Wolman and Miller (1960) originally suggested that a continuous, theoretical PDF could be used to represent the flow regime, it was not until three decades later that this theoretical approach to MFA was formalized (Nash 1994; Vogel et al. 2003; Goodwin 2004; Quader and Guo 2009; Klonksy and Vogel 2011). The theoretical approach to MFA involves multiplying a continuous PDF that is fit to the flow distribution (e.g., the log-normal or gamma distribution) with a sediment transport relation; which may be as simple as a power-law function that relates sediment transport to flow, or a more complex and threshold-driven relation. Metrics based on the resulting effectiveness curve equation may then be derived by analytical integration. The appeal of the theoretical approach to MFA lies in the ability to generate easily applied, closed-form solutions to MFA metrics such as Q_{eff} (Goodwin 2004) and the amount of sediment transported by discharges greater than Q_{eff} ($f+$) (Vogel et al. 2003). With these, one can expediently determine the relationship between MFA metrics and attributes of the flow regime (e.g., coefficient of variation, skewness, etc.), and/or sediment transport mode (e.g., empirical sediment rating curve exponent and critical shear stress for bed mobilization). Furthermore, one could use these relations to predict how a channel might respond to a change in flow variability or sediment supply due to environmental change assuming a correlation between Q_{eff} or another MFA metric, and Q_{bf}.

The theoretical work we have conducted on the relationship between grain size in a channel and the fraction of sediment transported above Q_{eff} ($f+$) has demonstrated that $f+$ tends to decrease overall as the threshold for sediment entrainment increases (Figure 2-2b). It also increases with the variability of the flow regime. This means that it will take on a very high value in fine-bed streams with flashy flow regimes. Soar and Thorne (2001) found that in fine-bed streams as flow variability increases, the ratio of Q_{eff} to Q_{bf} decreases, meaning that the effective discharge was much smaller than the bankfull discharge in flashy streams.

Therefore, in flashy, fine-bed streams, a single effective discharge may not be a reasonable metric for channel design. We also demonstrate that compound channel form—that is, channels with low, connected floodplains or benches—plays an important role in influencing $f+$ and hence Q_{eff} (Figure 2-2a). As flow variability increases, larger floods become more frequent, but they have less transport capacity in the floodplain thereby reducing the value of $f+$.
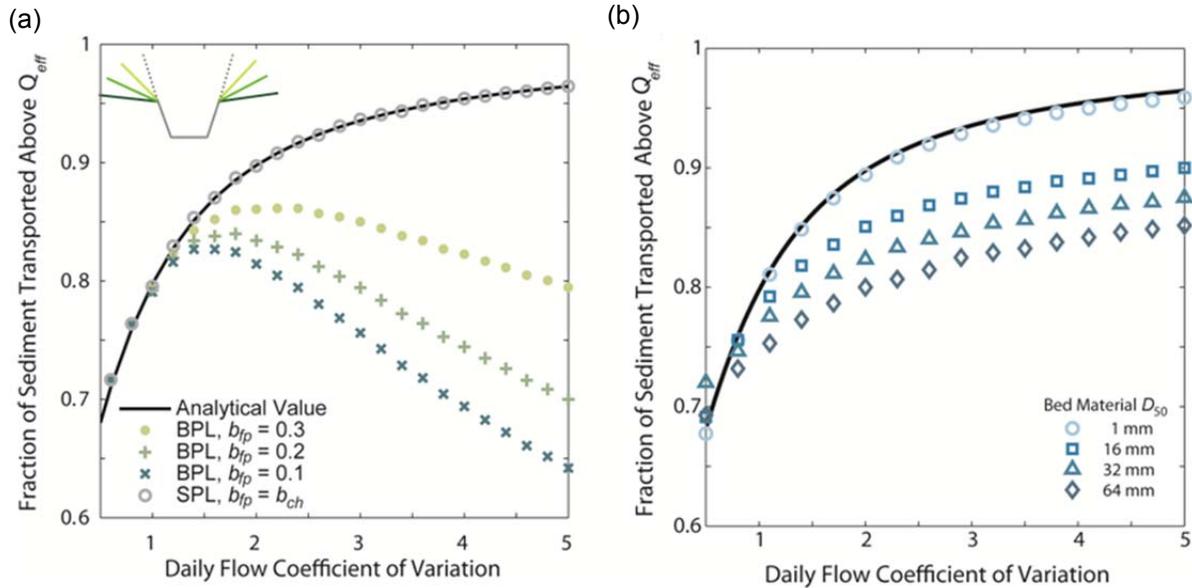
Figure 2-2. Fraction of sediment transported by discharges greater than Q_{eff} using analytical approaches of Vogel et al. (2003) for (a) compound channel form (BPL – broken power law) with varying floodplain lateral slope (b_{fp} – at-a-station hydraulic geometry floodplain exponent) compared to no floodplain example (SPL – single power law), and (b) an increasing threshold for sediment entrainment. Note that the black lines in both figures represent the closed-form equation for f+ assuming a power-law sediment rating curve and log-normal daily flow distribution (Vogel et al. 2003). The inset in (a) relates the colors of the data to the compound channel form that created them.

Our analyses indicate that the threshold for entrainment of bed material also influences the value and return interval of Q_{eff} in interesting ways. For flow distributions with low variability, large flows are rare. Transport of coarse sediment classes—and the most effective discharge for these sediment size classes— occur primarily in the right tail of the flow distribution resulting in a very large return interval (RI; Figure 2-3b). With increasing flow variability, flows less than the threshold for sediment entrainment become more frequent and push sediment transport further out into the right tail of the distribution and increasing the absolute value of Q_{eff} (Figure 2-3a).

In this case, RI drops precipitously with increasing C_v as the larger flows necessary to move the coarser sediment become more common (Figure 2-3b). However, the opposite is true in fine-grain streams with very low or negligible entrainment thresholds in which the effectiveness curve follows the flow frequency curve more closely. This means that the absolute value of Q_{eff} decreases with increasing flow variability. However, the recurrence interval remains relatively constant with flow variability due to the small absolute changes in the value of Q_{eff} (Figures 2.3a and 2.3b). Considering the sediment yield curves for fine- and coarse-grained systems can help explain these divergent relationships between Q_{eff} and C_v (Figure 2-4) as one follows the peak of the sediment yield curve as a function of C_v for fine (1 mm) and coarse (64 mm) bed streams. As flow variability increases in fine-bed channels, the peak of the sediment yield curve tracks to a smaller value resulting in smaller values of Q_{eff} (Figure 2-4a). In coarse-bed channels, the opposite is the case as less frequent flows become more effective (Figure 2-4c).
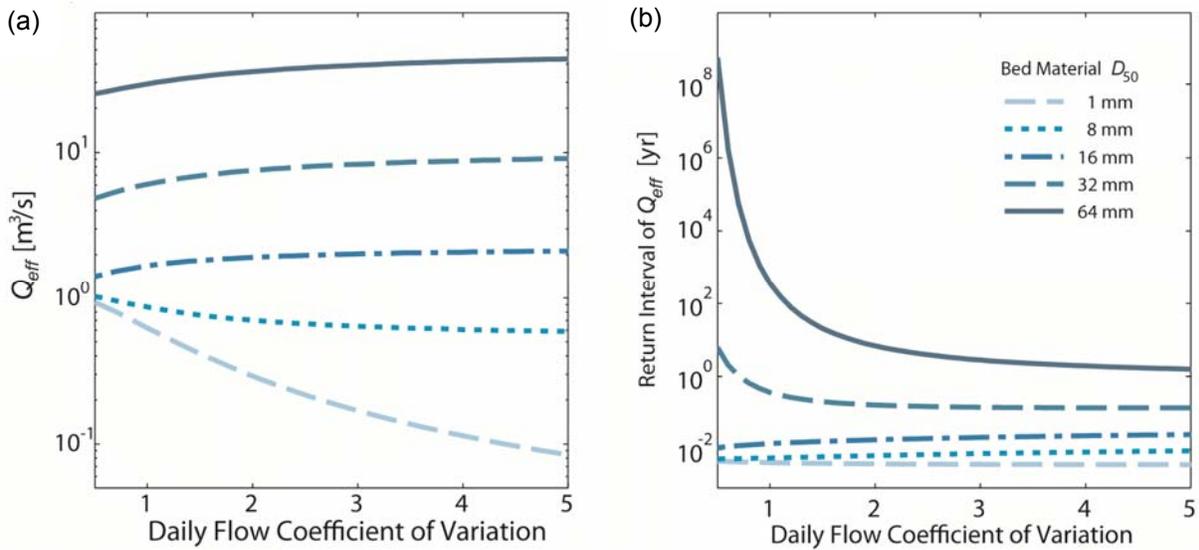
Figure 2-3. *The value of (a) Q_{eff} as a function of coefficient of variation (C_v) and sediment grain size (D₅₀), and (b) the return interval of Q_{eff} in years as a function of the same. Note that the Q_{eff} – C_v relationship changes from relatively small (sand to fine gravel) to relatively large (medium gravel to small cobble) sediment sizes. Plots are for a synthetic channel with Q_{bf} = 10 m³/s, and bottom width = 18 m. Relationships hold for channels of various sizes.*
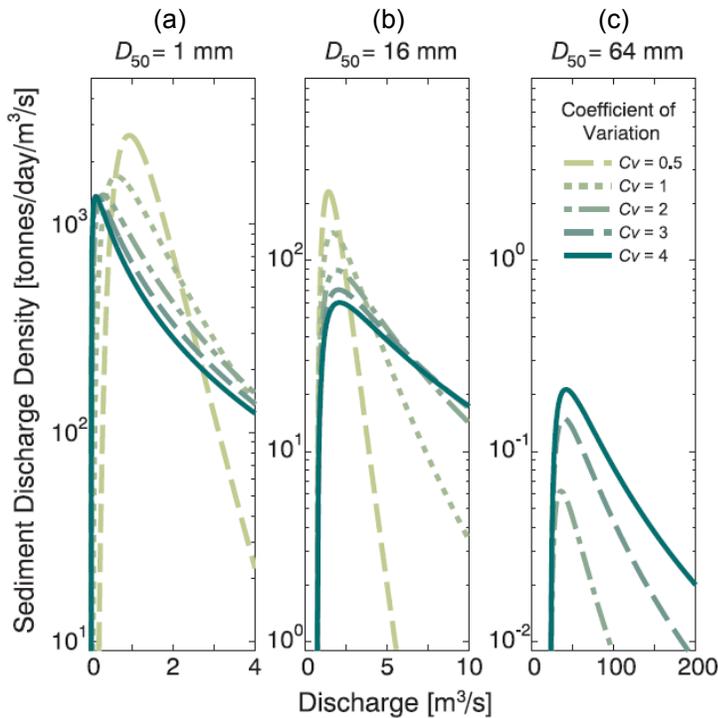
Figure 2-4. *Sediment yield curves for a range of grain sizes and C_v values. Note that the discharge associated with the peaks of these curves (Q_{eff}) decreases with increasing C_v for small grain sizes and increases with increasing C_v for large grain sizes.*

17

A final metric that we explore using this theoretical framework is the interquartile range of sediment yield centered on Q_{eff} ($Qeff.spread$) (Table 2-2, Figure 2-5). This metric helps describe the relative range of flows responsible for transporting this central 50% of sediment. A smaller number means that a smaller range of flows transports this central 50%, in which case a single-discharge metric may be suitable for channel design where sediment continuity is a concern. A larger number indicates that a wider range of flows is responsible for sediment continuity and a more sophisticated approach to channel design may be necessary. Compound channel form plays only a small role in influencing Q_{eff} for $Q_{eff} \leq Q_{bf}$ (Figure 2-5a). If $Q_{eff} > Q_{bf}$, then it will play a larger role in that as more flow has access to the floodplain (shallower sloped floodplain, short banks) then $Qeff.spread$ will increase, but only for very large values of C_v (very flashy systems). Sediment grain size plays a larger role on $Qeff.spread$ (Figure 2-5b). $Qeff.spread$ is generally larger in fine-bed streams and smaller in coarse-bed streams, meaning when sands dominate the bed, a larger range of flows is responsible for sediment transport and continuity, whereas this range tightens for gravel- to cobble-bed streams. Also, for all stream types, $Qeff.spread$ increases with C_v, but begins to level off for large values of C_v (>4 in coarse-bed streams).
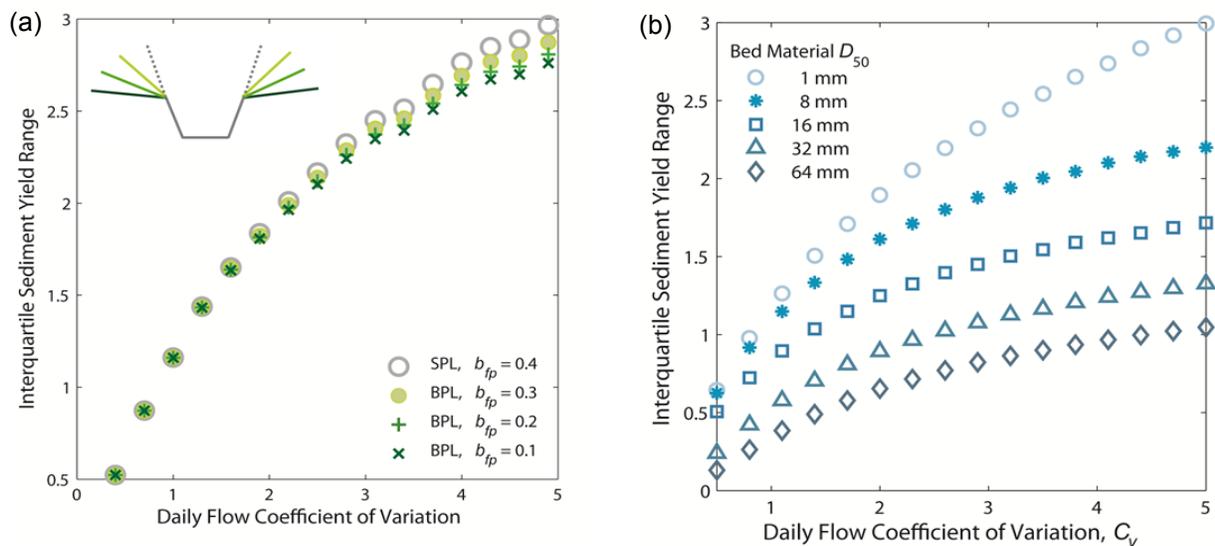
Figure 2-5. Interquartile sediment yield range centered on Q_{eff} ($Qeff.spread$) as a function of (a) C_v and compound channel form, as well as (b) bed sediment grain size.

Overall, these theoretical analyses provide information on how effective discharge estimates vary systematically with stream type and regional flow variability. Flow variability is also substantially affected by land use changes. As such, these analyses also provide insight into how future urbanization and other land use changes are likely to shift the range of geomorphically effective discharges that primarily influence stable channel morphology at stream crossings.

2.2.2   Empirical Study

Using a national flow and sediment load dataset, we explore empirical relationships between the drivers of sediment transport in rivers, namely the flow regime and sediment characteristics, and sediment yield metrics. This investigation has yielded relationships between the driver and response variables describing sediment yield that help inform to what physical drivers different river types are most sensitive.

18

We first collected data from stream sites included in published articles, as well as in government reports (Table 2-3). We have expanded this search to include other sites with a sufficient amount of sediment data ($n > 15$ samples) and a sufficiently long flow record straddling the time when the sediment data were collected. Site-specific information for all sites used in this portion of the study is provided in Appendix A.

Table 2-3. Bed-material load measurement sources.

	Reference	Region / Site
Coarse-bed Sites	Andrews (1994)	Sagehen Creek, California
	Andrews (2000)	East Fork Virgin River, Utah
	Bunte and Abt (2009)	Rocky Mountains, Colorado
	Erwin et al. (2011)	Pacific Creek, Wyoming
	Jones and Seitz (1980)	Clearwater River, Idaho
	King et al. (2004)	Rocky Mountains, Idaho
	Rankl and Smalley (1992)	Rocky Mountains, Wyoming
	Smalley et al. (1994)	Wind River, Wyoming
	USFS (2014b)	Rocky Mountains, Colorado and Wyoming
	USGS, National Water Information System (USGS NWIS) (2014)	California
Fine-bed Sites	Biedenharn and Thorne (1994)	Mississippi River
	Crowder and Knapp (2005)	Illinois
	Nash (1994)	Conterminous U.S.
	Nolan et al. (1987)	California
	Soar and Thorne (2001)	Midwestern and Eastern U.S.
	Watson et al. (1997)	Midwest U.S.
	USGS Sediment Data Portal (2014)	Conterminous U.S. and Puerto Rico

We collected a dataset of 93 fine (sand) bed sites in which ≥ 15 suspended-sediment samples have been collected where the fraction of sediment ≤ 0.0625 mm in diameter (sand/silt split) has been measured (Figure 2-6). We are interested in the sand portion of the suspended load only for this analysis because this approximates the bed-material load in sand-bed rivers, which is most responsible for channel form. Silt- and clay-sized particles are considered wash load and tend to not settle out of the water column, contributing little to channel form (Hey 1996). This dataset includes streams with drainage areas ranging from 10 to 1,000,000 km^2 across the continental U.S. and in Puerto Rico. Due to lack of data, not all regions in the U.S. are represented (e.g., Appalachia), but the overall range of hydrologic environments and channel types captured in the dataset should provide generally useful findings that can be applied across most of the country.
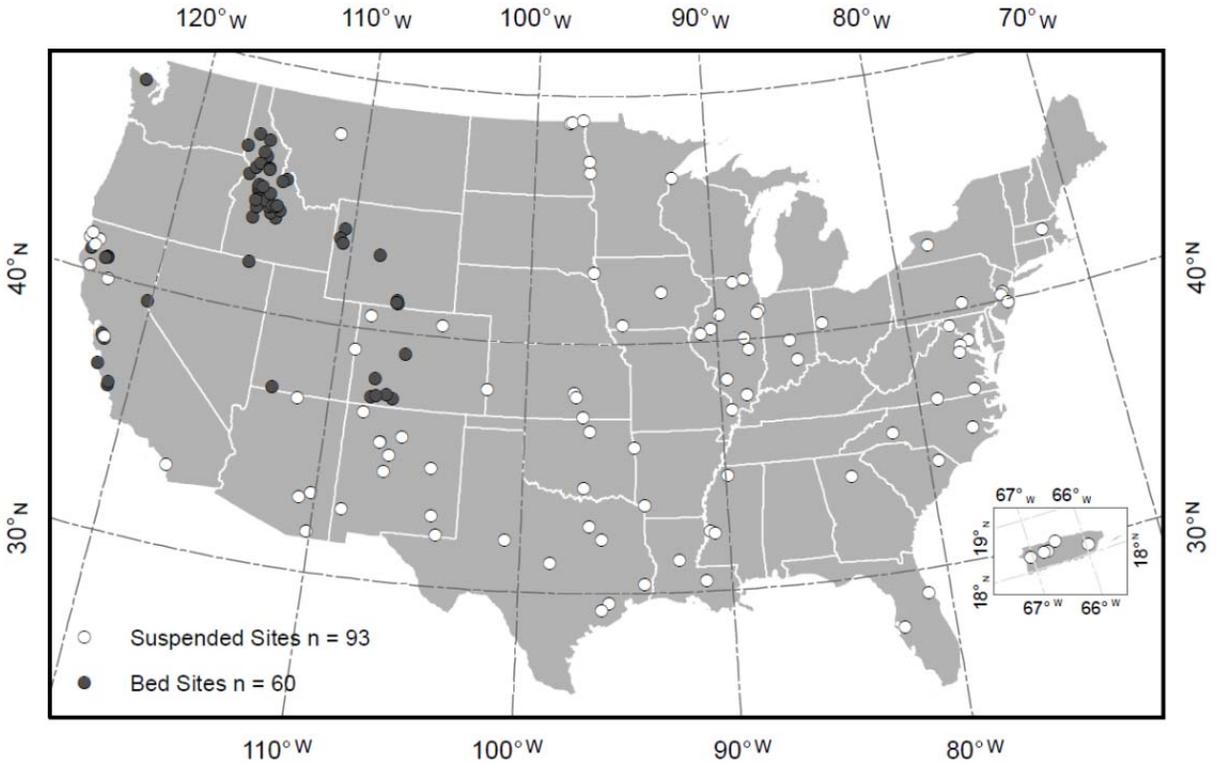
Figure 2-6. Map of suspended-load (white circles) and bedload (black circles) study sites.

We use bedload transport data to represent the bed-material load in coarse-bed streams. Existing bedload transport measurements for coarse-bed sites are much less common than suspended-load measurements and are primarily limited in geography to the Rocky Mountains, the Southwest, and the West Coast (Figure 2-7). Numerous inquiries at academic and government institutions for bedload data collected at or near stream gages in the Midwest and eastern U.S., resulted in no additional data. We use bedload data collected primarily with Helley-Smith bedload samplers, as these types of bedload samples are the most common and we want to compare similar bedload data. The drainage areas for bedload sites range from 10 to 15,000 km^2, over $n = 60$ sites.
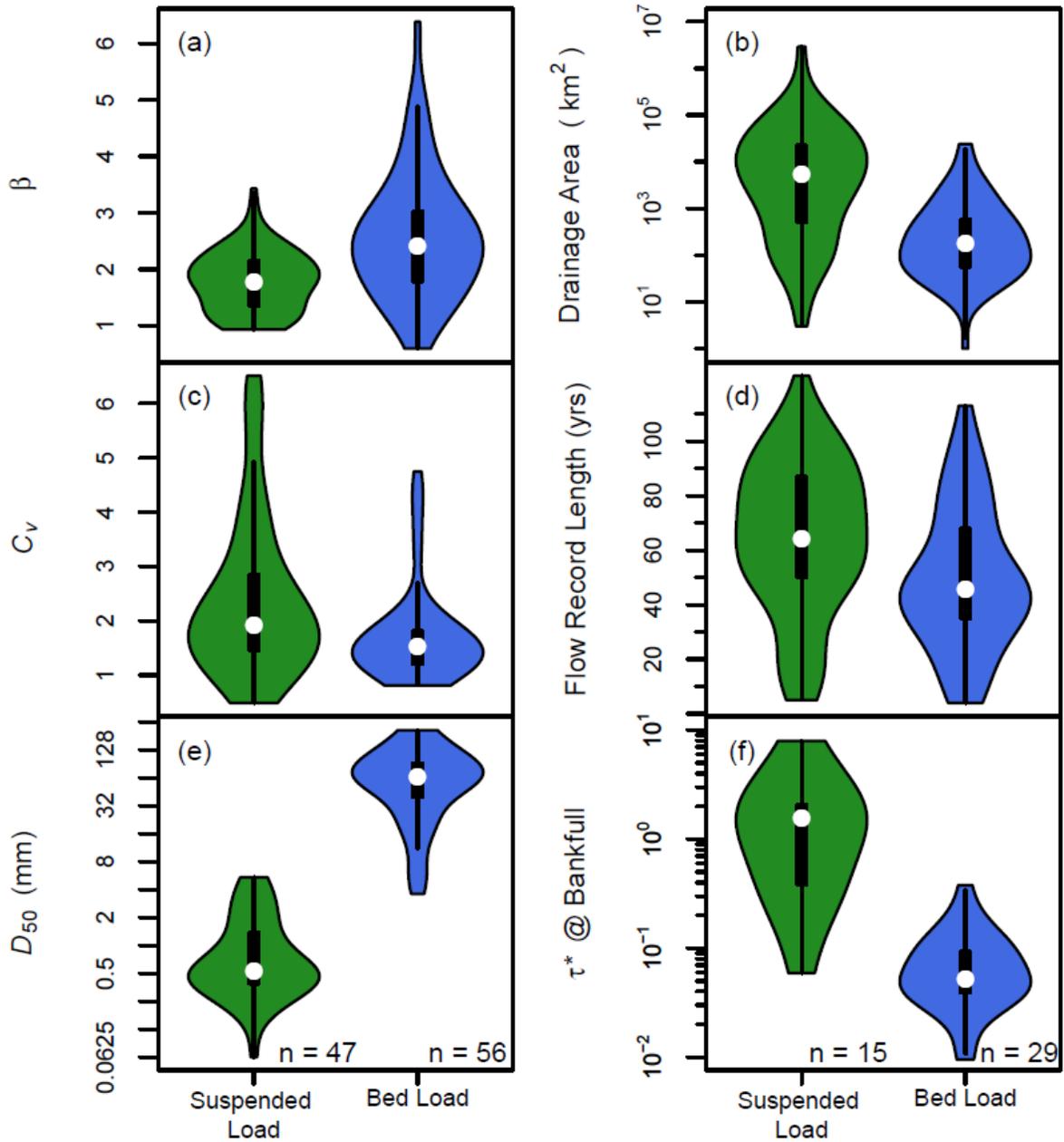
Figure 2-7. Empirical density functions (violin shapes) and interquartile ranges (black rectangles with white median dots) for site attributes. Unless otherwise noted, n = 93 fine-load sites and n = 60 coarse-bed sites.

2.2.2.1 Magnitude Frequency Analysis

We calculated the effective discharge for each site using the flow record coupled with the sediment rating of the form $Q_s = \alpha Q^{\beta}$, generated by robust log-linear regression methods, which give less weight to outliers (robust linear model (RLM) function, 'Modern Applied Statistics with S' (MASS) package (R CORE Team 2014a)). We completed a quality-control procedure to cull sites with poor rating curve fits (e.g., Pearson's correlation coefficient $R^2 < 0.50$), sparse data, or data that are deemed unrepresentative of

the minimum 10 yrs of flow record needed for analysis resulting in the final dataset used in this analysis. Other site attributes are summarized in Figure 2-7.

Many methods for effective discharge calculation exist (Soar and Thorne 2011). We tested the standard binning method (Biedenharn et al. 2000), the kernel density function method (Klonsky and Vogel 2011), the log-normal flow distribution fitting method (Goodwin 2004), and finally, the empirical flow distribution method (Orndorff and Whiting 1999). We deemed the empirical flow distribution method the most robust, consistent, and accurate method out of all of the methods we studied (Sholtes 2015). This is similar to the histogram method and often produced similar results. It involves numerically differentiating the empirical CDF of the flow record (sorted flow plotted as cumulative percentiles); however, by using a logarithmic bin spacing, this method is less susceptible to a few high flows in the right tail of the flow distribution overriding the MFA and resulting in the effective discharge being a very large and infrequent value. All reported results for the effective discharge were calculated using this method. The Q_{s50} is calculated from a flow record converted into a sediment yield record with a sediment rating curve. The sediment yield record is sorted and normalized by total sediment yield. The Q_{s50} is the discharge associated with 50% of cumulative sediment yield on this sorted sediment yield record. An example of this analysis for a suspended-load dominated site (Figure 2-8), shows the log-log rating curve analysis (Figure 2-8a), the daily flow distribution analysis (Figure 2-8b), the sediment yield curve (Figure 2-8c), from which Q_{eff} is calculated, and finally, the cumulative sediment yield curve (Figure 2-8d), from which Q_{s50} is calculated. The MFA methodology used herein is described in more detail in Sholtes (2015).

In addition to the sediment yield metrics, we calculated metrics that summarize various aspects of the flow regime (especially flow variability or flashiness, Table 2-2) and physical aspects of the channel and its boundaries: drainage area, sediment transport mode, grain size, as well as the bankfull flow (where available) and width:depth ratio. We then compared these aforementioned driving variables to the response variables, which are the metrics based on sediment transport MFA, what we are calling sediment yield metrics (Table 2-2). The objective here is to find relationships between the driving and response variables: What physical drivers most influence and best predict sediment yield metrics between suspended-load and bedload dominated rivers?
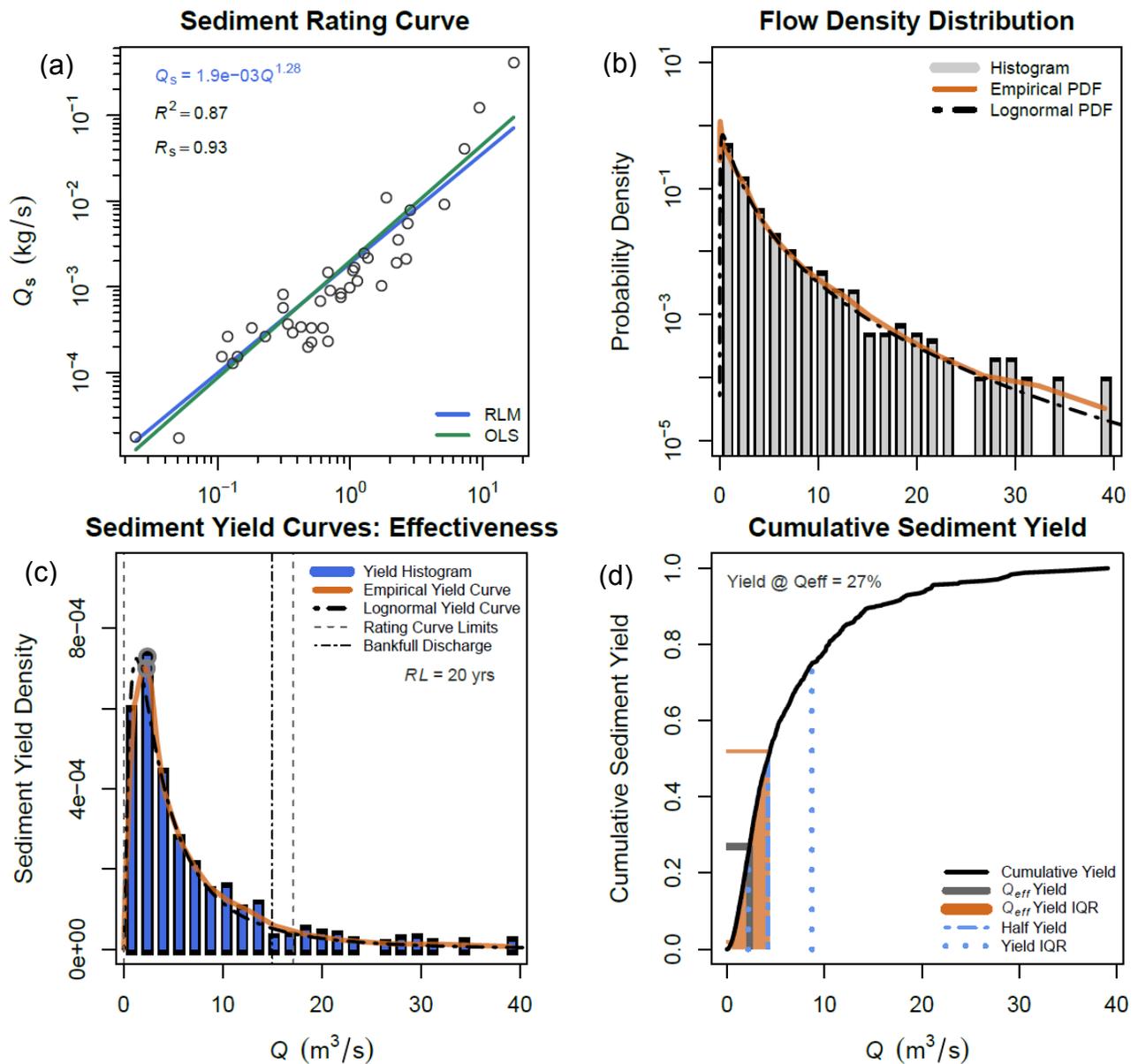
Figure 2-8. Example of MFA outputs for a suspended-load dominated site.

2.2.2.2 Sediment Yield Metric Analysis

The effective discharge for suspended-load sites covers a wide range of daily flow percentiles. The interquartile range (IQR) approximately spans the 70th – 95th, while the IQR of the effective discharge for the bedload sites was much narrower, spanning approximately the 92nd – 99th (Figure 2-9). We also calculated the percentiles of daily flow for the discharge associated with the interquartile range and median of cumulative sediment yield over the flow record (Q_{s25}, Q_{s50}, and Q_{s75}). The Q_{s25}, Q_{s50}, and Q_{s75} were calculated by determining the discharge value associated with 25%, 50%, and 75% of cumulative sediment transport over the sorted flow record, respectively. These flow interquartile ranges overlapped

much more, and expectedly, increased up to very high percentiles up to the Q_{s75} (100th percentile for median values for both types of sites). Return intervals of Q_{eff} tended to be at or less than 1.5 yrs according to the annual maximum flood series for sand-bed sites (Figure 2-10). Return intervals are slightly larger for Q_{s50} in fine-bed sites with an IQR ranging from just over 1 yr to approximately 1.75 yrs. In coarse-bed streams, the range of return intervals for Q_{eff} and Q_{s50} overlap well with median values of approximately 1.5 yrs and IQRs ranging from approximately 1.25 to 2.25 yrs.
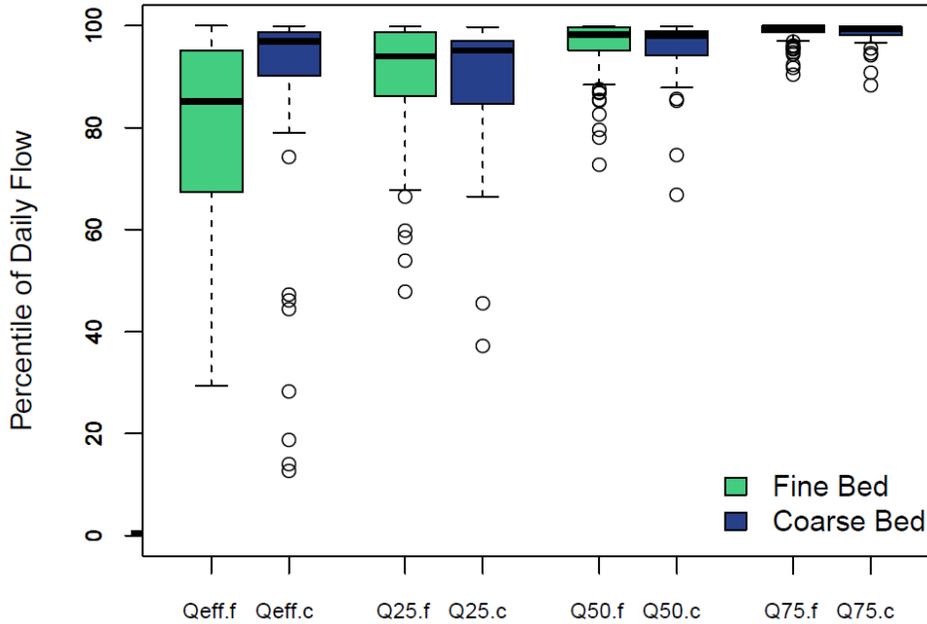
Figure 2-9. Daily flow percentiles for sediment yield metrics for fine-bed sites (".f," green), and coarse-bed sites (".c," blue).
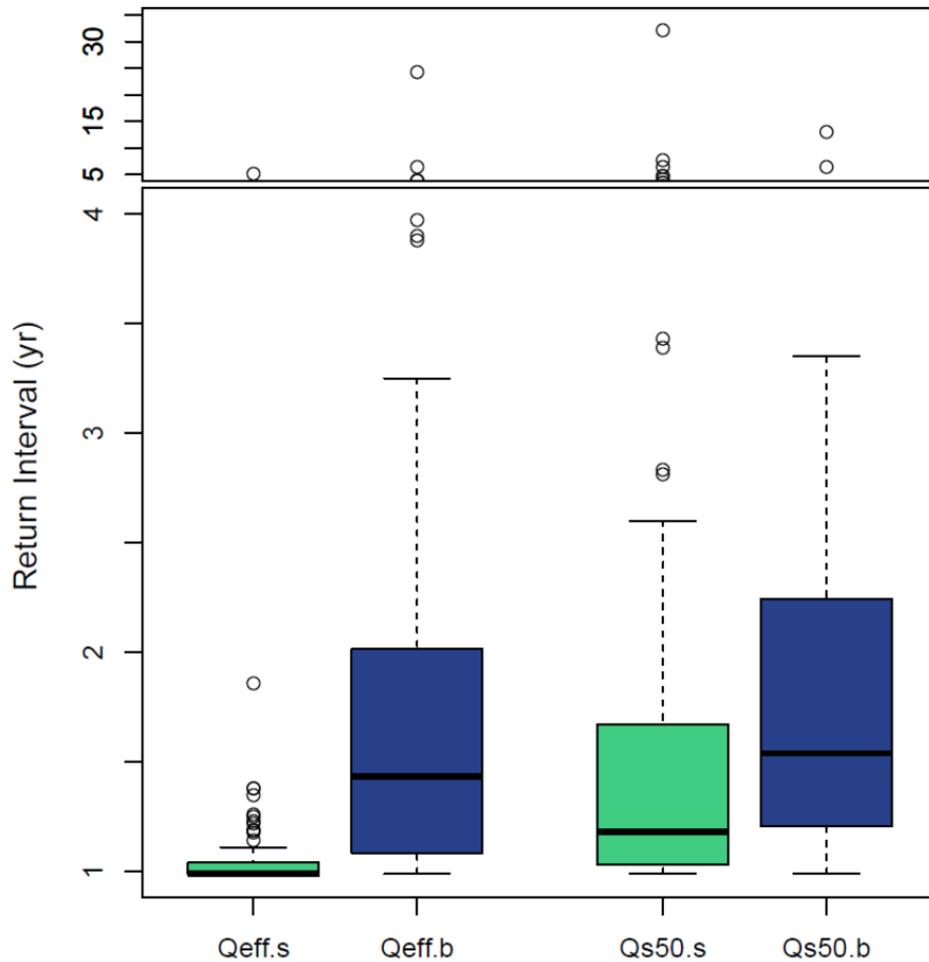
Figure 2-10. Return intervals (years) of sediment yield metrics for fine-bed sites (green), and coarse-bed sites (blue) based on the annual maximum flood series. Return interval values are censored at 1 yr.

As discussed in Section 2.2.1, C_v and β are two key driving variables that explain a large amount of variance in the values of several sediment yield metrics. Therefore, we consider sediment yield metrics as a function of combined flow and physical metrics: the product and ratio of C_v and β (Figure 2-11). These combined metrics are useful because C_v and β both range from 1 to 6 in absolute value. Both normalized values of Q_{eff} and Q_{s50} increase with the product of C_v and β (Figures 2-11a and 2-11d). This relationship is very strong for the normalized Q_{s50} values for both types of sites, and for the normalized Q_{eff} values for coarse-bed sites only. Klonsky and Vogel (2011) found that Q_{eff} and Q_{s50} normalized by the mean of daily flows both increase with C_v and β in a fairly tight relationship. We found a similar trend for both types of sites, with the relationship being much steeper for the normalized Q_{s50} for the fine-bed sites (Figure 2-11d). Because the maximum values of C_v at fine-bed sites are greater than those for the coarse-bed sites, flow variability may be dominating this steeper relationship for fine-bed sites.
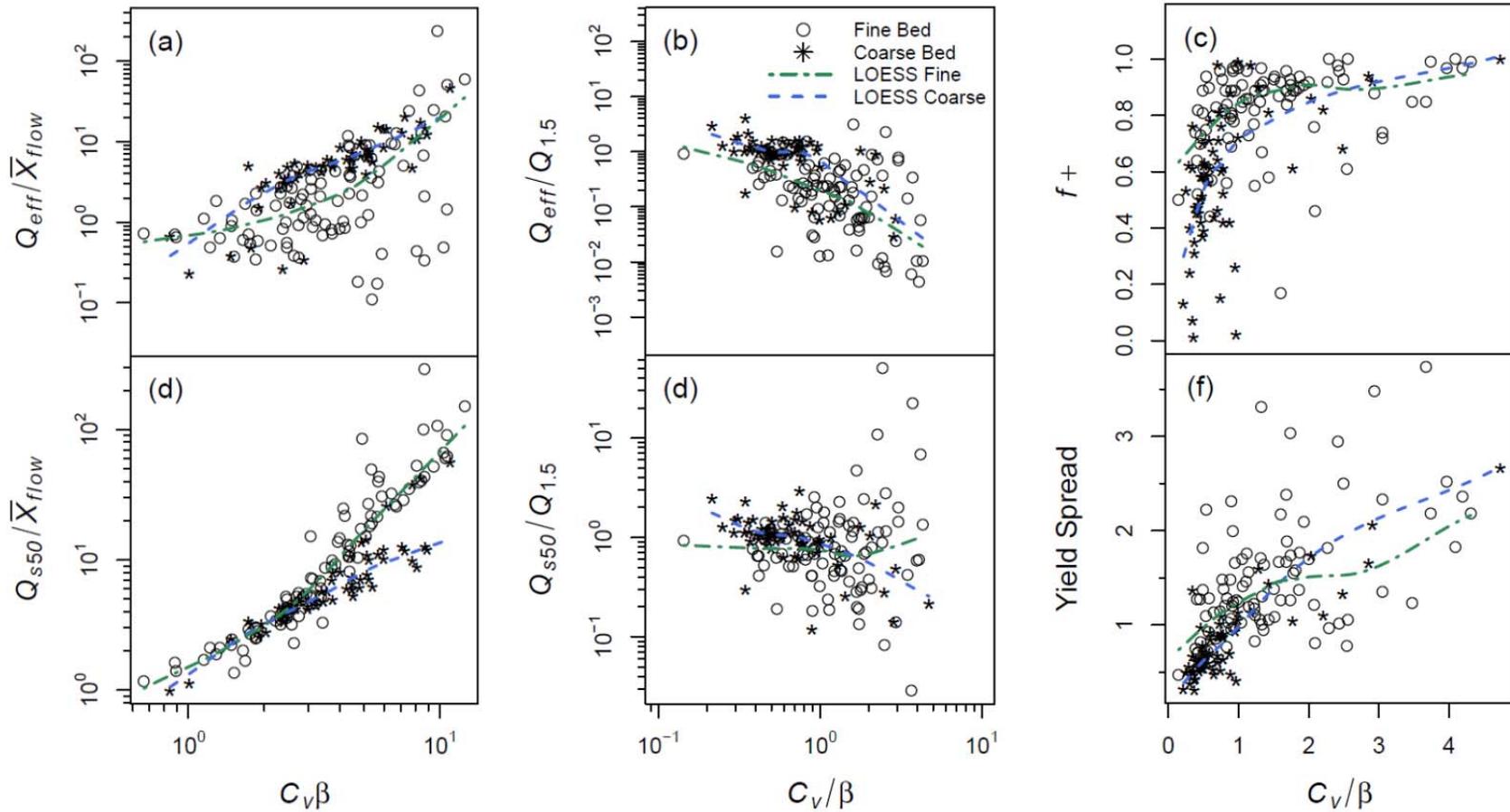
Figure 2-11. Logarithmic scatter plots of relationships between normalized Q_{eff} and Q_{s50} and the product (plots (a) and (d)) or ratio (plots (b) and (e)) of C_v and β. Plots (a) and (d) are normalized by mean annual flow and plots (b) and (e) are normalized by $Q_{1.5}$. Plots (c) and (f) show scatter plots of the ratio of f+ and yield.spread as a function of the ratio of C_v and β.

The ratio of C_v: β is perhaps a more intuitive compound driving variable than its product in that larger values indicate flow variability is high and β low, while smaller values indicate that flow variability is low and β high. Here, normalized Q_{eff} decreases, yield spread increases, and $f+$ increases with increasing C_v: β for both types of sites (Figures 2-11b, 2-11c, and 2-11f). When flow variability dominates the ratio, Q_{eff} becomes smaller and a wider range of flows are responsible for the middle 50% of cumulative sediment yield. When β dominates the ratio, Q_{eff} takes on a larger value and the range of flows responsible for the middle 50% of cumulative sediment transport shrinks.

We have presented some of the relationships found in our empirical analysis of the drivers of sediment yield and channel form in suspended-load and bedload-dominated rivers. With some exceptions, the observed relationships were similar in direction of response between both site types. However, the strength and slope of the response was greater for one site type over the other, depending on the metrics assessed. For example, the flow-sediment yield metric relationships observed for suspended-load sites were stronger than those of the bedload sites, and vice versa for the physical-sediment yield metrics. This means that flow variability likely exerts a stronger control on sediment transport in suspended-load dominated rivers, and physical boundary properties are more influential on bedload-dominated rivers. Flow variability increases the spread or range of flows about which the majority of sediment is transported for both site types. The grain size exerts significant influence on the sediment yield and frequency of most effective flows for bedload sites and less influence on suspended-load sites. Finally, the value of the sediment rating curve exponent (β) exerts strong control on the sediment yield. Greater values of β result in larger absolute and relative values of Q_{eff} and Q_{s50}, as well as the return intervals of these metrics. Greater β values also reduce the spread in sediment yield.
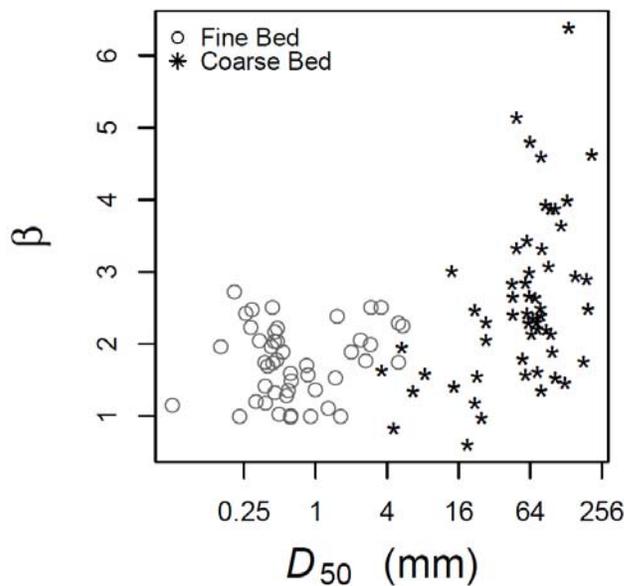
Figure 2-12. Relationship between grain size and sediment rating curve exponent, β for coarse-bed (black stars) and fine-bed (open circles) sites.

Sediment yield metric relationships with β are stronger for coarse-bed sites. This may in part be due to the fact that grain sizes in coarse-bed rivers and the shear stress necessary to mobilize the bed can vary by orders of magnitude (i.e., 4 to 256 mm), resulting in a wider range and greater values of β. Whereas in fine-bed rivers, sand-sized particles (0.063 to 2 mm) are often in motion over a wider range of flows (Figure 2-12). This is evident in the value of τ_c* for fine-bed sites, for which a majority are above the critical value range for incipient motion at Q_{bf} ($\tau_c* \in \{0.03, 0.07\}$, Figure 2-7f). An additional explanation

lies in transport capacity and supply limitation. Often, larger grain sizes in coarse-bed rivers are transport capacity limited as opposed to supply limited (Montgomery and Buffington 1997). In supply limited conditions, often found in lower gradient, fine-bed rivers, the grain size of the bed is less influential on the discharge-sediment load relationship as is indicated in Figure 2-12.

2.2.3   Discussion of Sediment Yield Metrics Relationships

Many of the relationships discussed above are qualitatively similar—or at least fall on the same spectrum of response—between the two types of sites due to the character of the empirical model used to represent the $Q – Q_s$ relationship for both coarse- and fine-bed sites. In some cases a well-defined relationship exists for one type of site and not another (e.g., *f+* versus C_v for fine-bed sites and *β* versus *Qs50.RI* and *yield.spread* for coarse-bed sites). In general, physical metrics tend to explain the variance in relationships with sediment yield metrics in coarse-bed sites, whereas flow variability tends to explain more variance in fine-bed sites.

Bed sediment grain size plays a dominant role in sediment yield in rivers, especially coarse-bed rivers. In fine-bed rivers, a larger range of discharges is responsible for sediment yield. This range of flow narrows as the grain size of the bed increases. In coarse-bed rivers, a narrower range of less frequent flows dominates sediment yield. The most effective discharge also increases in magnitude and decreases in frequency as grain size increases. We see this as a spectrum of responses based on flow hydrology and river-bed material. In flashier systems, $Q_{eff} < Q_{bf}$ if smaller more frequent flows are competent to transport sediment. However, if the bed is armored, then less frequent flows become more effective, and $Q_{eff} = Q_{bf}$, or $Q_{eff} > Q_{bf}$. In Figure 2-3, we show that in coarse-bed stream with low-flow variability, Q_{eff} might be some extremely rare and big flow because a large discharge is required to mobilize the bed and large discharges are relatively rare if the flow variability is low. Sediment yield and effectiveness in fine- and coarse-bed rivers respond differently to flow variability.

Some *differences* in sediment yield metric relationships between the two types of sites emerged from this study as well. When considering the theoretical relationship among Q_{eff}, C_v, and *β* in which a generic rating curve with no threshold is multiplied by the continuous lognormal PDF to represent the flow distribution (Section 2.2.1), both Q_{eff} and Q_{s50} generally monotonically increase with C_v and *β*, though the rate of increase in each is smaller at lower values of C_v and *β* (Figures 2-13a and 2-13b). For very small values of *β* (< 1.25, in this example), Q_{eff} actually decreases with C_v. When a sediment load-discharge relationship that includes an entrainment threshold is introduced, such as Parker (1979), Q_{eff} is no longer a monotonically-increasing function of C_v and, in this case, D_{50} (Figure 2-13c). Rather, Q_{eff} increases with C_v for larger sediment sizes, and decreases for smaller sizes. Though it is quantitatively different from the relationship among Q_{s50}, C_v, and *β*, Q_{s50} increases monotonically with C_v and D_{50} as well when an entrainment threshold is introduced.

Soar and Thorne (2001) found a similar relationship for fine-bed sites in their study of Midwestern and eastern U.S. sand-bed streams. In coarse-bed, semi-alluvial streams in the U.S. Rocky Mountains, Bunte et al. (2014) found that $Q_{eff} \gg Q_{bf}$, and in many cases, was equal to the maximum discharge value. Interpretation of their work also suggests that Q_{eff} should increase with flow variability in these coarse sites. This finding relates to the value of the sediment rating curve exponent: very large values of *β* lead to very infrequent flows being more effective, especially with increasing flow variability. Note that the sediment load measurement technique can influence this value as well, especially for bedload sites (Bunte and Abt 2009). As flow variability increases in coarse-bed streams, Q_{eff} takes on larger and larger values. The flow-sediment load relationships for coarse-bed streams observed in this study are generated from Helley-Smith bedload measurements and do not have such steep rating curves as those reported by Bunte et al. (2014), who use bedload traps and longer sampling times (Bunte et al. 2004). Nevertheless, we observe that Q_{eff} increases relative to Q_{bf}, and even exceeds Q_{bf}, in coarse-bed streams and this relationship is due to larger values of *β*.
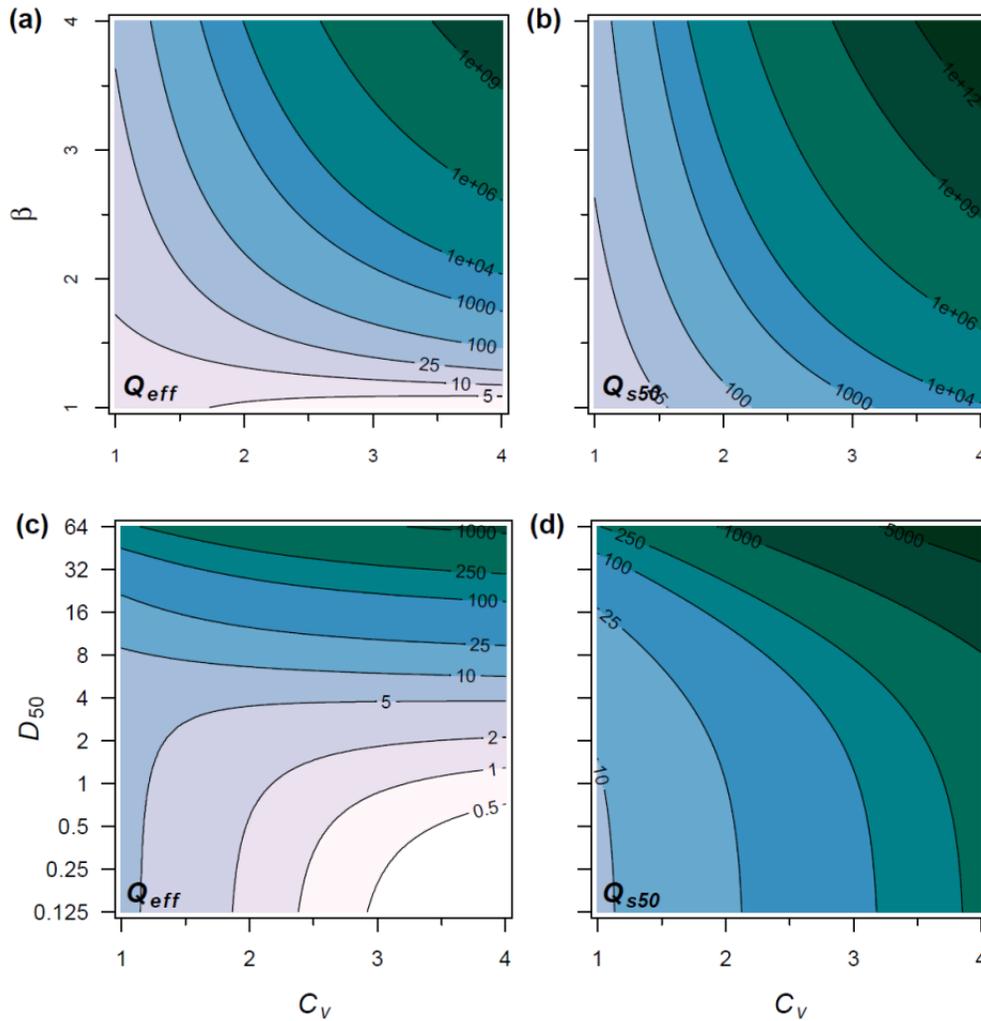
Figure 2-13. Contour plots of relationships between C_v, β, Q_{eff}, and Q_{S50} using a generic rating curve function to represent the sediment load-discharge relationship and a lognormal PDF to represent the flow distribution (plots (a) and (b)), and an entrainment threshold function (Parker 1979) to represent the sediment load-discharge relationship (plots (c) and (d)).

In summary, our findings indicate that the magnitude and frequency of sediment transport in all river types is sensitive to the variability of the flow regime, though fine-bed rivers are more sensitive. As flow variability increases, the range of discharges responsible for the bulk of sediment transport increases. Also, more sediment is transported by discharges greater than Q_{eff} as flow variability increases. This means that the bankfull discharge is likely to be greater than Q_{eff}, especially in fine-bed rivers.

These findings inform and relate the Stream Response Potential (SRP) conceptual model discussed in Chapter 5. Given the larger range of flows responsible for sediment yield, we find that fine-bed systems and flashy flow regimes tend to have a higher SRP and call for a greater depth of design analysis. Coarse-bed streams with low-flow variability tend to fall into low and medium stream response categories, and more simple design approaches may suffice in these systems.

2.3 Predicting Bankfull Discharge with Sediment Yield Metrics

Single design discharge approaches to channel design are based on the concept of the "dominant discharge." The dominant discharge is that which if held constant perpetually, would result in the same pattern, profile, and form of a river in dynamic equilibrium (Inglis 1947; Ackers and Charlton 1970). This concept may not apply in all rivers and its applicability is a function of flow regime and sediment supply quantity and quality. In some cases, Q_{bf} may have the properties of a dominant discharge in alluvial rivers in that sediment transport effectiveness may be at a maximum at bankfull (Wolman and Leopold 1957; Andrews 1980). Hence, Q_{bf} or some proxy, has been used as a design discharge for channel design (Hey and Thorne 1986; Shields et al. 2003; Doyle et al. 2007).

In many instances, especially in degraded streams adjusting to altered hydrology or sediment regimes, determining an appropriate value for bankfull discharge is not feasible. Therefore, proxies for Q_{bf} may be used. These include hydrologic predictors such as the 1.5- and 2-yr recurrence interval floods ($Q_{1.5}$ and Q_2, respectively), as well as MFA predictors (Q_{eff} and Q_{s50}). Excellent reviews of dominant discharge concepts and methods for estimating it for channel design are presented by Doyle et al. (2007) and Soar and Thorne (2011).

In this section, we compare the ability of hydrologic and MFA-derived proxies for dominant discharge to predict bankfull discharge in fine- and coarse-bed streams using a subset of the sites presented in previous sections for which field-based estimates of Q_{bf} were available. We present the log-log regression line between each flow metrics (MFA-based and hydrology-based) compared to the 1:1 line (Figure 2-14) and calculate various goodness-of-fit (GOF) and error estimates: root mean square deviation (RMSD), standard error of the estimate (SD), Thiel's (1958) measure of association (U) as well as metrics describing the fit of the log-log regression line (R^2, and slope and intercept values and p-values, Table 2-4).

The GOF analysis indicates that Q_{s50} is a good predictor of Q_{bf} for coarse- and fine-bed sites (Table 2-4). It predicts Q_{bf} about as well as Q_{eff} and $Q_{1.5}$ in coarse-bed sites. The effective discharge under-estimates Q_{bf} in fine-bed sites and the Q_2 tends to over-predict Q_{bf} for both types of sites. Log-log linear regression analysis indicates that all predictors in coarse-bed sites have imperfect fits with Q_{bf}. For example, the slopes of the log-log regression lines are all significantly different from unity (slightly less than unity). However, the slopes of the regression lines for Q_{s50} and $Q_{1.5}$ in fine-bed streams are not significantly different from unity, indicating a good 1:1 fit. Because no one predictor performs the best overall GOF metrics, we cannot conclude that one predictor is superior to the others. Nevertheless, this analysis indicates that Q_{s50} performs as well as and perhaps slightly better than Q_{eff}, an oft-cited predictor of dominant discharge, in coarse-bed sites and slightly better than $Q_{1.5}$ in fine-bed sites.

Figure 2-14. Comparison of Q_bf with Q_s25, Q_s50, Q_s75, Q_1.5, and Q_2.
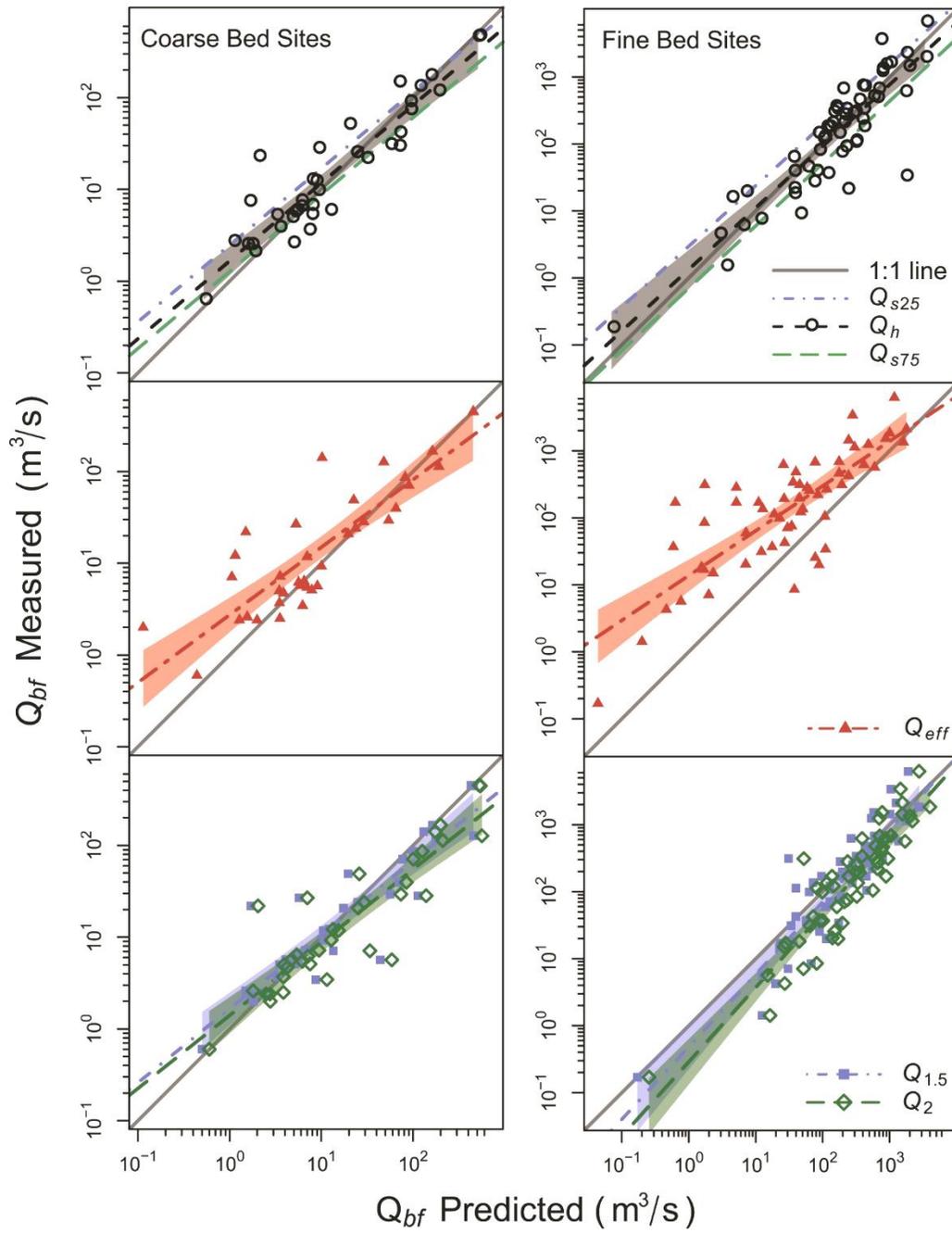
Figure 2-14. Comparison of Q_{bf} with Q_{s25}, Q_{s50}, Q_{s75}, $Q_{1.5}$, and Q_2.

Table 2-4. GOF metric for various Q_{bf} predictors.

	Q_{bf} Pred.	RMSD	U	SE	Lin. Slope	Lin. R^2	Log Slope[a]	Log Slope p	Log R^2	Intercept[b]	Intercept p[c]
Coarse-bed Sites	Q_{eff}	30	0.13	5	**0.94**	0.92	0.74	0.001	0.74	2.74	4.0E-05
	Q_{s50}	**25**	**0.10**	**4**	0.88	**0.96**	**0.85**	0.013	**0.86**	1.66	0.007
	$Q_{1.5}$	59	0.23	9	0.75	0.79	0.81	0.004	0.83	1.66	0.02
	Q_2	82	0.28	13	0.62	0.78	0.80	0.004	0.81	1.41	**0.14**
Fine-bed Sites	Q_{eff}	850	0.55	104	1.78	0.45	0.67	7.0E-06	0.64	13.72	2.7E-13
	Q_{s50}	**650**	**0.33**	**85**	1.07	**0.58**	**0.92**	**0.21**	0.79	1.34	**0.39**
	$Q_{1.5}$	730	0.40	95	1.25	0.49	**1.08**	**0.25**	0.81	0.48	**0.06**
	Q_2	**690**	**0.33**	90	**0.95**	0.52	1.11	**0.11**	**0.83**	0.29	2.3E-03

Notes: "Best" or values indicating good fit are denoted by bold font and shaded cells.

Statistic Definitions: p = probability; R^2 = coefficient of determination; RMSD = root mean square deviation; SE = standard error; and U = measure of association.

Variable Definitions: $Q_{1.5}$ and Q_2 = 1.5-yr and 2-yr return interval discharges, respectively [m³/s]; Q_{bf} = bankfull discharge [m³/s]; Q_{eff} = effective discharge [m³/s]; and Q_{s50} = discharge associated with 50% of cumulative sediment transport over the sorted flow record [m³/s].

[a]Log Slope p refers to the p-value associated with a t-test of the observed-predicted log-linear regression model diverging from unity with p-values ≤ 0.05 demonstrating that the slope of the regression line is significantly different from unity with a probability of 95%.

[b]Intercept values are back-transformed.

[c]Intercept p-values indicate whether the intercept is significantly different from zero.

Copeland et al. (2005) reported that the Q_{s75} best predicted Q_{bf}, but they used total suspended-load data, which included wash load and not simply suspended sand load (suspended bed material). This resulted in them predicting a larger sediment load for each discharge and likely upwardly biasing the cumulative sediment yield percentile most-closely associated with bankfull discharge. Fraction of cumulative sediment yield for Q_{eff} and Q_{bf} across all sites used in this part of the study are presented as box-and-whisker plots in Figure 2-15. Though there is considerable spread, the median value of cumulative sediment fraction at Q_{bf} is approximately 50% for fine- and coarse-bed sites.

The ability of the Q_{s50} to predict Q_{bf} for suspended-load sites is a novel finding and an argument for process-based methods for channel design for these sites. Calculating Q_{s50} either requires bed-material load data or, most likely, a calibrated sediment transport equation. We discuss the uncertainty associated with calculating Q_{s50} using sediment transport relations in Section 2.4.
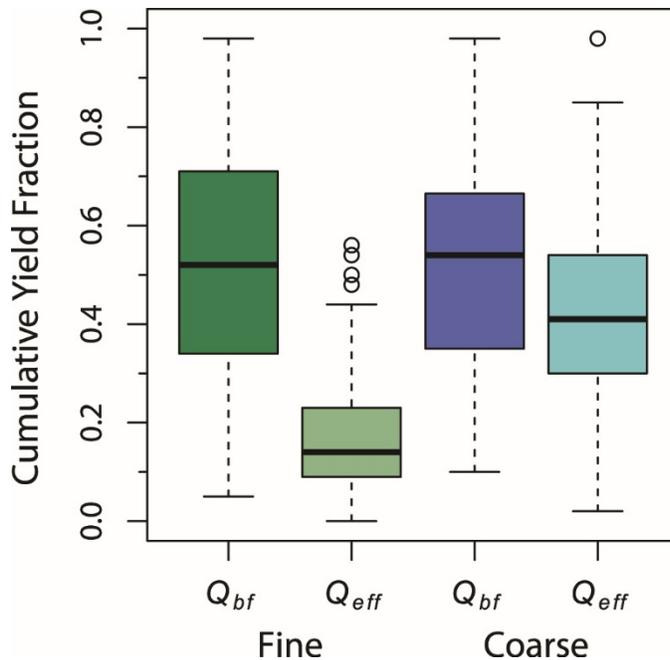
Figure 2-15. Cumulative sediment yield at bankfull and effective discharges for fine-bed and coarse-bed rivers.

2.4 Sediment Yield Metric Uncertainty

Up to this point we have explored the use and behavior of sediment yield metrics for channel design. Here, we explore and quantify the inherent uncertainty in estimating these metrics, what this uncertainty may be sensitive to, and present methods to quantify this uncertainty. We begin with a consideration of some of the dominant drivers of uncertainty in MFA and sediment yield metrics estimation (Section 2.4.1). This is followed by a comparison of estimates of sediment yield metrics made using measured sediment transport data versus those made with sediment transport equations (Section 2.4.2).

2.4.1 *Quantifying Uncertainty of Sediment Yield Metrics*

Quantifying uncertainty for sediment yield metrics based on MFA must incorporate uncertainty associated with the sediment load-discharge relationship as well as the flow record or other representation of the flow regime. A multitude of factors contribute to uncertainty in sediment yield estimation on rivers. These include measurement error, model specification and parameter error, hysteresis in the sediment load-discharge relationship, as well as the cumulative error associated with integrating sediment load predictions over an extended time series to name a few (Wilcock 2001; Bunte et al. 2004; Grams and Schmidt 2005; Schmelter et al. 2012; Grams et al. 2013). In the case of sediment yield metrics, we consider uncertainty from the perspectives of statistical uncertainty, environmental variability, as well as modelling error, and explore the sensitivity of sediment yield metric uncertainty these sources.

The largest source of uncertainty in sediment yield metric estimation comes from the sediment load-discharge relationship (Sholtes 2015). Here, we focus on quantifying the uncertainty in this relationship and propagating it through to the effective discharge and half-yield discharge calculations. The slope of the sediment rating curve in log-space (degree of nonlinearity) ultimately influences the value of Q_{eff} and Q_{s50} (Barry et al. 2008). To propagate the uncertainty of the log-log slope of the sediment rating curve, we take bootstrap samples (random data re-sampling with replacement) of the sediment load-discharge data pairs and fit new regression lines to these (Figure 2-16a). A bootstrapped sediment yield curve and Q_{eff}

estimate (Figure 2-16b), and cumulative sediment curve and Q_{s50} estimate (Figure 2-16c) are then created. The 2.5[th] and 97.5[th] percentiles of the bootstrapped sediment yield metric samples ($n = 1,000$ bootstrap samples) are then used to estimate a confidence interval for Q_{eff} and Q_{s50}.

To understand what factors result in greater uncertainty in sediment yield metric estimates (wider confidence intervals) we calculate the normalized width of these intervals (e.g., $Qs50.Spread = (Q_{s50,upp} - Q_{s50,low})/Q_{s50}$), and explore what aspects of flow regime and sediment load data influence the value of this normalized uncertainty width (Figure 2-17).
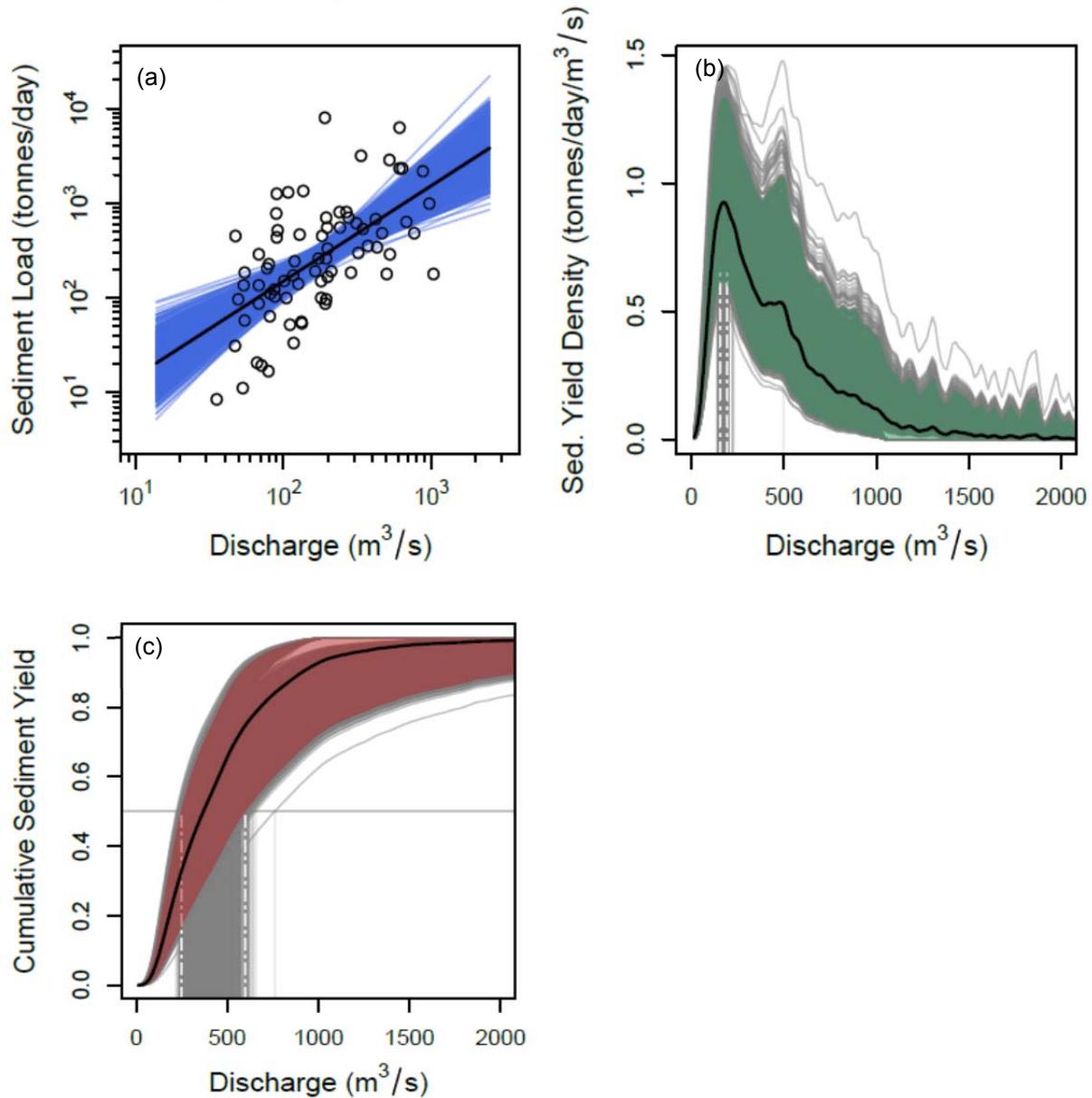
Figure 2-16. Uncertainty propagated (a) using bootstrapped samples of the sediment rating curves (b) to generate bootstrap samples of the sediment yield curve and Q_{eff}, and (c) cumulative sediment yield curve and Q_{s50} using sediment load and flow record data from the Dee Pee River at Pee Dee, South Carolina. Upper and lower 95% confidence intervals for Q_{eff} and Q_{s50} are displayed based on the bootstrap sample of these values (vertical white dashed lines). Pointwise confidence bands for the curves themselves ((b) shaded green and (c) red areas) are also plotted.
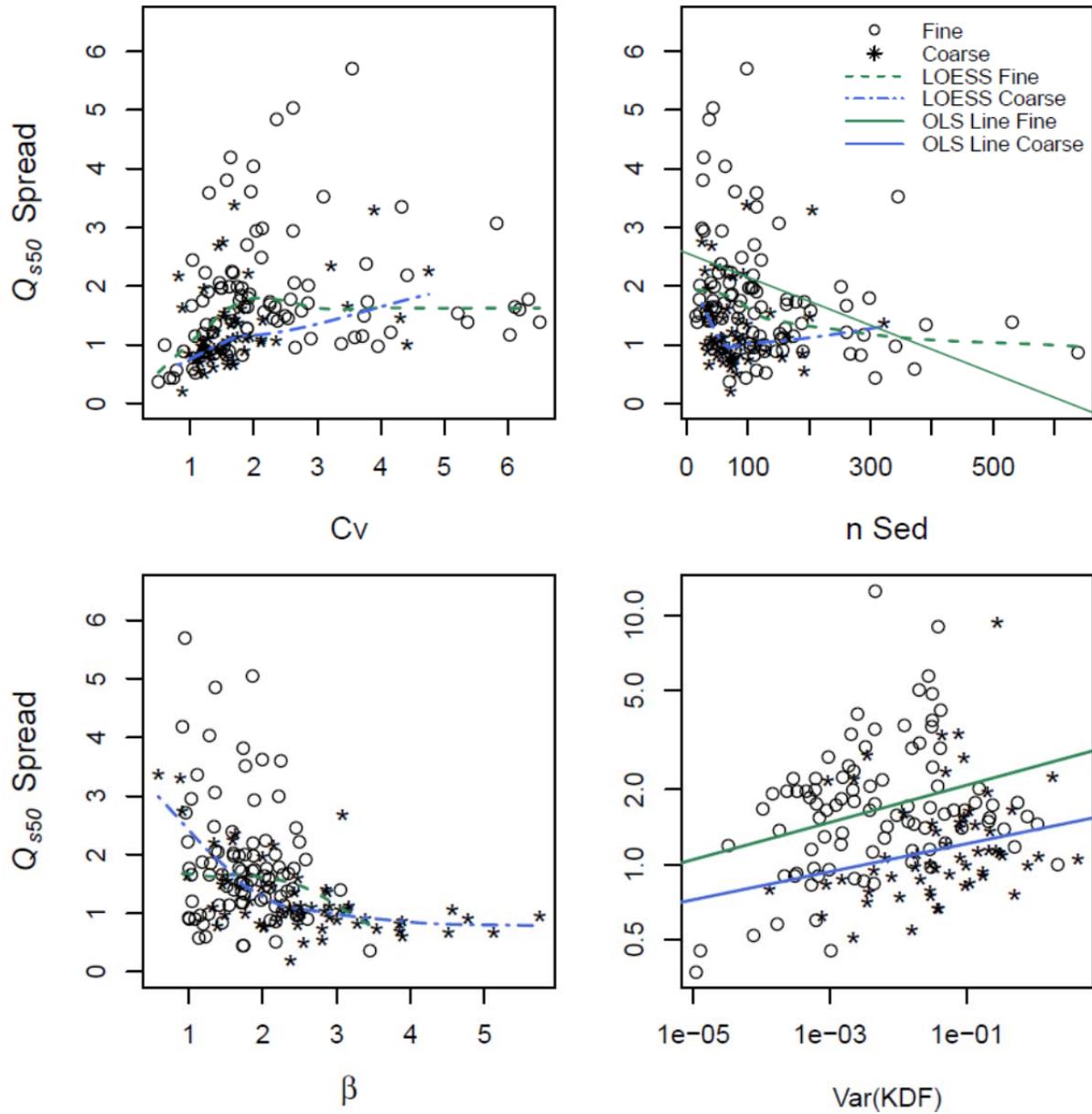
Figure 2-17. Relationships between the uncertainty spread in (a) Q_{s50} and the flow coefficient of variation (C_v), (b) the number of sediment load measurements (n_{sed}), (c) the value of the sediment rating curve exponent (β), and (d) the maximum value of the variance of the kernel density function of flows (Var(KDF)). Local regression scatterplot smoothing (LOESS) lines as well as log-linear ordinary least squares (OLS) lines are included to show trends where appropriate.

Results of the uncertainty sensitivity analysis (Figure 2-17) indicate the normalized width of the confidence interval of Q_{s50} (Qs50.Spread) tends to increase with flow variability (C_v, Figure 2-17a), decrease with sediment transport measurement sample size (Figure 2-17b), decrease with bed coarseness (and/or sediment rating curve β value), and increase with the variance of the kernel density function estimator (Var(KDF)) used to quantify the uncertainty of the flow regime (Figure 2-17d). The Var(KDF) term is a function of the width of the kernel, which in turn is inversely related to the sample size, which is very large for most streamflow records.

2.4.2   Modeled versus Measured Sediment Yield Calculation

Here we compare estimates of Q_{eff} and Q_{s50} generated from empirical, statistical models of log-transformed sediment load and instantaneous discharge data (empirical models) with those generated from calibrated, physically-based, sediment transport capacity models (physical models). Note that we use the phrase "physical models" here to refer to physically-based equations and not in the literal sense of a physical model. In general, sediment load data are not available for a particular stream or river of interest as they are time consuming and expensive to collect. Therefore, we evaluate how robust estimates of sediment yield metrics are to the additional uncertainty associated with the lack of such data and the need to model sediment transport. In a comprehensive study of effective discharge calculation using bedload sediment transport relations, Barry et al. (2008) found that the choice of equation largely did not influence the value of Q_{eff} for a particular site. This is because the steepness of the sediment transport-discharge relationship in log-space is what influences the position of the peak of the sediment yield curve. The absolute value of sediment yield (area under the sediment yield curve) is not important in this particular calculation, hence the absolute accuracy of estimating sediment yield does not come into play. Like Q_{eff}, the Q_{s50} yield metric is also only sensitive to the rate of increase in sediment transport with discharge (e.g., the value of β). This is because the cumulative sediment yield curve is normalized by the total yield value removing the influence of uncertainty in the absolute value of yield and hence the values of the coefficient, α.

We compare estimates of Q_{eff} and Q_{s50} using various physically-based models with those calculated from the empirical models (log-log regression of discharge-sediment load data) based on previously collected sediment load data as discussed above in Section 2.2. We conduct this analysis on two coarse-bed and two fine-bed sites to explore the strengths and weaknesses of various sediment transport models as well as representations of the modeled stage-discharge relationship (Table 2-5). In an effort to include a variety of flow regimes and channel geometries, we selected sites with relatively small and large drainage areas in each bed-material category.

Table 2-5. Modeled versus measured sediment yield site characteristics.

Site Number	Site Name	Type	Q-D Relation	DA [km^2]	Slope [m/m]	F_s [%]	D_{16} [mm]	D_{50} [mm]	D_{84} [mm]
1333850F	Trapper Ck, Idaho	Coarse	XS, HG	21	0.0414	5.2		79	210
13310700	South Fork Salmon River, Idaho	Coarse	XS, HG	855	0.0025	46		14	75
09260050	Yampa R. at Deerlodge, Colorado	Fine	XS, HG	20,541	0.0030	100	0.27	0.41	0.68
05568800	Indian Ck near Wyoming, Illinois	Fine	HG	162	0.0010	84	0.27	1.00	5.60

Variable Definitions: D_{16} and D_{84} = 16th and 84th percentile diameter of the bed sediment [m], respectively; D_{50} = median grain size [m]; DA = drainage area [m^2]; and F_s = approximate fraction of sand in bed sediments.
Abbreviations: HG = at-a-station hydraulic geometry relation based on field measurements of channel and flow geometry at a range of discharges; and XS = cross-section derived depth-discharge relationship (Q-D) using Manning's equation.

2.4.2.1   Sediment Transport Modeling Approach

For this comparison on coarse-bed sites, we use three physical models and three representations of the stage-discharge relationship to model sediment transport. The two coarse-bed sites studied are: Trapper Creek, Idaho (TC) and the South Fork of the Salmon River, Idaho (SR) (site numbers: 1333850F and 13310700, respectively). We use the following bedload models: Parker (1979), a single grain size, surface-based model; Wilcock and Kenworthy (2002), a two-fraction surface- or sub-surface based model; and Barry et al. (2004), a semi-empirical power-law model that is a direct function of discharge

rather than bed shear stress (referred to as Parker, Wilcock-Kenworthy (or WK), and Barry hereafter, respectively).

Using the Parker model, we also explore different representations of the stage-discharge relationship, an important aspect and additional source of uncertainty in sediment transport modeling. Using Manning's flow resistance equation, cross-section geometry, and channel slope, we calculate cross-section averaged depth, bed shear stress, width, velocity, and discharge as a function of water surface elevation (averaged depths). However, sediment transport can be highly spatially variable across a cross section. Because of the highly nonlinear relationship between sediment transport and discharge, using cross-section averaged values of hydraulic parameters to estimate sediment transport may introduce additional error. To evaluate this matter, we also calculated hydraulic variables for discrete vertical sections over the entire cross section. Sediment transport for the entire cross section at a given stage and discharge is then calculated as the sum sediment transport of sediment transported across all cross-section intervals. Finally, because a considerable number of stage, width, and flow area measurements were available for these two sites (Boise Adjudication Team (BAT; USFS 2014a) described by King et al. (2004)) and are generally available at all USGS gages, we also used at-a-station hydraulic geometry relations derived from these data to calculate cross-section averaged shear stress and width as a function of discharge (hydraulic geometry depths). All stage-discharge relationships (with the exception of the at-a-station hydraulic geometry relation) rely on an assumption of uniform, steady flow. This representation may be overly simplistic for many natural rivers requiring the use of a gradually-varied flow hydraulic model at a minimum.

The fine-bed sites included in this portion of the study are the Yampa River at Deerlodge, Colorado (YR) and Indian Creek near Wyoming, Illinois (IC) (USGS gage numbers: 09260050 and 05568800, respectively). Considerably less channel geometry data are available for the fine-bed sites introduced in Section 2.2. For these two sites, we relied on either a cross-section geometry derived from Light Detection and Ranging (LiDAR) and bathymetric surveys (YR), or hydraulic geometry data collected by the USGS at or near the stream gage as part of their regular field discharge measurements (YR and IC). We used the latter channel geometry data to create at-a-station hydraulic geometry relations for width, cross-sectional area, and average flow depth as a function of discharge. Channel slope was estimated from bed profile LiDAR data (YR) and from the topographic slope along the channel length as measured with a USGS topographic map in Google Earth (IC). We compare empirical models of sediment transport for these two sites with the following total load physical models: Yang's (1979) d_{50} sand model and Brownlie's (1981) total load and depth predictor model, both of which model suspended bed-material load (sand) (referred to as Yang and Brownlie hereafter, respectively). These models are driven by depth-, area- and velocity-discharge relationships derived from cross-sectional geometry and the Manning's flow resistance equation (YR) as well as at-a-station hydraulic geometry relations generated from USGS field measurements (YR and IC).

2.4.2.2 Modeled versus Measured Sediment Yield in Coarse-bed Sites

Though sediment yield metrics are insensitive to absolute values of predicted sediment yield, quite a range of values result when comparing empirical and physical models to calculate Q_{eff} and Q_{s50} (Figure 2-18, Table 2-6). The peak of the various sediment yield curves tend to match well for Trapper Creek (TC) and South Fork Salmon River (SR); however, in some cases an additional peak at smaller discharges associated with sand transport dominates over the central peak associated with gravel transport. In some models, including the empirical model for TC, this results in a very low predicted value of Q_{eff}. This "sand peak" becomes the most effective for sediment transport-discharge ($Q_s - Q$) relationships that have a milder slope in logarithmic space. The Parker equation becomes very steep in log space as the value of the dimensionless shear stress (τ^*) approaches the critical dimensionless shear stress τ_c^*, at smaller discharge values. This means that it under-estimates sand-bed load transport for TC. Indeed, it was derived for coarse gravel (> 16 mm) bedload transport (Parker 1979), suggesting it is not appropriate for

TC, which is a steep, armored channel whose bedload is dominated by sand- and fine-gravel transport over cobbles (Whiting et al. 1999; King et al. 2004).

The Barry model emulates a power-law equation whose coefficient is a function drainage area and whose exponent is a function of the ratio of critical shear stress for the surface and subsurface median sediment size: essentially a bed armoring ratio (Barry et al. 2004). This model was calibrated using sediment load data that included these two coarse-bed sites. The $Q_s - Q$ relationship it predicts matches that of the empirical model fairly well and tends to produce sediment yield metric estimates closest to those estimated from the empirical model.

To accommodate the transport of sand at smaller discharges evident in the TC sediment load data, we also implemented the Wilcock-Kenworthy (2002) two-fraction bedload model, which accounts for the sand-gravel interaction. The Wilcock-Kenworthy model over-estimates sediment load at both sites. However, it does capture the general slope of the $Q_s - Q$ relationship resulting in the same peak location in the sediment yield curve as predicted with the empirical model for TC (Figure 2-18a, middle graph).

The slope of the $Q_s - Q$ relationship from the sediment load data for SR is steeper than that of TC, indicating more gravel transport. This results in a peak in the empirical sediment yield curves which occurs in the middle of the range of flows. The $Q_s - Q$ relationship predicted by the Wilcock-Kenworthy model for SR is too mild relative to the empirical relationship resulting in a sediment yield curve peak that occurs at a much smaller discharge value relative to the position of the peaks predicted by the empirical and other physical models (Figure 2-18b). Again, the Barry model best predicts the location of Q_{eff}.

All physical models perform relatively poorly in predicting Q_{s50} in the two coarse-bed streams (Figure 2-18, right column). Differences in the slope of the $Q_s - Q$ relationship between the empirical and physical models result in cumulative error in predicting relative sediment yield as a function of the sorted flow regime. For TC, the Parker and Barry curves under-predict the rate of cumulative sediment transport for low flows resulting in large predicted values of Q_{s50}. The Wilcock-Kenworthy curve over-predicts cumulative transport of sand at low flows resulting in an underestimation of Q_{s50}. For SR, all physical models have milder $Q_s - Q$ slopes resulting in them over-predicting the rate of cumulative sediment transport at low discharges and underestimating Q_{s50}.

Some influence of the different methods for representing the 1-D stage-discharge relationship used to drive the physical models can be seen in the $Q_s - Q$ relationship for both sites; however, this influence does not translate to influencing estimates of Q_{eff}. The cross-section averaged and discrete width relationships also do not produce meaningful differences in the estimate of Q_{s50} with the Parker model. The at-a-station hydraulic geometry relation performs better than both cross-section methods in the case of TC and poorer in the case of SR. This could be due to how poorly single, 1-D estimates of channel geometry reflect the 3-D hydraulics at these sites.
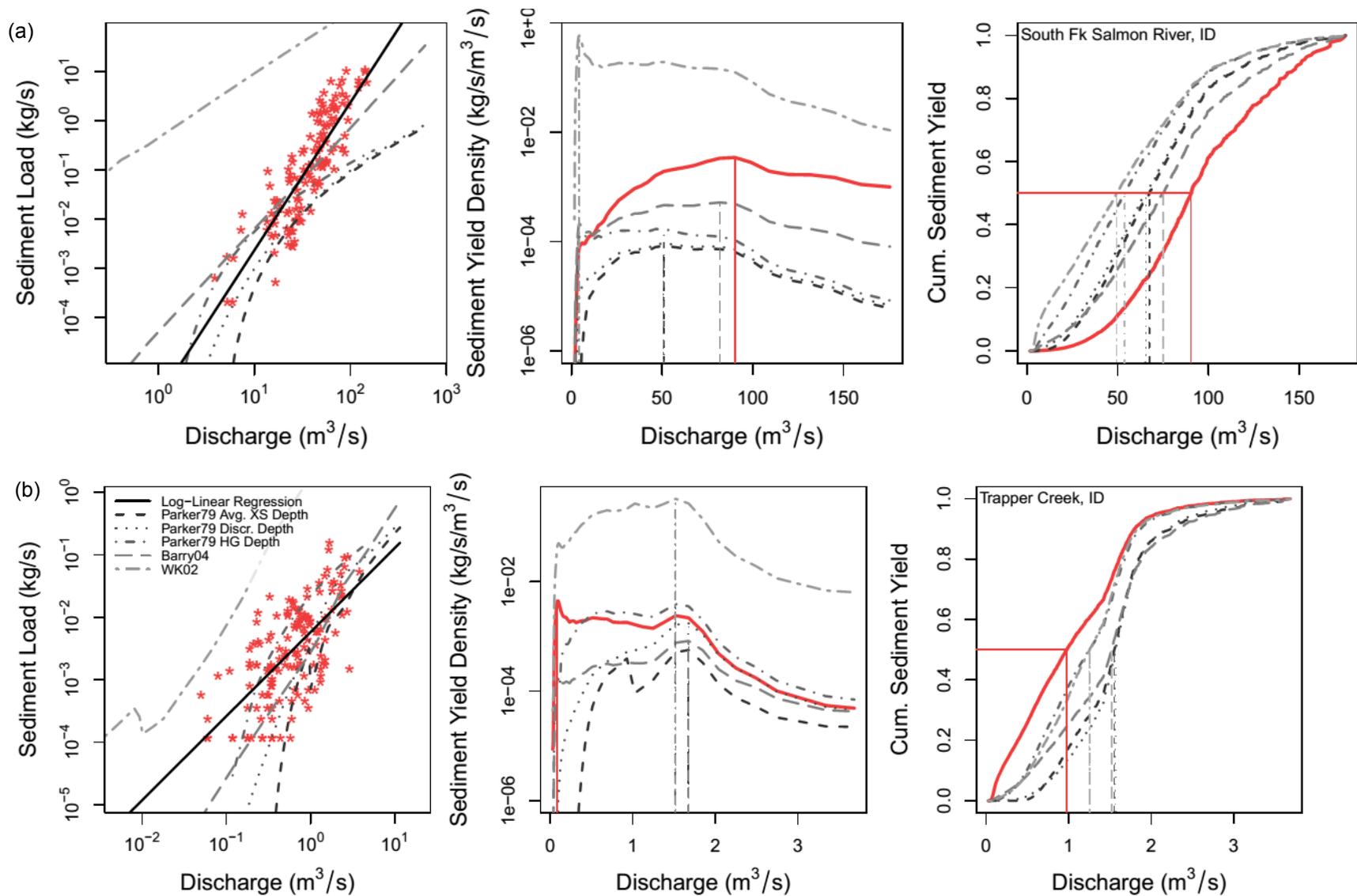
Figure 2-18. Comparison of sediment yield estimates and metric values calculated from empirical relations (log-linear regression), as well as calibrated sediment transport relations for bedload transport using various representations of the stage-discharge relationship for (a) Trapper Creek (TC) and (b) the South Fork of the Salmon River (SR).

Table 2-6. Sediment yield metric values calculated from various transport equations.

Site	Metric	RLM	Parker Average	Parker Disc.	Parker HG	Barry	Wilcock-Kenworthy	Brownlie	Brownlie HG	Yang	Yang HG
Trapper Creek	Q_{s50}	0.97	1.63	1.56	1.47	1.44	0.54				
	Q_{eff}	0.09	1.68	1.68	1.52	1.52	0.09				
	$\tau_c{}^*$		0.030	0.030	0.042	0.030					
South Fork of the Salmon River	Q_{s50}	90.3	67.4	65.4	53.8	75.0	49.3				
	Q_{eff}	90.1	50.8	50.8	50.8	81.9	4.3				
	$\tau_c{}^*$		0.030	0.030	0.030	0.030					
Yampa River	Q_{s50}	291						274	261	254	245
	Q_{eff}	278						228	11.6	11.6	11.6
Indian Creek	Q_{s50}	6.8							11.3		8.9
	Q_{eff}	1.55							1.98		1.98

Variable Definitions: Q_{eff} = effective discharge [m³/s]; Q_{s50} = discharge associated with 50% of cumulative sediment transport over the sorted flow record [m³/s]; and $\tau_c{}^*$ = critical dimensionless shear stress.
Abbreviations: RLM = robust linear model; and HG = at-a-station hydraulic geometry relation.

2.4.2.3 Measured versus Modeled Load in Fine-bed Sites

Total sediment load physical models for fine-bed streams estimate sediment yield metrics better than bedload physical models do in coarse-bed sites (Figure 2-19, Table 2-6). For our fine-bed sites (Yampa River and Indian Creek), we used the Brownlie and Yang total load models, as well as at-a-station hydraulic geometry and a cross-section averaged flow-resistance (Manning's) model for the relationship between flow, depth, area, and velocity.

Though these physical models tend to over-estimate absolute sediment load at YR, the slopes of both the Brownlie and Yang predicted $Q_s – Q$ relationships match those of the empirical models well at both sites. This results in the sediment yield curve peaks produced from the physical models lining up well with those from the empirical model for both sites. However, at YR a peak for very fine material results in very low values of Q_{eff} for all but the Brownlie-Manning and empirical models. Judging from the shape of the sediment yield curves for YR as well as the location of Q_{eff} from the empirical model, this small value of Q_{eff} is likely not the most effective discharge. Rather, the central peaks appear to be more effective and these line up well among all models. The sediment yield curves for IC are all unimodal and match well at relatively small discharge values.

All models and depth-discharge representations predict values of Q_{s50} relatively close to the empirical value for both sites. Because the physical models over-predict sediment load compared to the empirical model for YR, especially for smaller flows, they also over-predict the rate of cumulative sediment transport for small flows resulting in slight under-predictions Q_{s50}. The physical models for IC fit the data better, though slightly under-predict Q_s for lower discharges resulting in slightly greater predicted values of Q_{s50}. The hydraulic geometry relations result in $Q_s – Q$ relationships that are slightly closer to the empirical relationship for YR. A cross-section survey was not available for IC, therefore, only hydraulic geometry relations are used to drive the physical models.
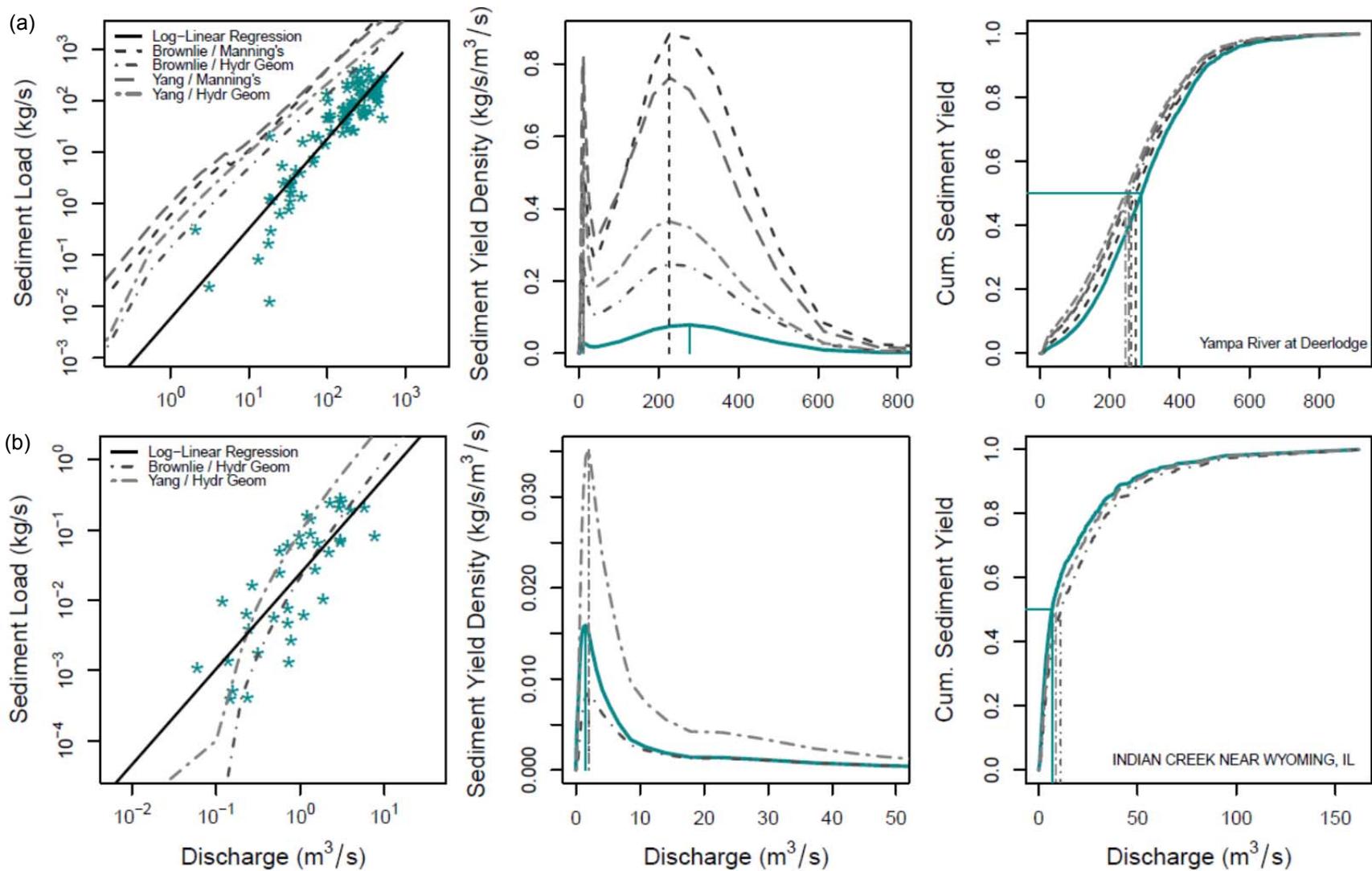
Figure 2-19. Comparison of sediment yield estimates and metric values calculated from empirical relations (log-linear regression), as well as calibrated sediment transport relations for total bed-material load (sand) transport using various representations of the stage-discharge relationship for the (a) Yampa River (YR) and (b) Indian Creek (IC).

41

On whole, using physical bedload and total load models to calculate sediment yield metrics produce similar results to empirical models for Q_{eff} for both coarse- and fine-bed sites, respectively. This finding parallels that of Barry et al. (2008), who studied this in coarse-bed streams. However, in cases of multimodal sediment yield curves, one must use their judgment in choosing a particular peak to represent Q_{eff}. This is especially true in modeled bedload scenarios where peaks for sand and fine gravel as well as coarse gravel may exist depending on the flow regime. The value of Q_{s50} is much more sensitive to model error for both types of sites due to cumulative error. Given the wide range of results produced from bedload equations, estimates of Q_{s50} in coarse-bed streams are likely to have large error in general. Because this portion of the study was not comprehensive and only includes two of each type of sites and physical models, we cannot make quantitative estimates of error or uncertainty associated with modeling bed-material load in calculating these sediment yield metrics. We recommend calculating Q_{s50} using multiple models and using the median or average value from these results in coarse-bed sites. These results indicate that estimating Q_{s50} in fine-bed streams using physical models produces much more accurate results. This is a welcomed finding because Q_{s50} performs most well in predicting bankfull discharge (Section 2.3).

2.5 Summary and Conclusions

In this chapter, we have explored the relationships between the drivers of sediment yield in rivers, namely the flow regime and physical properties of the sediment and channels, and the magnitude and frequency of sediment transport described by various metrics based on the sediment yield curve. We used theoretical approaches to explore these relationships in which a log-normal distribution function is assumed to represent the daily flow regime and various representations are used to represent the discharge sediment transport relationship. We also considered relationships based on flow, physical, and sediment yield metrics calculated from fine- and coarse-bed rivers across the continental U.S. and Puerto Rico.

Our findings indicate that the magnitude and frequency of sediment transport in all river types is sensitive to the variability of the flow regime, though fine-bed rivers are more sensitive. As flow variability increases, the range of discharges responsible for the bulk of sediment transport increases. Also, more sediment is transported by discharges greater than Q_{eff} as flow variability increases. This means that the bankfull discharge is likely to be greater than Q_{eff}, especially in fine-bed rivers.

Bed sediment grain size plays a dominant role in sediment yield in rivers, especially coarse-bed rivers. In fine-bed rivers, a larger range of discharges is responsible for sediment yield. This range of flow narrows as the grain size of the bed increases. In coarse-bed rivers, a narrower range of less frequent flows dominates sediment yield. The most effective discharge also increases in magnitude and decreases in frequency as grain size increases.

Sediment yield metrics inform the applicability of the dominant discharge concept (e.g., appropriateness of a single design discharge). A spectrum of responses of these metrics to flow hydrology and river-bed material exists. In flashier systems, $Q_{eff} < Q_{bf}$ if smaller more frequent flows are competent to transport sediment. However, if the bed is armored, then less frequent flows become more effective, and $Q_{eff} = Q_{bf}$ or $Q_{eff} > Q_{bf}$. In Figure 2-3, we show that in coarse-bed stream with low-flow variability, Q_{eff} might be some extremely rare and big flow because a large discharge is required to mobilize the bed and large discharges are relatively rare if the flow variability is low. Sediment yield and effectiveness in fine- and coarse-bed rivers respond differently to flow variability.

When considering what design discharge to use to approximate the channel-forming discharge, the $Q_{1.5}$ provides a reasonable estimate of the bankfull discharge in coarse-bed rivers and in some fine-bed rivers. In fine-bed rivers, this static flood event does not predict the bankfull discharge well in cases of greater flow variability. The discharge at which 50% of cumulative sediment yield occurs (Q_{s50}, half-yield discharge) predicts Q_{bf} the best under most flow regimes in single-thread, perennial fine-bed river as well as coarse-bed rivers. This indicates that process-based approaches to channel design that consider sediment transport are important for channel design in fine-bed rivers. However, identifying an

appropriate design discharge is one of many basic stream-restoration design criteria including longitudinal slope and bankfull dimensions.

These findings inform and relate the SRP conceptual model discussed in Chapter 4. Given the larger range of flows responsible for sediment yield as indicated by the *yield.spread* metric, we find that fine-bed systems and flashy flow regimes tend to have a higher SRP and call for a greater depth of design analysis. Coarse-bed streams with low-flow variability tend to fall into low and medium stream response categories, and more simple design approaches may suffice in these systems.

CHAPTER 3

Computational Tools for Hydrologic Analysis and Stable Channel Design

3.1 Introduction

To better facilitate application of novel hydrologic metrics and sediment transport analysis in design hydrology for stream crossings, we developed a number of new web- and spreadsheet-based tools in addition to drawing upon some existing tools. These tools also address the objective of accessible and user-friendly tools in response to guidance from state DOT agencies. This chapter describes the associated toolset which assists with: (1) desktop watershed assessment, (2) flow summary metrics, (3) computation of a FDC, both using gage-based computations and model estimation, (4) sediment yield computations, including both effective discharge and half-load discharge, and (5) Capacity-Supply Ratio (CSR), where the sediment continuity of an upstream channel is contrasted to the restoration reach.

3.2 Watershed Assessment

The rapid desktop assessment of the drivers, constraints, and data available in a watershed is vital to the comprehensive understanding of what types of questions should be asked in a stream-crossing design. A practical yet powerful tool for rapid watershed assessment is the Watershed Rapid Assessment Program (WRAP) available at https://erams.com/wrap/. Development of this tool was supported by several initiatives that were leveraged for this NCHRP project through extensive collaboration with the eRAMS development team to ensure its applicability to design hydrology analyses for stream crossings. This tool extracts a broad range of climate, hydrology, geology, land use, and water quality. Specific to the design of stream crossings, the following data could be obtained in this tool:

> See tutorial in Appendix B (Section B.3): *Rapid Watershed Assessment* for a walkthrough of this process.

- **Stream discharge**: availability of flow gage data is vital to understanding your computational options should a FDC be required for design (next section for more details).
- **Land use trends**: will help you start to get an idea of whether the use of historic discharge data is appropriate for a given location. Note that data are only available as far back as the National Land Cover Database (NLCD) in 1992.

3.3 Flow Summary Metrics

The Flow Analysis tool in Environmental Risk Assessment & Management (eRAMS) includes a fairly comprehensive list of metrics for summarizing gage data which can be downloaded as a comma separated value (CSV) file. The metric used directly in this analysis is the Richards-Baker Flashiness Index (R-B Index) (discussed in detail in Section 4.2.2). The R-B Index is used to quantify the frequency and rapidity of short-term changes in streamflow. Land use and water management changes may lead to increased or decreased flashiness. This flashiness index is typically based on mean daily flows and calculated by dividing the path length of flow oscillations for a time interval (i.e., the sum of the absolute values of day-to-day changes in mean daily flow) by total discharge during that time interval.

> See tutorial in Appendix B: *Flow Summary Metrics* for a walkthrough of accessing the flow summary metrics.

3.4 Flow Duration Curves

Flow frequency, as represented by a FDC is a graphical representation of the frequency, or the fraction of time that a discharge magnitude is equaled or exceeded. More specifically, FDCs and flow frequency curves both express the same information, the former as a CDF and the latter as a PDF. Representation of the entire runoff hydrograph time series (typically daily runoff, but can be hourly, or even 15-minute) in a single curve makes the FDC a compact signature of streamflow variability. It is a valuable tool to understand precipitation-runoff responses in gaged watersheds, and to regionalize them to ungaged watersheds. FDCs are an essential part of effective discharge and channel stability analysis. At ungaged sites, and gaged sites with inadequate data (short record length and poor representation of land use changes), it is necessary to compute an estimated FDC. FDCs can be estimated in ungaged basins using a variety of methods including regression methods (e.g., Hawley and Bledsoe (2011)), index methods (e.g., basin-area and regional scaling), continuous simulation modeling (e.g., HEC-HMS, HSPF, SWMM, and SWAT), geostatistics, and methods that use short runoff records (Castellarin et al. 2012). Continuous simulation may be especially advantageous for areas undergoing rapid land use changes and with flashy flow regimes that require a shorter time step for adequate characterization of sediment transport potential.

This project supported the development and/or refinement of three tools for estimating FDCs: (1) a single-gage FDC computation tool for all flow gage sites in the eRAMS database (includes all USGS NWIS and U.S. Environmental Protection Agency, STOrage and RETrieval (EPA STORET) sites, as well as some regional data (mainly for Colorado), (2) a regional FDC estimation tool which pulls data from multiple representative gage locations, and (3) a customized version of the SWAT model which has been tailored to focus on the computation of FDCs given land use changes in the basin.

3.4.1 Single-gage FDC Computation

The standard method for FDC computation from gage data involves downloading daily-average flow data (often from the USGS NWIS websites) and then programming the FDC computations based upon this gage data into standard spreadsheet software (i.e., Microsoft Excel®). Our eRAMS-based tool unites flow data and a FDC computational tool into one map-based and user-friendly process. Another advantage of this single-gage FDC tool is that users can rapidly examine seasonal trends or look at the changes in the FDC over multiple time periods. These trends can then be correlated with land use / land cover changes in the watershed for a more comprehensive understanding of the watershed hydrology.

> See tutorial in Appendix B (Section B.4): *Single-gage FDC Computation within eRAMS* for a walkthrough of this process.

3.4.2 Regional FDC Estimation Tool

As an example of a regional scaling (or index method), a regionally representative FDC may be developed by normalizing flows from similar gages with some reference discharge or watershed drainage area. In this approach, bankfull discharge is not recommended because it can be highly variable among streams and observers. Instead, a regional estimate of the Q_2 (median annual peak flow from USGS regional regressions available throughout the U.S.) or some other metric can be used to normalize discharges (Watson et al. 1997). A FDC for a comparable ungaged site may then be computed by substituting the flow used to normalize the FDC(s) from the gaged site(s). The USGS now has regional regression relationships for certain percentiles of FDCs in many states, but these do not provide a complete FDC for use in effective discharge analysis. Other metrics that can be used to scale and non-dimensionalize FDCs include, mean annual flow (available for the entire U.S. from Castellarin et al. (2012)), median streamflow from USGS flood regression equations where available, or watershed drainage area. The Q_2 is commonly used by the practitioner community when a confident estimate is available (could use USGS StreamStats (http://water.usgs.gov/osw/streamstats/) for an estimate of Q_2 at an ungaged location; however, these are regionalized estimated and the accuracy of the selected value will directly affect the accuracy of the regional FDC) for an ungaged location and drainage area when Q_2 is highly uncertain.

When evaluating an ungaged location, the regionalized FDC tool in eRAMS allows a user to estimate a FDC by selecting multiple representative gages in the region around the ungaged stream and collapse the curves down to a single regional FDC. The first step in this process is the computation of the FDCs for each selected gage, followed by normalization of each FDC using a normalizing metric

> See tutorial in Appendix B (Section B.5): *Regional FDC Estimation within eRAMS* for a walkthrough of this process.

(typically drainage area, mean annual flow, or 2-yr peak flow). Finally, the FDC is re-scaled to the ungaged location.

3.4.3 SWAT Model

The SWAT model (Arnold et al. 1998; Arnold and Fohrer 2005) has proven to be an effective tool for assessing watershed problems for a wide range of scales and environmental conditions across the globe. SWAT is a freely available basin-scale, continuous-time model that is designed to predict the impact of management on water and sediment yields in ungaged watersheds. The model is physically-based, computationally efficient, and capable of continuous simulation over long time periods. Both urban and agricultural water management practices can also be simulated in SWAT.

The process of configuring SWAT for a given watershed has also been greatly facilitated by the development of geographic information systems (GIS) based interfaces (such as eRAMS), which provide a straightforward means of translating digital land use, topographic, and soil data into model inputs. Dr. Jeffrey Arnold (U.S. Department of Agriculture, Agricultural Research Service (USDA-ARS)) and Dr. Peter Allen (Baylor University) have been collaborating for several years on applying SWAT to channel stability assessments. This channel stability assessment process (called SWAT-DEG (Soil and Water Assessment Tool – channel DEGgradation)) includes the computation of FDCs in ungaged watersheds with complex land use. Although the decision support tool discussed below (Chapter 5) will not exclusively prescribe a single modeling framework such as SWAT, the development of these interface tools helps facilitate the adoption of continuous hydrologic simulation in standard practice as one means of developing a FDC for magnitude-frequency and sediment continuity analysis at ungaged sites to augment gage extrapolation methods. The eRAMS web-based interface essentially works like the USGS StreamStats approach where users can click on a particular point of interest, delineate a watershed, and run the model based on a weighted average behavior of the hydrologic units intersected by the basin of interest.

This browser-based hydrologic modeling tool will allow users to create a hydrologic model and then adjust land use and climate variables to explore how changes in the FDC might result. Specifically, land use changes may be represented by changing the NRCS Curve Number and the time of concentration in the user interface.

3.4.3.1 SWAT Parameterization

At the time this project was proposed, the authors of SWAT were working to develop a national database which would allow users to perform a continuous simulation at any ungaged location in the U.S. based on SWAT models that are calibrated for larger hydrologic units. Unfortunately, the first round of national-scale parameterization returned less reliable data than they had anticipated. Hence, at the time of publication of this report, there is no way to automatically parameterize the SWAT model to local flow gage data. Thus uncalibrated FDC estimates (under current and future land use / climate scenarios) are best viewed relative to one another for the same watershed as opposed to stand alone output which could be readily compared to gage-based FDCs.

However, users do have the ability to manually perform their own calibration by following these steps:

- run the SWAT model for your watershed under existing land use and climate conditions;
- select local or representative flow gages;
- create FDCs from the selected gages; and
- iteratively adjust the key input parameters to the SWAT model (NRCS Curve Number and time of concentration) until the gage FDC and SWAT FDC closely match.

3.5 Sediment Yield: Computation of Both Effective and Half-load Discharge Metrics

The computation of effective and half-load discharge metrics are both derived from a sediment yield curve which is the product of the FDC (water discharge versus % of time) and a sediment transport rating curve (water discharge versus sediment transport) (Figure 2-1).

Each sediment transport equation currently available in the eRAMS Cross Section tool requires its own unique set of parameters (Table 3-1 and Appendix B).

Table 3-1. Input parameters required for sediment transport equations.

Parameter	Yang (1996)	Brownlie (1981)	Bagnold as modified by Martin and Church (2000)	Wilcock-Kenworthy (2002)	Power Function
Transported Sediment Diameter [mm]	√	√	√		
Gravel Sediment Diameter [mm]				√	
Sand Sediment Diameter [mm]				√	
Percent Sand [%]				√	
Bed Sediment d_{50} [mm]		√			
Bed Sediment d_{84} [mm]		√			
Bed Sediment d_{16} [mm]		√			
Manning's n	√	√	√	√	√
Bottom Width [m]			√	√	
Bed Slope [m/m]	√		√	√	
Energy Grade Line Slope [m/m]	√				
Friction Slope [m/m]		√			
Power-function Coefficient					√
Power-function Exponent					√
Power-function Units					√

3.6 Capacity Supply Ratio

This section covers the background and development methodologies of the CSR Tool. This tool was developed to aid in the application of the research concepts produced for this report in stable channel design. The CSR Tool ultimately outputs a 'family of channel slope and width combinations' which provide continuity of water and sediment across the full range of flows (as represented by a flow frequency curve or FDC) (see Figure 3-2). The following will give a background on the CSR concept in the context of channel design, the approach of the tool code structure, and verification of the tool's functionality. An overview of running the CSR Tool and associated examples with screenshots are presented in Appendix B.

3.6.1 Background

There is a diverse and eclectic array of methods used in the current practice of river-channel design; however, the most common methods usually involve a particular reliance on the use of analog reaches and designing the channel to a single 'dominant' discharge. This single discharge is often relied on as the discharge that will be most influential on channel form and assumed to be a good proxy of all flows that influence channel form in the flow regime. Choosing a single 'channel-forming' discharge is usually identified through bankfull field indicators, recurrence interval analysis of peak flows, regional flood regression relationships, or a combination of these methods. Many problems can arise if care and astuteness is not taken while choosing the proper discharge and recognizing the limitations of comparing to a reference system. These techniques have great uncertainty and often oversimplify the site-specific processes that govern channel stability. Furthermore, even if great effort is put into finding a single representative discharge, resulting designs may still lead to an unstable channel design because other influential flows were not accounted for in the analysis. An alternative approach to help alleviate some of these uncertainties is analytical channel design. This approach is often referred to as a process-based approach, because it relies on finding a site-specific equilibrium state of the processes governing the overall stability of the channel such as the sediment transport continuity. A well-known application of this method is the Copeland method in the stable channel design feature of HEC-RAS. This method can

perform a sediment balance analysis for channel design which can lower the uncertainty of relying on the aforementioned methods. However, this method still relies on calculating the sediment balance using a single representative discharge that does not account for the sediment transported by any other flows. The assumptions associated with using a single discharge in this methodology can lead to unstable channel designs, since systems often have other influential flows that effect sediment transport.

An alternative approach that aims at taking the Copeland method a step further to help alleviate this uncertainty, is the CSR method first introduced in Soar and Thorne (2001). This method quantifies the balance of total sediment entering the design reach (Supply) versus the total sediment that the design reach has potential to convey through (Capacity). This approach is analogous to the Copeland method; however, it balances the total sediment moved across the entire FDC rather than just a single representative discharge. This approach can produce stable channel designs with more efficacy than using a single discharge because it accounts for the influence of flows across the entire FDC helping alleviate the uncertainty of selecting and assuming the encompassing influence of a single discharge (Soar and Thorne 2011). ***Thus, there is a pressing need for a tool that can perform this analysis and give the user a means to produce the full spectrum of information that can be used to aid in the stable channel design process.***

The CSR Tool was developed to perform this analysis for a given reach of interest and to produce a range of possible stable channel design solutions with capacity / supply ratios equal to 1.

3.6.1.1 Copeland Method

The Copeland method was developed by Dr. Ronald Copeland at the USACE for use in the SAM software package (Copeland 1994). It is an analytical channel design approach that was developed solely to design sand-bed channels by estimating sediment continuity in a design reach using the total load sediment transport equation created by Brownlie (1981). For a given design discharge, the model solves for stable depth and slope for a range of bottom widths for trapezoidal cross sections.

The Copeland method requires an incoming sediment load which can be entered by the user, or the program can estimate the concentration using a user-defined trapezoidal cross section that represents an upstream supply reach that will produce the incoming sediment load.

The user must then define the desired characteristics of the design reach and enter a single design discharge that will be used in the analysis. This discharge will be assumed to represent the most channel-forming flow that can be seen in the flow record for the channel. The HEC-RAS reference manual suggests the use of a 2-yr frequency flood (perennial streams), 10-yr frequency flood (ephemeral streams), bankfull discharge, or effective discharge for the design discharge. The program can then solve for depth, slope, and width combinations that will successfully pass the incoming sediment load through the design channel based on its estimated sediment transport potential using Brownlie (1981). The results from the model produce a family of channel slope and width combinations which provide continuity of water and sediment (Figure 2-1).

3.6.1.2 CSR Method

The CSR concept was first introduced by Soar and Thorne (2001). They used this concept to analyze the faults in a design that led to a failed river-restoration project at White Marsh Run, Maryland. The CSR is a simple balance between the ability of a given river reach to transport sediment (Capacity), to the sediment that is being transported into the reach of interest (Supply). This is the same sediment balance concept as used in the Copeland method, however, the difference comes from which discharge(s) the sediment transport capacity is calculated with. More specifically, the CSR can be described as Equation (3-1):

$$\text{CSR} = \frac{\int_{\text{time}} \text{ transport capacity of Design Reach}}{\int_{\text{time}} \text{ transport capacity of Supply Reach}} \qquad \textbf{(3-1)}$$

Equation (3-1) describes the CSR as the time-integrated ratio of sediment transport capacity of a design reach to the incoming sediment supply. In other words, "*The CSR is defined as the bed-material load transported through the river reach by a sequence of flows over an extended time period divided by the bed-material load transported into the reach by the same sequence of flows over the same time period*" (Wohl et al. 2015). Ultimately, the CSR method balances the total average sediment yield over the entire flow record rather than just for a single representative discharge as in the Copeland method.

If the capacity of the reach to transport sediment exceeds the sediment entering the reach from upstream, then degradation or erosion can be expected in the reach with a CSR > 1. On the other hand, if the sediment entering the reach exceeds the capacity of the reach to transport it, then aggradation or sediment accumulation is expected with a CSR < 1. A CSR within 10% of unity will be the most likely to have sediment balance with minimal aggradation or degradation in the channel (Soar and Thorne 2001).

3.6.1.3 Effectiveness Analysis

In order to find the time-integrated sediment transport, a MFA needs to be performed to find the total 'effectiveness' for each reach. In the context of this tool, the sequence of flows over an extended time period is derived from a user-defined gage flow record, or a FDC from another source for the river reach of interest. These flows are used to calculate the probability that a given flow will occur on average in the associated reach in a given day. Then, the potential that the given flow has to move sediment is estimated with an appropriate sediment transport equation. The effectiveness or the sediment transported on average over a period of time is calculated by multiplying the probability of the given flow by the potential sediment that can be transported by that flow. The effectiveness for each flow in the record is summed to get the total effectiveness or time-integrated sediment transport capacity of the reach.

3.6.1.4 Using the CSR/Effectiveness in the Stable Channel Design Tool

The CSR Stable Channel Design Tool (CSR Tool) requires the input of hydrology information and the dimensions and hydraulic characteristics of a supply reach to perform the CSR analysis. The information is used to perform a MFA for the supply reach to estimate the total effectiveness or sediment supply entering the design reach of interest downstream. The hydrologic information for the supply reach is assumed to be the same for the design reach, and the sediment transported by the supply reach is assumed to be the value that is entering the design reach. The program also requires dimensions and hydraulic characteristics for a potential design reach except a width and slope. Then, the program loops through width and slope combinations that produce an effectiveness that balances with the calculated incoming sediment from the supply reach giving a CSR = 1. The black line in Figure 3-1 represents a family of channel slope and width combinations which provide continuity of water and sediment (i.e., CSR = 1). This curve is analogous to the output produced by the Copeland method of HEC-RAS. Any slope/width values above this line can expect degradation or erosion, while any below could expect aggradation or sediment accumulation.
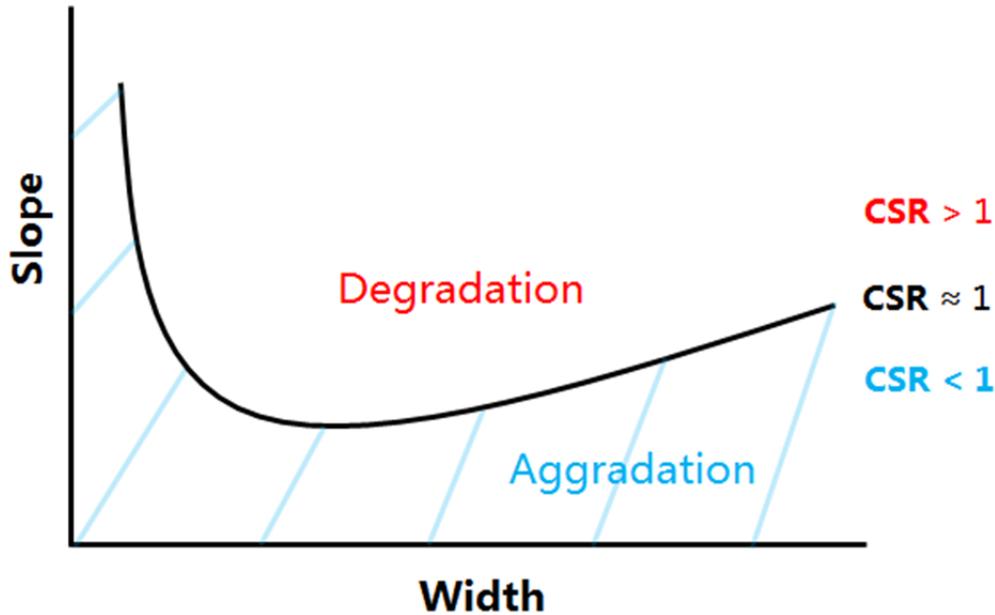
Figure 3-1. Family of width and slope combinations which provide continuity of water and sediment.

Figure 3-2 shows a visual representation of the methodology behind the tool using a CSR analysis. The figure shows a delineated upstream supply reach and downstream design reach. Each reach shows an idealized flow frequency / probability distribution (A), an idealized sediment discharge curve (B), and the resulting product of (A) and (B) which gives the effectiveness curve (C). The area under the effectiveness curve represents the total sediment moved by each reach and is used to find the sediment balance of the design reach using the CSR. The curves are colored-coded to correspond with the CSR equation shown at the top of Figure 3-2. The bottom of Figure 3-2 shows a simplified trapezoidal channel with the associated required inputs used for the supply and design reach of the tool. The channel bed Manning's *n* is not a required input because it is calculated through the sediment transport calculations, and all inputs are representative average values for the reach of interest.

$$\text{Capacity/Supply Ratio(CSR)} = \frac{\int_{time} \text{Sediment transport capacity of Design Reach}}{\int_{time} \text{Sediment transport capacity of Supply Reach}}$$
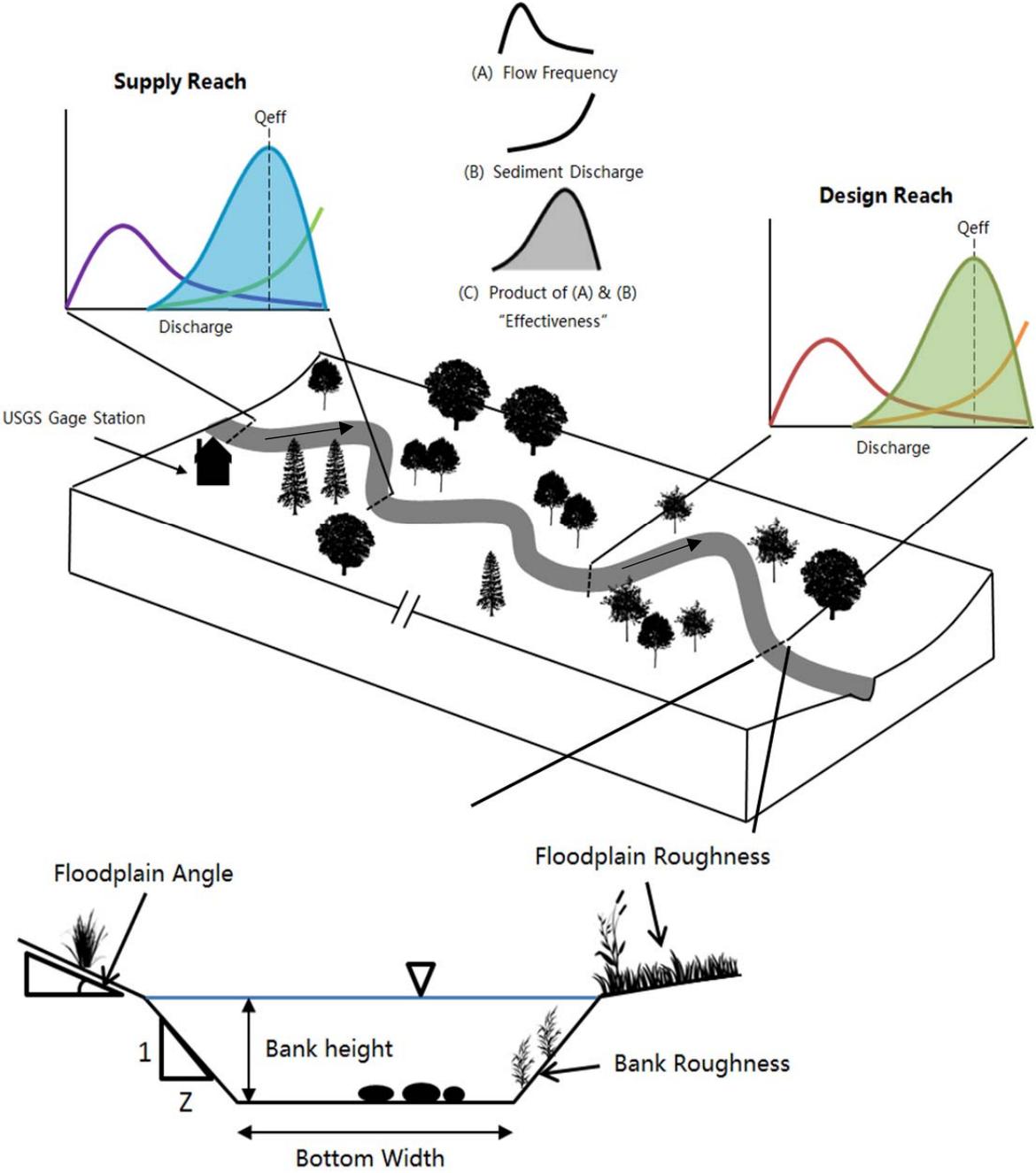
Figure 3-2. Visual representation of CSR analysis and simplified trapezoidal channel geometry assumed in tool.

3.6.2 CSR Tool Development

The basic methodology of the code behind the CSR Tool was closely modeled after the Copeland method in HEC-RAS (Copeland 1994). This is to provide a means of comparison between the two methods and a means to verify the accuracy of the tool output to a well-reviewed and respected method. Some of the main assumptions used in this approach to model flow are listed below:

- 1-D steady, uniform flow;
- a simplified trapezoid is used to represent the actual channel cross section;
- the channel is split into bank and bed components;
- sediment transport is only on the bed of the channel; and
- the bed and bank components have the same velocity which is the cross-section averaged velocity of the entire channel.

For a detailed review of all the equations used in the calculations of the CSR Tool and explanations of their application within the tool, refer to the CSR Tool Reference Manual (Appendix D of this NCHRP 24-40 final report). A list of some of the additions in the CSR Tool that are not present in the Copeland method of HEC-RAS follows:

- Sediment transport is calculated using the entire FDC associated with the design reach rather than just a single representative discharge and, therefore, accounts for the morphological influence of the other flows.
- Overbank flow is modeled and considered in transport calculations unlike the Copeland method. This can help avoid overestimating the effectiveness of overbank flows.
- The tool is capable of performing the CSR analysis for not only sand-bed streams but also gravel-/ cobble-bed streams using the Wilcock and Crowe (2003) equation (referred to as Wilcock-Crowe hereafter) and Parker (1990a) equation.
- Additional planform outputs and sediment percentiles are listed for each solution.

3.6.2.1 Hydrology Calculations

A more extensive hydrologic analysis is required by the CSR Tool in order to estimate the time-integrated sediment transport capacity of the reaches over the entire FDC rather than a single discharge. The CSR Tool can use a flow gage record, or a pre-derived FDC. These flow characteristics are assumed to be the same and representative of the flows seen by the supply and design reach.

If a gage record is chosen for the hydrology data, then the program will sort the discharges using an arithmetic binning procedure. This method splits the flows into a specified number of equal interval bins. A total number of bins must be defined by the user or the program defaults to 25 bins as recommended by Biedenharn et al. (2000). The process starts at 25 arithmetic discharge bins and reduces the amount of bins until there are no bins with zero frequency. In cases where there is still zero frequency at 10 bins then the process starts again at 25 bins and combines the discharges above the zero frequency bin into one. Each bin represents a range of discharges that the flows of the record could fall into. The probability of occurrence for the flows in each range are calculated and ultimately used to find the total effectiveness or sediment yield for the supply and design reaches.

The most common method to perform a MFA is using a flow record when possible; however, it is rare in practice to have a sufficiently long flow record for a stable reach upstream of the design reach. In these instances, the CSR Tool can take a user-defined FDC, such as the output from SWAT-DEG in eRAMS. An example of using SWAT-DEG is presented in Chapter 5 of this report. SWAT-DEG creates a very detailed FDC and outputs a table of exceedance probabilities versus discharges that can be directly pasted into the CSR Tool. This FDC is very detailed and often thousands of cells long so the user is required to define a lower number of bins to consolidate the FDC for use in sediment calculations. The

> More detail on the equations used for the hydrology calculations can be found in the CSR Tool Reference Manual (Appendix D of this NCHRP 24-40 final report).

default is set to 25 bins but the user can choose up to 50 bins. The user can then run the associated tab to consolidate the original FDC. The larger FDC is sampled logarithmically for the user-defined number of bins. This is converted to a CDF, then to a PDF by differentiating each point on the CDF with the central difference method. The PDF can then be used in the sediment transport calculations for the tool.

3.6.2.2 Sediment Transport Calculations

The CSR Tool can run the CSR analysis to find stable channel design solutions for both sand-bed and gravel- / cobble-bed streams.

The sand-bed portion of the tool uses the Brownlie (1981) total load sediment transport equation to estimate transport rate just like the Copeland method in HEC-RAS. Two bedload sediment transport equations, the Parker (1990a) and Wilcock-Crowe (2003) equations are available to estimate sediment transport rates in gravel- and cobble-bed streams. The Parker (1990a) bedload equation is appropriate for use with rivers of gravel size (> 2 mm diameter) and larger substrate. The Wilcock-Crowe (2003) bedload equation can be used for use with gravel- and cobble-bed streams that include a sand fraction (< 2 mm diameter).

> Refer to the CSR Tool Reference Manual (Appendix D of this NCHRP 24-40 final report) for further selection guidance on stream type.

The code methodology for the gravel- / cobble-bed portion was matched as closely as possible to the sand-bed structure. The biggest difference between the methodologies for the calculation of hydraulic parameters is with the hydraulic roughness. The sand-bed portion of the tool uses the Manning's equation and the built-in roughness predictor for bed forms in the Brownlie (1981) sand-bed sediment transport equation. It was chosen to use the Manning's equation and the Limerinos (1970) equation to calculate the roughness in the channel for the gravel-bed portion of the tool. The Limerinos (1970) equation was calibrated to account for mostly grain roughness of larger particles from gravels to boulders.

3.6.2.3 CSR Analysis Code Structure

The CSR Tool was programmed using the Microsoft Visual Basic for Applications (VBA) programming language. The main routine performed by the CSR Tool is running the design reach to perform the CSR analysis and search for stable channel designs. This part of the tool is run after the incoming sediment load is calculated for the supply reach using the given hydrologic information. The CSR Tool code structure went through many iterations to find the most reliable and efficient configuration. The average runtime for the tool is 2 to 8 seconds depending on the example and computer speed. The final code methodology for calculating stable channel design solutions is outlined in Figure 3-3.
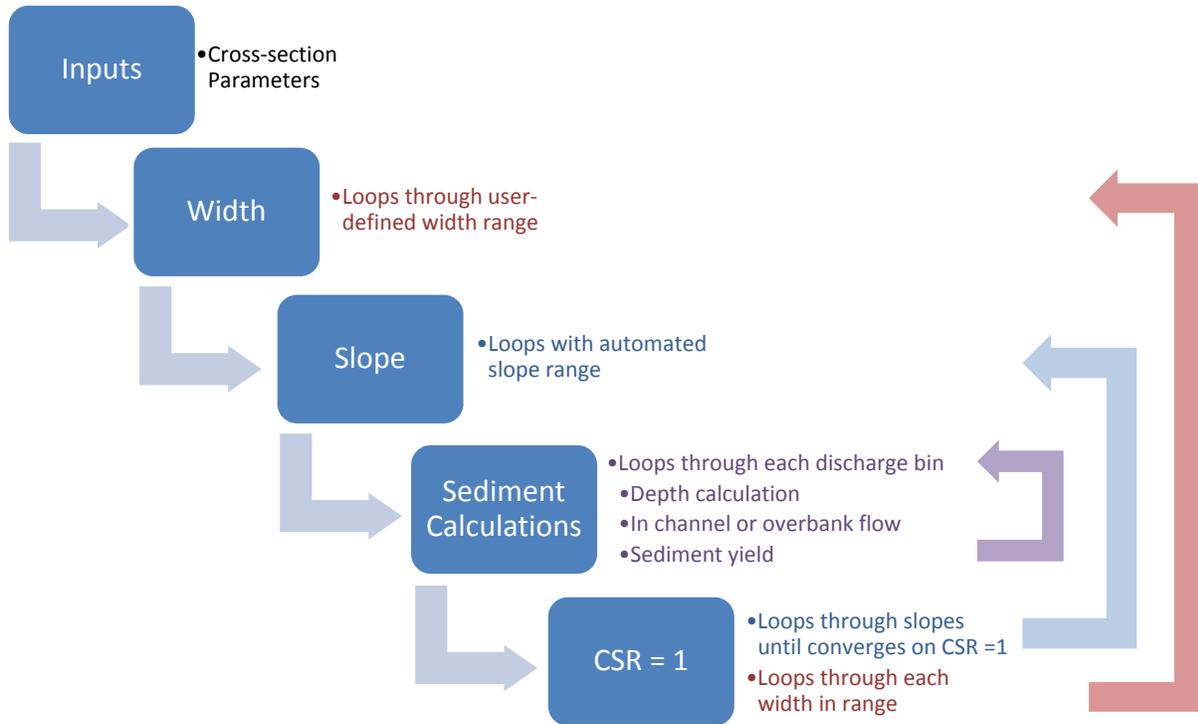
Figure 3-3. Schematic of Design Reach code methodology.

Firstly, the program reads the cross-sectional information entered by the user. Screenshots of the required inputs for the supply and design reaches are shown in Figure 3-4. The user provides a range of channel widths, and the program loops through this range in 2-m increments. For each width in the range, the slope corresponding to CSR = 1 is iteratively determined. The program guesses an initial slope and calculates the depth, in channel or overbank flow, and upper or lower regime to calculate sediment yield for each average discharge in the binned FDC. The sediment yield summed over all discharges is compared with the supply reach total sediment yield to calculate the CSR for that slope estimate. The slope is then updated using a bisection method until it converges on the slope that will give a CSR = 1 within a tolerance of 0.025 for each width in the defined range.

Supply Reach:

Design Reach:

Inputs For Supply Reach		
Main Channel		
Bottom Width	*	m
Bank Height	*	m
Bank Angle	*	H:V
Slope	*	m/m
Right Bank (n)	*	
Left Bank (n)	*	
Grain Size		
D16	*	mm
D50	*	mm
D84	*	mm
Floodplain		
Floodplain Angle	*	H:V
Floodplain (n)	*	

Run Supply Reach

Tab Guidance

Required Inputs
(-) Auto-updated values

Inputs for Design Reach		
Main Channel		
Bank Height	*	m
Bank Angle	*	H:V
Right Bank (n)	*	
Left Bank (n)	*	
Grain Size		
D16	-	mm
D50	-	mm
D84	-	mm
Floodplain		
Floodplain Angle	*	H:V
Floodplain (n)	*	
Planform/ Valley (Optional)		
Valley Slope, Sv	*	m/m
Max Meander Beltwidth	*	m
Beltwidth Buffer	*	m
Program Constraints		
Min Bottom Width	1	m (default)
Max Bottom Width	*	m

Run CSR Tool

Tab Guidance

Required Inputs
Optional Inputs
(-) Auto-updated values

Figure 3-4. Required inputs for the Supply Reach and the Design Reach of the CSR Tool.

3.6.2.4   CSR Tool Validation

When the CSR Tool is given a single discharge rather than a full FDC, its results can be directly compared to the implementation of the Copeland method in the HEC-RAS stable channel design tool. We have found very similar results between HEC-RAS output and single-discharge calculations from the CSR Tool, which fosters confidence in the validity of the tool's output. Figure 3-5 is an example of the CSR Tool's output with a single discharge for Big Racoon Creek in Indiana compared to HEC-RAS's stable channel design using the Copeland method.
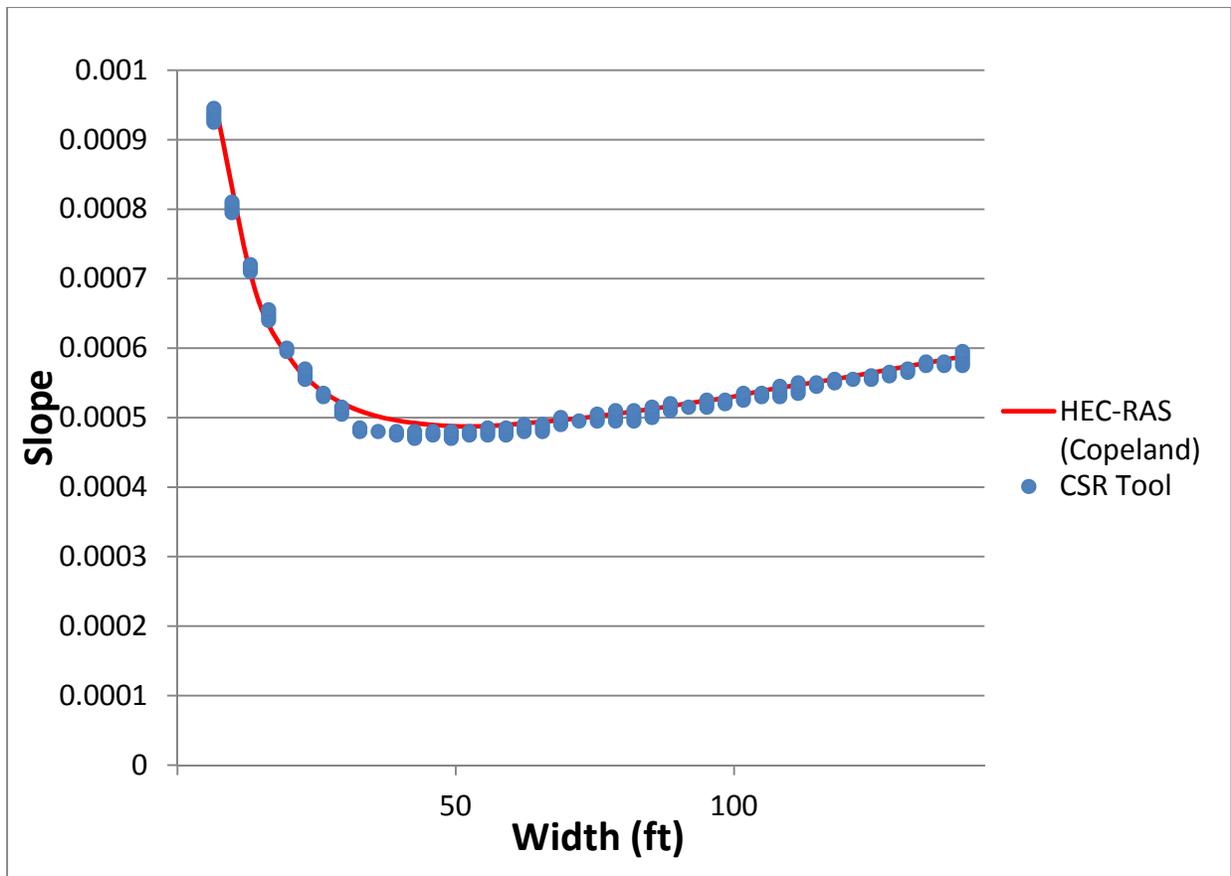
Figure 3-5. Comparison of CSR Tool with HEC-RAS stable channel design using the Copeland method with the same channel dimensions, grain size distribution, and single discharge.

The CSR Tool estimated a total sediment concentration of 279 ppm at 1,246 cfs and HEC-RAS estimated a total sediment concentration of 286 ppm at 1,246 cfs. The data for this example were taken from Soar and Thorne (2001).

The gravel-bed portion of the tool could not be validated for single-discharge design through comparison with output from Copeland's method in HEC-RAS or SAM (Thomas et al. 2002) because the Parker (1990a) and Wilcock-Crowe (2003) equations are not currently available in those software packages. The code used in the CSR Tool for the Parker (1990a) and Wilcock-Crowe (2003) bedload relations was obtained directly from a VBA-based tool created by Gary Parker called the 'acronym' series (Parker, 1990b). Gary Parker also added the use of the Wilcock-Crowe (2003) relationship in his tool in a later version. These codes were directly implemented in the CSR Tool and adapted to fit the methodology of the CSR analysis. Outputs from the CSR Tool were then compared to results from both Gary Parker's original tools and manual calculations to confirm the output of estimated sediment yield.

3.6.2.5 Planform Characteristics

Several additional outputs were added to the results page of the tool including a width-to-depth ratio for each stable channel solution. Also, if a valley slope of the design reach is entered then each stable channel solution found will have an output of sinuosity, meander belt width, and a channel braiding risk associated with each stable slope and width combination. The meander belt width is an estimation of the total planform width the river will span to support the projected dimensions and sinuosity of the design

(Hagerman and Williams 2000). This can be useful for visualizing the size of the design and determining whether planform width constraints exist in the design area. The user can define a maximum allowable meander belt width between the edge of the river and any planform constraint such as infrastructure. If any solution is over this amount then it will be highlighted in red in the outputs, so the user can know which solutions might conflict with this lateral restriction. Braiding risk is calculated for each slope and width combination using equations developed by van den Berg (1995). The level of risk for each design is calculated based on how close the design is to a braiding threshold. Figure 3-6 shows a visual representation of these planform concepts.

Refer to the CSR Tool Reference Manual (Appendix D of this NCHRP 24-40 final report) for further explanation of these concepts and the associated
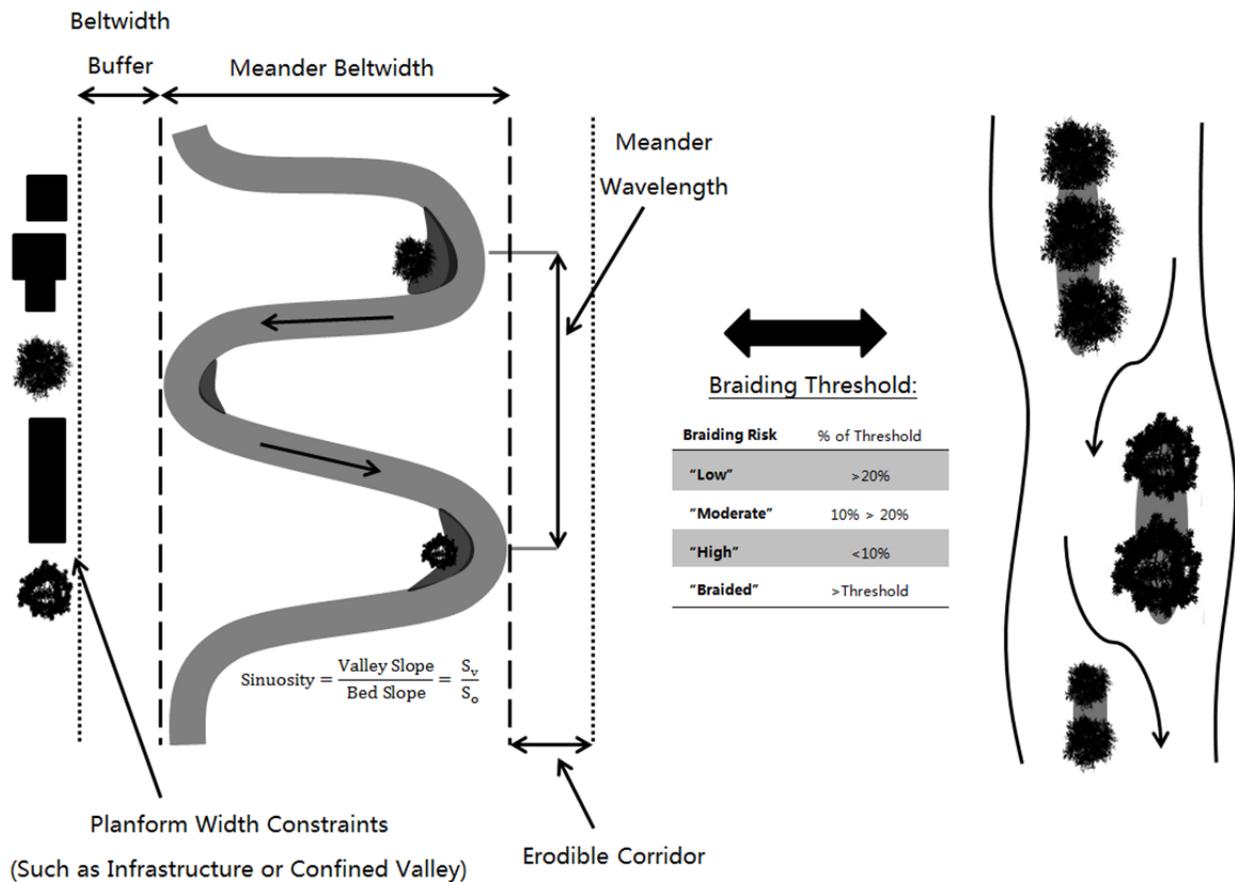
Figure 3-6. Visual representation of the planform characteristics included in the tool.

3.6.2.6 CSR Tool Outputs

The following shows examples of the output solutions produced by the CSR Tool for a sand-bed stream (Figure 3-7) and a gravel-bed stream (Figure 3-8). Figure 3-7a shows the plot of the family of channel slope and width combinations which provide continuity of water and sediment (i.e., CSR = 1) for the associated design. Figure 3-7b shows the associated table of solutions with the planform characteristics listed for each design. These outputs are shown on the 'Results' tab of the CSR Tool.

58

This example was developed using data retrieved from Soar and Thorne (2001) for a reach on Big Raccoon Creek in Indiana.

Figure 3-9 shows an example output from the 'Detailed Results' tab of the CSR Tool. This is a summary of the 'effectiveness' in tons/day for each average bin discharge for the supply reach. The 'effectiveness' table (Table 3-9b) shows the associated sediment percentiles summary (see the CSR Tool Reference Manual (Appendix D) for more information). This output is generated for each stable channel design solution as well and is displayed on the 'Detailed Results' tab of the CSR Tool.

Figure 3-9a shows the plot of the family of channel slope and width combinations which provide continuity of water and sediment (i.e., CSR = 1) for the associated design. Figure 3-9b shows the associated table of solutions with the planform characteristics listed for each design. This example was developed using data retrieved from King et al. (2004) for a reach on the Red River in Idaho.

Stable Channel Design Solutions

Slope vs Bottom Width (ft)

(b)
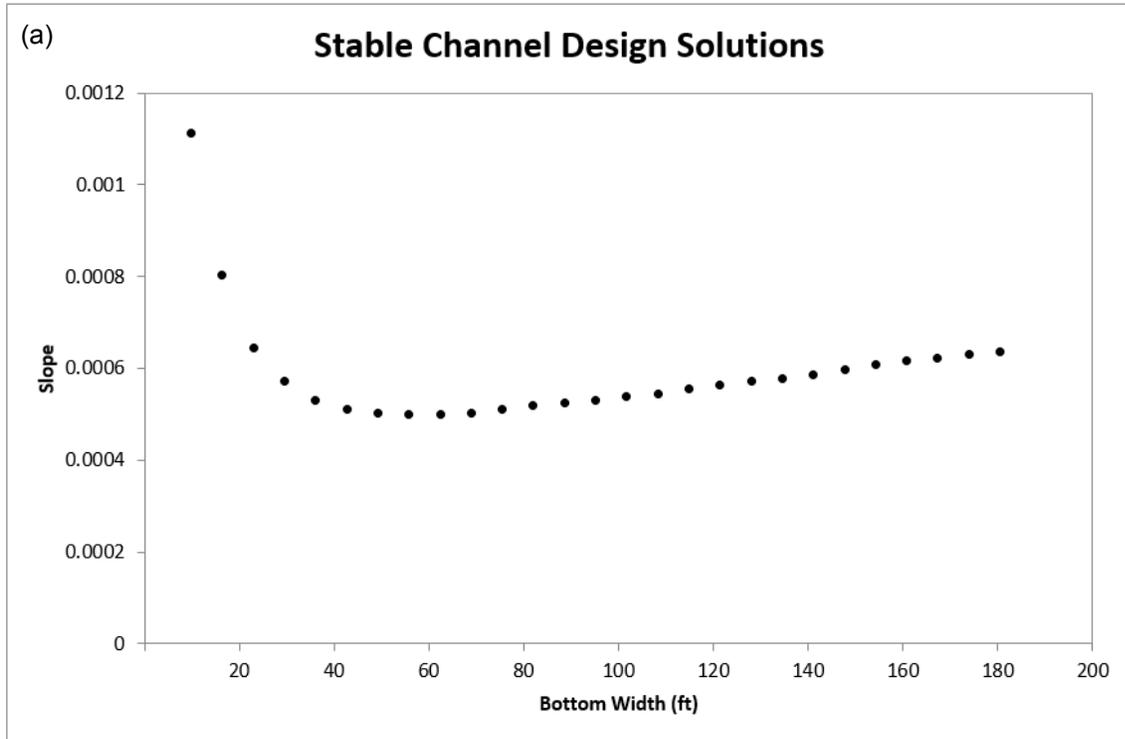
Stable Geometries   **Planform Characteristics**

Width (ft)	Width (m)	Slope	CSR	w/h Ratio	Sinuosity	Braiding Risk	Belt Width(m)	Min Wavelength(m)	Max Wavelength(m)
10	3	0.001112	0.999	1	< 1	Low	-	34	37
16	5	0.000803	1.002	2	< 1	Low	-	56	62
23	7	0.000646	1.002	3	1.00	Low	36	79	87
30	9	0.000571	1.000	3	1.13	Low	85	101	112
36	11	0.000531	0.999	4	1.22	Low	112	124	137
43	13	0.00051	1.002	5	1.27	Low	131	146	162
49	15	0.000503	1.000	6	1.29	Low	145	169	187
56	17	0.000499	1.002	7	1.30	Low	158	191	212
62	19	0.000501	1.000	7	1.29	Low	168	214	237
69	21	0.000503	0.999	8	1.29	Low	178	236	262
75	23	0.00051	0.999	9	1.27	Low	184	259	287
82	25	0.000518	1.002	10	1.25	Low	189	282	312
89	27	0.000524	0.999	10	1.24	Low	195	304	337
95	29	0.000531	0.998	11	1.22	Low	199	327	362
102	31	0.000539	1.000	12	1.20	Low	201	349	387
108	33	0.000545	0.999	13	1.19	Low	205	372	412
115	35	0.000555	1.001	13	1.17	Low	203	394	436
121	37	0.000563	1.000	14	1.15	Low	202	417	461
128	39	0.000571	1.001	15	1.13	Low	200	439	486
135	41	0.000579	1.000	16	1.12	Low	196	462	511
141	43	0.000586	0.998	16	1.11	Low	192	484	536
148	45	0.000598	1.001	17	1.08	Low	178	507	561
154	47	0.00061	1.001	18	1.06	Low	162	529	586
161	49	0.000617	1.002	19	1.05	Low	151	552	611
167	51	0.000621	1.001	20	1.04	Low	147	574	636
174	53	0.000632	0.998	20	1.03	Low	125	597	661
180	55	0.000637	1.002	21	1.02	Low	115	619	686

Figure 3-7. (a) Plot of family of width and slope combinations which provide continuity of water and sediment and (b) output table of stable geometries and planform characteristics for each solution. Example: Big Raccoon Creek, Indiana.

Supply Reach Summary

Discharge (cms)	Supply Effectiveness
4.80	2.16
12.26	4.77
19.71	5.98
27.17	4.33
34.62	4.76
42.08	3.79
49.54	6.06
56.99	4.38
64.45	4.54
71.90	1.07
79.36	1.22
86.81	.93
94.27	.79
101.72	.89
109.18	.66
116.63	1.08
124.09	.82
131.54	.89
139.00	.48
146.45	2.06
153.91	.55
161.36	.59
168.82	1.88
176.27	.67
183.73	.71

Qs Percentiles	Discharge (cms)
Qs50	44.83
Qs75	73.16
Qs90	142.10
Qeff	49.54

Figure 3-8. Example output on 'Detailed Results' tab. Example: Big Raccoon Creek, Indiana.

(a) Stable Channel Design Solutions

(b)

Stable Geometries | | | | **Planform Characteristics**

Width (ft)	Width (m)	Slope	CSR	w/h Ratio	Sinuosity	Braiding Risk	Belt Width(m)	Min Wavelength(m)	Max Wavelength(m)
3	1	0.00737	1.002	1	1.03	Low	13	11	12
7	2	0.00603	0.999	2	1.26	Low	33	23	25
10	3	0.00582	0.999	4	1.31	Low	41	34	37
13	4	0.00578	0.998	5	1.31	Low	47	45	50
16	5	0.00582	0.998	6	1.30	Low	52	56	62
20	6	0.00586	1.001	7	1.30	Low	57	68	75
23	7	0.00593	0.998	8	1.28	Low	61	79	87
26	8	0.00616	1.000	10	1.23	Low	62	90	100
30	9	0.00621	0.999	11	1.22	Low	66	101	112
33	10	0.00636	0.999	12	1.20	Low	67	113	125
36	11	0.00646	1.001	13	1.18	Low	68	124	137
39	12	0.00659	0.999	14	1.15	Low	68	135	150
43	13	0.00663	1.001	15	1.15	Low	70	146	162
46	14	0.00682	1.000	17	1.11	Low	66	158	175
49	15	0.00698	0.999	18	1.09	Low	62	169	187
52	16	0.00704	1.002	19	1.08	Low	62	180	200
56	17	0.00715	1.000	20	1.06	Low	58	191	212
59	18	0.00728	1.000	21	1.04	Low	51	203	224
62	19	0.00734	1.002	23	1.04	Low	49	214	237
66	20	0.00756	1.002	24	1.01	Low	32	225	249

Figure 3-9. (a) Plot of family of width and slope combinations which provide continuity of water and sediment and (b) output table of stable geometries and planform characteristics for each solution. Example: Red River, Idaho.

3.7 Prospectus for eRAMS and CSR Analytical Channel Design Tools

The eRAMS-based tools (desktop watershed assessment, flow summary metrics, FDC computation, and sediment yield computations) provide a user-friendly and data-rich interface to perform multiple required computations supporting the overall analysis outlined in this report. As a cloud-based toolset which also is relied upon for multiple other federal (e.g., EPA, National Science Foundation (NSF), and USDA), state, and local agencies, these tools will continue to be maintained and improved into the future.

Future research and improvements to these tools include more-detailed watershed assessment, calibration of the SWAT model to gage data, and the integration of a 1-D flow model into eRAMS. At the time of publication of this report, the watershed assessment tool is fairly new with near-term plans to include easier data downloads of assessment report data and possibly the integration of multi-metric assessments of watershed condition. The calibration of SWAT models to flow data already in the eRAMS platform is supported by the USDA-ARS team which developed SWAT and will be accomplished at some time in the near future. The eRAMS team has been in conversation with the USACE to determine if it is appropriate (and possible) to incorporate either the computations or outputs of the HEC-RAS model into eRAMS or if developing a stand-alone 1-D river model would be appropriate. Additionally, as all of the eRAMS tools can be accessed independent of the GIS interface, using a REST-based protocol, the site-based tools could be used for broader-spatial analysis including optimizing projects in a watershed.

The CSR Tool provides a user-friendly interface to apply the full spectrum CSR analysis to produce a family of width and slope combinations which provide continuity of water and sediment for a design reach of interest. This analysis can help alleviate some of the uncertainties involved with choosing a single 'channel-forming' discharge and not considering the morphological influences of other flows. The solutions from this tool can provide strong support to aid in the process of designing stable channel stream crossings.

The CSR Tool also provides a platform for further research in stable channel design. It is suggested that further research is performed to test the applicability of the CSR technique in practical stable channel design. This could include testing the tool against channel designs that have been implemented to compare with results shown in the field. Also, further theoretical comparisons can be made to help support the question: "When is the CSR method most needed over the single discharge method?" Preliminary results have shown that the CSR method is the most needed when the stream has a "flashy" hydrograph and/or in fine-grain streams. The CSR Tool can also support the question: "What single discharge or sediment percentile best represents the full spectrum output produced by the CSR?" Preliminary results from this project suggest that the single discharge that aligns with the CSR output is often bracketed between the Q_{s50} and Q_{s75} designs. Further research is necessary to pinpoint what factors lead to the CSR result being closer to Q_{s50} or Q_{s75}.

Decision Support for FDC Generation and Sediment Yield Calculations

4.1 Introduction

As described in Chapter 2, calculations of sediment yield, the half-load discharge (Q_{s50}), or the effective discharge (Q_{eff}) rely upon FDCs, which describe the frequency, or fraction of time that a discharge magnitude is equaled or exceeded. In Chapter 3, we presented tools that can be used to estimate FDCs for gaged or ungaged locations.

Because of the typically highly non-linear relationship between discharge and sediment transport, large, infrequent flows at the tail of a FDC can have an important impact on sediment yield calculations and channel design based on those calculations. It is important to understand, therefore, how land use changes may affect FDC generation, and the circumstances under which sediment yield calculations may be affected by the temporal resolution at which data used to generate FDCs were collected. Based on an overwhelming call for tool simplicity among DOT practitioners, this chapter continues to document when certain simplified analyses are appropriate for design hydrology and provides case studies that address the following questions:

- In what situations are sub-daily streamflow data required in order to achieve a reasonable estimation of the sediment yield curve? This is addressed in Section 5.2.
- How does watershed urbanization affect the FDC, and what are the possible implications for computing sediment yield metrics? This is addressed in Section 5.3.

We then present guidance on estimating Q_{s50}, as well as worked examples using the tools developed as part of this project.

4.2 Appropriate Flow Data Resolution for Sediment Transport Calculations

4.2.1 Background

The decision to use either daily-averaged or sub-daily streamflow records has the potential to impact the calculation of effective discharge, sediment yield, and other sediment transport metrics. By using daily-averaged discharge data in sediment transport calculations, one must assume that the flow record does an adequate job of representing the flow regime. However, studies have shown that small (Ågren et al. 2007), urban (Graf 1977; Walsh et al. 2005), and arid watersheds (Allan and Castillo 2007) can exhibit rapid short-term variations in streamflow during runoff events. This type of streamflow behavior is termed "flashy." In "flashy" watersheds, because of the highly non-linear relationship between discharge and sediment transport, high sediment transporting discharges may happen infrequently and for very brief periods of time. Therefore, in these situations, daily-averaged flow data may not adequately represent the actual flow regime.

It was recognized long ago that using sediment rating curves with daily-averaged flow data could present errors in the computation of sediment discharge if the daily-average discharge is not representative of the flow rate throughout the day (Colby 1956). A study of six watersheds in East Devon, England, showed that sediment yield calculations from daily flow records could vary by up to 10% from those made with instantaneous records (Walling 1977). However, it is not clear how flashiness was related to the error in sediment yield calculations for these watersheds.

More recently, in a study of small to medium watersheds (smaller than 620 km^2) of the Yazoo River basin in northwest Mississippi, it was found that when the sediment yield curve was created from daily-averaged flow data, it deviated from the 15-minute sediment yield curve by 0 to more than 100% (Hendon 1995). This was because the highest discharges, occurring less than 3% of the time, were not represented in the daily-averaged data. Missing these discharge rates is problematic because high discharge rates correspond to high sediment transport rates (Hendon 1995). In another study from the same basin, use of daily-average flow data was found to under-predict sand yield by 51% and the total suspended sediment yield by 59% (Dubler 1997).

To the best of our knowledge, the effect of flow data resolution on sediment transport calculations has not been investigated outside of the Yazoo River Basin and East Devon, England, or with a large set of sites. Additionally, while the aforementioned studies investigated the effect of flow data resolution on sediment yield calculations, the relationship with flashiness in still unquantified. Here we present our findings from a nationwide study of the effect of flow data resolution on sediment transport metrics for both bedload and suspended-load transport. Our objectives are threefold:

(1) To quantify the effect of flow data resolution (daily-averaged and sub-daily) on sediment yield calculations in light of stream flashiness.
(2) To identify the situations in which using daily-averaged flow data for sediment transport calculations is acceptable and when it is not.
(3) To investigate the potential impacts on channel design parameters when daily-averaged flows are used in situations where sub-daily flows are more appropriate.

4.2.2 Methods

4.2.2.1 Data Selection

This analysis drew from bedload and suspended-load sites described in Chapter 2 and are listed in Appendix A. Sites were analyzed individually for continuity in flow records and effects of flow regulation. In total, 39 sites with bedload measurements and 99 sites with suspended-load measurements were chosen to be included in this analysis (Figure 4-1). The sites cover a wide range of the conterminous U.S. and represent drainage areas ranging from approximately 10 to 2,500,000 km^2. Basins were chosen such that a wide range of flow regimes would be analyzed including flashy and non-flashy systems.
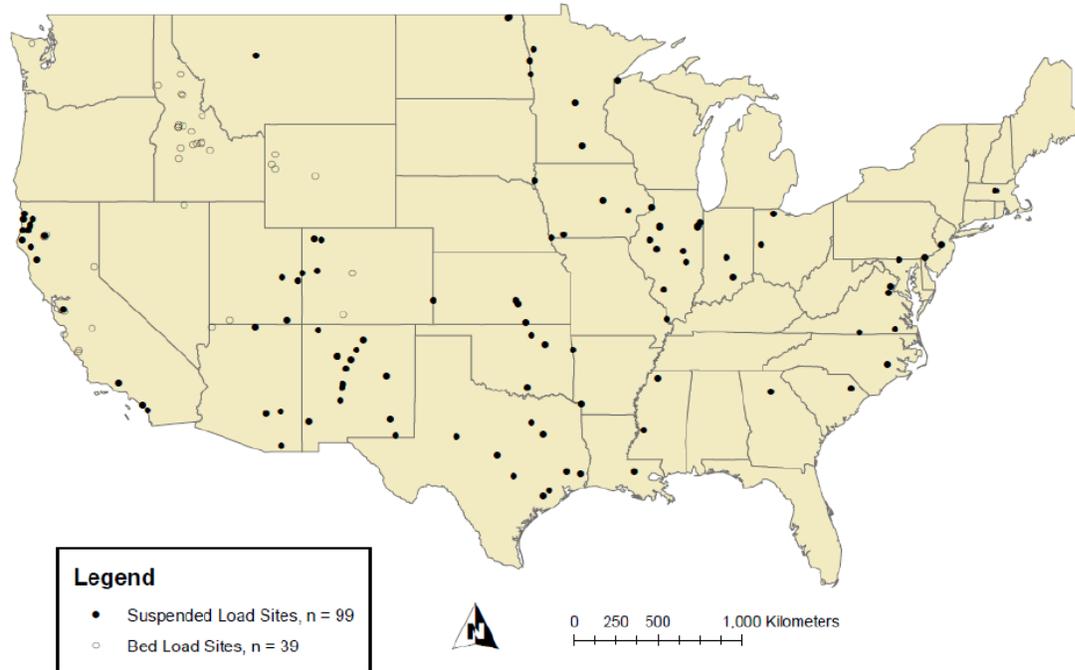
Figure 4-1. Map of sites used in this study.

The USGS was used as the source of all flow data required in this study. Daily flow data and sub-daily flow data (after 10/1/2007) were downloaded from the USGS NWIS website. Sub-daily flow data (prior to 10/1/2007) were obtained through the USGS Instantaneous Data Archive (IDA). The record length of flow data retrieved varied by site but ranged from the first day in which sub-daily flow data were available through the water year 2013, if possible. Some gages were discontinued prior to 2013; in that case, data were retrieved through the date in which the gage ceased operations. In total, 80 percent of sites used in this analysis contained more than 10 yrs of flow data.

4.2.2.2 Data Filtering

Flow data downloaded from the USGS were filtered prior to analysis. All blank observations and observations of "ice" (i.e., no flow measurements occurred) were removed. Additionally, due to lapses in both the daily and sub-daily flow data, the flow data had to be filtered so that time series of both datasets were identical. For example, if the month of September 1995 was missing from the sub-daily flow data, the month of September 1995 was removed from the daily-averaged data, and vice versa. Additionally, because sub-daily flow data prior to 10/1/2007 are stored by the USGS in the IDA, while data after this date are accessible from the NWIS, the sub-daily flow data had to be stitched together to create a seamless time series.

4.2.2.3 Flow Metrics

In order to characterize the flow conditions at each site, flow metrics were calculated using daily-averaged flow data. The primary flow characteristic of interest was flashiness as it was hypothesized that sub-daily flow data would be most useful for flashy systems where use of daily-averaged flow data would be unable to adequately represent the flow regime. While the R-B Index (Baker et al. 2004) was

ultimately chosen for use in this analysis, another flashiness metric termed T_{Qmean} (Konrad and Booth 2002) was also investigated, but deemed to not be as useful at the Richards-Baker metric.

The R-B Index is calculated by first calculating the path length of flow changes over a given period of time. The path length is equal to the sum of the absolute values of day-to-day changes in discharge. This path length is then divided by the sum of mean daily flows. The R-B Index is high for flashy hydrographs and low when hydrographs rise and fall gradually (Table 4-1):

$$\text{R - B Index} = \frac{\sum_{i=1}^{n} |q_i - q_{i-1}|}{\sum_{i=1}^{n} q_i} \qquad \textbf{(4-1)}$$

where:
q = daily-averaged discharge [m^2/s];
i = day; and
n = total number of days in the flow record.

Table 4-1. Classes corresponding to different design hydrology strategies based on bed material and flow regime flashiness.

R-B Index	R-B Index ≤ 0.2	0.2 < R-B Index ≤ 0.5	0.5 < R-B Index
Degree of Flashiness	Low	Moderate	High

4.2.2.4 Sediment Rating Curves

In order to characterize the rate at which sediment is transported as a function of flow, sediment rating curves were employed. Sediment rating curves often take the form of a simple power function: $Q_s = aQ^b$; where Q_s is the sediment discharge rate, Q is the water discharge rate, and a and b are best-fit regression parameters (Asselman 2000). The process of developing these curves is described in detail in Chapter 2.

4.2.2.5 Sediment Transport Metrics

In order to characterize sediment discharge at each site, three sediment transport metrics were calculated using both the daily-averaged and the sub-daily flow data. The three sediment transport metrics utilized in this study are the effective discharge (Q_{eff}), the half-yield discharge: the discharge below which 50% of the sediment is transported (Q_{s50}), and the sediment yield (*SY*).

As described in Chapter 2, the term "effective discharge" refers to the discharge that transports more sediment than any other (Emmett and Wolman 2001). For many systems, the effective discharge is often considered to be the "channel-forming discharge" and nearly equivalent to bankfull discharge (Andrews 1980). The effective discharge is generally computed by first subdividing the range of streamflows during a period of record into a number of classes or bins from which the total sediment quantity transported by each class is calculated. This is achieved by multiplying the frequency of flow occurrence in each class by the median sediment load for that flow class (Biedenharn et al. 2000), resulting in a sediment yield. The sediment load for a flow was calculated using a sediment rating curve. The effective discharge (Q_{eff}) is the median discharge of the flow class with the maximum sediment yield.

To compute the effective discharge using actual flow records, the discharge data first need to be discretized into a histogram. The bins of the histogram can be spaced either arithmetically or logarithmically. For this study, effective discharge was calculated using an arithmetic binning procedure. Effective discharge has been calculated by others using both arithmetic and logarithmic bins, however, the majority of analyses have chosen arithmetic bins (Soar and Thorne 2001). Initially 25 bins were used in the analysis, however, if the effective discharge fell into the first bin, the first bin was subdivided into

three new bins and the analysis was repeated. This was done to prevent the over-estimation of effective discharge. If the effective discharge fell into the first bin again, the original first bin was subdivided into 5 bins. This process was repeated until the effective discharge no longer landed in the first bin or until the original first bin has been subdivided into 11 or more bins. Once the bin with the maximum sediment yield was identified, the median flow in that bin was said to be the effective discharge.

To calculate the sediment yield, the sediment rating curve and water discharge time series were utilized to first create a sediment discharge time series. By performing a trapezoidal integration procedure on the sediment discharge time series (trapz function, 'pracma' package (R CORE Team 2014b)), the sediment yield for the period of record was obtained.

Lastly, to calculate Q_{s50}, an ordered vector of sediment discharges was created by sorting the water discharges and applying the sediment rating curve. The ordered sediment discharge vector was then cumulatively summed. Q_{s50} was then determined by locating the water discharge that corresponded to 50% of the cumulative sediment transport.

4.2.2.6 Response Variables

In order to investigate the effect of flow data resolution on Q_{eff}, SY, and Q_{s50}, we divided the sediment transport metrics computed from daily-averaged flow data by those which were computed with sub-daily flow data: SY_{Daily} / SY_{15}, $Q_{eff\text{-}Daily} / Q_{eff\text{-}15}$, $Q_{s50\text{-}Daily} / Q_{s50\text{-}15}$. Here, the "Daily" subscript denotes the value of the metrics derived from average daily flow records, and the "15" subscript denotes those generated from 15-minute data. The response variable was then plotted against a predictor variable such as flashiness.

4.2.2.7 Quantile Regression

Quantile regression (Koenker and Bassett 1978) was used to analyze the relationships between our response variables (SY_{Daily} / SY_{15}, $Q_{eff\text{-}Daily} / Q_{eff\text{-}15}$, $Q_{s50\text{-}Daily} / Q_{s50\text{-}15}$) and flashiness. While most regression applications estimate rates of change in the mean of the response variable, quantile regression estimates rates of change for all portions of a probability distribution of the response variable (Cade and Noon 2003). Depending on the variables of interest, quantile regression can be a powerful tool for visualizing the relationship between predictor and response variables.

4.2.2.8 Multiple Linear Regression

Multi-variable linear regression was utilized to model the response variables. By regressing the response variables, we may find a suitable set of parameters for modeling error in our sediment transport metrics. A database of site characteristics and flow metrics were analyzed to identify the best subsets (regsubsets function, 'leaps' package (R CORE Team 2014c)) of predictor variables. Best subsets of 1, 2, and 3 variables were identified. Use of an interaction variable was also explored. The database of predictor variables included drainage area, annual precipitation, bed sediment sizes, sediment rating curve parameters, and common flow metrics. Predictor variables identified in each best subset were checked for cross-correlation before being regressed.

4.2.3 Results

4.2.3.1 Effective Discharge

Analysis of the effect of flow data resolution on effective discharge yielded unclear results. Flashiness was not observed to impact the ratio of effective discharge computed with daily-averaged flow data ($Q_{eff\text{-}Daily}$) to effective discharge computed with sub-daily flow data ($Q_{eff\text{-}15}$) (Figure 4-2). Of the bedload sites, approximately 60% had a $Q_{eff\text{-}Daily} / Q_{eff\text{-}15}$ ratio that was larger than one. Similarly, of the

suspended-load sites, 40% had a $Q_{eff\text{-}Daily}$ / $Q_{eff\text{-}15}$ ratio that was larger than one. Overall, there was little pattern in the relative size of Q_{eff} calculated with daily-averaged flow data to Q_{eff} calculated with sub-daily flow data.
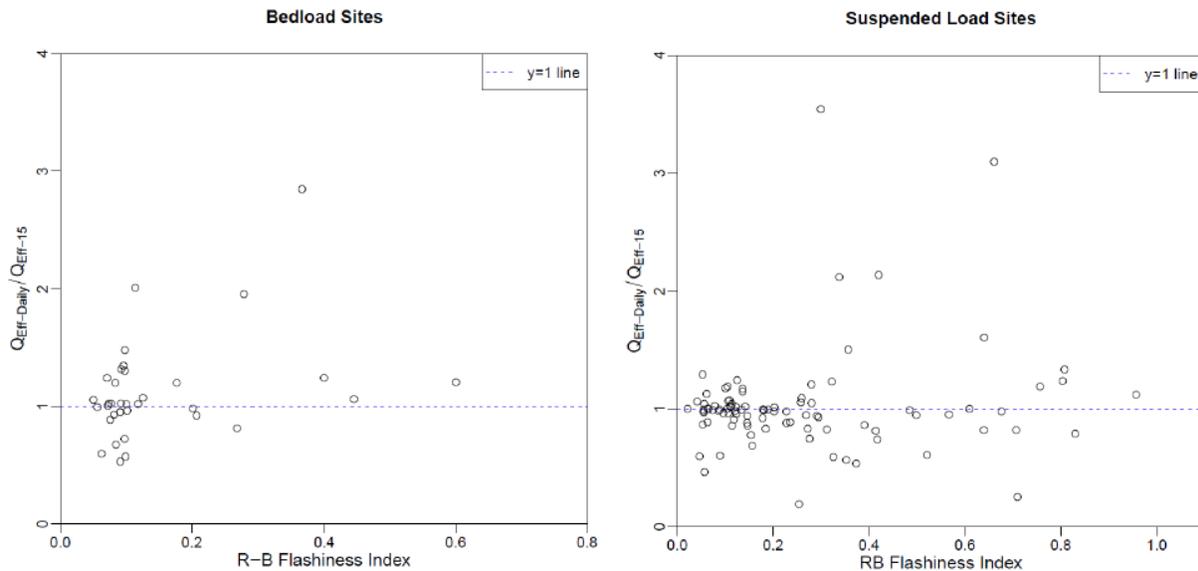
Figure 4-2. Ratio of effective discharge computed with daily-averaged flow to sub-daily flow versus the R-B Index.

4.2.3.2 Quantile Regression

<u>Sediment Yield</u>

Sediment yield computed with daily-averaged flow data (SY_{Daily}) was found to generally be less than sediment yield computed with sub-daily flow (SY_{15}) (Figure 4-3). The ratio of SY_{Daily} / SY_{15} was found to decrease with increasing flashiness in a wedge-shaped fashion for both bedload and suspended-load sites. That is that for non-flashy sites ($RB \approx 0$), SY_{Daily} / SY_{15} was found to be nearly equal to 1, while for flashy sites ($RB > 0.4$), SY_{Daily} / SY_{15} was found to range from 1 to 0.4. Because there was more than one rate of change of SY_{Daily} / SY_{15} observed in Figure 4-3, quantile regression was used to highlight the heterogeneous response of SY_{Daily} / SY_{15} to flashiness. It was also observed that the sediment rating curve parameter b, contributed to the degree of response of SY_{Daily} / SY_{15} to flashiness. Specifically, for sites with flashy flow characteristics, is was observed that as rating curve parameter b increases, the ratio of SY_{Daily} / SY_{15} decreases.
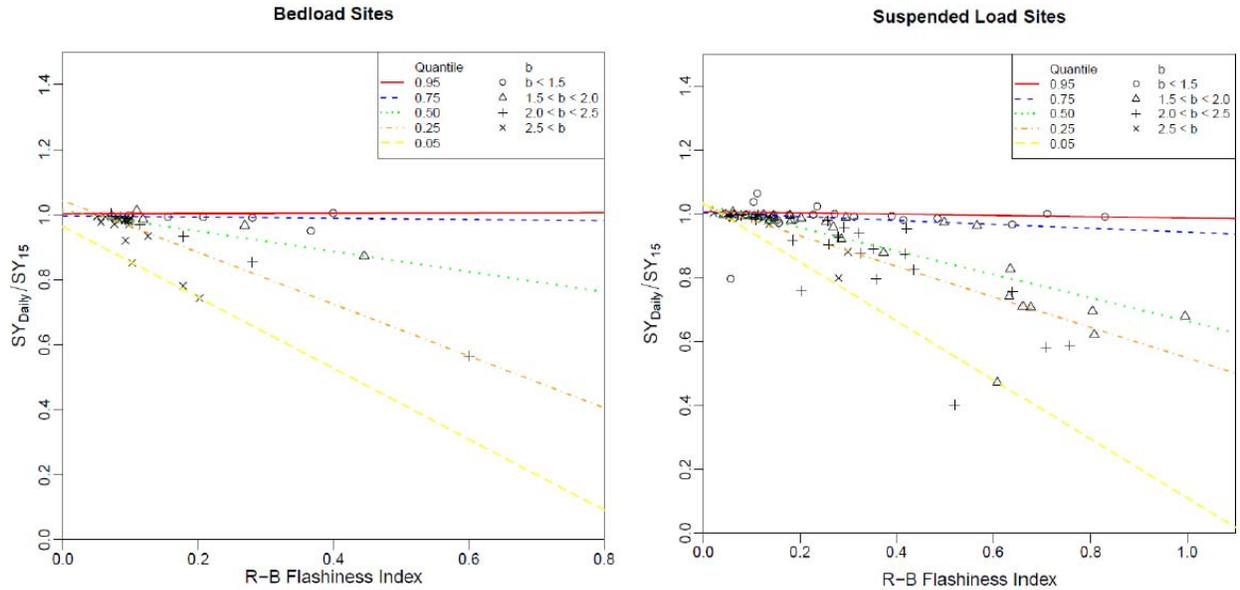
Figure 4-3. Ratio of sediment yield computed with daily-averaged flow to sub-daily flow versus the R-B Index.

4.2.3.3 Half-yield Discharge, Q_{s50}

The discharge below which 50% of cumulative sediment is transported calculated with daily flow data ($Q_{s50\text{-}Daily}$) was found to generally be less than when it was calculated with sub-daily flow data ($Q_{s50\text{-}15}$) (Figure 4-4). Much like the *SY* data, the Q_{s50} data were observed to fit a wedge-shaped pattern in which sediment rating curve parameter b influenced the degree of response of $Q_{s50\text{-}Daily}$ / $Q_{s50\text{-}15}$. That is that for non-flashy sites ($RB \approx 0$), $Q_{s50\text{-}Daily}$ / $Q_{s50\text{-}15}$ was found to be nearly equal to 1, while for flashy sites ($RB > 0.4$), $Q_{s50\text{-}Daily}$ / $Q_{s50\text{-}15}$ was found to range from 1 to 0.2. It was also observed that the sediment rating curve parameter b, contributed to the degree of response of $Q_{s50\text{-}Daily}$ / $Q_{s50\text{-}15}$ to flashiness. Specifically, for sites with flashy flow characteristics, is was observed that as rating curve parameter b increases, the ratio of $Q_{s50\text{-}Daily}$ / $Q_{s50\text{-}15}$ decreases.

70
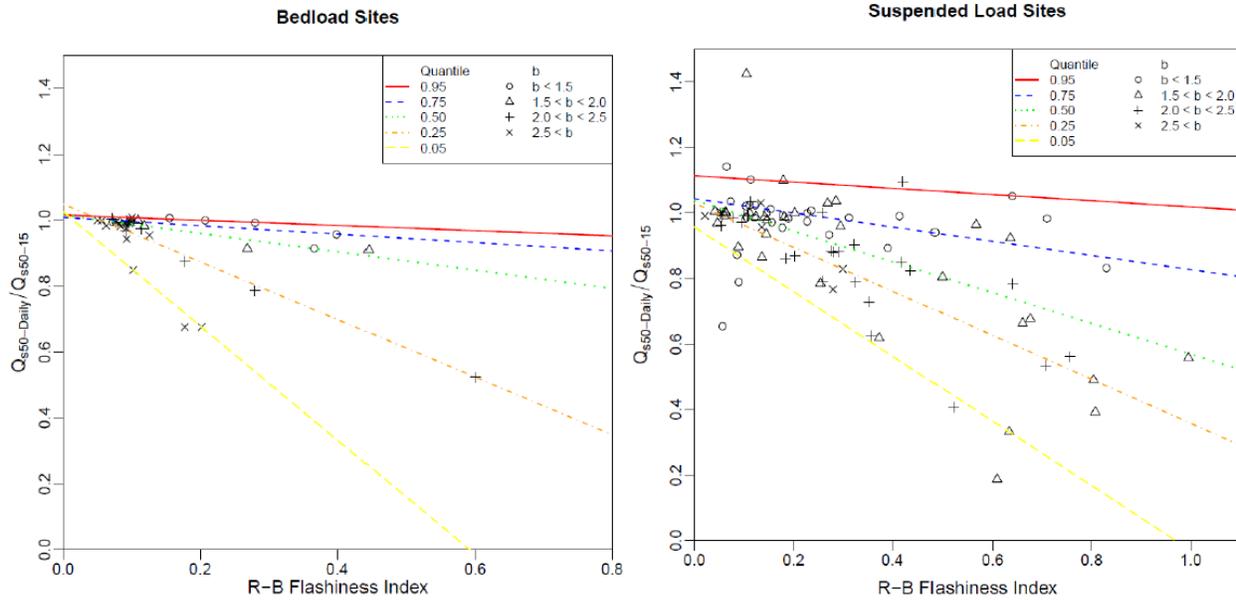
Figure 4-4. Ratio of discharge below which 50% of sediment is transported computed with daily-averaged flow to sub-daily flow versus the R-B Index.

4.2.3.4 Multiple Linear Regression Analysis

The best predictors of change in SY_{Daily} / SY_{15} and $Q_{s50\text{-}Daily}$ / $Q_{s50\text{-}15}$ were identified through multiple linear regression analysis (Table 4-2). Variables used in the analysis include the R-B Index, T_{qmean}, average annual precipitation, drainage area, median sediment size (d_{50}), 84th percentile sediment size (d_{84}), best-fit sediment rating curve exponent (b), and best-fit sediment rating curve coefficient (a). *RB* was found to be the best single predictor of change in both in SY_{Daily} / SY_{15} and $Q_{s50\text{-}Daily}$ / $Q_{s50\text{-}15}$ for both bedload and suspended-load sites as it explained the more variance than any other single variable (higher R^2 value). The second and third best indicators for all models were found to be d_{50} and b. The predictive ability of each model was also seen to increase from a 1-variable model to a 3-variable model based on R^2 values. For coarse- and fine-bed sites, the best model was found to be a 2-parameter model that utilized an interaction variable. For the sediment yield response variable, the 2-parameter interaction model utilized R-B Index and sediment rating curve parameter b. For the Q_{s50} response variable, the 2-parameter interaction model utilized R-B Index and d_{50} sediment size.

71

Table 4-2. Linear regression models relating error in hydrologic / sediment transport metrics to flow flashiness (*RB*) and exponent on sediment rating curve (*b*).

Bedload / Suspended Load	Dependent Variable[a]	Number of Regression Model Parameters	Best Regression Model[b]	R^2
Bedload	SY_{Daily} / SY_{15}	1	$1.0184 - 0.4472\ RB$	0.39
Bedload	SY_{Daily} / SY_{15}	2	$1.1123 - 0.55\ RB - 0.29\ b$	0.53
Bedload	SY_{Daily} / SY_{15}	2 + interaction	$0.95 + 0.6297\ RB + 0.03937\ b - 0.5715\ RB * b$	0.84
Bedload	SY_{Daily} / SY_{15}	3	$1.107 - 0.519\ RB - 0.0252\ b - 3.36\text{E-}05\ D_{50}$	0.61
Bedload	$Q_{s50-Daily} / Q_{s50-15}$	1	$1.0279 - 0.5511\ RB$	0.4
Bedload	$Q_{s50-Daily} / Q_{s50-15}$	2	$1.064 - 0.5607\ RB - 0.00029\ D_{50}$	0.56
Bedload	$Q_{s50-Daily} / Q_{s50-15}$	2 + interaction	$0.9831 - 0.105\ RB + 0.00102\ D_{50} - 0.01019\ RB * D_{50}$	0.82
Bedload	$Q_{s50-Daily} / Q_{s50-15}$	3	$1.111 - 0.5983\ RB - 0.0232\ b - 0.000015\ D_{50}$	0.64
Suspended Load	SY_{Daily} / SY_{15}	1	$1.0328 - 0.3903\ RB$	0.5
Suspended Load	SY_{Daily} / SY_{15}	2	$1.147 - 0.3915\ RB - 0.06224\ b$	0.57
Suspended Load	SY_{Daily} / SY_{15}	2 + interaction	$0.97 + 0.4483\ RB + 0.03312\ b - 0.456\ RB * b$	0.72
Suspended Load	SY_{Daily} / SY_{15}	3	$1.203 - 0.494\ RB - 0.0962\ b + 0.0206\ D_{50}$	0.62
Suspended Load	$Q_{s50-Daily} / Q_{s50-15}$	1	$1.0387 - 0.5016\ RB$	0.41
Suspended Load	$Q_{s50-Daily} / Q_{s50-15}$	2	$1.0792 - 0.707\ RB + 0.00156\ D_{50}$	0.49
Suspended Load	$Q_{s50-Daily} / Q_{s50-15}$	2 + interaction	$1.134 - 0.8834\ RB - 0.02437\ D_{50} + 0.097\ RB * D_{50}$	0.53
Suspended Load	$Q_{s50-Daily} / Q_{s50-15}$	3	$1.194 - 0.6897\ RB - 0.07368\ b + 0.02472\ D_{50}$	0.52

[a]Dependent Variables are defined in the *List of Abbreviations, Acronyms, Initialisms, and Symbols*.
[b]Variable Definitions: b = best-fit exponent from sediment rating curve; D_{50} = median grain size [m]; and *RB* = Richards-Baker Flashiness Index computed with daily-average flow data.

4.2.4   Discussion

4.2.4.1   Effective Discharge

Analysis of the effect of flow data resolution on effective discharge yielded unclear results.   Among bedload and suspended-load sites, the ratio of $Q_{eff-Daily} / Q_{eff-15}$ was both less than 1 and greater than 1 in nearly equal abundance. Flashiness, as well as other flow metrics did not appear to exhibit any control on the ratio. We believe that these results are a byproduct of the inherently variable process of determining Q_{eff}. The number and size of the arithmetic bins in the calculation of effective discharge played a large role in the resultant Q_{eff} and subsequent results. In this analysis, 25 arithmetic bins were used. When the effective discharge landed in the first bin, as it frequently did, the first bin was subdivided and the process was repeated, as to not over-estimate Q_{eff}. The result was that depending on the analysis, a variable number of bins and bin sizes were used. Because we believe that Q_{eff} is both variable and highly dependent on the binning procedure, we recommend consideration be given to using Q_{s50} in its place. Q_{s50} is the most accurate and least biased estimator of the bankfull discharge in suspended-load channels, and performs as well as Q_{eff} in bedload channels.

4.2.4.2   Sediment Yield and Q_{s50}

Daily-averaged flow data were found to be inadequate for capturing high-magnitude flows at flashy sites. Under these circumstances, high sediment transporting flow rates were diminished by low flows in the averaging process, ultimately causing an underestimation of sediment transport. Sediment yield and Q_{s50} computed with daily-averaged flow data were both found to differ by varying degrees from that which was calculated from sub-daily flow data. The primary control on how SY_{Daily} and $Q_{s50-Daily}$ varied from SY_{15} and Q_{s50-15} was flashiness. Non-flashy systems had SY_{Daily} and $Q_{s50-Daily}$ values that were very

similar to SY_{15} and Q_{s50-15}. Alternatively, flashy systems had SY_{15} and Q_{s50-15} values that were either similar or very different from SY_{Daily} and $Q_{s50-Daily}$ depending on the magnitude of b (low or high). For flashy sites with a high value of b, the difference was great; for flashy sites with a low value of b, the difference was small. For flashy sites, b was found to be an important secondary control on the ratio of SY_{Daily}/SY_{15} (Figure 4-3). Figure 4-5 shows that for flashy sites, as b increases, the ratio of SY_{Daily}/SY_{15} decreases in a linear manner.
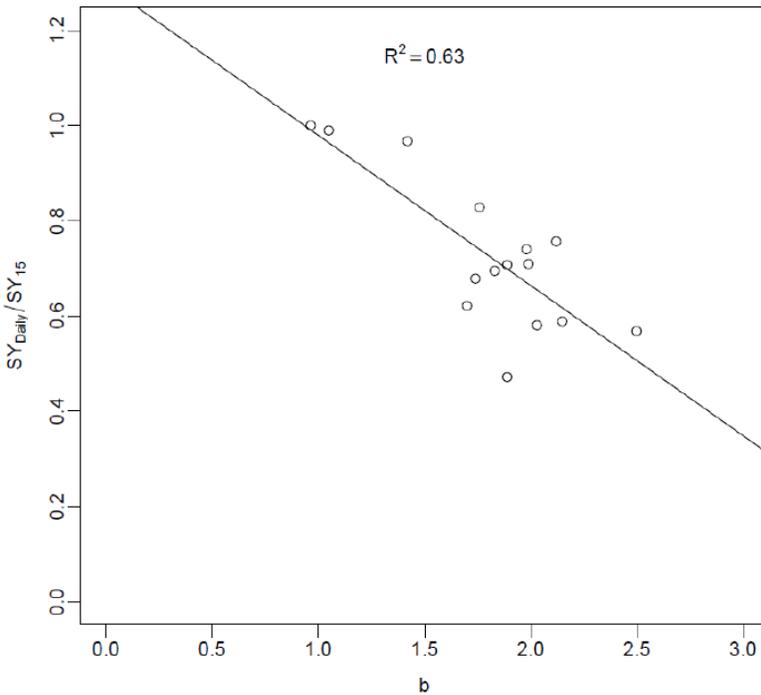
Figure 4-5. Relationship between underestimation of sediment yield and sediment rating curve best-fit exponent (b) for suspended-load sites with a RB flashiness greater than 0.6.

4.2.4.3 Design Implications

The exponent of the sediment transport rating curve (b) represents a number of physical watershed characteristics including the erosive power of the river and the extent to which new sediment sources become available as discharge increases (Asselman 2000). Additionally, b has been found to correlate with average air temperature and basin relief (Syvitski et al. 2000). Syvitski found that b was positively correlated with basin relief (0.616) and negatively correlated with average air temperature (-0.445).

If one were to use daily-averaged flow data to calculate the sediment yield of a flashy system with a moderate to large b value, they would be at risk of greatly underestimating sediment yield. In order to quantify the potential effect of underestimating sediment yield on design, Henderson proportionalities were used (Henderson 1966). Henderson combined the Einstein sediment transport function as revised by Brown (1950), the Chezy flow resistance formula, and momentum and mass conservation for steady uniform flow into a single proportionality:

$$q_s \propto \frac{q^2 S^2}{D^{\frac{3}{2}}}$$

(4-2)

73

Rearranging for channel slope yields:

$$S \propto \sqrt{\frac{D^{\frac{3}{2}} q_s}{q^2}}$$

(4-3)

where:
q_s = unit sediment transport rate [m²/s];
q = unit water discharge [m²/s];
S = gradient [m/m]; and
D = grain size [m].

Comparing a slope resulting from daily-averaged discharges to one resulting from sub-daily discharges yields:

$$\frac{S_{Daily}}{S_{Sub}} \propto \frac{\sqrt{\dfrac{D^{\frac{3}{2}} q_{s\text{-}Daily}}{q_{Daily}^2}}}{\sqrt{\dfrac{D^{\frac{3}{2}} q_{s\text{-}Sub}}{q_{Sub}^2}}}$$

(4-4)

Assuming that bed sediment size remains constant and simplifying yields:

$$\frac{S_{Daily}}{S_{Sub}} \propto \sqrt{\frac{q_{s\text{-}Daily}}{q_{s\text{-}Sub}}} * \left| \frac{q_{Daily}}{q_{Sub}} \right|^{-1}$$

(4-5)

Using SY as a surrogate for q_s (both measures for sediment transport) and Q_{s50} as a surrogate for q (both measures of discharge) we can relate the underestimation of SY and Q_{s50} to design slope:

$$\frac{S_{Daily}}{S_{Sub}} \propto \sqrt{\frac{SY_{Daily}}{SY_{Sub}}} * \left| \frac{Q_{s50\text{-}Daily}}{Q_{s50\text{-}Sub}} \right|^{-1}$$

(4-6)

where:
S_{Daily} = channel slope generated from average daily flow records [m/m];
S_{Sub} = channel slope generated from sub-daily flow records [m/m];
D = grain size [m];
$q_{s\text{-}Daily}$ = unit sediment transport rate generated from average daily flow records;
q_{Daily} = discharge per unit width generated from average daily flow records [m²/s];
$q_{s\text{-}Sub}$ = unit sediment transport rate generated from sub-daily flow records;
q_{Sub} = discharge per unit width generated from sub-daily flow records [m²/s];
SY_{Daily} = sediment yield generated from average daily flow records [m³];
SY_{Sub} = sediment yield generated from sub-daily flow records [m³];
$Q_{s50\text{-}Daily}$ = discharge associated with 50% cumulative sediment transport over average daily flow records [m³/s]; and

$Q_{s50\text{-}Sub}$ = discharge associated with 50% cumulative sediment transport over sub-daily flow records [m³/s].

Using the relationship Equation (4-6), we can plot how the underestimation of S_{Daily} increases with RB and b (Figure 4-6). One can see in Figure 4-6 that when using daily-averaged flow data, the degree to which channel slope can be underestimated increases with RB and b. Underestimation of channel slope can lead to channel aggradation. However, if b is low (low sediment supply, or low erosive power), even in very flashy conditions, the design slope will not be underestimated when using daily-averaged flow data. In order for the design slope to be greatly underestimated the system must exhibit rapid short-term variations in streamflow (have a high R-B Index) and have a moderate to steep rate of sediment transport (b).
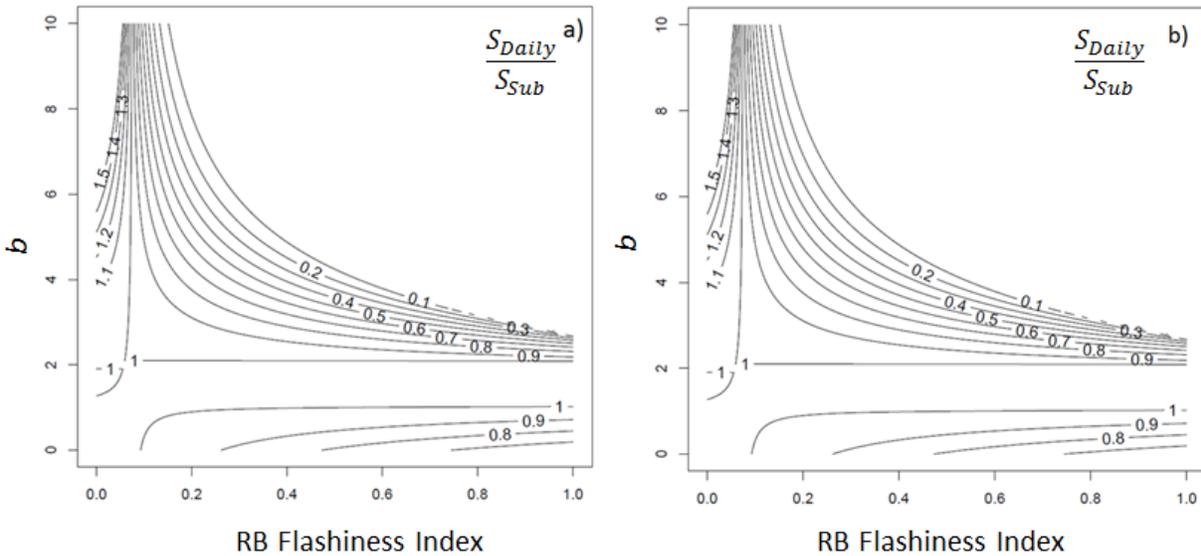
Figure 4-6. Ratio of design slope calculated with daily flow data (S_{Daily}) to the design slope calculated with sub-daily flow data (S_{Sub}): (a) bedload sites and (b) suspended-load sites.

4.3 Urbanization Effects on FDCs

4.3.1 Motivation

Physiographic changes associated with urbanization can dramatically alter the hydrologic response in a watershed undergoing urban development, which in turn can have cascading effects on aquatic habitat, flood risk, and stream channel morphology (e.g., Booth and Jackson (1997) and Booth and Bledsoe (2009)). While it is known that urbanization can cause larger peak flow magnitudes for a given precipitation event than natural land use conditions (Hollis 1975; Vogel et al. 2011), there is less literature on how urbanization impacts the entire spectrum of flows that make up the flow regime. Because of the wide range of useful applications FDCs have, it is important to understand how they change in response to urbanization.

Here we present a case study on the effect of urbanization on FDCs for select streams in the Puget Sound Region of western Washington. In this study, we use a 50-yr analysis period starting in 1960 and ending in 2010. Our objectives include:
- to tabulate urbanization growth in the selected watersheds;
- to evaluate precipitation trends;

- to quantify the effects of urbanization on FDCs and stream flashiness; and
- to relate hydrologic changes to potential changes in channel morphology.

4.3.2   Methods

4.3.2.1   Study Area

The extent of this study is the Puget Sound basin of western Washington, U.S. The Puget Sound basin is bordered on the east by the Cascade mountain range and on the west by the Olympic Mountains. To the north, the basin extends towards Canada, with a small portion of the basin lying within British Columbia. To the south, the basin terminates in the foothills near the City of Olympia. The area of the basin is approximately 31,000 km^2 (Cuo et al. 2011).

The region receives approximately 1,000 mm of precipitation annually, with higher elevations receiving greater amounts. The majority of precipitation occurs as rain in the fall and winter months, with over 75% of precipitation occurring between October and the end of March (Kruckeberg 1991).

The basin has seen tremendous population growth in recent decades. The population of the four-county region of King, Kitsap, Pierce, and Snohomish Counties has grown from 1,500,000 in 1960 to 3,690,000 in 2010 (Washington State 2012).   In 2010, the basin comprised 70% of the state's population (Cuo et al. 2009).

4.3.2.2   Site Selection

Because most highly urban watersheds in the Puget Sound basin have small drainage areas, this analysis was limited to watersheds with a drainage area less than 200 km^2. To maintain a similar climate and precipitation amongst watersheds, only watersheds with a mean elevation less than 300 m above sea level were included in this analysis. Lastly, selected watersheds were required to have at least 25 yrs of "adequate" discharge data available from a USGS gaging station. A year of flow record was considered "adequate" if more than half of the daily discharge observations were present. Years of record were not required to be continuous; however, they were required to be between the years 1960 and 2010. A map of the selected watersheds is shown in Figure 4-7. Table 4-3 gives each watershed's drainage area, analysis period, and gage station number.
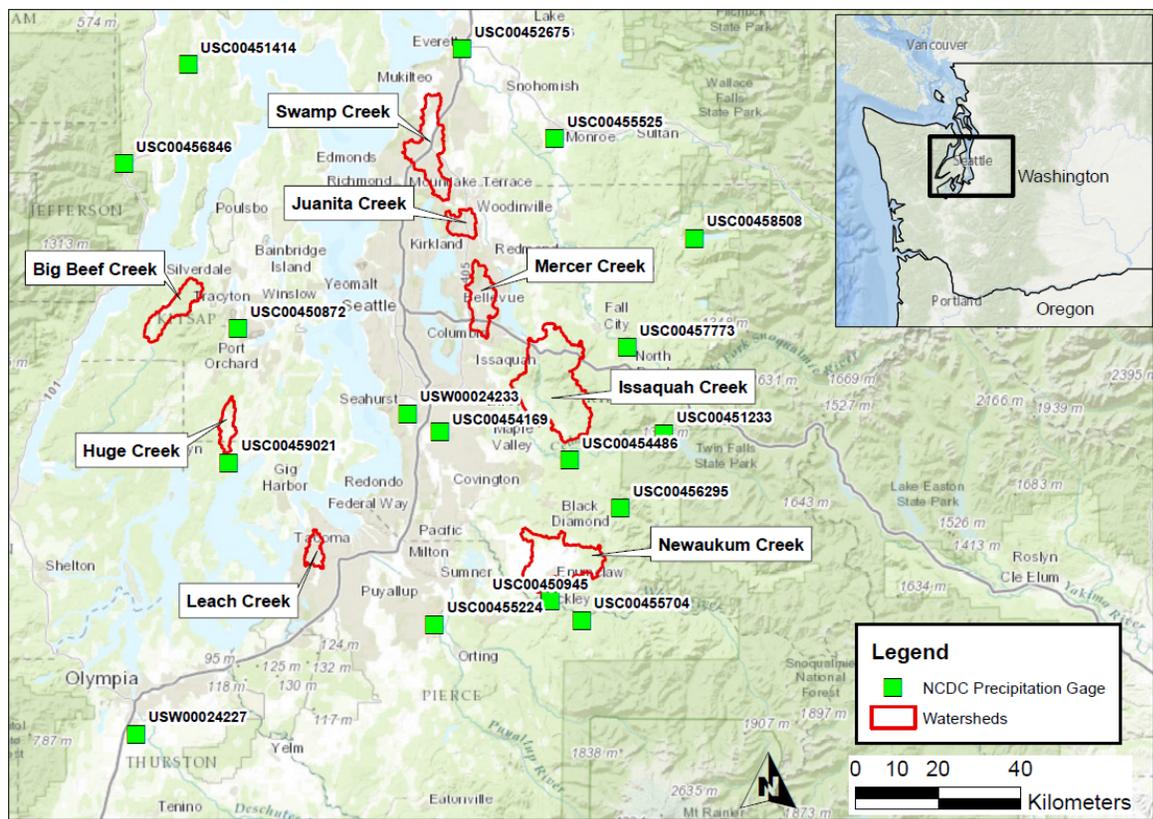
Figure 4-7. Map of watersheds and NCDC rain gages selected for analysis.

Table 4-3. USGS stations.

Station Name	USGS Gage Number	Analysis Period	Drainage Area [km²]
Juanita Creek near Kirkland, WA	12120500	1964-1989	17
Mercer Creek near Bellevue, WA	12120000	1960-2010	31
Swamp Creek at Kenmore WA	12127100	1964-1989	25
Big Beef Creek near Seabeck, WA	12069550	1970-1981, 1992-2007, 2009-2010	35
Huge Creek near Wauna, WA	12073500	1960-1969, 1978-2010	17
Newaukum Creek near Black Diamond, WA	12108500	1960-2010	70
Issaquah Creek near mouth near Issaquah, WA	12121600	1964-2010	145
Leach Creek near Fircrest, WA	12091200	1960-1986, 1989-2010	12.2

4.3.2.3   Watershed Urbanization Analysis

The degree of impervious surfaces in a watershed is an important indicator of watershed urbanization. Increased streamflow rates and runoff volumes following urbanization are widely recognized to be caused by increases in impervious surface area (Boyd et al. 1993; Smith et al. 2002).

77

While watershed imperviousness is useful in quantifying urbanization, datasets in the Puget Sound region are limited temporally. Satellite-derived estimates of land imperviousness are available through the NLCD beginning in the year 2001 (Homer et al. 2004). However, because this study examines urbanization from 1960 to 2010, population density was chosen as the main indicator of urbanization. Strong relationships between watershed imperviousness and population density have been suggested in the literature (Stankowski 1972; Sheng and Wilson 2009). It is important to note that when reliable imperviousness information is available, it should certainly be used over population density as the primary indicator of watershed urbanization. Small, highly commerical, or industiral watersheds may have extremely small populations, while maintaining very high amounts of impervious surfaces. In these locations, satellite-derived estimates of impervious surfaces (i.e., Multi-Resolution Land Characteristics Consortium (MRLC)) should be used for current analyses. Analyses of historical conditions in these locations will require other forms of local information (maps, photographs, or personal knowledge) and should be exercised with abundant caution.

In order to quantify the population and population density in our watersheds over time, historic U.S. Census tract data were utilized. Geographic maps of census tract boundaries and associated population tables were obtained for censuses conducted in 1960, 1970, 1980, 1990, 2000, and 2010 (Minnesota Population Center 2011). Census information is gathered in geographic units of varying size including: states, counties, tracts, and block levels. Census blocks offer population data at the finest spatial resolution but were not available for this region until the year 2000 (Minnesota Population Center 2011). The finest resolution population data available for the Puget Sound region from 1960 to 2010 were found to be census tract data.   Therefore, census tract data were used to develop population estimates.

Figure 4-8 shows the relationship between the percent imperviousness in 2011 and population density in 2010. In total, the relationship between population density and impervious cover was analyzed for more than 1,200 census tracts. For census tracts with less than 50% impervious surface, as is the case with our eight study watersheds, population density was found to explain 74% of the variance in percent imperviousness (Figure 4-8), suggesting that population density is a reasonable surrogate for impervious surfaces for watersheds that are less than 50% impervious.

Watershed populations for each decade were estimated from census tract data in a fashion similar to that used in another study (Sheng and Wilson 2009). Census tracts for each decade were re-mapped to the watershed boundaries in ArcGIS. For census tracts located only partially within the watershed, it was assumed that the census tract population density was uniform, and the population was split in proportion to the census tract area within the watershed. Population density (people/km^2) was then calculated by dividing the estimated watershed population (number of people) by the watershed area (km^2).
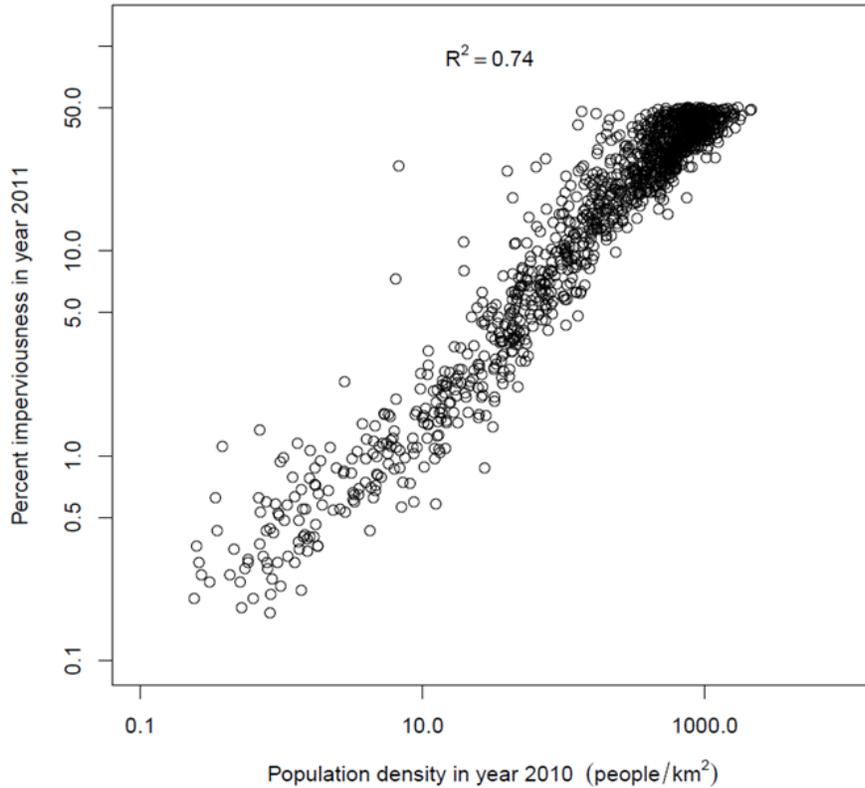
Figure 4-8. Relationship between impervious surfaces (computed from the 2011 NLCD (Homer et al. 2015)) and population density for census tracts in the State of Washington that are less than 50% impervious.

Following the quantification of population density in each of the watersheds over time, the watersheds were grouped into three categories based on their degree of urbanization in the year 2010:

(1) **urban watersheds:** watersheds with an estimated population density exceeding 1,000 people/km^2;

(2) **semi-urban watersheds:** watersheds with population densities exceeding 100 people/km^2; and

(3) **rural watersheds:** watersheds with population densities below 100 people/km^2.

4.3.2.4 Precipitation

Daily precipitation series for each watershed from 1960 to 2010 were spatially interpolated from nearby National Climatic Data Center (NCDC) daily precipitation gages (5.8). An inverse distance weighting (IDW) procedure (Chen and Liu 2012; Li and Heap 2011; Lu and Wong 2008) was utilized. The equations used to perform the IDW procedure are provided as Equations (4-7) and (4-8):

$$R_p = \sum_{i=1}^{N} w_i R_i \tag{4-7}$$

$$w_i = \frac{d_i}{\sum\limits_{i=1}^{N} d_i}$$

(4-8)

where:

R_p = unknown rainfall at the watershed of interest [mm];
N = number of rainfall stations, which was the 5 nearest for this analysis;
w_i = weighting of rainfall station i;
R_i = rainfall at station i [mm]; and
d_i = distance from rainfall station i to the centroid of the watershed of interest [km].

Daily rainfall sequences were used to calculate a number of metrics aimed at quantifying different precipitation characteristics. To quantify the total magnitude of precipitation, the precipitation was summed on an annual basis. To capture the intensity of single and multiple day precipitation events, we calculated the maximum annual 1-, 2-, 3-, and 7-day precipitation total. Lastly, to quantify variability in precipitation we calculated the coefficient of variation of each year of daily precipitation records. The coefficient of variation is calculated by dividing the standard deviation of the distribution by the mean of the distribution.

4.3.2.5 Flow Metrics

Temporal changes in streamflow were monitored through analysis of the FDC. In order to track changes in the FDC temporally, a "cumulative-yearly" approach was taken. This means that a FDC was created for each year of the flow record using all years of record prior. To avoid any bias that may be introduced to the analysis by starting the analysis on an abnormally wet or dry year, the first cumulative FDC was created for the fifth year of record utilizing the 5 prior years of flow record. For each year after year five, a new FDC was created using the entire flow record to that given year.

Another flow characteristic of interest to us in this analysis was the rate at which streamflow varies over time. Streams and rivers that experience rapid variations in streamflow over time are often termed "flashy." Watershed urbanization has been linked to flashy streamflow behavior in previous studies (Walsh et al. 2005). In order to characterize this streamflow behavior, the R-B Index (Baker et al. 2004) was utilized.

4.3.2.6 Baseflow Analysis

Baseflow is a component of total streamflow that enters a stream from a persistent and slowly varying source (Sophocleous 2002). While source of baseflow can vary, hydrologists agree that most baseflow originates from saturated flow from groundwater storage (Meyer 2005). Urbanization has been linked to the decline of stream baseflow in certain instances (Price 2011; Simmons and Reynolds 1982). This result is generally thought to be the result of impervious surfaces limiting the infiltration of precipitation into the subsurface layers; however, declining baseflow can also be caused by shallow groundwater extractions (Sophocleous 2002).

In order to examine trends in baseflow over the analysis period, the long-term hydrograph was separated into baseflow and runoff components. To isolate the baseflow in the long-term hydrograph, the Web-based Hydrograph Analysis Tool (WHAT) was utilized (Lim et al. 2005). WHAT allows users to select a baseflow separation method. For this study, a recursive digital filter method was used with default values for "perennial streams with porous aquifers." Although the base flow component of the hydrograph identified by this technique may not directly reflect groundwater contributions to streamflow, this methodology removes the subjective aspects from manual hydrograph separation and provides a fast and reproducible means to separating hydrographs over long periods of time (Lim et al. 2005). Upon

separation of the hydrograph into baseflow and direct runoff components, the average daily baseflow and direct runoff were computed for each year of record during the analysis period. Additionally, the baseflow index was calculated for each year of the analysis. The baseflow index, which is the long-term ratio of baseflow to total streamflow (Bloomfield et al. 2009), is useful for parametrizing streamflow by its origin.

4.3.2.7   Statistical Test for Trends

The non-parametric Mann-Kendall test (Mann 1945; Kendall 1975) was used to identify statistically significant trends in FDC percentiles, average annual baseflow, average annual runoff, and precipitation metrics. The Mann-Kendall rank correlation coefficient τ was computed for each watershed from the time series of each flow and precipitation metric. The test is particularly useful as missing values are allowed and the data do not need to conform to any particular distribution (Gilbert 1987). In this test, a null hypothesis of no statistically significant trend is used as a default. The null hypothesis is rejected if the calculated probability value p is less than *a priori* specified value (Gilbert 1987), 0.05 (5%) used in this study. The smaller the p-value, the more convincing the trend. The trend is an upward trend if the Mann-Kendall test statistic is positive. Likewise, the trend is downward if the test statistic (τ) is negative.

The R-B Index is calculated by first calculating the path length of flow changes over a given period of time. The path length is equal to the sum of the absolute values of day-to-day changes in discharge (q). This path length is then divided by the sum of mean daily flows (Equation (4-9)). The R-B Index is high for flashy hydrographs and low when hydrographs rise and fall gradually:

$$\text{R - B Index} = \frac{\sum_{i=1}^{n} |q_i - q_{i-1}|}{\sum_{i=1}^{n} q_i} \tag{4-9}$$

where:
q = daily-averaged discharge [m^2/s];
i = day; and
n = total number of days in the flow record.

4.3.2.8   Analysis of Channel Design Parameters

Two methods were used to relate hydrologic changes to potential changes in channel design parameters. First, to relate changes in the FDC to changes in design slope, Henderson proportionalities were used (Henderson 1966). Henderson combined the Einstein sediment transport function as revised by Brown (1950), the Chezy flow resistance formula, and momentum and mass conservation for steady uniform flow into a single proportionality, Equation (4-10):

$$q_s \propto \frac{q^2 S^2}{D^{\frac{3}{2}}} \tag{4-10}$$

Rearranging for channel slope yields:

$$S \propto \sqrt{\frac{D^{\frac{3}{2}} q_s}{q^2}} \tag{4-11}$$

81

where:

q_s = unit sediment transport rate [m²/s];
q = unit water discharge [m²/s];
S = gradient [m/m]; and
D = grain size [m].

The relationship in Equation (4-6) can be utilized to estimate change in channel slope. To do this, the channel slope (S_1) is estimated at one point in time from the unit sediment transport rate (q_{s1}) and unit discharge rate (q_1) at that same point in time. This can be done again at a second point in time to estimate the new channel slope (S_2). Together S_1 and S_2 can be used to estimate change in slope over an analysis period as shown in Equation (4-12).

For this study, unit sediment transport capacity was estimated at the 98th percentile discharge using a corrected version of the Meyer-Peter and Müller bedload transport equation (Wong and Parker 2006). The bed material was taken as gravel (Konrad et al. 2005). Channel geometry as a function of depth was calculated using information from field measurements collected and made available by the USGS:

$$\frac{S_1}{S_2} \propto \frac{\sqrt{\dfrac{q_{s1}}{q_1^2}}}{\sqrt{\dfrac{q_{s2}}{q_2^2}}} \tag{4-12}$$

where:

S_1 = channel slope at one point in time [m/m];
S_2 = new channel slope at a second point in time [m/m];
q_{s1} = unit sediment transport rate at one point in time [m²/s];
q_1 = unit discharge rate at one point in time [m²/s];
q_{s2} = unit sediment transport rate at a second point in time [m²/s]; and
q_2 = unit discharge rate at a second point in time [m²/s].

Secondly, hydraulic geometry relationships were utilized to relate changes in hydrology to likely changes in channel width. In an analysis of streams in the Puget Sound Lowland, many of which also appear in this study, Konrad et al. (2005) found that channel width could be related to the 90th percentile discharge reasonably well through a power function. This relationship is expressed in Equation (4-13):

$$w = 9.2 Q_{90}^{0.39} \tag{4-13}$$

where:

w = channel width [m]; and
Q_{90} = streamflow exceeded 10% of the time [m³/s].

4.3.3 Results

4.3.3.1 Urbanization Analysis

Analysis of decadal populations in the watersheds revealed a wide range of population densities (Figure 4-9). Huge Creek and Big Beef Creek, located west of Seattle in Kitsap County were found to have the lowest population density over the analysis period. Newaukum Creek and Issaquah Creek, were found to have slightly higher population densities, but both had slow growth rates similar to those in Huge and Big Beef Creeks. The remaining watersheds, Juanita, Mercer, Swamp, and Leach Creeks, were found to have very large growth rates over the analysis period. Juanita Creek had the greatest population growth, growing from approximately 154 people/km² in 1960 to over 1,900 people/km² in 2010. Mercer,

Swamp, and Juanita Creeks all had similar growth trends to a lesser extent, growing from less than 300 people/km^2 in 1960 to more than 1,500 people/km^2 in 2010. Leach Creek was nearly urbanized in 1960 and, therefore, saw lesser population growth over the analysis period.
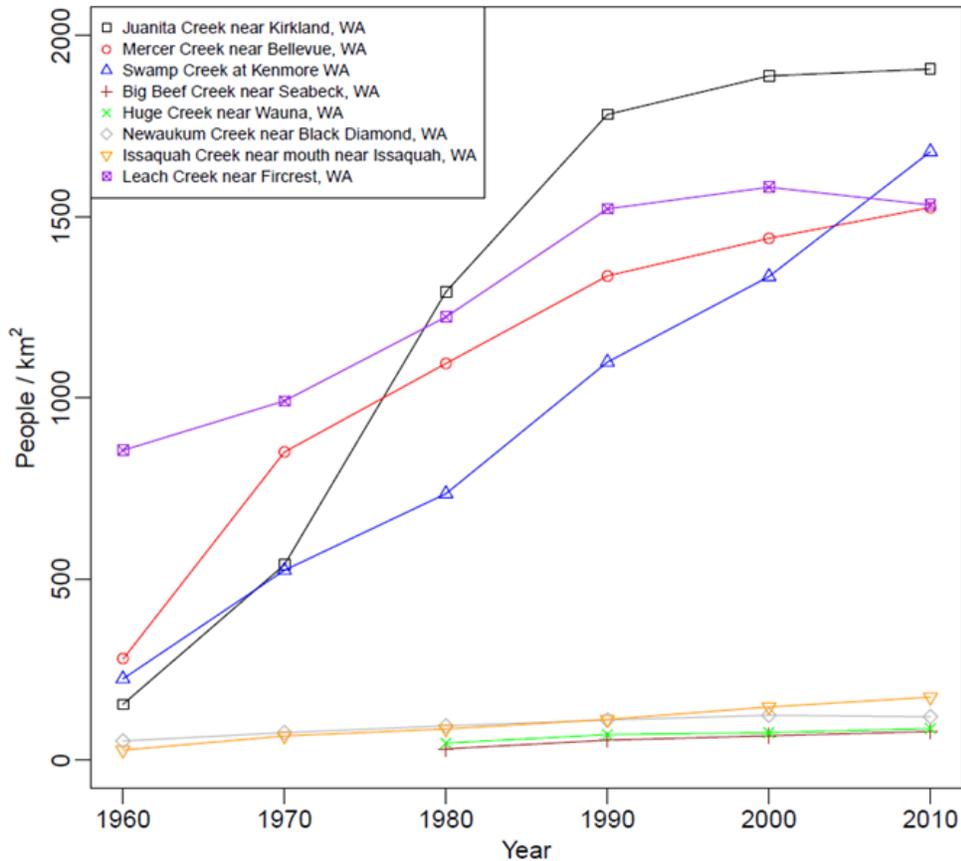
Figure 4-9. Estimation of watershed population density.

Based on these results, the watersheds were categorized into three groups according to population density in 2010:

(1) **urban watersheds:** watersheds with the highest amount of population growth over the analysis period and a population density greater than 1,000 people/km^2 in 2010;

(2) **semi-urban watersheds:** watersheds with slower population growth, and more than 100 people/km^2 in 2010; and

(3) **rural watersheds:** watersheds with the slowest rate of population growth, and a population density of less than 100 people/km^2 in 2010.

The results of this categorization are shown in Table 4-4.

Table 4-4. Watershed categorization table.

Station Name	USGS Gage No.	2010 Estimated Population Density	Average Population Growth 1960-2010 [people/ km^2 / yr]	Class
Juanita Creek near Kirkland, WA	12120500	1908	35.1	Urban
Mercer Creek near Bellevue, WA	12120000	1526	24.9	Urban
Swamp Creek at Kenmore WA	12127100	1680	29.1	Urban
Leach Creek near Fircrest, WA	12091200	1533	13.5	Urban
Newaukum Creek near Black Diamond, WA	12108500	120	1.3	Semi-Urban
Issaquah Creek near mouth near Issaquah, WA	12121600	174	2.9	Semi-Urban
Big Beef Creek near Seabeck, WA	12069550	79	1.6	Rural
Huge Creek near Wauna, WA	12073500	87	1.3	Rural

4.3.3.2 Precipitation

Results of the precipitation analysis showed no statistically significant trends in total annual precipitation (Table 4-5). Two of the four urban watersheds (Mercer Creek and Leach Creek) and both of the rural watersheds were found to have statistically significant increasing trends in multi-day precipitation maximums. All of the other watersheds showed slight but non-significant increases in multi-day precipitation maximums. Two of the eight watersheds (Leach Creek and Huge Creek) were found to have significant increasing trends in precipitation variability.

Table 4-5. Mann-Kendall τ values for precipitation metrics.

		Mann-Kendall τ Values					
		Annual Precipitation	Annual Maximum Precipitation				Coefficient of Variation
Station Name	Land Use		1-day	2-day	3-day	7-day	
Juanita Creek near Kirkland, WA	Urban	-0.16	-0.04	0.02	0.08	0.06	-0.09
Mercer Creek near Bellevue, WA	Urban	-0.05	0.09	0.22	0.20	0.16	0.00
Swamp Creek at Kenmore WA	Urban	-0.15	0.04	-0.04	0.08	0.14	-0.13
Leach Creek near Fircrest, WA	Urban	0.03	0.33	0.32	0.32	0.26	0.21
Newaukum Creek near Black Diamond, WA	Semi-urban	-0.11	0.05	0.11	0.02	0.03	-0.07
Issaquah Creek near mouth near Issaquah, WA	Semi-urban	-0.07	0.15	0.08	0.06	0.02	0.11
Big Beef Creek near Seabeck, WA	Rural	-0.02	0.24	0.21	0.25	0.21	0.18
Huge Creek near Wauna, WA	Rural	0.01	0.31	0.33	0.38	0.35	0.27

Significant Upward Trend
Significant Downward Trend

4.3.3.3 Flow Analysis

Three of the four urban watersheds were found to have statistically significant increasing trends over time in both the lower and higher regions of the FDC (Table 4-6). For high magnitude discharges ($Q_{90} - Q_{99}$), Leach Creek was found to have the strongest increasing trend. Swamp Creek was the only urban watershed to not have an increasing trend in the upper portion of the FDC. Swamp Creek did, however, have increases to the lower portion of the FDC. Combined, the urban watersheds experienced a 35% increase on average in the magnitude of the 98th (Q_{98}) and 99th (Q_{99}) percentile discharges (Table 4-7). The lower end of the FDC also increased in the urban watersheds but to a lower degree (Table 4-7).

Table 4-6. Mann-Kendall τ values for FDC percentiles.

Station Name	Land Use	Q_{10}	Q_{25}	Q_{50}	Q_{75}	Q_{90}	Q_{95}	Q_{98}	Q_{99}	RB Flashiness
Juanita Creek near Kirkland, WA	Urban	0.85	0.82	0.30	-0.11	0.56	0.71	0.75	0.75	1.00
Mercer Creek near Bellevue, WA	Urban	0.47	0.28	-0.07	-0.16	0.10	0.63	0.81	0.85	0.99
Swamp Creek at Kenmore WA	Urban	0.87	0.79	0.56	0.09	-0.47	-0.48	-0.44	-0.35	0.97
Leach Creek near Fircrest, WA	Urban	0.38	0.41	0.47	0.91	0.92	0.93	0.95	0.95	0.74
Newaukum Creek near Black Diamond, WA	Semi-Urban	-0.71	-0.84	-0.85	-0.65	-0.47	-0.61	-0.55	-0.35	0.13
Issaquah Creek near mouth near Issaquah, WA	Semi-Urban	-0.84	-0.91	-0.83	-0.85	-0.76	-0.77	-0.51	-0.32	0.84
Big Beef Creek near Seabeck, WA	Rural	-0.44	-0.16	-0.10	-0.10	-0.29	-0.25	-0.23	-0.28	0.45
Huge Creek near Wauna, WA	Rural	-0.81	-0.66	-0.61	-0.47	-0.52	-0.26	0.22	0.34	0.67

Variable Definition: RB = R-B Index; and Q_{10}, Q_{25}, Q_{50}, Q_{75}, Q_{90}, Q_{95}, Q_{98}, and Q_{99} = 10th, 25th, 50th, 75th, 90th, 95th, 98th, and 99th percentile discharges [m^3/s], respectively.

Significant Increasing Trend
Significant Decreasing Trend

Table 4-7. Average percent change in flow metrics over analysis period.

Land Use	Q_{10}	Q_{25}	Q_{50}	Q_{75}	Q_{90}	Q_{95}	Q_{98}	Q_{99}	RB Flashiness
Urban	15.9	13.5	6.5	7.0	20.6	30.5	35.0	36.1	46.6
Semi-urban	-13.6	-15.2	-8.4	-9.3	-5.5	-8.5	-0.9	-1.7	4.1
Rural	-12.6	-14.8	-20.4	-21.2	-16.6	-12.3	-6.1	-2.5	14.3

The two semi-urban watersheds (Newaukum Creek and Issaquah Creek) were found to have statistically significant decreasing trends for all portions of the FDC. The magnitude of the decreasing trends for the semi-urban watersheds was found to be greatest in the lower part of the FDC. The 25th and 10th percentile flows were found to have decreased on average by 15% and 13%, respectively (Table 4-6).

One of the two rural watersheds was found to have decreasing trend in the FDC. Huge Creek had statistically significant decreasing trends for nearly all parts of the FDC except the 99th percentile discharge (Q_{99}), which had an increasing trend. The other rural watershed (Big Beef Creek) saw no statistically significant increasing or decreasing trend with the exception of the 10th percentile discharge (Q_{10}). The magnitude of the decreasing trends for the semi-urban watersheds was found to be greatest for mid-range flow ($Q_{25} - Q_{75}$).

Results of our analysis on watershed flashiness yielded similar results across all watershed types. All watersheds with the exception of Newaukum Creek, experienced statistically significant increasing trends in the R-B Index over time. The strongest increasing trends were generally found in the urban watersheds. Combined, the average increase in flashiness for urban watersheds was 46% (Table 4-6). The rural and semi-urban watersheds saw flashiness increase by 14% and 4%, respectively.

4.3.3.4 Hydrograph Analysis

Analysis of the hydrograph's baseflow and runoff components showed statistically significant decreases in baseflow index for three of the four urban watersheds (Table 4-7). A decrease in baseflow index can be caused by a decrease in baseflow, an increase in total streamflow, or both. In these three

watersheds, the decrease in baseflow index was accompanied by a strong increase in runoff, and subsequently an increase in total streamflow. Only one of these three watersheds (Mercer Creek) saw both an increase in runoff and a decrease in baseflow. While Swamp Creek saw a decreasing trend in baseflow index over the analysis, the trend was not strong enough to be statistically significant. In total, the urban watersheds experienced a 43% increase in average daily runoff over the analysis period (Table 4-8).

Both of the semi-urban watersheds were found to have statistically significant downward trends in annual daily average baseflow (Table 4-8). However, because of their decline in total streamflow, these watersheds were not found to have a statistically significant decrease in baseflow index. No significant trends in baseflow, runoff, or baseflow index were found in the two rural watersheds. However, the rural watersheds were found to have a 13% reduction in the magnitude of average daily baseflow and a 12% reduction in average daily runoff (Table 4-9).

Table 4-8. Mann-Kendall τ values for hydrograph analysis.

Station Name	Land Use	Baseflow Index	Annual Daily Average	
			Runoff	Baseflow
Juanita Creek near Kirkland, WA	Urban	-0.553	0.353	-0.053
Mercer Creek near Bellevue, WA	Urban	-0.569	0.255	-0.191
Swamp Creek at Kenmore WA	Urban	-0.231	-0.003	-0.188
Leach Creek near Fircrest, WA	Urban	-0.236	0.461	0.425
Newaukum Creek near Black Diamond, WA	Semi-urban	-0.101	-0.031	-0.167
Issaquah Creek near mouth near Issaquah, WA	Semi-urban	-0.075	-0.130	-0.260
Big Beef Creek near Seabeck, WA	Rural	0.127	-0.048	-0.111
Huge Creek near Wauna, WA	Rural	-0.110	0.028	-0.087

Significant Upward Trend
Significant Downward Trend

Table 4-9. Average percent change in daily runoff and baseflow magnitude.

Land Use	Runoff	Baseflow
Urban	43.4	4.8
Semi-urban	-1.5	-9.8
Rural	-12.1	-13.8

4.3.3.5 Channel Design Parameters

Using locally calibrated bankfull geometry relationships (Konrad et al. 2005) and Henderson proportionalities (Henderson 1966), we were able to qualitatively estimate the potential change in channel bankfull width and channel slope over the analysis period. Findings from this analysis indicate the urban streams had significant potential for channel degradation estimated as a 5% reduction in channel slope and a 7% increase in channel bankfull width (Table 4-10). Rural and semi-urban streams were found to have a small potential for channel aggradation estimated as a negligible change in channel slope and a 2% reduction in channel width for semi-urban watersheds. The rural watersheds saw a potential 2% increase in channel slope and nearly a 7% decrease in channel width (Table 4-10).

Table 4-10. Average potential percent change in channel width and slope over analysis period.

Land Use	Channel Slope	Channel Width
Urban	-5.1	7.1
Semi-urban	0.4	-2.2
Rural	2.3	-6.9

4.4 Decision Support for Estimating Q_{s50}

In Section 4.2, we found that accurate computation of sediment yield metrics such as Q_{s50} will depend on flow data resolution for flashy (high RB) or fine-bedded (high b value) rivers. Our case study of urbanizing watersheds (Section 4.3) indicated that flashiness, and the upper tails of the FDC, are affected by land use change.

In Figure 4-10, we present a decision tree designed to provide practical guidance on the computation of sediment transport metrics such as Q_{s50}. The decision tree presents a series of questions regarding land use change, potential non-stationarity of the flow record, and the availability of stream gage data and sediment transport measurements, to guide the user toward the best approach for calculating Q_{s50}. Section 4.5 provides details on how to approach each node in the decision tree, and Section 4.6 provides some worked examples where Q_{s50} is calculated using the decision tree and the tools described in Chapter 3.
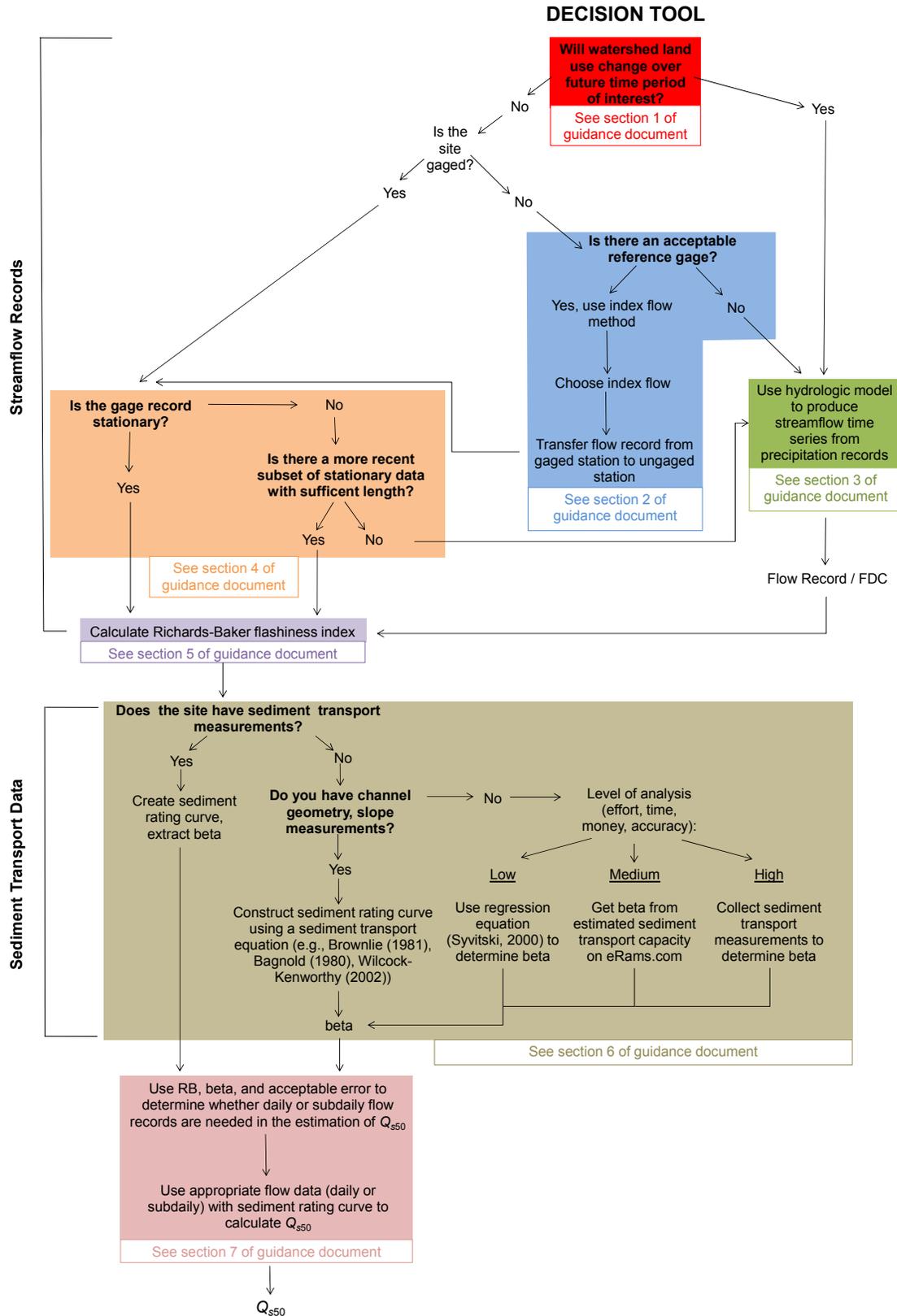
DECISION TOOL

Figure 4-10. Decision tree supporting Q_{s50} calculations.

4.5 Guidance for Calculating the Half-load Discharge

4.5.1 Section 1: Will Watershed Land Use Change Substantially Over the Future Time Period of Interest?

If a substantial change in land use in your basin is expected over your time period of interest, historical streamflow records may not act as a good predictor of future streamflow behavior. Hydrological models can be used to assess how much the flow regime is likely to change with changes in land use, and if significant changes are likely to occur, models may be used to generate streamflow data consistent with future land use.

Many hydrological models have been applied to evaluate potential hydrologic impacts of basin-scale climate change and urban development (Praskievicz and Chang 2009), and some state agencies employ their own models for continuous hydrologic simulation (e.g., Western Washington Hydrology Model (WWHM 2012)). Regardless of the chosen hydrological model, the hydrologic importance of potential future land use change may be evaluated by comparing model-predicted FDCs for current and projected land use scenarios. If a shift in the FDC due to land use change is predicted, it may be more appropriate to use the model-predicted FDC than historical streamflow records. Although uncalibrated models may accurately predict the direction of change in streamflow associated with land use change, accurate prediction of the magnitude of those changes likely requires a spatially calibrated model (Niraula et al. 2015).

> See Example 1 for an illustration of how the SWAT-DEG tool in eRAMS may be used to assess shifts in a FDC due to potential land use changes.

4.5.2 Section 2: Choosing a Reference Streamflow Gage and Indexing Flow Records

At locations in which streamflow gaging records are unavailable, it becomes necessary to synthesize streamflow data from another source. In this document we propose using the index flow method to transfer streamflow records from a gaged location to an ungaged location. The reliability of this method is a function of the quality of the gaged record and the physiographical similarity of the watersheds.

Is There an Acceptable Reference Gage?

In order to produce a streamflow record for an ungaged basin using the index flow method, a reference gage is needed. The selection of a good reference gage is critical as its flow record will be scaled to the ungaged location using an index discharge. The reference gage should be located in a climate similar to the ungaged location as climate impacts both the magnitude and slope of a basin's FDC (Castellarin et al. 2012). Characteristics such as topography, vegetation, land use, soils, and watershed shape shall also impact FDC characteristics (Fennessey and Vogel 1990; Burt and Swank 1992; Musiake et al. 1975) and should be similar amongst analog and ungaged watersheds. Other factors being equal, nearby gages provide better relations for indexing streamflow records than remote stations

> **Choosing the Index Flow**
>
> When indexing a FDC for an ungaged basin, consideration must be given to selecting an appropriate index flow. Commonly used index flows include the mean annual runoff (Smakhtin 1997; Ganora et al. 2009), median daily runoff (Ley et al. 2011), and 2-yr discharge (Watson et al. 1997). The index flow must be able to be estimated for the ungaged location, often this is accomplished with regional regression equations (USGS 2012).

(Searcy 1959). However, usable relations have been established between stations as far apart as 50 miles (Searcy 1959). Professional judgement is required to make a determination of whether an "acceptable" reference gage exists.

Estimating Streamflow Records at Ungaged Stations
(summarized from Biedenharn et al. (2000))

1. Using a streamflow record from a gaged site in a physiographically similar watershed.

2. Divide the discharge series by the index discharge for the gaged site. This creates a dimensionless flow record for the gaged site. If more than one reference gage site is available, an average dimensionless flow record for all the sites can be developed. This step can be completed using eRAMS. The flow analysis tool within eRAMS allows users to create a dimensionless FDC from a number of stream gages. This tool is useful because it allows users to visually compare the slope and shape of FDCs they are considering using in their analysis. Ideally, the gages selected for creating your regional FDC will have a similar shape and collapse onto each other when indexed.

3. Compute the index flow for the ungaged site using regional regression equations (http://water.usgs.gov/osw/programs/nss/index.html).

4. Calculate the streamflow record for the ungaged site by multiplying the dimensionless flow record by the index discharge for the ungaged site.

4.5.3 Section 3: Using a Hydrologic Model to Produce Streamflow Time Series from Precipitation Records

Many methods and software packages exist for rainfall runoff modeling, for an introduction, see Beven (2011). The SWAT-DEG tool within eRAMS is a great resource for developing streamflow records from climatic data for watersheds throughout the country. An example of this application is given below for Box Elder Creek in Northern Colorado.

> See Example 2 for an example application of rainfall-runoff modeling using the SWAT-DEG tool in eRAMS.

4.5.4 Section 4: Checking the Stationarity of Streamflow Records

Because some regions may be experiencing changes in climate that render historical hydrologic records less effective (Milly 2007), it is critical that we check the stationarity of a hydrologic record before using it. Methods for testing the stationarity of historical hydrologic records include Mann-Kendall testing (Hamed 2008; Kumar et al. 2009), Spearman's rank correlation method (Villarini et al. 2009; Kahya and Kalayci 2004), and Sen's slope (Kahya and Kalayci 2004). If the streamflow record is highly non-stationary, a hydrologic model may be appropriate for developing streamflow records. For gaged sites, a flow record of at least 15 to 20 yrs is needed to detect non-stationary behavior, especially for watersheds with inherently high values of R-B Index (see next section) and coefficient of variation.

> The RB index can be calculated at gaged sites using the eRAMS Flow Analysis tool. This is illustrated in Example 3.

4.5.5 *Section 5: Calculating the R-B Index*

The R-B Index is calculated by first calculating the path length of flow changes over a given period of time. The path length is equal to the sum of the absolute values of day-to-day changes in discharge. This path length is then divided by the sum of mean daily flows. The R-B Index is high for flashy hydrographs and low when hydrographs rise and fall gradually. The R-B Index is Equation (4-14):

$$\text{R - B Index} = \frac{\sum_{i=1}^{n} |q_i - q_{i-1}|}{\sum_{i=1}^{n} q_i} \qquad \textbf{(4-14)}$$

where:

q = daily-averaged discharge [m^2/s];
i = day; and
n = total number of days in the flow record.

4.5.6 *Section 6: Obtaining a Sediment Rating Curve*

Gaged Sites

If sediment transport measurements exist at a given site for a range of discharges, a sediment rating curve can be constructed. Sediment rating curves often take the form of a simple power function: $Q_s = aQ^b$; where Q_s = sediment discharge rate [kg/s], Q = water discharge rate [m^3/s], and a, b = best-fit regression parameters (Asselman 2000).

Ungaged Sites

For sites in which sediment transport measurements are not available, a range of options exist for synthesizing a sediment rating curve. If the channel geometry and slope measurements are available at the site, total load sediment transport equations can be used to create a sediment rating curve. Total load equations (e.g., Bagnold (1966), Brownlie (1981), Einstein (1950), and Yang (1973)) provide an estimate of sediment transport rate for a given discharge, by estimating the sediment transport at a range of discharges, a sediment rating curve can be established.

> In instances where channel geometry measurements are not available, and collecting sediment transport data is cost or time-prohibitive, other methods exist for estimating sediment rating curve parameters. The eRAMS platform has the functionality to provide sediment transport capacity estimates at varying discharges for either extracted or imported cross sections. To make these estimates, eRAMS allows the user to choose between using the Brownlie (1981), Bagnold (1980), and Wilcock-Kenworthy (2002) equations. The eRAMS platform will also perform the necessary regression and provide the user with the resultant sediment rating curve parameters. These capabilities are located within the channel cross-section analysis application (currently available at https://beta.erams.com/).

Sediment rating curves can also be estimated through use of regression equations. This method, while universally applicable, may only provide a broad estimate of the sediment rating curve parameters. Syvitski et al. (2000) developed a number of regression equations for estimating both the rating curve coefficient and exponent based off of factors such as basin relief, mean annual air temperature and latitude.

Streamflow gaging stations in the U.S. generally provide data in both daily-averaged and 15-minute increments. Daily-averaged discharges, while convenient to use, may not always be appropriate for sediment transport calculations. Streams in urban areas, arid climates, or with small drainage areas may exhibit rapid short-term variations in streamflow (Ågren et al. 2007; Graf 1977; Walsh et al. 2005). This type of streamflow is often termed "flashy." Flashy streams may have flood events lasting only a few hours, causing the peak discharge to be much greater than the corresponding mean daily discharge (Biedenharn et al. 2000). In these situations, sediment transport can be underestimated. The degree of underestimation is a function of stream flashiness and the logarithmic slope of the sediment rating curve, b (Rosburg 2015). Using Figure 4-11, one can estimate the underestimation in Q_{s50} that would result from using daily-averaged flow data, instead of hourly flow data, as a function of the R-B Index (Baker et al. 2004) and sediment rating curve parameter b.
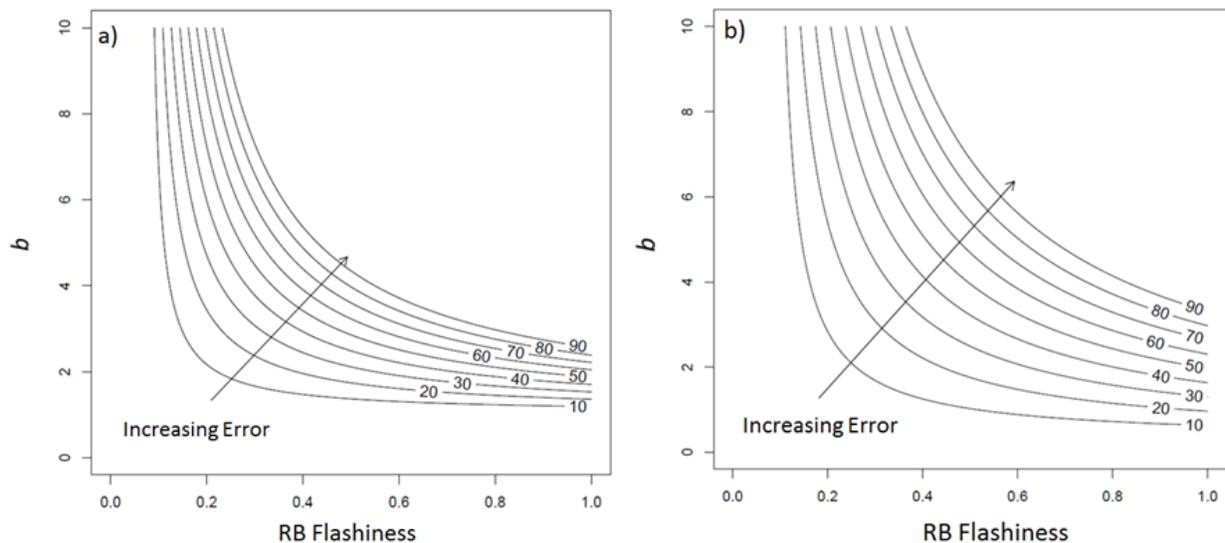
Figure 4-11. Percent of underestimation of the half-load discharge (Q_{s50}) (values labeled at the top of contours) when it is calculated with daily-averaged flow data instead of hourly flow data for: (a) bedload sites and (b) suspended-load sites. Figure originally from Rosburg (2015).

4.6 Examples

Much of the analysis needed to determine Q_{s50} for a given site can be facilitated using tools built into eRAMS. These capabilities are illustrated through the following four examples.

4.6.1 Example 1: Projecting Hydrologic Changes Caused by Changing Land Use for the Fourmile Creek Watershed in Central Iowa (Section 1)

The Fourmile Creek watershed is a 300 km^2 basin located north and east of Des Moines, Iowa (Figure 4-12). Here we explore the hydrologic sensitivity of Fourmile Creek to urbanization using the eRAMS SWAT-DEG tool. As of the year 2010, 36% of the watershed was classified as urban (Table 4-11), and it is expected that the proportion of urban area will increase. Therefore, two hypothetical scenarios were developed to explore how increases in urban area would impact hydrologic conditions. In Scenario

> Example 4 includes sample calculations of gage stationarity using the Mann-Kendall test.

1, urban area was increased to 50% of watershed area and cropland decreased to 38%. In Scenario 2, urban area was increased to 75% of watershed area and cropland was decreased to 13% (Table 4-11).

Running SWAT-DEG within eRAMS requires, at a minimum, watershed information, channel information, and climate data for the time period of interest. Once a new project has been created, one can populate the watershed properties by extracting data from a user-defined watershed, or can simply enter the data directly if it is known. To facilitate the use of climate data, eRAMS allows users to download daily climate observations from the Global Historical Climatology Network – Daily (GHCND). The eRAMS interface where the data are input is shown in Figure 4-13.
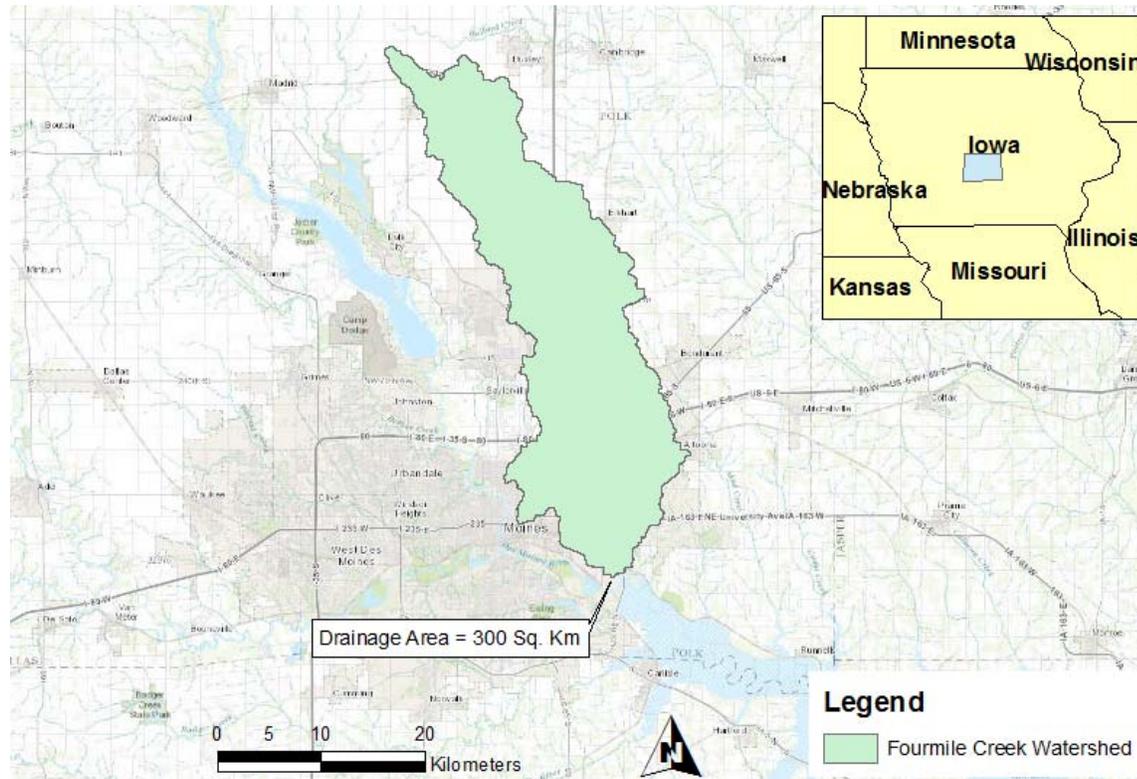
Figure 4-12. Fourmile Creek watershed.

Table 4-11. Current and future land use scenarios.

Land Use	Year 2010 (adapted from Snyder & Associates Inc. (2013))	Future Scenario 1	Future Scenario 2
Urban and Rural Residential	36%	50%	75%
Forest	1%	1%	1%
Crop Land	52%	38%	13%
Pasture/Grassland	11%	11%	11%
Other	0%	0%	0%
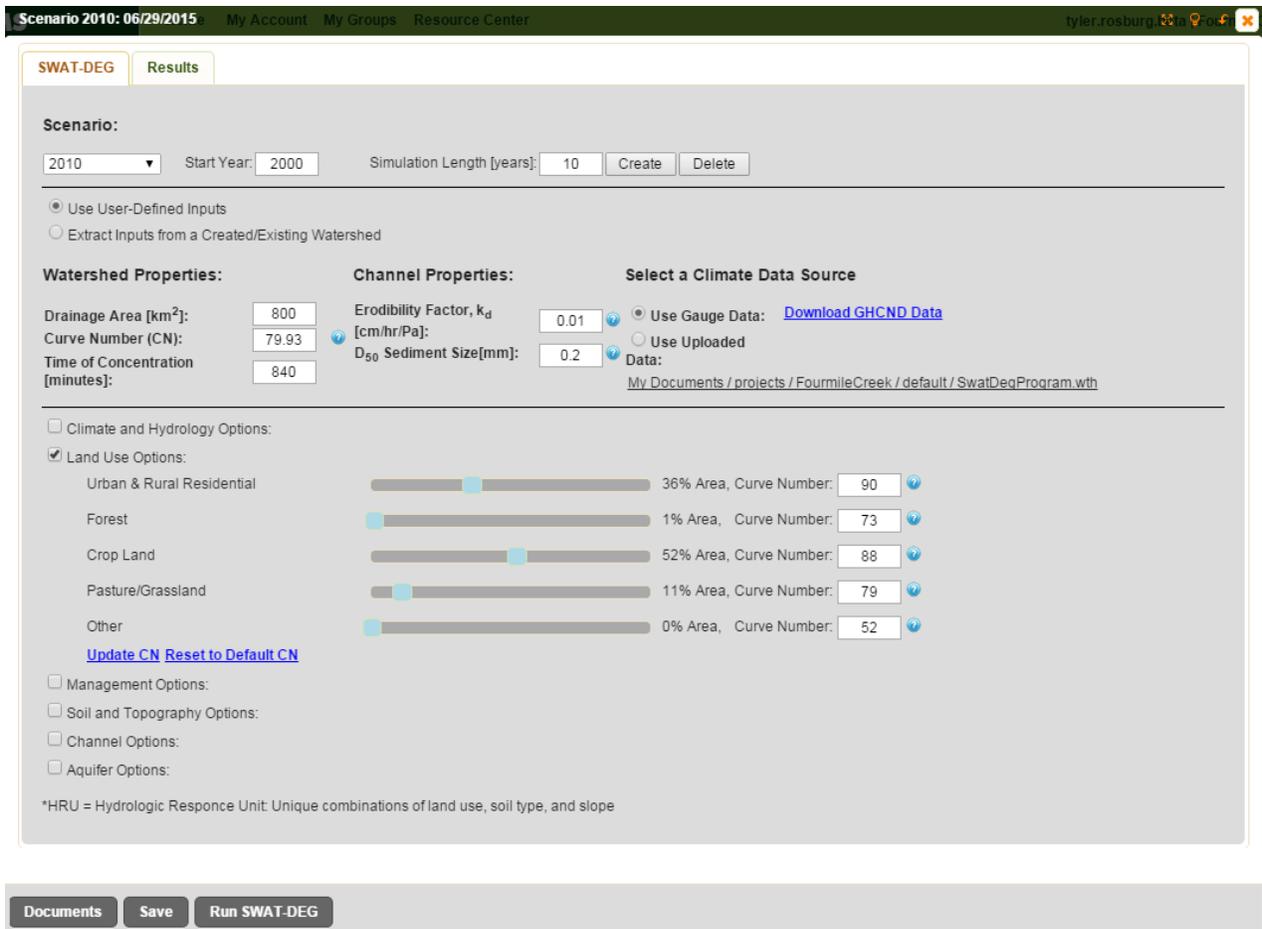
Figure 4-13. eRAMS SWAT-DEG interface.

Following the data input, the user can click "Run SWAT-DEG" to run the model and view the results. The "Results" tab displays the various scenarios the user created and allows users to choose and graph outputs. Outputs can also be downloaded in a variety of formats for post processing. Our investigation into the hydrologic impacts of urbanization for Fourmile Creek suggest that increases in urbanization are projected to cause increases in the magnitude of the FDC across nearly all exceedance levels (Figure 4-14). This demonstrates that historic streamflow records may not be appropriate for future land use conditions.
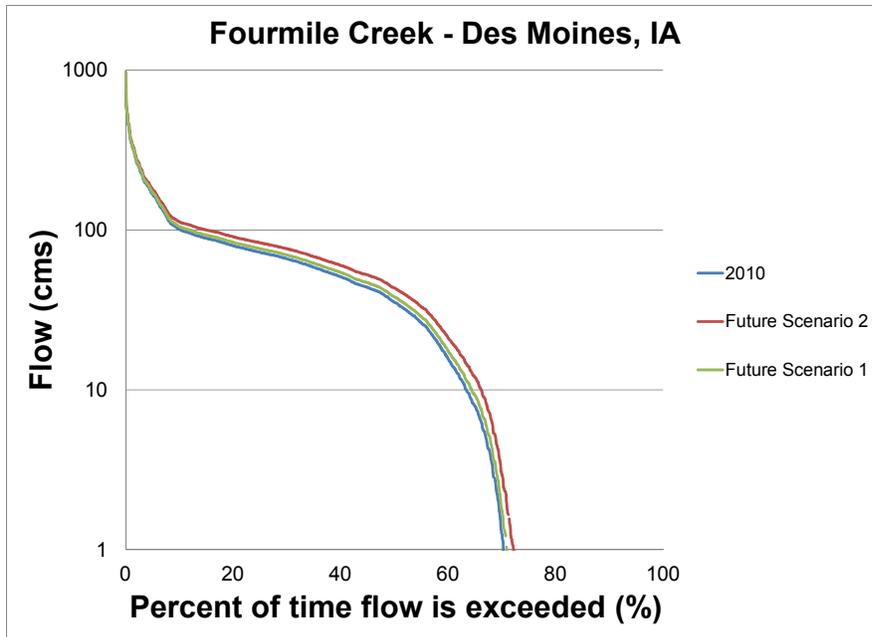
Figure 4-14. Comparison of current and future land use FDCs for Fourmile Creek. Created with data produced by eRAMS SWAT-DEG tool.

4.6.2   Example 2: Rainfall Runoff Modeling of Box Elder Creek (Section 3)

Box Elder Creek is a 750 km² watershed located in northern Colorado and southern Wyoming (Figure 4-15). Because the creek is ungaged, streamflow records are unavailable. Additionally, because the southern portion of the basin is undergoing rapid urbanization, indexing a flow record from a similar and nearby gage is not the best option. This leaves hydrologic modeling as the best remaining option for obtaining a streamflow series at this site.
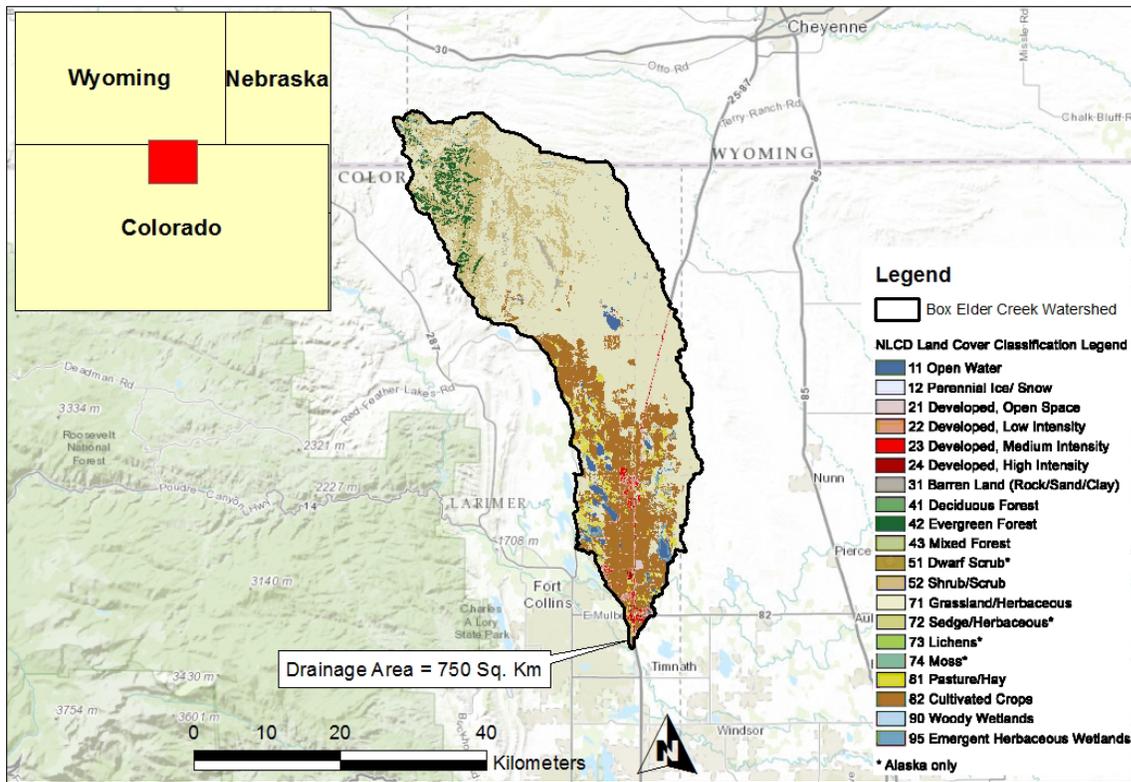
Figure 4-15. Box Elder Creek watershed.

After logging into eRAMS and starting a new SWAT-DEG project, you are required to input watershed properties, channel information, and climate data for the time period of interest. One can populate the watershed properties by extracting data from a user-defined watershed, or can simply enter the data directly if it is known. To obtain climate data, eRAMS allows users to download GHCND data. The required input information for Box Elder Creek is shown in Figure 4-16.
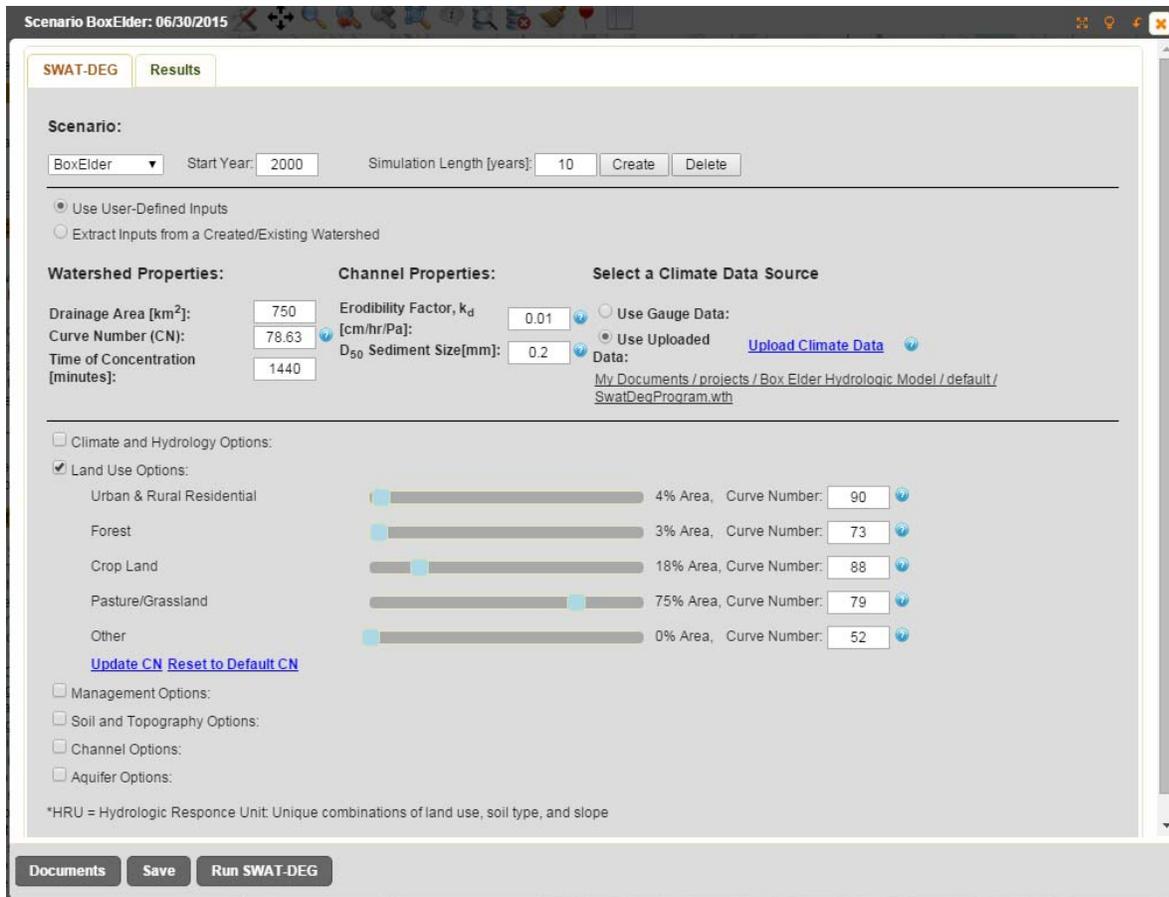
Figure 4-16. eRAMS SWAT-DEG inputs for Box Elder Creek, Colorado.

After fully populating the input screen, the model can be run by clicking "Run SWAT-DEG." This runs the model and launches the output screen. Streamflow data can then be obtained by selecting the appropriate scenario and output parameter and clicking "Graph Output." A plot of the streamflow time series will then be made available as shown in Figure 4-17**.** The start and end of the streamflow time series correspond to the start year and simulation length selected when the scenario was developed. It is important to note that you are required to have climatology data for the entire simulation period.

After running the model, the raw streamflow data can be downloaded by clicking in the upper right-hand corner of the graph and choosing a preferred file format. Currently, streamflow data are only available in millimeters/day. This can be converted to cubic meters per second (cms) by multiplying by the drainage area (m^2) and 86.4. Future versions of eRAMS will do this conversion automatically and provide streamflow in cubic meters per second.
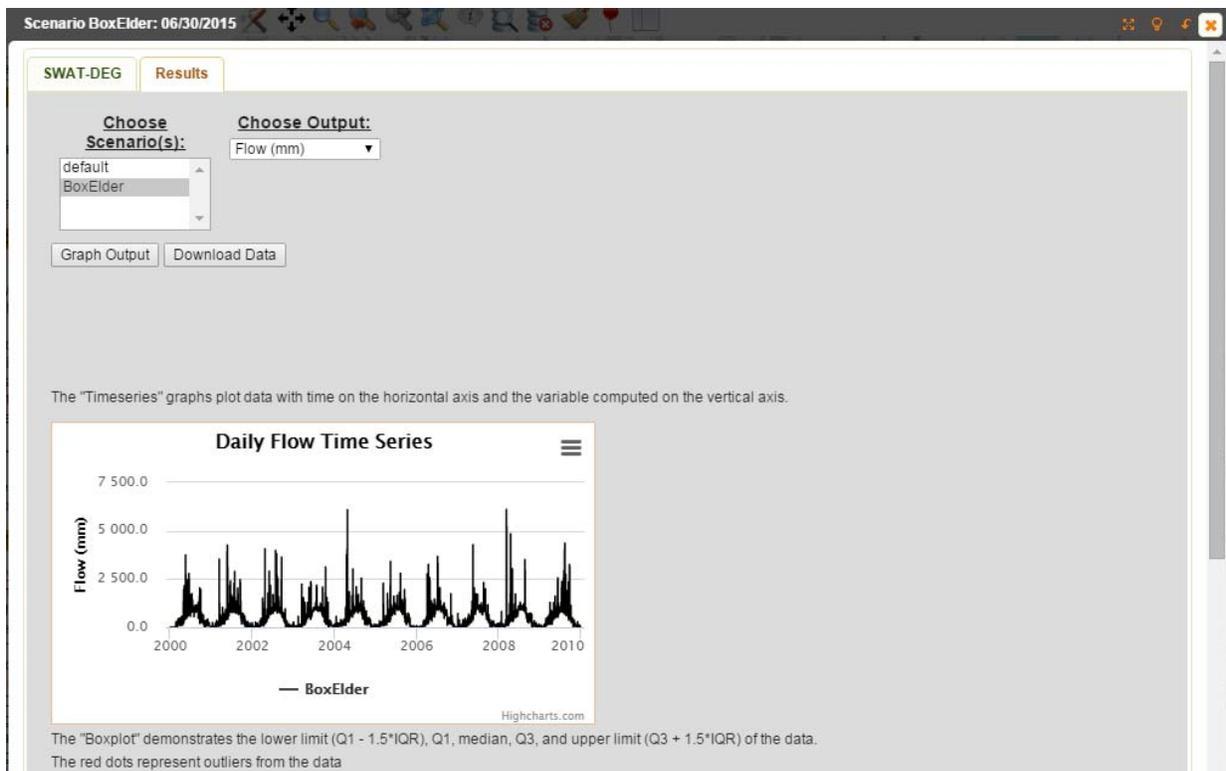
Figure 4-17. Daily series of streamflow for Box Elder Creek.

4.6.3 Example 3: Using eRAMS to Calculate the R-B Index of the Iowa River near Iowa City, Iowa (Section 5)

After signing into eRAMS.com and starting a new "Flow Analysis" project, select your streamflow gage of interest. This can be accomplished by searching for a USGS station by name or keyword, or also by drawing a rectangle or polygon on the map. Once you have selected your gage, click the "Flow Analysis Model" link to launch the application (Figure 4-18).
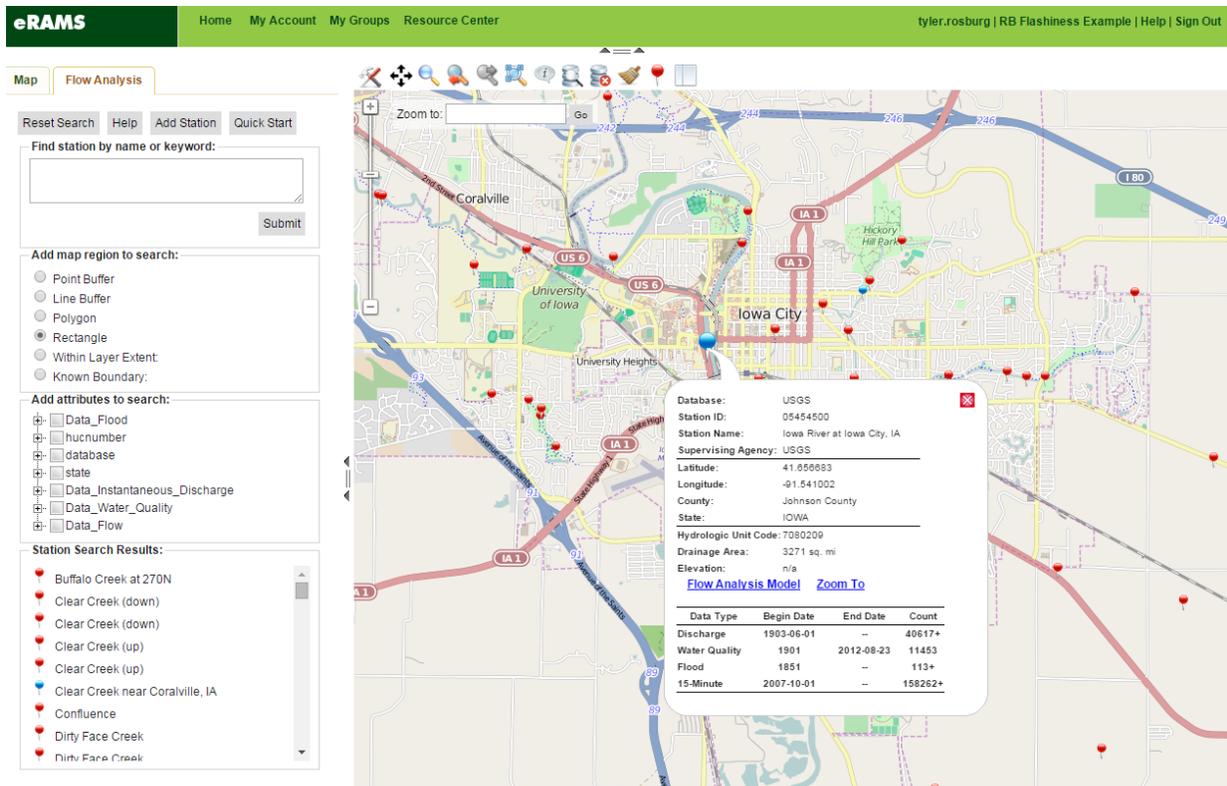
Figure 4-18. Selecting a streamflow gage with eRAMS.

Next, proceed to the "Data" tab and specify your preferred time series, analysis period, and parameter. Finally, click "Run Model" to obtain the output (Figure 4-19).
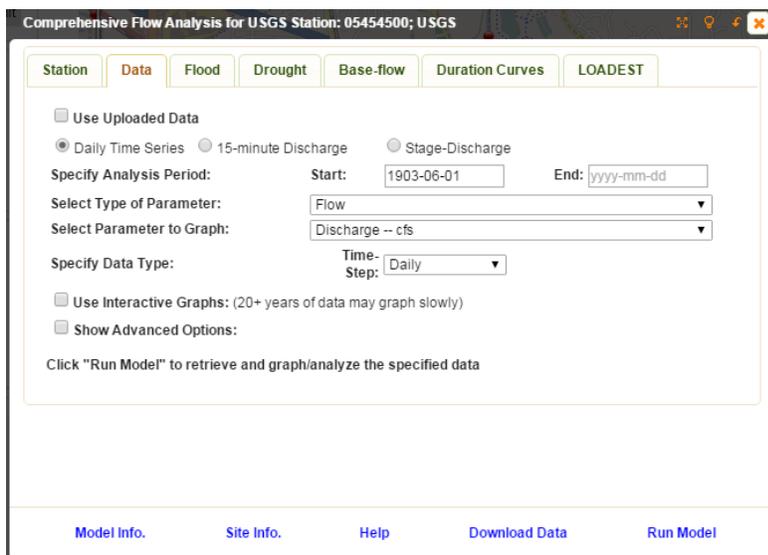
Figure 4-19. eRAMS Flow Analysis Tool input.

Clicking "Run Model" launches the output screen (Figure 4-20). From here we can download a host of streamflow statistics including the R-B Index by clicking "Download Add'l Stats." The statistics are made available on an annual basis as well as for the entire period selected.
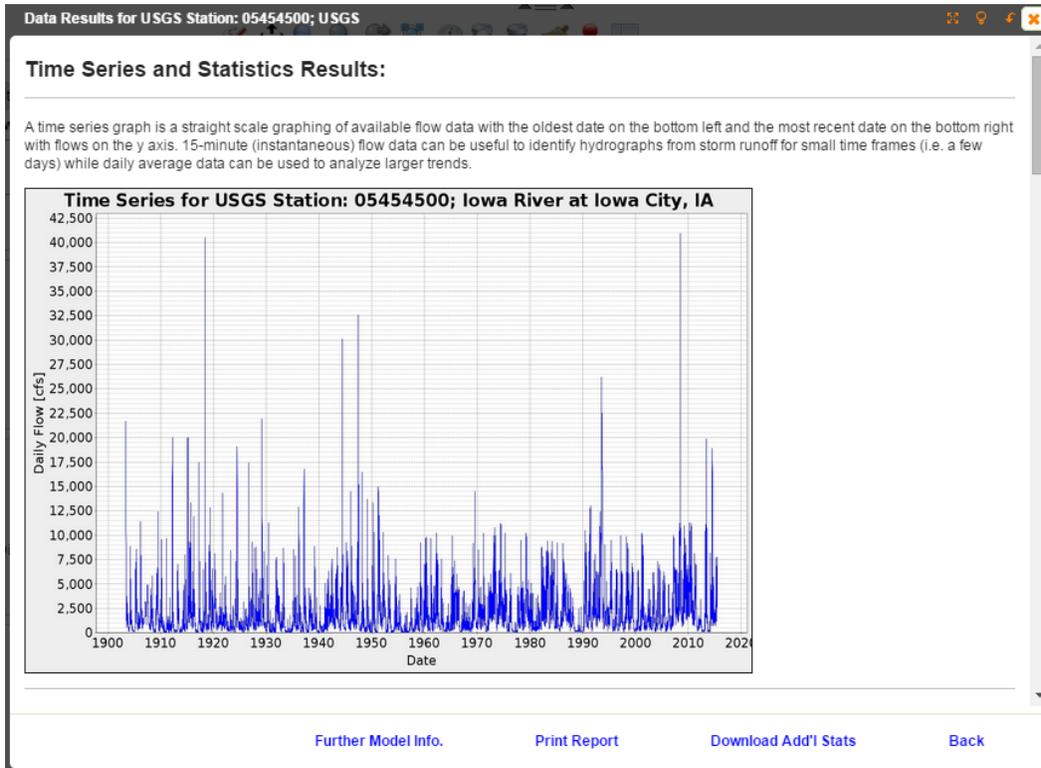
Figure 4-20. eRAMS Flow Analysis Tool output screen.

4.6.4 Example 4: Using the Qs50 Decision Tree for Determining Qs50 for the Iowa River near Iowa City, Iowa (Sections 1 through 5)

The Iowa River near Iowa City, Iowa, is a sand-bed river that drains over 8,400 km^2 of land in northern Iowa (Figure 4-21). Land use in the basin is predominantly agricultural. Because of the basin's large size and agricultural setting, land use is not expected to change significantly in the future.
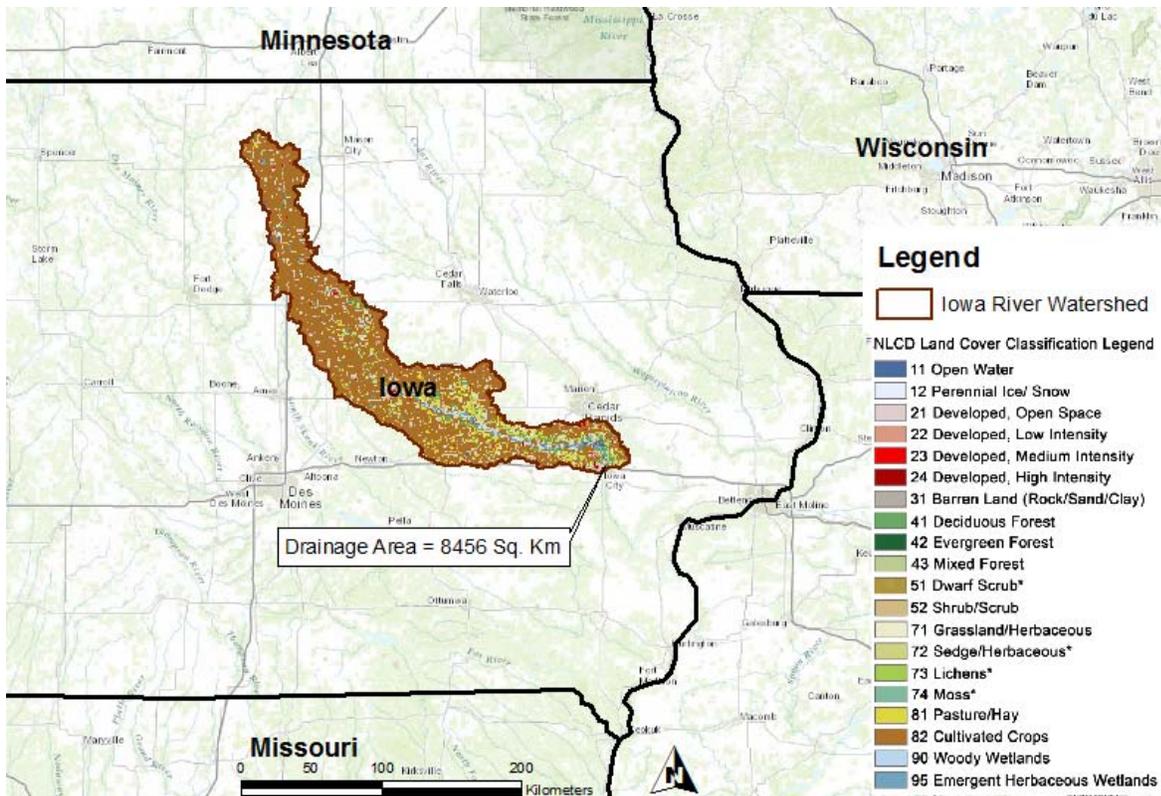
Figure 4-21. Iowa River watershed with 2011 land cover.

Hydrologic Data

Daily-averaged streamflow measurements are available from the USGS beginning in 1903. Because the site is gaged, on-site historical streamflow data should be the first choice source for hydrologic data. However, before these data can be used in the calculation of Q_{s50}, they must be checked for trends.

Stationarity Check

To check for trends in our gaged streamflow record caused by either changes in land use or climate, we will use the Mann-Kendall test (Mann 1945; Kendall 1975) on our annual maximum flow series. The Mann-Kendall test is designed to detect increasing or decreasing trends in data. The test is particularly useful as missing values are allowed and the data do not need to conform to any particular distribution (Gilbert 1987). The Mann-Kendall test statistic (τ) is calculated as shown in Equation (4-15), where n is the total number of data points:

$$\tau = \sum_{k=1}^{n-1} \sum_{j=k+1}^{n} sign(x_j - x_k)$$

(4-15)

where:
$sign(x_j - x_k) = 1$ if $(x_j - x_k) > 0$;
$sign(x_j - x_k) = 0$ if $(x_j - x_k) = 0$; and
$sign(x_j - x_k) = -1$ if $(x_j - x_k) < 0$.

In this example, a p-value of 0.05 was used to identify significant trends. Performing the Mann-Kendall test on our annual maximum flow series yields a Mann-Kendall τ value of 0.108 and a p-value of 0.244. Because τ is greater than 0, there is an upward trend in our flow data. However, because the p-value is greater than 0.05, the trend is not statistically significant. For this reason, we will classify our flow data as stationary and proceed to calculating the R-B Index (Baker et al. 2004).

Richards-Baker Flashiness Index

We calculate the R-B Index using daily streamflow data in Equation (4-15), which results in a R-B Index of 0.089 for Iowa River at Iowa City. This indicates that the Iowa River is not very flashy, likely a result of the large drainage area.

Sediment Data

Suspended sediment transport measurements are available from the USGS for the Iowa River near Iowa City. These measurements taken at discrete points in time can be paired with streamflow data to create a sediment rating curve. The sediment rating curve for the Iowa River is shown in Figure 4-22.

$$Q_s = 2.7e{-}04Q^{1.74}$$
$$R^2 = 0.72$$
$$R_s = 0.87$$
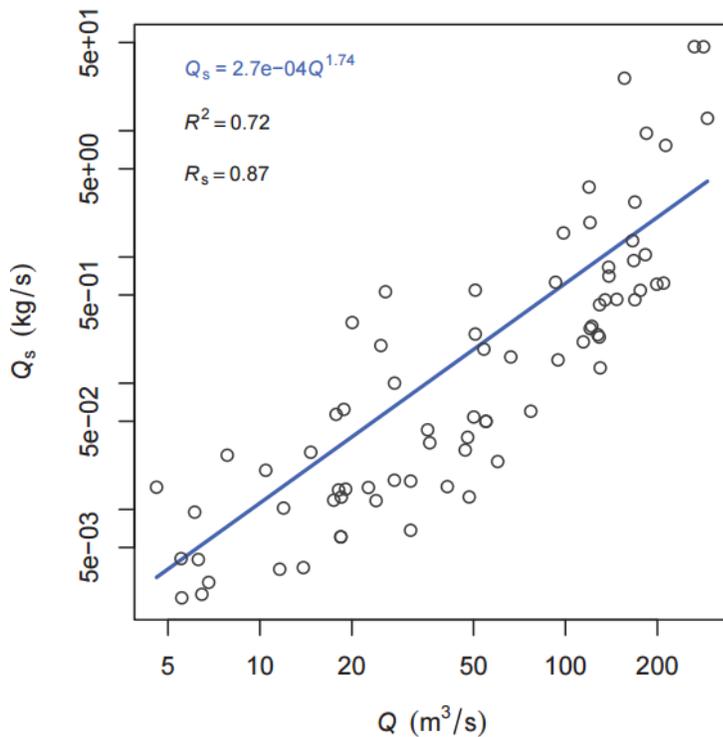
Figure 4-22. Sediment Rating Curve for Iowa River at Iowa City, Iowa.

Streamflow Data Resolution

Percent error in the underestimation of half-load discharge (Q_{s50}) calculated with daily-averaged flow data at bedload sites and suspended-load sites are shown in Figure 4-23.
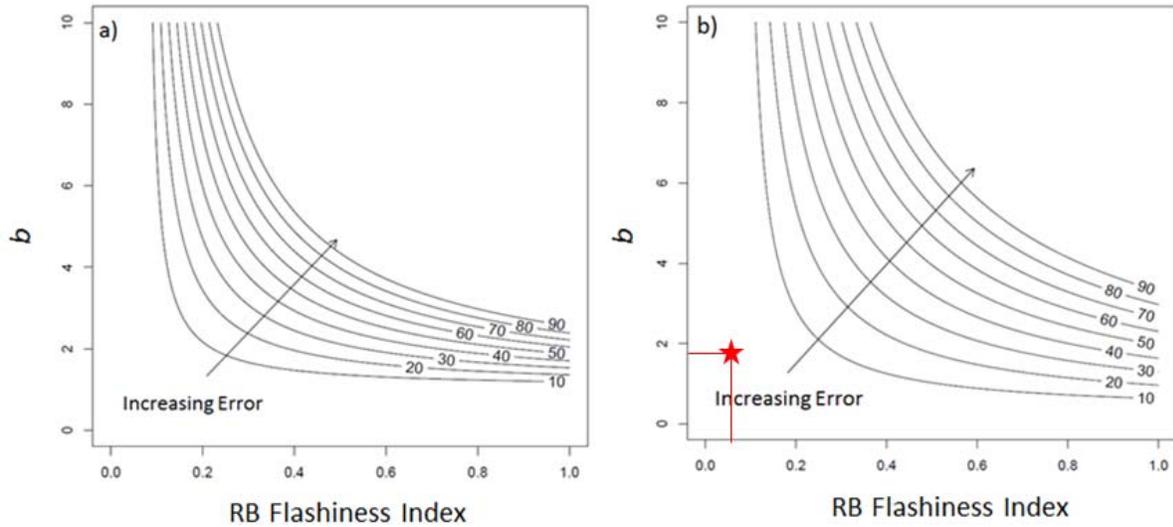
Figure 4-23. Percent error in half-load discharge (Q_{s50}) calculated with daily-averaged flow data at (a) bedload sites and (b) suspended-load sites. For the Iowa River, use of daily-averaged flow data is estimated to cause no more than 10% error (red star).

Calculation of Q_{s50}

Calculation of Q$_{s50}$

Step 1: Order the streamflow data from smallest to largest.

Step 2: Calculate the sediment transport rate for each flow value using the sediment rating curve.

Step 3: Cumulatively sum the sediment transport rates calculated in Step 2 to calculate a cumulative sediment transport rate column.

Step 4: Divide each value in the cumulative sediment transport rate column by the total cumulative sediment transport (the sum of the rates calculated in Step 2) to calculate the percent of cumulative sediment transport associated with each flow.

Step 5: Identify the streamflow associated with 50% of cumulative sediment transport, using linear interpolation if necessary. This is Q_{s50}, the half-load discharge.

Table 4-12 illustrates the calculation of Q_{s50} for this site.

Table 4-12. Sample calculation of Q_{s50}.

	Vector 1	Vector 2	Vector 3	Vector 4	
			Cumulative Sediment	**% of Cumulative**	
Date	**Flow** $[m^3/s]$	**Sediment Transport** $[kg/s]$	**Transport**	**Sediment Transport**	
5/3/2015	3	5.48E-05	5.48E-05	0.05	
5/6/2015	3.3	6.47E-05	1.20E-04	0.11	
5/1/2015	4	9.04E-05	2.10E-04	0.19	
5/7/2015	5.5	1.57E-04	3.67E-04	0.34	
5/2/2015	5.9	1.78E-04	5.45E-04	0.50	Q_{s50}
5/4/2015	6.3	1.99E-04	7.45E-04	0.68	
5/5/2015	8.6	3.43E-04	1.09E-03	1.00	
	Sum	1.09E-03			

 As shown in Table 4-12, this sample calculation of the half-load discharge (Q_{s50}) was found to be 5.9 m^3/s.

Design Hydrology Commensurate with the Geomorphic Setting: Decision Support Tools for Understanding Channel Susceptibility and the Optimum Level of Analysis

In response to DOT requests to include guidance on when simple versus complex approaches are appropriate; this chapter describes three general types of decision support tools that inform the hydrologic design process:

(1) decision tables for relating channel response potential to an appropriate level of design analysis guidance (Section 5.1; Tables 5-1 and 5-2, and Figure 5-1);

(2) a decision table to guide selection of analog reaches (Section 5.2; Table 5-3); and

(3) tool for RGAs of channel instability and susceptibility at stream crossings (Section 5.3; Figures 5-6 through 5-9).

In developing these tools, the research team strived for user-friendly structures (e.g., decision tables or trees) based on our discussions on current practices with state DOTs. The tools described in this chapter are integrated with another decision support tool focused on generating FDCs and performing sediment yield computations (Chapter 4) to provide a general framework for design hydrology (Chapter 6).

5.1 Relating Channel Response Potential to an Appropriate Level of Design Analysis Guidance

This section focuses on a decision support tool that relates the hydrologic and geomorphic context of a channel to a set of design hydrology options detailed in Chapter 6. It is increasingly evident that ecological and geomorphic resistance to human impacts such as urban development and roadways varies across both natural and legacy attributes (Utz et al. 2016). For example, channel enlargement, an inverse measure of geomorphic resistance, has been shown to exponentially increase with watershed imperviousness in the fine-grained channels of southern California (Hawley and Bledsoe 2013), whereas the coarser-bed streams of northern Kentucky exhibit less enlargement (Hawley et al. 2013; Figure 5-1). Furthermore, within settings of equal resistance (e.g., two cobble-bed streams), the likelihood of channel instability increases with increasing erosive energy of the setting (Bledsoe and Watson 2001; van den Berg 1995).
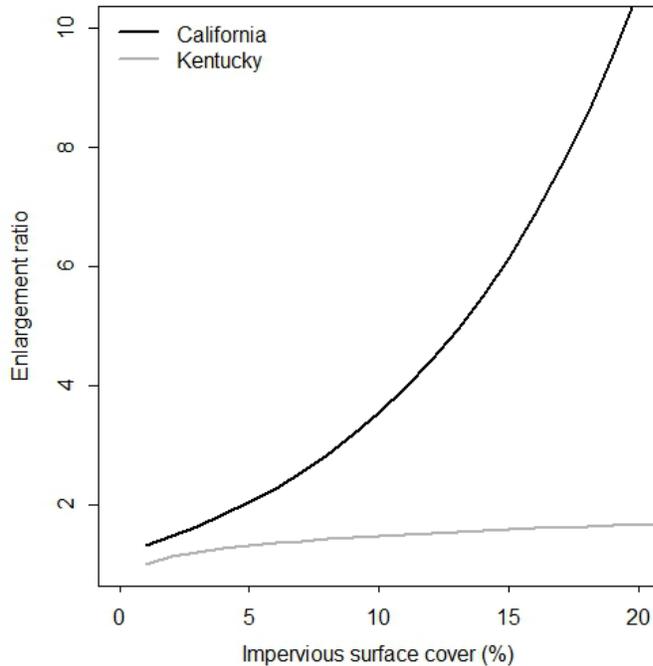
Figure 5-1. Channel enlargement (post-urban cross-sectional area / pre-urban cross-sectional area) varies by stream type and resistance, with southern California streams (n = 66, median particle diameter = 3.8 mm; data from Hawley and Bledsoe (2013)) exhibiting greater susceptibility to channel instability than northern Kentucky streams (n = 88, median particle diameter = 55 mm; data from Hawley et al. (2013)), adapted from Utz et al. (2016).

The recommended framework (Tables 5-1 and 5-2 presented later in Section 5.1.1, and Figure 5-2 presented later in Section 5.1.2) is based on two primary factors: (1) flow variability and (2) channel type (bed material or flow energy relative to bed material). Such a hydrogeomorphic framework allows one to associate a mix of design hydrology tools ranging from the simple to the complex (peak flow only to analog approaches to design approaches based on novel hydrologic metrics developed in this study, e.g., Q_{s50}) to provide a stronger physical basis for designing stable channel geometry at stream crossings. Given the reliance on a single discharge to represent the relative energy of the system in the tools presented below, we also incorporate flow flashiness as a previously discussed surrogate for the relative erosivity of the flow regime (see Section 2.1).

5.1.1 Identifying Hydrogeomorphic Types that Require Different Design Hydrology Approaches

The first step of the framework is applying a simple classification that integrates hydrologic regime (variability and flashiness) with channel type in the four degrees of SRP (Table 5-1). Dominant bed material (or stream power relative to bed-material size as discussed below) is used as the primary geomorphologic indicator of inherent SRP because it serves as a simple proxy for mode of sediment transport and sensitivity to inflowing sediment load. These ratings of Low to Very High can then be related to different design hydrology methodologies such that the depth of analysis is commensurate with the level of channel lability and response potential.

106

Table 5-1. SRP decision table used to define classes corresponding to different design hydrology strategies based on bed material and flow regime flashiness.

Bed Material[a]	Flow Regime Flashiness[b]		
	R-B Index $\leq$ 0.2	0.2 < R-B Index $\leq$ 0.5	0.5 < R-B Index
Boulder / resistant hard pan	Low	Low	Medium
Armored cobble / coarse gravel with assorted sizes tightly packed, overlapping, and possibly imbricated; most material >4 mm (0.16 in.); F_s < 20%, mostly boulders/ cobbles/coarse gravel	Medium	Medium	High
Transitional – unarmored containing moderately packed to loose assortment with 20% < F_s < 50%.	Medium	High	Very High
Live bed – very loose assortment with no packing; large amounts of material <4 mm (0.16 in.); F_s > 50%, mostly sand and finer.	High	Very High	Very High

[a]F_s = approximate fraction of sand in bed sediments.
[b]For braiding and/or rapid urbanization (~10% increase in urban land cover per decade) move to next higher category.

A physically robust variable that is missing from Table 5-1 is flow energy relative to boundary material resistance. A channel with relatively large bed material and flow energy could have large sediment supply and be more responsive to its range of inflowing water and sediment loads than a channel with fine bed material, low sediment supply, and a very stable flow regime that is fed by groundwater. An alternative and more physically-based approach to the simple approach depicted in Table 5-1 is to include flow energy relative to dominant bed grain size. Recent process-based stream classifications have used hydraulic parameters (most notably dimensionless shear stress (τ^*) referenced to the median grain diameter of the channel bed (D_{50})) to relate flow and bed material to not only channel form but also potential instability and sensitivity to perturbations in inflowing water and sediment (Church 2006). Recent research also indicates that dimensionless specific stream power (ω^*), a robust predictor of sediment transport capacity (Eaton and Church 2011), has more information content than τ^*, and is less sensitive to variability in slope and grain size compared to τ^* (Ferguson 2012). Dimensionless specific stream power is defined as:

$$\omega^* = \frac{\omega}{\rho[g(G-1)D_{50}]^{3/2}} \tag{5-1}$$

where:
ω = specific stream power [W/m^2] ($\omega = \rho gQS/w$), where: ρ = density of the fluid mixture [kg/m^3], g = gravitational acceleration [m/s^2], Q = median annual peak flow (Q_2) [m^3/s], S = channel slope [m/m], and w = channel top width [m];
G = specific gravity of sediment; and
D_{50} = median grain size of the bed material [m].

A very important advantage of using dimensionless specific stream power (ω^*) to represent relative flow strength is that ω can be estimated from simple measures of peak discharge (for example Q_2), channel width (w), and gradient (S) of the stream ($\omega = \rho gQS/w = \rho gqS$, where q = water discharge per unit width [m^2/s]), whereas estimates of τ^* require that a flow resistance equation be employed to estimate

the water depth. This means that ω^* can be determined directly from the continuity equation, while it is necessary to invoke a flow resistance equation to relate τ^* to discharge, thereby introducing additional uncertainty associated with the chosen flow resistance equation. This is the basic practical difference between a stream power-based approach and a shear-stress based approach (Eaton and Church 2011). In addition, the threshold of incipient particle motion is relatively constant around a ω^* value of 0.1 and shows less variability than τ^* across a range of grain sizes and channel slopes (Ferguson 2012).

These attributes of ω^* bode well for its use as a single physical factor that is relatively robust in distinguishing between different hydrogeomorphic settings that require different design hydrology approaches. For example, the decision table in Table 5-1 can be modified to use ω^* in conjunction with flow variability as a more quantitative means of delineating among hydrogeomorphic settings that differ in response potential, lability, and sensitivity to inflowing sediment load (Table 5-2).

Table 5-2. SRP decision table used to define classes corresponding to different design hydrology strategies based on dimensionless specific stream power at the median annual flood (Q_2) and flow regime flashiness.

Flow Power at Q_2 Relative to Bed Material (ω^*)	Flow Regime Flashiness		
	R-B Index $\leq$ 0.2	0.2 < R-B Index $\leq$ 0.5	0.5 < R-B Index
ω^* << O[0.1]	Low	Low	Medium
ω^* ~ O[0.1]	Medium	Medium	High
ω^* ~ 0.3 to O[1]	Medium	High	Very High
ω^* ~ O[1] or higher	High	Very High	Very High

Abbreviations: O = on the order of; and ω^* = dimensionless specific stream power.

5.1.2 Relating Hydrogeomorphic Types and Levels of Channel Response Potential to Hydrologic Design Strategies

Ultimately, different hydrogeomorphic types and levels of channel response potential must be cross-referenced with a set of hydrologic design strategies that reflect a spectrum of inherent complexities and risks. Figure 5-2 presents a framework for determining an appropriate level of analysis for a stream channel design. This guidance takes the form of a decision table that takes into account the SRP and whether or not an acceptable analog channel is available. The decision table is meant to help answer the following questions: (1) What level of hydrologic analysis should be undertaken? (2) Is it necessary to perform some sort of sediment transport analysis, and if so, what type of analysis is needed? (3) What domain (i.e., how far upstream and/or downstream from the project location) should be considered in the analysis? (4) When should an analog channel be used as a basis for design? The fundamental philosophy underlying this analysis decision table is that, as SRP increases, it becomes necessary to conduct a deeper analysis over a larger area of influence.

Potential analyses fall into three categories: (1) hydrologic analysis, (2) sediment transport analysis, and (3) analog analysis. For channels with low SRP, the "hydrologic analysis" for a channel design project can be a simple process of using gage data or regression equations to determine the peak flow that the channel must convey. For channels that are expected to be more sensitive to disturbance, however, it is important to account for the full range of flows (and their effects on sediment transport and channel morphology), so the full FDC should be considered.
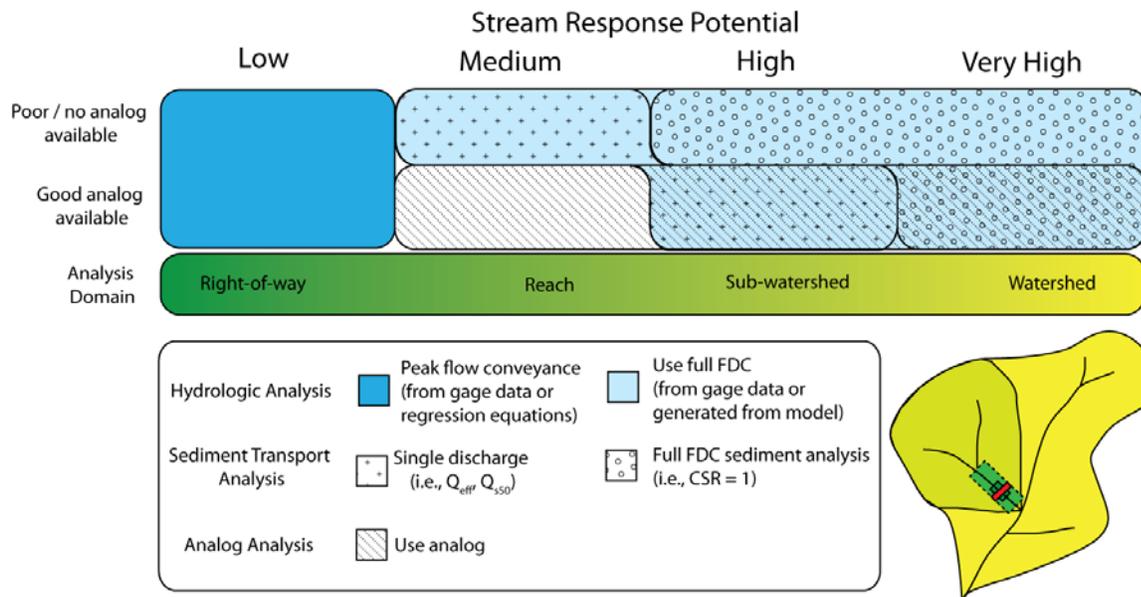
Figure 5-2. Decision table providing guidance on the level of design hydrology analysis. Note that if a field rapid geomorphic assessment (RGA) indicates High or Very High susceptibility and response potential in the design reach, then shift to the next higher level of stream response potential (SRP) and design analysis.

The level of "sediment transport analysis" called for in the decision table is also a function of the SRP. In general, channels with low response potential are assumed to be largely insensitive to disturbance, so it is unlikely that any sediment transport analysis is necessary for those cases. However, channels that are more susceptible to disturbance are likely to benefit from sediment continuity considerations. For channels with intermediate response potential, this may involve a sediment transport analysis resulting in a single design discharge (e.g., effective discharge or calculation of the Q_{s50}), whereas channels with greater response potential may warrant analysis resulting in a full design FDC (e.g., a design capacity supply ratio, CSR = 1).

In general, for all cases except those where the SRP is Low, if an appropriate "analog" channel is available, it is suggested that insight from that analog be incorporated into the analysis. Because an analog can help inform channel design, the reliance upon deep hydrologic and sediment transport analyses is relaxed when an appropriate analog is available.

The "analysis domain" is schematized in the cartoon watershed in the lower right-hand side of Figure 5-2, which suggests that the spatial domain that should be considered in a design project increases as the SRP increases. Thus, at locations with a low SRP, simply considering the right-of-way might be sufficient. However, as the potential instability of the channel increases, it becomes necessary to consider larger spatial areas due to the increased likelihood of upstream (e.g., propagating headcuts) and downstream (e.g., incision, aggradation, or widening) feedbacks.

Ultimately, a set of analysis tools is associated with each of the design approaches depicted in Figure 5-2 as described in Chapter 6. For example, the intermediate design approach for a moderately responsive channel in Figure 5-2 relies on $Q_{1.5}$ as a proxy for Q_{s50} in bedload channels and thus only requires a peak flow estimate. In contrast, a flashy, fine-grained system with high response potential would require determination of a FDC as input into an effective discharge type analysis in order to determine Q_{s50} and the channel geometry that best approximates sediment continuity across the entire FDC.

109

5.2 Identifying and Evaluating the Utility of Upstream Supply / Analog Reaches as Part of the Design Process

The concept of using analog reaches as a template or blueprint for design is a staple of stream-restoration practice. As the science of predicting the river form is still evolving, analog reaches offer a template of potentially stable dimensions for regionally similar stream settings. As described in this report, the use of analog reaches (also referred to as the 'analogy method' (see NRCS (2007)) is just one of multiple channel design options. To date, the analogy method has sometimes been used recklessly in practice as streams from different watersheds and even different physiographic regions with disparate hydrologic and sediment supply characteristics have been used to define channel geometry in dissimilar settings. This section introduces a decision support tool for identifying upstream analogs and supply reaches that are very similar in terms of key criteria including the valley setting, boundary conditions, and inflowing loads of water and sediment. When these criteria are met, the analog reach may provide a fundamentally important line of evidence that complements and can be integrated with all design hydrology approaches.

5.2.1   Decision Support Tool for Identifying Upstream Analogs and Sediment Supply Reaches

Identifying and analyzing an analog reach is a challenging task. There are a number of interacting factors which must be considered in the selection process. In an attempt to streamline the selection process, these factors have been translated into a series of questions (Tables 5-3 and 5-4). The first four questions in Table 5-3 are *required*, if the analyst is unable to find an appropriate analog reach with a similar drainage area, similar channel type, similar hydrology, or that is stable, then an analytical design method is recommended. The second set of questions are *important* (Table 5-4); hence, it is recommended that at least 6 of 8 are satisfied to ensure the analog reach is an appropriate analog. If the analog reach is not on the same river, then the first question does not apply and that criteria are not met.

Table 5-3. *Required* **questions for analog reach selection. The analog reach must meet 100% (4/4) criteria.**

Topic	Question	Criteria Met if:	Context	References
Flow Regime	Do the sites have similar drainage area (within 20%)?	Answer to question is 'yes.'	Rivers and streams are scaled in size by their drainage areas.	• eRAMS online tool for delineation (simplified version in development) • StreamStats online tool (USGS 2012) • Arc Hydro Tools ArcGIS Toolkit
Flow Regime	Is the hydro-climatic system the same (i.e., how and when does the precipitation come: snow, winter rain, convective rain, monsoon)?	Answer to question is 'yes.'	This is often less troublesome if the analog reach is close to the restoration reach, but can become an issue in mountainous areas with strong orographic effects (i.e., wet and dry side of the mountains)	• Cheng et al. (2012) • Poff (1996) • Reidy Liermann et al. (2012) • Sawicz et al. (2014)

Topic	Question	Criteria Met if:	Context	References
Channel Type	Are the channel types the same?	Answer to question is 'yes.'	Target channel type represents: (1) prevailing historical channel type that was previously stable (diagnose why departure occurred) in that location under current land use; OR (2) channel type is stable under same current land use, flow, and sediment supply in analog reach.	• Table 5-2 • Church (2006) • Lagasse et al. (2012) • Montgomery and Buffington (1997) • Rosgen (1994)
Stability	Is the analog reach largely stable?	Answer to question is 'yes.'	CEM stage I or V per Schumm et al. (1984; Figure 5-3) banks stable, no evidence of trends in aggradation / degradation, planform change, etc. over engineering time scales.	• Lagasse et al. (2012) • Schumm et al. (1984) • Hawley et al. (2012a)

Again, we define 'stable' after Biedenharn et al. (1997): "*In summary, a stable river, from a geomorphic perspective, is one that has adjusted its width, depth, and slope such that there is no significant aggradation or degradation of the stream bed or significant planform changes (meandering to braided, etc.) within the engineering time frame (generally less than about 50 years).*"

Table 5-4. *Important* **questions for analog reach selection. The analog reach must meet 75% (6/8) criteria.**

Topic	Question	Criteria Met if:	Context	References
Location	If on the same river, is the analog reach upstream of the project reach? (If analog reach is not on the same river, that criterion is not met).	Answer to question is 'yes.'	Restoration is often in response to disequilibrium (or instability), thus if instability exists at the restoration site, it is likely that this instability may persist downstream.	• Learn more about the National Hydrography Dataset Viewer at http://nhd.usgs.gov/index.html
Flow / Sediment Regime Alterations	Are there any noteworthy tributaries, dams, or intervening flow augmentations or extractions?	Answer to question is 'no.'	Tributaries, dams, and flow augmentations or extractions can initiate changes in the flow and sediment regimes.	• Learn more about the National Hydrography Dataset Viewer at http://nhd.usgs.gov/index.html

Topic	Question	Criteria Met if:	Context	References
Valley Type Energy	Is the valley stream power (defined as the $S_v * Q_2^{0.5}$, where S_v = valley slope and Q_2 = 2-yr return interval discharge) similar (within 20%)?	Answer to question is 'yes.'	Stream power is the stream's ability to do work including the entrainment and transport sediment.	Desktop estimates for the required parameters can be estimated using: • Valley slope ➔ Google Earth (see link for more details) and • Q_2 (for most locations in the U.S.) ➔ StreamStats (USGS, 2012) • Bledsoe and Watson (2001) • van den Berg (1995)
Valley Type Lateral Constraints	Are the lateral constraints (i.e., the influence or connectivity of the valley walls) similar? (Is the ratio of floodplain width to channel width within 30% between the analog and project reaches?)	Answer to question is 'yes.'	The narrower and steeper the valley walls, the more connection (and influence) they will have on a river's planform, sediment inputs, and ability to self-adjust.	• Desktop estimates can come from Google Earth imagery • Nanson and Croke (1992) • Whiting and Bradley (1993)
Flow Regime	Same hydrologic flashiness (within 30%)?	Answer to question is 'yes.'	Flashiness (i.e., the frequency and rapidity of short term changes in streamflow) influences the stability of a river channel.	• Estimates for gaged sites can be found using the Flow Analysis toolkit in eRAMS (variable currently in downloadable data summary) • Baker et al. (2004)
Land Use	Are the extent and nature of land use (e.g., curve number) similar between the two watersheds (within 20%)?	Answer to question is 'yes.'	Watershed land use influences both flow regime and sediment supply in a river.	• Can use SWAT-DEG tool in eRAMS (currently in beta version) to estimate composite curve number for a watershed • NRCS (1986)
Geologic Setting	Analogous physiographical region/geologic setting with respect to topography / valley slopes, soil types, and vegetation cover?	Answer to question is 'yes.'	These watershed characteristics influence the magnitude and timing of runoff.	• Booth et al. (2010) • Reid and Dunne (1996) • Vigil et al. (2000)

Topic	Question	Criteria Met if:	Context	References
Bed Surface Sediment Characteristics	Are the bed surface grain size distributions similar (do not differ by more than ± one half phi class for D_{50} and D_{84})	Answer to question is 'yes.'	The bed surface grain size is linked to sediment supply (e.g., Dietrich et al. (1989)).	• Bunte and Abt (2001)

INCISED CHANNEL EVOLUTION PHASES
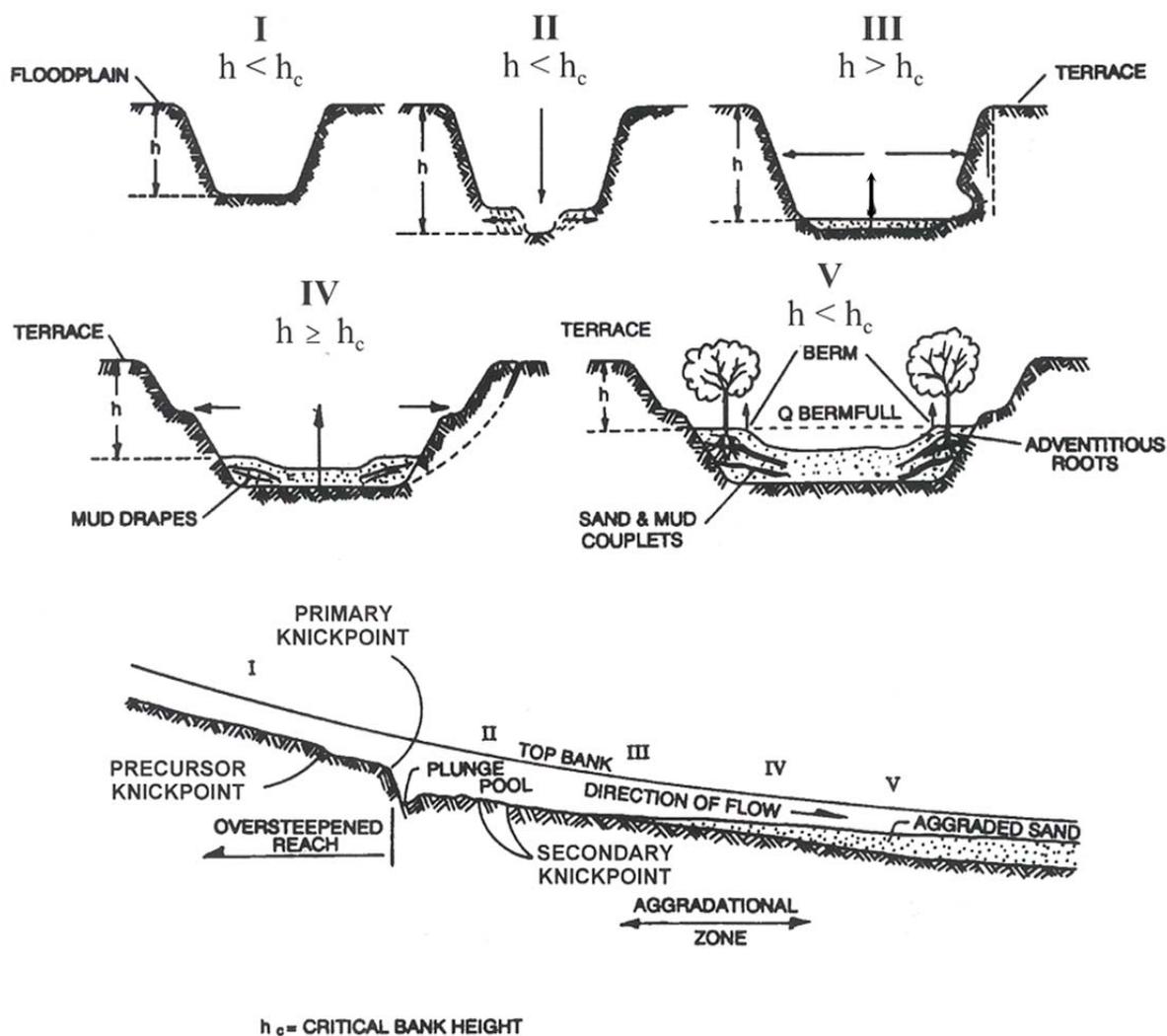
Figure 5-3. Incised Channel Evolution Sequence (after Schumm et al. (1984)).

113

5.2.2 The Risks of Misapplying the Analog Reach Approach

Informing a design with a survey of other stable streams from a region has been a standard of the restoration practice for many decades. Analog reaches can be extremely valuable to a designer, particularly when they are from similar geomorphic settings within the region (i.e., Tables 5-3 and 5-4). However, when used without regard for differences in key factors such as sediment supply, the geomorphic setting, flashiness, and watershed urbanization, the analog reach approach can be prone to failure. Some of the most notable abuses have come in the form of 'regional curves' which plot the cross-sectional geometry of a handful of stable streams from a region against their respective drainage areas (Figure 5-4) and often become the channel restoration sizing equation for any stream in a region or state without regard for the standard errors inherent in the models or their relatively limited datasets (e.g., 15 sites in the outer Bluegrass Ecoregion of Kentucky (Brockman et al. 2012); 50 sites for all of Ohio (Sherwood and Huitger 2005)). Rather than attempting to find an analog channel in a nearby catchment from a similar hydrogeomorphic setting, the regional curve approach has resulted in streams being sized based on the average stream size for the associated drainage area from the entire ecoregion or state. But just as designers know that channel slope has an extremely strong influence on its hydraulics, the same can be said for its geomorphic stability and the associated stable cross-sectional geometry. A flat channel typically needs a much deeper cross section to transport the same sediment load as a steep channel with the same load. Because regional curves are only a function of drainage area, the role of channel slope in shaping the geometry is inherently overlooked.

Relationship of bankfull area to drainage area at different levels of catchment imperviousness in Kentucky, USA
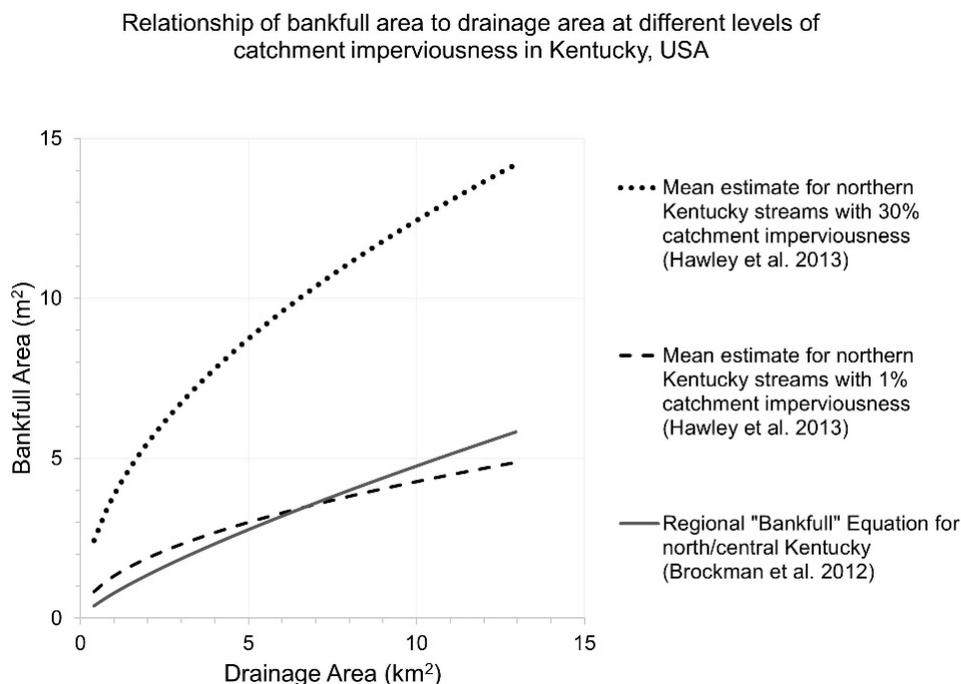
Figure 5-4. Bankfull area predictably increases with drainage area within similar regions such as north/central Kentucky; however, watershed urbanization can induce channel instability that can enlarge unarmored channels by ~two- to three-fold compared to undeveloped watersheds (adapted from Smith et al. (2016)).

The regional curve approach can be particularly problematic in urban channels. For example, in an analysis of 88 samples from northern Kentucky, Hawley et al. (2013) showed that the size of channels in undeveloped watersheds tracked reasonably well with the regional equations from Brockman et al.

(2012), which used 15 sites from a broader region (including northern Kentucky). However, the northern Kentucky dataset showed that watersheds with 30% impervious area could induce trajectories of channel instability that correspond to a ~two- to three-fold increase in channel size for a given drainage area compared to an undeveloped catchment (Figure 5-4). Regional curve designs that did not adequately account for the enlargement phenomenon evident in such urban settings (e.g., via two-stage channel designs and/or armoring commensurate with the increased erosive power of the urban flow regime) could be inherently prone to failure, as has been documented in numerous studies (e.g., Smith and Prestegaard (2005)).

Despite these challenges, the analog reach approach can have great utility when designers can identify an analog reach in the field that is truly representative of their design reach, There are numerous factors to consider when screening for an appropriate analog reach (Tables 5-3 and 5-4), which can make finding an ideal analog reach challenging, particularly in regions with expansive urbanization. It may not always be feasible to identify a suitable analog reach, which is why the design decision table (Figure 5-2) can accommodate designs that lack an appropriate analog. However, an appropriate analog can be very informative of the types of restoration strategies and channel forms that can be functional in a given setting. Particularly on more susceptible systems, analogs can add a degree of confidence when model output designs align with what one can see as being already functional in the field in a good analog reach.

5.2.3   Selection of a Sediment Supply Reach

Crossing designs rarely have the luxury of having sediment transport monitoring data for their site. Consequently, the industry standard approach is to develop a design that matches the sediment transport capacity of the upstream reach. By matching the ability of the upstream reach to transport sediment, the crossing design should inherently be able to transport the sediment load that is delivered to it. Fundamental to this approach is the ability to select an upstream reach that is truly representative in characterizing the long-term sediment supply. The dynamic nature of fluvial systems can make this task challenging to even the most well-trained designer.

This task can be especially confounded in urban/suburban settings, which often include numerous crossings such as roadways (Chin and Gregory 2001) or other infrastructure that can serve as vertical channel hardpoints similar to natural bedrock or engineered grade control structures (Hawley et al. 2012a). These artificial hardpoints can mask potential system imbalances of energy and resistance by creating a vertical limit to channel incision. Even more importantly, in regards to channel design, they can bias the bed-material composition in the vicinity of the crossing, artificially fining the upstream reach and coarsening the downstream reach relative to a reach further removed from the influence of artificial grade control and hydraulic constrictions (Figure 5-5).
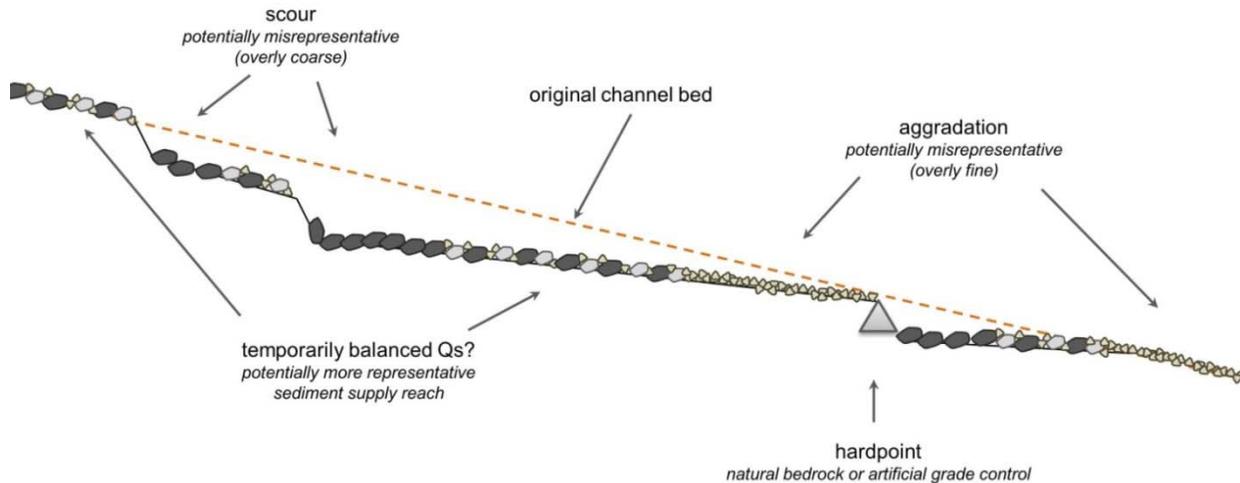
Figure 5-5. When selecting the sediment supply reach, the designer should use the reach or subreach that is most representative for sediment continuity. Avoid scour areas immediately downstream of headcuts or hardpoints, as well as aggradational areas immediately upstream of hardpoints. Subreaches that appear to be transporting their bedload without incision or aggradation (even temporarily) are more representative than segments that are more clearly downcutting or aggrading.

Given the high sensitivity of sediment transport models to grain size (e.g., Meyer-Peter and Müller (1948) and Wilcock and Crowe (2003)), a poorly-selected sediment supply reach would inevitably have an adverse influence on the effective discharge calculation and crossing design. For example, Hawley et al. (2012b) documented substantial fining of the bed-material gradation in a reach immediately upstream of a channel hardpoint (i.e., VRN-C, Figure 5-6), negatively biasing the flow that corresponded to the critical shear stress for incipient motion by an order of magnitude from 5% of Q_2 at VRN-C compared to 50 to 54% of Q_2 at the more representative reaches within the analysis domain. Such broad discrepancies that could be introduced from poor site/reach selection could negatively affect both the shape of the sediment-discharge rating curve, and likely the estimate of Q_{eff}.
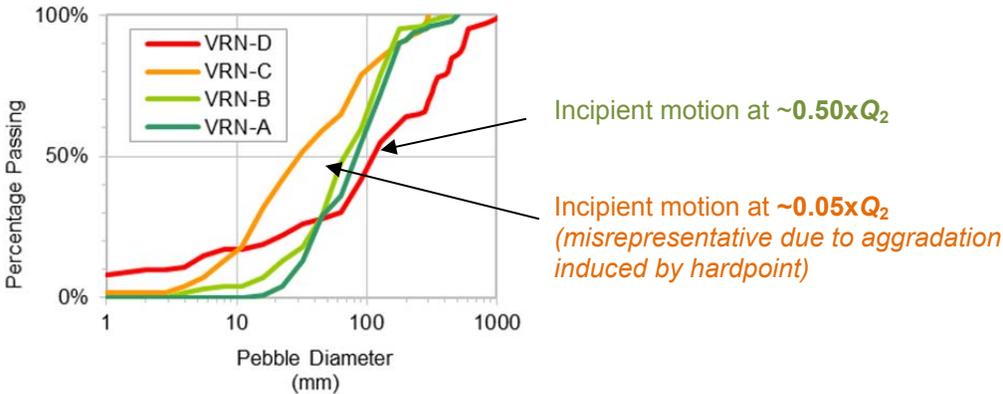
Figure 5-6. Bed-material gradations from four hydrogeomorphically-unique reaches along a 2-km analysis domain in an urban catchment in northern Kentucky (adapted from Hawley et al. (2012b)). Site VRN-C was substantially finer than the more representative reaches due to the proximity of a downstream hardpoint that induced deposition. In contrast, the upper tail of site VRN-D was influenced by active incision (CEM II and III), resulting in bed coarsening in the upstream-most portion of the analysis domain compared to more representative reaches (VRN-B and VRN-A).

We suggest the following approaches to reduce the risk of mischaracterizing the sediment supply reach:

(1) **Find an equilibrium reach** (even if it is short and/or temporary): Even in cases where the upstream sediment supply reach is currently unstable, attempt to select a subreach that is closest to sediment continuity, such as a reach between an upstream degradational zone and a downstream aggradational zone (Figure 5-5). A subreach that appears to be passing the sediment supply without substantial downcutting or aggradation, even if the relative equilibrium is temporary, is more likely to be representative of the sediment supply than a subreach with active incision, widening, or aggradation.

(2) **Collect data from multiple subreaches**: Streams with existing infrastructure crossings, particularly in an urban/suburban setting may not have an ideal reach or subreach that is truly representative of the long-term sediment supply. Collecting geomorphic data (bed material and channel geometry) from multiple subreaches reduces the risk of being solely dependent on what might otherwise be an outlier in a broader sample size (e.g., VRN-C in Figure 5-6).

(3) **Consider using multiple subreaches in modeling**: Fluvial systems are increasingly thought of as processes in time as opposed to things in space. Complex response sequences associated with headcutting, geotechnical mass wasting, and aggradation are likely to deliver episodic pulses of sediment that are challenging to represent using a static sediment supply reach. Compounding the uncertainty is the potential for future land use change and its associated effects on discharge and sediment regimes. Computing analytical CSR designs from multiple sediment supply reaches might facilitate a design selection that maintains sediment continuity under multiple sediment supply regimes.

(4) **Take proactive measures in final design commensurate with the setting susceptibility**: Even the best designs for sediment continuity can be undermined by factors that designers cannot control (e.g. installation of a poorly designed infrastructure crossing upstream that creates a sediment supply bottleneck or an impact downstream that induces headcutting that migrates upstream to the crossing location). Incorporating precautionary controls in higher risk settings, such as buried grade control structures, can reduce the risk of downcutting that might otherwise be induced by future factors that are outside the control of the design project.

5.3 Decision Support Tool for RGA of Channel Instability and Susceptibility

Stream instability risk is directly linked to structural risk at stream crossings. In performing field reconnaissance for design hydrology, there are often opportunities to simultaneously assess other risk factors. In this section, we describe a decision support tool for RGAs of channel instability and susceptibility at stream crossings that proceed concurrent with the hydrologic design process. Although we did not formally ask questions on the use of RGAs as a component of the design hydrology process in our practitioner survey, conversations with practicing engineers and anecdotal reports indicate that implementation of existing RGA tools that have been sanctioned for stream crossings (e.g., Johnson et al. (1999) as described in HEC-20 (*Hydraulic Engineering Circular No. 20*, Lagasse et al. 2012) is not widespread in practice. Therefore, this project reviewed existing RGA tools and focused on potential opportunities for streamlining and simplifying these tools with the aim of making them more likely to be adopted in practice.

5.3.1   Background on RGAs

Many stream crossings involve channels that are far removed from dynamic equilibrium whether it is caused by legacy (e.g., valley bottom aggradation, channelization, mill dams, or tie drives) or contemporary effects (e.g., urbanization, floodplain encroachment, or dredging), or a combination thereof. With complex response sequences that can last for decades or longer, sustainable stream-crossing designs are critically dependent on an understanding of current and future channel evolution trajectories (e.g., Hawley et al. (2012a) and Schumm et al. (1984)). Designs can be affected by a pulsed delivery of excess sediment from upstream channel instability, as well as be undermined by headcut migration from actively unstable downstream reaches (Hawley et al. 2012b). Conventional approaches to stream-crossing design that exclusively focus on maintaining sediment continuity might also ignore an even more common bank failure mechanism – geotechnical mass wasting of banks – which would clearly be an undesirable *a priori* risk factor at a crossing location.

Developing tools for predicting channel instability as a result of changing water and sediment inputs is challenging for several reasons including geomorphic thresholds and non-linear lagged responses, historical legacies, and a large number of interrelated variables that can simultaneously respond to watershed changes. Despite these difficulties, the need for practical tools in stream management have prompted many efforts to develop qualitative or semi-quantitative methods for understanding the potential response trajectories of channels based on their current state. In particular, Channel Evolution Models (CEMs) provide an attractive framework for understanding channel response and instability across diverse geomorphic settings. The well-known incised-channel CEM of Schumm et al. (1984) documents a sequence of five stages of adjustment and ultimate return to quasi-equilibrium that has been observed and validated in many regions and stream types. Process-based CEMs provide a framework for understanding response trajectories and developing strategies for mitigating the impacts of processes likely to dominate channel response in the future (Simon 1995). The original incised-channel CEM has been subsequently modified and expanded upon by many researchers (e.g., Simon (1989), American Society of Civil Engineers (ASCE 1998), Bledsoe et al. (2002), Watson et al. (2002), and Hawley et al. (2012a)).

More recent tools for assessing channel instability and response potential, especially in the context of managing bridge crossings and other infrastructure, have included elements of incised-channel CEMs and various descriptors of boundary conditions, and resisting versus erosive forces. Simon and Downs (1995) and Johnson et al. (1999) developed rapid assessment techniques for alluvial channels based on diverse combinations of metrics describing bed material, CEM stage, existing bank erosion, vegetative resistance, and other controls on channel response. Although based on a strong conceptual foundation of the underlying mechanisms controlling channel form, the assessment ratings provided by most of these tools

are based on aggregated scores that can mask which factors are ultimately driving the final risk ratings. Table 5-5 summarizes four of the most known and/or widely implemented RGAs.

Table 5-5. Partial list of variables utilized in previously-published tools for performing rapid stability assessments and assessing channel susceptibility.

Simon and Downs (1995) Variables	Johnson et al. (1999) Variables	Bledsoe et al. (2012a) Variables	Caltrans (2014) Variables
• degree of incision • Simon six-stage CEM for incised channels • primary bed material • degree of constriction • bed/bank protection • streambank erosion – mass wasting versus fluvial • streambank instability – % banks failing • woody vegetation cover – "riparian" • bank accretion • hillslope material • % hillslope eroding • severity of side slope erosion	• shear stress ratio • bed material consolidation and armoring • vegetative bank protection • mass wasting or bank failure • high-flow angle of approach to bridge • distance from meander impact point • percentage of channel constriction • bank soil texture and coherence • average bank slope angle • bar development • bank cutting • debris jam potential • obstructions, flow deflectors, and sediment traps	• D_{50} / armor potential • CEM stage • grade control distance, spacing, and condition • proximity to geomorphic threshold • valley confinement • bank angle and height • bank materials / consolidation	• watershed and floodplain activity and impacts • flow characteristics • channel pattern • entrenchment / channel confinement • bed material • bar development • obstructions • bank soil texture and coherence • average bank slope angle • vegetative or engineered bank protection • bank erosion • mass wasting or bank failure • stream-crossing alignment with flow

5.3.2 Adapting a Regional RGA / Screening Tool for Wider Applicability

We adapted a regional RGA developed by the Co-Principal Investigators as a complement to the design hydrology guidance (see http://www.waterboards.ca.gov/academy/courses/riverrat/606_hydromod scrntool_fldmanl.pdf; Bledsoe et al. (2010)). A variety of potential metrics were considered for inclusion in this tool. Initial sets of metrics and schemes for assigning relative weights were identified through a review of previously-published tools for assessing channel stability (Simon and Downs 1995; Johnson et al. 1999; Bledsoe et al. 2012; Caltrans 2014) (Table 5-5). We initially considered an extensive array of over 60 hydrogeomorphic metrics across watershed, valley, and reach scales. This included standard metrics such as drainage area, valley slope, and grain size, along with other factors such as proximity of downstream grade control and natural hardpoints in limiting upstream channel incision.

The goal of the variable reduction process is to identify metrics with a clear and direct physical linkage with channel response in either the vertical or lateral dimension, and that could be rapidly assessed in the field. The original pool of metrics considered for inclusion in the RGA was reduced by grouping the variables by the processes that they represent in either the vertical or lateral dimension (e.g., erosive power versus boundary resistance versus proximity to threshold) and ranking the various descriptors in terms of their fidelity to the key physical processes, and their ease of measurement / data requirements. Selection of metrics is ultimately based on a tradeoff between the level of effort required to quantify or measure a particular metric and the degree to which it enhances the physical basis and prediction accuracy of the tool. For this project, we initially reduced the set of candidate variables for inclusion in the RGA tool to seven (Figure 5-7).
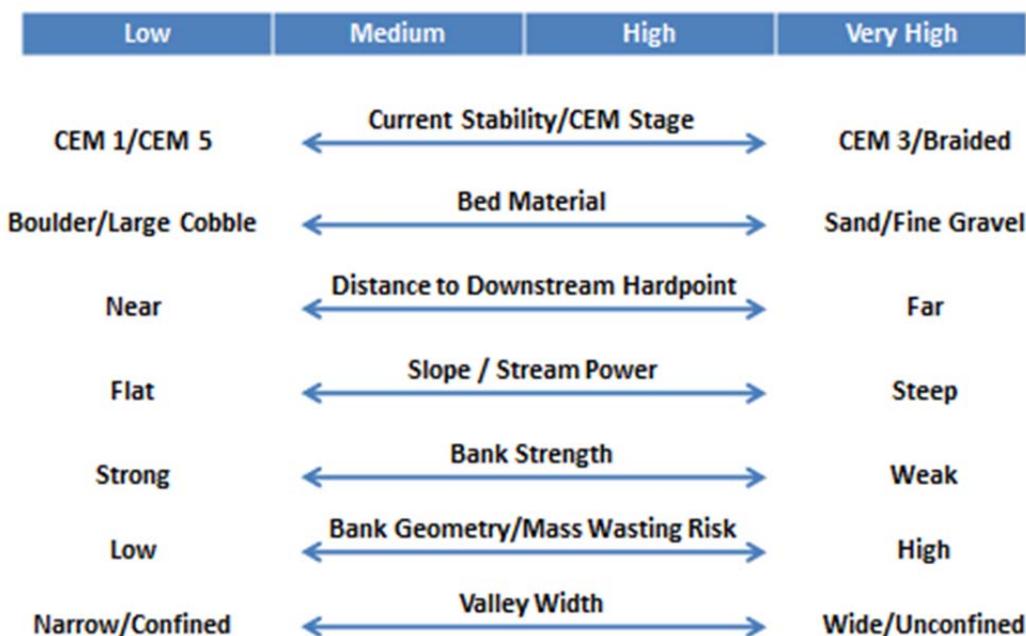
Figure 5-7. Seven candidate stability indicators recommended for inclusion in an RGA, performed as part of the hydrologic design process.

Based on feedback provided in the survey of DOT engineers and by the NCHRP Panel, we reduced the seven candidate stability indicators to four by recognizing the inter-correlation between some of the vertical and lateral stability factors:

(1) current stability status – CEM stage, braiding, alluvial fan;

(2) dominant bed material / armoring potential;

(3) distance to downstream hardpoint / grade control; and

(4) bank strength.

Among these factors, several indicators control channel stability to the extent that they are indicative of early 'off ramps' in the RGA process. Boulder-bed streams are indicative of systems with bed mobility that is likely to be rare (e.g., threshold discharge for incipient motion on the order of ~3 to 10 times the magnitude of the 2-yr discharge, Hawley and Vietz (2016); Figure 5-8). As such, boulder-bed streams would represent the Low risk category.

In contrast, streambeds dominated by sand- and fine-gravel would likely be indicative of extremely frequent mobility (e.g., on the order of 0.0001 to 0.01 times the 2-yr discharge, Hawley and Vietz (2016), Figure 5-8). Such geomorphically sensitive systems would represent the Very High risk category. Other immediate indicators of Very High risk would be channel braiding or a CEM stage of III (geotechnical mass wasting bank failure and active downcutting and widening (Schumm et al. 1984)). These early 'off ramps' are summarized in Figure 5-9.
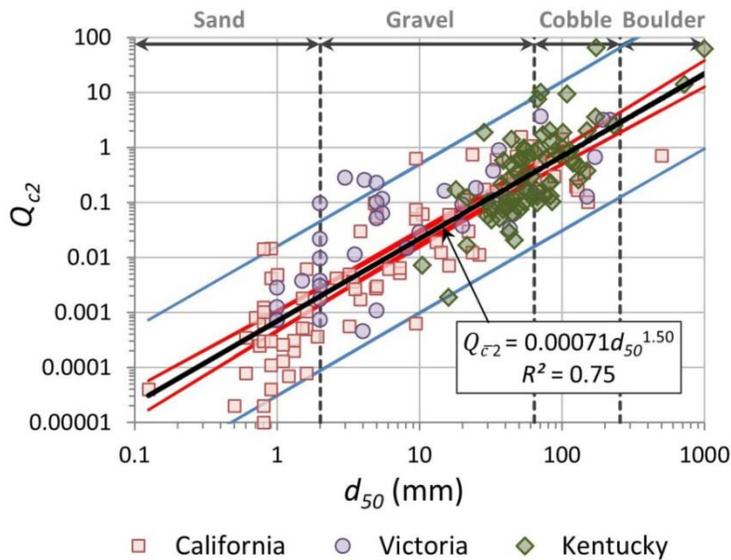
Figure 5-8. Critical discharge for incipient motion (Q_c) standardized by the predevelopment 2-yr peak discharge (Q_{c2}) versus bed-material size represented by the median particle (d_{50}) from each site. The figure is adapted from Hawley and Vietz (2016) using data from 195 sites in California and Kentucky (U.S.) and Victoria (Australia). Lines depict the mean estimate (black), the 95% confidence interval (CI) of the mean estimate (red), and the 95% CI of individual site estimates (blue).

Low	Medium	High	Very High
Boulder			Sand/Fine Gravel
			CEM III
			Braiding

Figure 5-9. Early 'off ramps' in the RGA of Low risk (boulder-dominated streams) and Very High risk (sand- / fine-gravel dominated streams, CEM III (mass wasting banks), or active braiding).

Streams not exhibiting the early 'off ramp' conditions would warrant examination of the secondary factors mentioned above. For example, a streambed dominated by medium to coarse gravels could be as sensitive as a Very High risk category if its banks were weak (alluvium lacking vegetation) and it lacked grade control. However, the same streambed could be Low risk if it had strong banks (bedrock/boulder) and frequently spaced grade control. Cases in between would be either Medium or High risk according to Figure 5-10. Likewise, bed-material dominated by very coarse gravels / small cobbles would range from Low to High risk class depending on bank strength and hardpoint frequency, and beds dominated by large cobbles would range from Low to Medium (Figure 5-10).

Bed Material = Medium to Coarse Gravel

Frequency of Hardpoint(s)	Strong Banks (bedrock/boulder/ coarse cobble)	Moderate (cohesive/ well vegetated)	Weak Banks (alluvium/ poorly vegetated)
None/infrequent	High	High	Very High
Intermediate	Med	High	High
Frequent	Low	Med	High

Bed Material = Small Cobbles/Very Coarse Gravel

Frequency of Hardpoint(s)	Strong Banks (bedrock/boulder/ large cobble)	Moderate (cohesive/ well vegetated)	Weak Banks (alluvium/ poorly vegetated)
None/infrequent	Med	Med	High
Intermediate	Low	Med	Med
Frequent	Low	Low	Med

Bed Material = Large Cobbles

Frequency of Hardpoint(s)	Strong Banks (bedrock/boulder/ large cobble)	Moderate (cohesive/ well vegetated)	Weak Banks (alluvium/ poorly vegetated)
None/infrequent	Low	Med	Med
Intermediate	Low	Low	Med
Frequent	Low	Low	Low

Figure 5-10. RGA risk categories for beds ranging from coarse gravels to large cobbles across a gradient of bank strength and hardpoint (grade control) frequency.

5.3.3   Analysis Domain for Applying the RGA

Channel responses may propagate for significant distances downstream (and sometimes upstream) from a point of influence such as a stormwater outfall or stream crossing. Accordingly, it may be necessary to conduct field reconnaissance across a domain spanning multiple channel types/settings and property owners. We recommend that the typical analysis domain for conducting the RGA will be at least 20 channel widths upstream and downstream in accordance with the recent Caltrans (2014) guidance.

Begin by defining the points or zones along the channel reach(es) where changes in discharge or channel type are likely to occur (e.g., potential locations of outfalls or tributary inputs). Document any observed outfalls for final desktop synthesis and define the upstream and downstream extents of analysis as follows:

- **Downstream** – until reaching the closest of the following:
  - at least one reach downstream of the first grade control point (but preferably the second downstream grade control location);
  - tidal backwater/lentic waterbody;
  - equal order tributary (Strahler, 1952);[1] and
  - a two-fold increase in drainage area.[2]
- **Upstream** – extend the domain upstream for a distance equal to 20 channel widths OR to grade control in good condition – whichever comes first. Within that reach, identify hardpoints that could check headward migration, evidence that headcutting is active or could propagate unchecked upstream.

Within the analysis domain there may be several reaches that should be assessed independently based on either length or change in physical characteristics. In more urban settings, segments may be logically divided by other stream crossings (Chin and Gregory 2002), which may offer grade control, create discontinuities in the conveyance of water or sediment, etc. In more rural settings, changes in valley/channel type, natural hardpoints, and tributary confluences may be more appropriate for delineating assessment reaches. In general, the following criteria should trigger delineation of a new reach and hence a separate susceptibility assessment:

- 200 m or *ca.* 20 bankfull widths – it is difficult to integrate over longer distances;
- distinct or abrupt change in grade or slope due to either natural or artificial features;
- distinct or abrupt change in dominant bed material or sediment conveyance;
- distinct or abrupt change in valley setting or confinement; and
- distinct or abrupt change in channel type, bed form, or planform.

5.3.4   Connection between RGA and Design Hydrology

Performing a RGA parallel with the design hydrology process has a number of potential benefits. First, additional risk factors such as incised-channel evolution, braiding, distance to hardpoint, bank strength, etc. can help inform whether assumptions of the hydrologic analyses are valid. Mobile boundary modeling of channels is generally infeasible for most projects, and the standard sediment continuity analyses that are feasible typically assume static channel geometry. Performing a RGA and considering additional risk factors provides insight into the acceptability of the quasi-equilibrium geometry assumption used in effective discharge type analyses. In highly unstable channels where this assumption is sufficiently violated, it may be beneficial to take some of the precautionary steps discussed in Section 4.2.3 such as running analyses with different channel geometries that correspond to different stages of channel evolution and/or proactively installing channel armoring/grade control.

Second, departures between the actual channel response versus the anticipated channel sensitivity inferred from flow type and grain size can occur where hydrologic analysis does not capture other risk factors. For example, whether a channel incises or widens in response to land use change depends on local variations in boundary resistance and vegetation. Moreover, if a streambed is large cobbles/boulders, but the crossing occurs at the canyon mouth on an alluvial fan with obvious braiding, the engineer would

---

[1] In the absence of proximate downstream grade control or backwater, the confluence of an 'equal order tributary' should correspond to substantial increases in flow and channel capacity that should, in theory, correspond to significant flow attenuation; however, there is no scientific basis to assume that downstream channels of higher stream order are less susceptible than their upstream counterparts.

[2] An increase in drainage area greater than or equal to 100% would roughly correspond to the addition of an equal-order tributary.

logically recognize a higher risk situation compared to upstream in the confined step-pool canyon. One might be able to create sediment continuity with a simplified modeling approach, but the designer should probably consider reinforcing the banks/abutments, doing some channel 'restoration' downstream, etc. in order to provide channel geometry the ability to maintain sediment continuity. Finally, many design hydrology approaches are focused on bed-material mobility and transport, and the hydrogeomorphic types used to identify the appropriate level of hydrologic design rely heavily on bed-material size. Active channel instability at the crossing and/or upstream (e.g., bank failures) can confound efforts to obtain a representative grain size distribution needed for performing design hydrology analyses that consider sediment transport. This RGA, performed as part of the hydrologic design process, can provide important information on the uncertainty of inputs used in the analysis.

CHAPTER 6

Conclusions and Suggested Research

This project achieved its goal of developing scientifically supported methods for defining the design hydrology for stream crossings along with developing tools for understanding how design hydrology might adapt to land use changes. The methods and tools developed in this study were influenced by a survey of state DOT engineers aimed at understanding their design hydrology needs. As a result, emphasis was placed on developing approaches and tools that are physically-based yet as straightforward and user-friendly as possible.

6.1 Novel Design Hydrology Metrics

In the initial phase of the project, we explored relationships between the drivers of sediment yield in rivers and streams, namely the flow regime and physical properties of the sediment and channels, and the magnitude and frequency of sediment transport described by various metrics based on the sediment yield curve. Theoretical approaches were used to explore relationships based on flow, physical characteristics, and sediment yield metrics calculated from fine- and coarse-bed rivers across the continental U.S. and Puerto Rico. This work expands on previous MFA studies by applying a uniform method of bed-material yield analysis across a wide range and a large number of river types to characterize the relationships between properties of the flow regime and bed material, and the range, magnitude, and frequency of the most effective flows.

Sediment yield metrics inform the applicability of the dominant discharge concept (e.g., the appropriateness of a single design discharge). Our findings indicate that the magnitude and frequency of sediment transport in all river types is sensitive to the variability of the flow regime; however, sediment yield and effectiveness in fine- and coarse-bed rivers respond differently to flow variability. Sediment yield metrics in fine-bed, suspended-load dominated streams are more sensitive to flow variability, whereas coarse-bed streams are more sensitive to physical aspects of the channel and bed sediment size. Bed sediment grain size plays a dominant role in sediment yield in rivers, especially coarse-bed rivers. In fine-bed rivers, a larger range of discharges is responsible for sediment yield. This range of flow narrows as the grain size of the bed increases. In coarse-bed rivers, a narrower range of less frequent flows dominates sediment yield. The most effective discharge also increases in magnitude and decreases in frequency as grain size increases.

In many cases, sediment yield metrics respond in a continuum from flashy and fine-bed to stable and coarse-bed. In flashier systems, $Q_{eff} < Q_{bf}$ if smaller more frequent flows are competent to transport sediment. If the streambed is armored, then less frequent flows become more effective, and $Q_{eff} = Q_{bf}$, or $Q_{eff} > Q_{bf}$. As flow variability increases, the range of discharges responsible for the bulk of sediment transport increases. Also, more sediment is transported by discharges greater than Q_{eff} as flow variability increases. This means that the bankfull discharge is often likely to be greater than Q_{eff}, especially in fine-bed rivers.

We also tested the predictive ability of several metrics in estimating bankfull discharge (Q_{bf}), an important channel design variable. Estimates of Q_{eff} are very sensitive to the MFA methodology used, and Q_{eff} tends to produce very scattered relationships with physical- and flow-related metrics. The discharge at which 50% of cumulative sediment yield occurs (Q_{s50}, half-yield discharge) predicts Q_{bf} the

best under most flow regimes in single-thread, perennial fine-bed river as well as coarse-bed rivers. Q_{s50} tends to be a much less variable estimate and is less sensitive to the MFA methodology. In addition, it tends to predict the bankfull discharge better than Q_{eff} across a wide range of river types. However, unlike Q_{eff}, estimating Q_{s50} is estimated from the absolute value of cumulative sediment transport and, therefore, is sensitive to the sediment transport relation used if sediment transport measurements are not available and a calibrated relation is used.

The 1.5-yr flood ($Q_{1.5}$) predicts Q_{bf} approximately as well as Q_{s50} and Q_{eff} for bedload-dominated sites. When considering what design discharge to use to approximate the channel-forming discharge, the $Q_{1.5}$ often provides a reasonable estimate of the bankfull discharge in coarse-bed rivers and in some fine-bed rivers. In fine-bed rivers, this peak flow metric does not predict the bankfull discharge well in cases of greater flow variability.

In summary, Q_{s50} is an attractive alternative to Q_{eff} for single-discharge design as it appears more informative and useful than Q_{eff}, especially when equilibrium bankfull channel dimensions are not apparent from stable upstream supply reaches. When compared to Q_{eff} and the 1.5- and 2-yr floods, Q_{s50} is the least biased estimator of Q_{bf} and has the lowest mean absolute percent error and root mean square error (RMSE) for fine-bed sites. In coarse-bed streams the 1.5-yr annual maximum flood predicts Q_{bf} just as well as Q_{s50}, indicating that a sediment yield-based approach to channel design is especially important for fine-bed streams and rivers.

6.2 Effects of Flow Data Resolution on Design Hydrology

We found that accurate computation of sediment yield metrics such as Q_{s50} will depend on flow data resolution for flashy (high *RB*) or fine-bedded (high b value) rivers. Results of our analysis on the effect of flow-data resolution on sediment transport calculations for 39 bedload sites and 99 suspended-load sites suggest that the use of daily-averaged flow data is not always appropriate. In instances where the flow regime at the site is flashy and the values of the sediment rating curve exponent (b) is medium to high (e.g., > 2), sediment yield and Q_{s50} were greatly underestimated by using daily-averaged flow data. This underestimation of sediment yield was shown to have considerable impacts on channel design. Henderson (1966) proportionalities were used to relate the underestimation of sediment yield to error in design slope, which could ultimately cause channel aggradation. As flashiness increases, the stable design slope predicted using average daily data decreases dramatically from that predicted using 15-minute data. This departure become more severe with larger values of b. Additionally, it was shown that even in instances where flashiness was high, a value of b (e.g., close to 1) mitigated the magnitude of error in sediment yield and Q_{s50} calculations, causing it to be quite low.

6.3 Effects of Land Use Change on Design Hydrology

Our case study of urbanizing watersheds indicated that flashiness, and the upper tails of the FDC, are substantially affected by land use change. An analysis of the effect of urbanization on FDCs for the Puget Sound region revealed that urbanization caused upward shifts in the magnitude of the entire FDC for nearly all urban watersheds. This upward shift was greatest for the high magnitude flows (90th – 99th percentile) and on average represented an approximate increase of 35% over the analysis period. The upward shift was lesser for the low magnitude flows (10th – 25th percentile) and on average represented an approximate increase of 15% over the analysis period. Semi-urban and rural watersheds were found to have decreases in the magnitude of small discharges (10th – 25th percentile). This result was attributed to a reduction in baseflow caused by extensive groundwater extraction. Streamflow in nearly all the watersheds was also found to be becoming significantly flashier. Urban watersheds saw on average a 46% increase in the R-B Index over the analysis period, while semi-urban and rural watersheds saw increases of 4% and 14%, respectively. This R-B Index is strongly related to behavior of sediment yield curves, especially fine-grained channels.

An analysis of population trends in the case study showed that all watersheds experienced population growth over the analysis period of 1960 to 2010. Watersheds with the highest population density and growth were categorized as "urban" while the remaining watersheds were either categorized as "semi-urban" or "rural." Analysis of precipitation trends from 1960 to 2010 revealed that none of the eight watersheds had any significant increasing or decreasing trends in annual precipitation. The precipitation analysis did reveal, however, that half of the watersheds were experiencing increasing trends in the variability and intensity of precipitation.

Hydrologic trends for both urban and non-urban watersheds were related to potential changes in channel morphology. Urban watersheds that saw upward shifts in the FDC were found to have potential for channel degradation over the analysis period. Conversely, the semi-urban and rural watersheds which saw downward shift in the FDC were found to have potential for channel aggradation. Case studies illustrate the dynamic nature of watershed hydrology, as increasing precipitation intensity and variability and changes in population density over time were found to impact hydrology over the analysis period.

6.4 Novel Tools for Design Hydrology

Five primary design support / analysis tools were developed during the course of this project. In developing these tools, the research team strived for user-friendly structures (e.g., decision tables, decision trees, and spreadsheet tools) based on our discussions on current practices with state DOTs. Field reconnaissance is a critical component of the recommended approach. The tools are summarized below.

(1) A decision tree with complementary web-based hydrologic analysis tools was developed to provide practical guidance on generating the FDCs required for the computation of robust design hydrology metrics such as Q_{s50}. The decision tree presents a series of questions regarding land use change, potential non-stationarity of the flow record, and the availability of stream gage data and sediment transport measurements, to provide a standardized approach for calculating Q_{s50}.

(2) Decision tables are provided for relating channel response potential to an appropriate level of design analysis guidance. The decision tables account for inherent SRP and whether or not an acceptable analog channel is available in answering the following questions: (1) What level of hydrologic analysis should be undertaken? (2) Is it necessary to perform sediment transport analysis, and if so, what type of analysis is needed? (3) What spatial domain (i.e., how far upstream and/or downstream from the project location) is recommended for conducting the analysis? The fundamental philosophy underlying this analysis decision table is that, as SRP increases, it becomes necessary to conduct a deeper analysis over a larger area of influence.

(3) A decision table was developed to guide selection of analog reaches that may provide an additional line of evidence in design hydrology analyses. The analogy method has sometimes been used recklessly in design as streams from different watersheds and even different physiographic regions with disparate hydrologic and sediment supply characteristics have been used to define channel geometry in dissimilar settings. This decision support tool helps users identify upstream analogs that are very similar in terms of key criteria including the valley setting, boundary conditions, and inflowing loads of water and sediment, and to define supply reaches for sediment continuity analysis.

(4) A tool that supports RGAs of channel instability and susceptibility at stream crossings was developed. This overtly simple approach is not intended to supplant more comprehensive and rigorous methods, most notably HEC-20 (Lagasse et al. 2012). Instead, it is intended to complement more in-depth approaches by orienting the design hydrology designer to some key considerations during field reconnaissance early in the design hydrology process. To develop the simplified RGA, we reduced a large pool of potential indicators to four:

i. current stability status – CEM stage, braiding, alluvial fan;

ii. dominant bed material / armoring potential;

iii.   distance to downstream hardpoint / grade control; and

iv.   bank strength.

High ratings of stream susceptibility based on these indicators trigger a deeper level of design hydrology analysis as defined by the design decision table described under item 2. above, and underscore the need for a greater stability analysis using more rigorous and comprehensive tools such as HEC-20.

(5) The CSR Tool was developed in VBA to compute analytical channel designs based on the CSR, a robust design hydrologic metric that accounts for the full spectrum of sediment transporting events. Additional conclusions regarding the CSR Tool are provided in the following section.

The suite of tools developed in this project to provide a general framework for design hydrology. This framework is summarized in a separate guidance document (Appendix C of this NCHRP 24-40 final report) that provides a concise summary and step-by-step procedures for performing the recommended design hydrology analyses.

Table 6-1 summarizes which types of streams to which this guidance and tools apply versus those to which it does not apply.

Table 6-1. Streams and situations to which the guidance and tools apply versus situations where it is not directly applicable.

Applies:	Does Not Apply:
• Alluvial channels	• Non-alluvial channels
• Dune/ripple, pool-riffle, plane bedforms	• Multi-thread, braided, fan channels
• Single-thread	• Channel slope > ~ 0.03
• Channel slope ≤ ~ 0.03	• Ephemeral, dryland rivers
• D_{50} of sand and larger	• Abrupt transitions
• Near-perennial flow	• Channels that lack capacity to transport inflowing sediment load at valley slope
	• Severely backwatered / tidal situations
	• CSR Tool does not apply to boulders

6.5 CSR Tool

A growing body of scientific literature has converged on the conclusion that a sediment continuity or "sediment impact analysis" should underpin the design of most alluvial channels (Copeland et al. 2005; Soar and Thorne 2001, 2011; NRCS 2007; Shields et al. 2003, 2008; Doyle et al. 2007), especially "live bed" or "labile" channels (Church 2006). Existing analytical stable channel design techniques like the Copeland method in SAM (Thomas et al. 2002) and HEC-RAS rely on a single design discharge and inflowing sediment load. Therefore, there is an implicit and often dubious assumption that if sediment transport capacity is matched at the one presumed design discharge, it is sufficiently matched across the *full spectrum* of sediment transporting flows. Unfortunately, this is frequently not the case, especially in fine-grained channels, because the channel geometry that minimizes differences between the cumulative sediment transport capacity of an upstream supply reach and a design reach is not the channel geometry indicated by examining only one design discharge.

To address this gap in the design hydrology toolbox, this project developed a tool for applying the Capacity-Supply Ratio metric: the CSR Tool. The CSR Tool computes analytical channel designs based on the CSR, a design hydrologic metric that accounts for the full spectrum of sediment transporting events. The spreadsheet-based tool ultimately outputs a family of channel slope and width combinations (analytical solutions) which provide continuity of water and sediment across the full range of flows as represented by a flow frequency curve or FDC. The CSR is defined as the bed-material load transported

through the design reach by a sequence of flows over an extended time period divided by the bed-material load supplied to the reach by the same sequence of flows over the same time period. Thus, the CSR method balances the total average sediment yield over the entire flow record rather than just for a single representative discharge as in existing software tools for performing analytical channel design. It explicitly accounts for the morphological influence of flows other than Q_{eff} and Q_{s50}. If the capacity of the reach to transport sediment exceeds the sediment supplied from upstream, then degradation or erosion can be expected in the reach with a CSR > 1. Alternatively, if the sediment entering the reach exceeds the capacity of the reach to transport it, then aggradation or sediment accumulation is expected with a CSR < 1. A CSR near unity will be the most likely to have sediment balance with minimal aggradation or degradation in the channel. The FDC input into the CSR Tool can reflect current or projected future flow regimes that result from land use change.

6.6 Suggested Research

Analyses and case studies of land use change effects on hydrologic regimes underscore the need for robust strategies for forecasting temporal shifts in the hydrologic record. Because FDCs are widely used by scientists and engineers for a wide range of applications including channel design and magnitude frequency analysis, future work that provides locally calibrated estimates of FDC change with land use would be a valuable contribution to the field. Perhaps this could take the form of locally calibrated equations for regressing FDC percentiles based on local factors and level of urbanization.

The value of the sediment rating curve exponent (b) was found to exhibit strong control on the error created by using daily-averaged flow data in sediment yield and Q_{s50} calculations. Additional research that provides a greater understanding of the physical meaning of b, and perhaps a method of estimation, would be useful extension of this research. Currently, our only means of estimating b, is to use a series of sediment discharge measurements and corresponding flow rates to create a best-fit rating curve. Because existing sediment discharge measurements, especially bedload, are few and far in between and because taking new measurements can be cost-prohibitive, a reliable estimation technique would be useful. With an estimation procedure for b, and simple flashiness calculations computed from USGS streamflow data, one can determine if daily-averaged flow data are appropriate for use in sediment transport calculations.

Future research and improvements to the web-based tools include more-detailed watershed assessment, calibration of the SWAT model to gage data, and the integration of a 1-D flow model into eRAMS. At the time of publication of this report, the watershed assessment tool is fairly new with near-term plans to include easier data downloads of assessment report data and possibly the integration of multi-metric assessments of watershed condition. The calibration of SWAT models to flow data already in the eRAMS platform is supported by the USDA-ARS team which developed SWAT and will be accomplished at some time in the near future. The eRAMS team has been in conversation with the USACE to determine if it is appropriate (and possible) to incorporate either the computations or outputs of the HEC-RAS model into eRAMS or if developing a stand-alone 1-D river model would be appropriate. Additionally as all of the eRAMS tools can be accessed independent of the GIS interface, using a REST-based protocol, the site-based tools could be used for broader-spatial analysis including optimizing projects in a watershed.

The CSR Tool also provides a platform for further research in stable channel design. It is suggested that additional research further test the applicability of the CSR technique in practical stable channel design. This could include testing the tool against channel designs that have been implemented to compare with results shown in the field. Also, further theoretical comparisons can be made to more precisely address the question, "When is the CSR method most needed over the single discharge method?" Preliminary results have shown that the CSR method is the most needed for fine-grained and or flashy streams. The CSR Tool can also support the question, "What single discharge or sediment percentile most closely matches designs based on the full spectrum of flows accounted for by the CSR?" Preliminary results suggest that the single discharge that produces design equivalence with the CSR output is often bracketed between Q_{s50} and Q_{s75} depending on the system.

FDCs that are input into the CSR Tool can reflect current or projected future flow regimes that result from land use change. However, this yields a caveat: sediment supply will also change with land use. Thus, further research is needed on how to best implement scenario analysis that examines sediment and water continuity of both near bankfull and overbank flood flows under potential future loadings / hydrologic futures is recommended. Research relating land use changes to departures between the supply reach and design reach sediment yield curves within specific bins and ranges of the sediment yield curve, and ultimately translating these departures into improved understanding of channel morphologic response is also needed.

Although the design hydrology approach described herein is applicable to a wide range of stream types, further research is needed on design hydrology for supply-limited systems, braided rivers, alluvial fans, ephemeral systems (where the typical dominant flow often has a recurrence interval of 10 to 25 yrs), and other non-equilibrium situations. This includes situations where high sediment loads and infrastructure constraints necessitate the design of a non-alluvial "flume" or "slurry channel" with transport capacity exceeding supply. Further integration of ecological aspects including aquatic organism passage (Hotchkiss and Frei 2007) into analytical channel design remains an important consideration and research need.

REFERENCES

Ackers, P., and F. Charlton. 1970. "Meander Geometry Arising from Varying Flows." *Journal of Hydrology*, Vol. 11, No. 3, pp. 230–252, DOI: 10.1016/0022-1694(70)90064-8.

Ågren, A., I. Buffam, M. Jansson, and H. Laudon. 2007. "Importance of Seasonality and Small Streams for the Landscape Regulation of Dissolved Organic Carbon Export." *Journal of Geophysical Research: Biogeosciences*, Vol. 112, No. G3, DOI: 10.1029/2006JG000381.

Allan, J.D., and M.M. Castillo. 2007. *Stream Ecology*. Second Edition, Springer Science+Business Media B.V., Netherlands, 436 p.

American Society of Civil Engineers (ASCE), Task Committee on Hydraulics and Modeling of River Width Adjustment. 1998. "River Width Adjustment, II: Modeling." *Journal of Hydraulic Engineering*, Vol. 124, No. 9, pp. 903–917, DOI: 10.1061/(ASCE)0733-9429(1998)124:9(903).

Andrews, E.D. 1980. "Effective and Bankfull Discharges of Streams in the Yampa River Basin, Colorado and Wyoming." *Journal of Hydrology*, Vol. 46, No. 3, pp. 311–330.

Andrews, E.D. 1994. "Marginal Bed Load Transport in a Gravel Bed Stream, Sagehen Creek, California." *Water Resources Research*, Vol. 30, No. 7, pp. 2241–2250, DOI: 10.1029/94WR00553.

Andrews, E.D. 2000. "Bed Material Transport in the Virgin River Utah." *Water Resources Research*, Vol. 36, No. 7, pp. 585–596, DOI: 10.1029/1999WR900257.

Andrews, E.D. and J.M. Nankervis. 1995. Effective Discharge and the Design of Channel Maintenance Flows for Gravel-bed Rivers. Pages 151–164 in J.E. Costa, A.J. Miller, K.W. Potter, and P.R. Wilcock (Eds.): *Natural and Anthropogenic Influences in Fluvial Geomorphology*, Vol. 89, American Geophysical Union, Washington, DC.

Arnold, J.G. and N. Fohrer. 2005. "SWAT2000: Current Capabilities and Research Opportunities in Applied Watershed Modelling." *Hydrological Processes*, Vol. 19, No. 3, pp. 563–572, DOI: 10.1002/hyp.5611.

Arnold, J.G., R. Srinivasan, R.S. Muttiah, and J.R. Williams. 1998. "Large Area Hydrologic Modeling and Assessment, Part 1: Model Development." *Journal of the American Water Resources Association*, Vol. 34, No. 1, pp. 73–89, DOI: 10.1111/j.1752-1688.1998.tb05961.x.

Ashmore, P.E. and T.J. Day. 1988. "Effective Discharge for Suspended Sediment Transport in Streams of the Saskatchewan River Basin." *Water Resources Research*, Vol. 24, No. 6, pp. 864–870, DOI: 10.1029/WR024i006p00864.

Asselman, N.E.M. 2000. "Fitting and Interpretation of Sediment Rating Curves." *Journal of Hydrology*, Vol. 234, Nos. 3–4, pp. 228–248, DOI: 10.1016/S0022-1694(00)00253-5.

Bagnold, R.A. 1966. "An Approach to the Sediment Transport Problem from General Physics." *Professional Paper 422-I*, U.S. Geological Survey, Washington, DC, 42 p.

Baker, D.B., R.P. Richards, T.T. Loftus, and J.W. Kramer. 2004. "A New Flashiness Index: Characteristics and Applications to Midwestern Rivers and Streams." *Journal of the American Water Resources Association*, Vol. 40, No. 2, pp. 503–522, DOI: 10.1111/j.1752-1688.2004.tb01046.x.

Barry, J.J., J.M. Buffington, and J.G. King. 2004. "A General Power Equation for Predicting Bed Load Transport Rates in Gravel Bed Rivers." *Water Resources Research*, Vol. 40, No. 10, W10401, DOI: 10.1029/2004WR003190.

Barry, J.J., J.M. Buffington, P. Goodwin, J.G. King, and W.W. Emmett. 2008. "Performance of Bed-load Transport Equations Relative to Geomorphic Significance: Predicting Effective Discharge and its Transport Rate." *Journal of Hydraulic Engineering*, Vol. 134, No. 5, pp. 601–615, DOI: 10.1061/(ASCE)0733-9429(2008)134:5(601).

Benson, M.A. and D.M. Thomas. 1966. "A Definition of Dominant Discharge. *International Association of Scientific Hydrology Bulletin*, Vol. 11, No. 2, pp. 76–80, DOI: 10.1080/02626666609493460.

Beven, K.J. 2011. *Rainfall-Runoff Modelling: The Primer*. Second Edition, John Wiley & Sons, West Sussex, UK, 488 p.

Biedenharn, D.S., and C.R. Thorne. 1994. "Magnitude-frequency Analysis of Sediment Transport in the Lower Mississippi River." *Regulated Rivers: Research and Management*, Vol. 9, No. 4, pp. 237–251, DOI: 10.1002/rrr.3450090405.

Biedenharn, D.S., C.M. Elliott, and C.C. Watson. 1997. "The WES Stream Investigation and Streambank Stabilization Handbook." U.S. Army Corps of Engineers, Waterways Experiment Station, Vicksburg, MS, October, 436 p., URL: http://citeseerx.ist.psu.edu/viewdoc/download?doi=10.1.1.122.4798&rep=rep1&type=pdf.

Biedenharn, D.S., R.R. Copeland, C.R. Thorne, P.J. Soar, R.D. Hey, and C.C. Watson. 2000. "Effective Discharge Calculation: A Practical Guide." *Technical Report No. ERDC/CHL TR-00-15*, U.S. Army Corps of Engineers, Engineer Research and Development Center, Vicksburg, MS.

Bledsoe, B.P., and C.C. Watson. 2001. "Logistic Analysis of Channel Pattern Thresholds: Meandering, Braiding, and Incising." *Geomorphology*, Vol. 38, No. 3, pp. 281–300, DOI: 10.1016/S0169-555X(00)00099-4.

Bledsoe, B.P., C.C. Watson, and D.S. Biedenharn. 2002. "Quantification of incised channel evolution and equilibrium." *Journal of the American Water Resources Association*, Vol. 38, No. 3, pp. 861–870, DOI: 10.1111/j.1752-1688.2002.tb01002.x.

Bledsoe, B.P., R.J. Hawley, E.D. Stein, and D.B. Booth. 2010. "Hydromodification Screening Tools: Field Manual for Assessing Channel Susceptibility." *Technical Report 0606*, Southern California Coastal Water Research Project (SCCWRP), Costa Mesa, CA, March, 41 p. + appendices, URL: http://www.waterboards.ca.gov/academy/courses/riverrat/606_hydromodscrntool_fldmanl.pdf.

Bloomfield, J.P., D.J. Allen, and K.J. Griffiths. 2009. "Examining Geological Controls on Baseflow Index (BFI) using Regression Analysis: An Illustration from the Thames Basin, UK." *Journal of Hydrology*, Vol. 373, No. 1, pp. 164–176, DOI: 10.1016/j.jhydrol.2009.04.025.

Booth, D.B., and C.J. Jackson. 1997. "Urbanization of Aquatic Systems – Degradation Thresholds, Stormwater Detention, and the Limits of Mitigation." *Water Resources Bulletin*, Vol. 33, No. 5, pp. 1077–1090, DOI: 10.1111/j.1752-1688.1997.tb04126.x.

Booth, D.B., and B.P. Bledsoe. 2009. "Streams and Urbanization." Pages 93–123, Chapter 6 in: *The Water Environment of Cities* (Ed. L.A. Baker), Springer Science+Business Media, LLC, 375 p.

Booth, D.B., S.R. Dusterhoff, E.D. Stein, and B.P. Bledsoe. 2010. "Hydromodification Screening Tools: GIS-based Catchment Analyses of Potential Changes in Runoff and Sediment Discharge." *Technical Report #605*, Southern California Coastal Water Research Project (SCCWRP), Costa Mesa, CA, 35 p., URL: http://ftp.sccwrp.org/pub/download/DOCUMENTS/TechnicalReports/605_HydromodScreeningTools_GIS.pdf.

Boyd, M.J., M.C. Bufill, and R.M. Knee. 1993. "Pervious and Impervious Runoff in Urban Catchments." *Hydrological Sciences Journal*, Vol. 38, No. 6, pp. 463–478, DOI: 10.1080/02626669309492699.

Brice, J.C. 1975. "Airphoto Interpretation of the Form and Behavior of Alluvial Rivers." Final Report, U.S. Army Research Office, St Louis, MO, 13 p.

Brockman, R.R., C.T. Agouridis, S.R. Workman, L.E. Ormsbee, and A.W. Fogle. 2012. "Bankfull Regional Curves for the Inner and Outer Bluegrass Regions of Kentucky." *Journal of the American Water Resources Association*, Vol. 48, No. 2, pp. 391–406.

Brown, C.B. 1950. *Sediment Transportation in Engineering Hydraulics*. Wiley, New York, pp. 769–857.

Brownlie, W.R. 1981. "Prediction of Flow Depth and Sediment Discharge in Open-channels." *Report No. KH-R-43A*, California Institute of Technology, W.M. Keck Laboratory, Pasadena, CA.

Bunte, K., and S.R. Abt. 2001. "Sampling Surface and Subsurface Particle-size Distributions in Wadable Gravel- and Cobble-bed Streams for Analyses in Sediment Transport, Hydraulics, and Streambed Monitoring." *General Technical Report RMRS-GTR-74*, U.S. Department of Agriculture, Forest Service, Rocky Mountain Research Station, Fort Collins, CO, 428 p., URL: http://www.stream.fs.fed.us/publications/PDFs/rmrs_gtr74.pdf.

Bunte, K. and S.R. Abt. 2009. "Transport Relationships between Bedload Traps and 3-inch Helley-Smith Sampler in Coarse Gravel-bed Streams and Development of Adjustment Functions." U.S. Army Corps of Engineers, Federal Interagency Sedimentation Project, Vicksburg, MS, December, 138 p., URL: http://water.usgs.gov/fisp/docs/091221_Bunte_and_Abt_Trap_HS_comparison_and_adjustment_functions_final.pdf.

Bunte, K., S.R. Abt, J.P. Potyondy, and S.E. Ryan. 2004. "Measurement of Coarse Gravel and Cobble Transport Using a Portable Bedload Trap." *Journal of Hydraulic Engineering*, Vol. 130, No. 9, pp. 879–893, DOI: 10.1061/(ASCE)0733-9429(2004)130:9(879).

Bunte, K., K.W. Swingle, S.R. Abt, and D. Cenderelli. 2013. "Steep Gravel Bedload Rating Curves Obtained from Bedload Traps Shift Effective Discharge to Flows Much Higher than 'Bankfull'." ePoster EP41A-0774 presented at the American Geophysical Union Fall Meeting, San Francisco, CA, December 3-17, 2012.

Burt, T.P., and W.T. Swank. 1992. "Flow Frequency Responses to Hardwood-to-grass Conversion and Subsequent Succession." *Hydrological Processes*, Vol. 6, No. 2, pp. 179–188, DOI: 10.1002/hyp.3360060206.

Cade, B.S., and B.R. Noon. 2003. "A Gentle Introduction to Quantile Regression for Ecologists." *Frontiers in Ecology and the Environment*, Vol. 1, No. 8, pp. 412–420, DOI: 10.1890/1540-9295(2003)001[0412:AGITQR]2.0.CO;2.

Caltrans. 2014. "Caltrans Hydromodification Requirements Guidance: Storm Water Best Management Practices, Rapid Assessment of Stream Crossings, Higher Level Stream Stability Analysis." *Report CTSW-OT-14-314.05*, California Department of Transportation, Storm Water Liaison, Caltrans Division of Environmental Analysis, Sacramento, CA, June, 156 p., URL: http://www.dot.ca.gov/hq/oppd/stormwtr/guidance/CT-Hydromodification-Requirements-Guidance-06-2014.pdf.

Carling, P. 1988. "The Concept of Dominant Discharge Applied to Two Gravel-bed Streams in Relation to Channel Stability Thresholds." *Earth Surface Processes and Landforms*, Vol. 13, No. 4, pp. 355–367, DOI: 10.1002/esp.3290130407.

Castellarin, A., G. Botter, D.A. Hughes, S. Liu, T.B.M.J. Ouarda, J. Parajka, D. Post, M. Sivapalan, C. Spence, A. Viglione, and R.M. Vogel. 2012. "Prediction of Flow Duration Curves in Ungauged Basins." Pages 135–162, Chapter 7 in: *Runoff Prediction in Ungauged Basins: Synthesis across Processes, Places and Scales* (Eds. G. Blöschl, M. Sivapalan, T. Wagener, A. Viglione, and H. Savenije), Cambridge University Press, New York, NY.

Chen, F.W., and C.W. Liu. 2012. "Estimation of the Spatial Rainfall Distribution using Inverse Distance Weighting (IDW) in the Middle of Taiwan." *Paddy and Water Environment*, Vol. 10, No. 3, pp. 209–222, DOI: 10.1007/s10333-012-0319-1.

Cheng, L., M. Yaeger, A. Viglione, E. Coopersmith, S. Ye, and M. Sivapalan. 2012. "Exploring the Physical Controls of Regional Patterns of Flow Duration Curves–Part 1: Insights from Statistical Analyses." *Hydrology and Earth System Sciences*, Vol. 16, No. 11, pp. 4435–4446, DOI: 10.5194/hess-16-4435-2012.

Chin, A., and K.J. Gregory. 2001. "Urbanization and Adjustment of Ephemeral Stream Channels." Annals of the Association of American Geographers, Vol. 91, No. 4, pp. 595–608, DOI: 10.1111/0004-5608.00260.

Church, M. 2006. "Bed Material Transport and the Morphology of Alluvial River Channels." *Annual Review of Earth and Planetary Sciences*, Vol. 34, pp. 325–354, DOI: 10.1146/annurev.earth.33.092203.122721.

Colby, B.R. 1956. "Relationship of Sediment Discharge to Streamflow." *U.S. Geological Survey Open File Report 56-27*, Reston, VA, 170 p.

Copeland, R.R. 1994. "Application of Channel Stability Methods – Case Studies." *Technical Report HL-94-11*, U.S. Army Corps of Engineers, Waterways Experiment Station, Vicksburg, MS, September, 60 p., URL: http://www.dtic.mil/dtic/tr/fulltext/u2/a285625.pdf.

Copeland, R.R., P.J. Soar, and C.R. Thorne. 2005. "Channel-forming Discharge and Hydraulic Geometry Width Predictors in Meandering Sand-bed Rivers." Pages 1 – 12 in R. Walton (Ed.): *Impacts of Global Climate Change*, World Water and Environmental Resources Congress 2005, Anchorage, AL, May 15-19, DOI: 10.1061/40792(173)568.

Crowder, D.W., and H.V. Knapp. 2005. "Effective Discharge Recurrence Intervals of Illinois Streams." *Geomorphology*, Vol. 64, Nos. 3–4, pp. 167–184, DOI: 10.1016/j.geomorph.2004.06.006.

Cuo, L., D.P. Lettenmaier, M. Alberti, and J.E. Richey. 2009. "Effects of a Century of Land Cover and Climate Change on the Hydrology of the Puget Sound Basin." *Hydrological Processes*, Vol. 23, No. 6, pp. 907–933, DOI: 10.1002/hyp.7228.

Cuo, L., T.K. Beyene, N. Voisin, F. Su, D.P. Lettenmaier, M. Alberti, and J.E. Richey. 2011. "Effects of Mid-twenty-first Century Climate and Land Cover Change on the Hydrology of the Puget Sound Basin, Washington." *Hydrological Processes*, Vol. 25, No. 11, pp. 1729–1753, DOI: 10.1002/hyp.7932.

Dietrich, W.E., J.W. Kirchner, H. Ikeda, and F. Iseya, F. 1989. "Sediment Supply and the Development of the Coarse Surface Layer in Gravel-bedded Rivers." *Nature*, Vol. 340, pp. 215–217, DOI: 10.1038/340215a0.

Doyle, M.W., D. Shields, K.F. Boyd, P.B. Skidmore, and D. Dominick. 2007. "Channel-forming Discharge Selection in River Restoration Design." *Journal of Hydraulic Engineering*, Vol. 133, No. 7, pp. 831–837, DOI: 10.1061/(ASCE)0733-9429(2007)133:7(831).

Dubler, D. 1997." Effective Discharge Determination in the Yazoo River Basin, Mississippi." Colorado State University, Department of Civil Engineering, Fort Collins, CO.

Eaton, B.C., and M. Church. 2011. "A Rational Sediment Transport Scaling Relation Based on Dimensionless Stream Power." *Earth Surface Processes and Landforms*, Vol. 36, No. 7, pp. 901–910, DOI: 10.1002/esp.2120.

Einstein, H.A. 1950. "The Bed Load Function for Sediment Transport in Open Channel Flows." *Technical Bulletin No. 1026*, U.S. Department of Agriculture, Soil Conservation Service, Washington, DC.

Emmett, W.W., and M.G. Wolman. 2001. "Effective Discharge and Gravel-bed Rivers." *Earth Surface Processes and Landforms*, Vol. 26, No. 13, pp. 1369–1380, DOI: 10.1002/esp.303.

Erwin, S., J. Schmidt, and N. Nelson. 2011. "Downstream Effects of Impounding a Natural Lake: The Snake River Downstream from Jackson Lake Dam, Wyoming, USA." *Earth Surface Processes and Landforms*, Vol. 36, No. 11, pp. 1421–1434, DOI: 10.1002/esp.2159.

Fennessey, N., and R.M. Vogel. 1990. "Regional Flow-Duration Curves for Ungauged Sites in Massachusetts." *Journal of Water Resources Planning and Management*, Vol. 116, No. 4, pp. 530–549, DOI: 10.1061/(ASCE)0733-9496(1990)116:4(530).

Ferguson, R.I. 2012. "River Channel Slope, Flow Resistance, and Gravel Entrainment Thresholds." *Water Resources Research*, Vol. 48, W05517, DOI: 10.1029/2011WR010850.

Ganora, D., P. Claps, F. Laio, and A. Viglione. 2009. "An Approach to Estimate Nonparametric Flow Duration Curves in Ungauged Basins." *Water Resources Research*, Vol. 45, No. 10, pp. 1–10, DOI: 10.1029/2008WR007472.

Gilbert, R.O. 1987. Statistical Methods for Environmental Pollution Monitoring. John Wiley & Sons, New York, NY.

Goodwin, P. 2004. "Analytical Solutions for Estimating Effective Discharge." *Journal of Hydraulic Engineering*, Vol. 130, No. 8, pp. 729–738, DOI: 10.1061/(ASCE)0733-9429(2004)130:8(729).

Graf, W.L. 1977. "Network Characteristics in Suburbanizing Streams." *Water Resources Research*, Vol. 13, No. 2, pp. 459–463, DOI: 10.1029/WR013i002p00459.

Grams, P.E., and J.C. Schmidt. 2005. "Equilibrium or Indeterminate? Where Sediment Budgets Fail: Sediment Mass Balance and Adjustment of Channel Form, Green River Downstream from Flaming Gorge Dam, Utah and Colorado." *Geomorphology*, Vol. 71, Nos. 1–2, pp, 156–181, DOI: 10.1016/j.geomorph.2004.10.012.

Grams P.E., D.J. Topping, J.C. Schmidt, J.E. Hazel Jr., and M. Kaplinski. 2013. "Linking Morphodynamic Response with Sediment Mass Balance on the Colorado River in Marble Canyon: Issues of Scale, Geomorphic Setting, and Sampling Design." *Journal of Geophysical Research Earth Surface*, Vol. 118, No. 2, 361–381, DOI: 10.1002/jgrf.20050.

Gregory, K.J., and A. Chin. 2002. "Urban Stream Channel Hazards." *Area*, Vol. 34, No. 3, pp. 312–321, DOI: 10.1111/1475-4762.00085.

Hagerman, J.R., and J.D. Williams. 2000. "Meander Shape and the Design of Stable Meanders." In: Proceedings of the American Water Resources Association, Spring Specialty Conference: *Riparian Ecology and Management in Multi-land Use Watersheds*, Anchorage, AK, April 30 - May 4, pp. 563–568.

Hamed, K.H. 2008. "Trend Detection in Hydrologic Data: The Mann-Kendall Trend Test under the Scaling Hypothesis." *Journal of Hydrology*, Vol. 349, Nos. 3–4, pp. 350–363, DOI: 10.1016/j.jhydrol.2007.11.009.

Hassan, M.A., D. Brayshaw, Y. Alila, and E. Andrews. 2014. "Effective Discharge in Small Formerly Glaciated Mountain Streams of British Columbia: Limitations and Implications." *Water Resources Research*, Vol. 50, No. 5, pp. 4440–4458, DOI: 10.1002/2013WR014529.

Hawley, R.J. and B.P. Bledsoe. 2011. "How do Flow Peaks and Durations Change in Suburbanizing Semi-arid Watersheds? A Southern California Case Study." *Journal of Hydrology*, Vol. 405, pp. 69–82, DOI: 10.1016/j.jhydrol.2011.05.011.

Hawley, R.J., and B.P. Bledsoe. 2013. "Channel Enlargement in Semiarid Suburbanizing Watersheds: A Southern California Case Study." *Journal of Hydrology*, Vol. 496, pp. 17–30, DOI: 10.1016/j.jhydrol.2013.05.010.

Hawley R.J., and G.J. Vietz. 2016. "Addressing the Urban Stream Disturbance Regime." *Freshwater Science*, Vol. 35, No. 1, DOI: 10.1086/684647.

Hawley R.J., K.R. MacMannis, and M.S. Wooten. 2013. "Bed Coarsening, Riffle Shortening, and Channel Enlargement in Urbanizing Watersheds, Northern Kentucky, USA." *Geomorphology*, Vol. 201, pp. 111–126, DOI: 10.1016/j.geomorph.2013.06.013

Hawley, R.J., B.P. Bledsoe, E.D. Stein, and B.E. Haines. 2012a. "Channel Evolution Model of Semiarid Stream Response to Urban-induced Hydromodification." *Journal of the American Water Resources Association*, Vol. 48, No. 4, pp. 722–744, DOI: 10.1111/j.1752-1688.2012.00645.x.

Hawley, R.J., M.S. Wooten, B.C. Vatter, E. Onderak, M.J. Lachniet, T. Schade, G. Grant, B. Groh, and J. DelVerne. 2012b. "Integrating Stormwater Controls Designed for Channel Protection, Water Quality, and Inflow/infiltration Mitigation in Two Pilot Watersheds to Restore a More Natural Flow Regime in Urban Streams." *Watershed Science Bulletin*, Vol. 3, No. 1, pp. 25–37, URL: http://www.cwp.org/images/stories/Images/wsb/wsbpdf/WSBsp12.pdf.

Henderson, F. 1966. *Open Channel Flow*. Macmillian Company, New York, NY, 544 p.

Hendon, S. 1995. "Comparison of 15-minute versus Mean Daily Flow Duration Curves from the Yazoo Basin." M.S. Thesis, Colorado State University, Department of Civil Engineering, Fort Collins, CO.

Hey, R.D. 1996. "Channel Response and Channel Forming Discharge." U.S. Army, European Research Office, University of East Anglia, 216 p.

Hey, R.D., and C.R. Thorne. 1986. "Stable Channels with Mobile Gravel Beds." *Journal of Hydraulic Engineering*, Vol. 112, No. 8, pp. 671–689, DOI: 10.1061/(ASCE)0733-9429(1986)112:8(671).

Hollis, G.E. 1975. "The Effect of Urbanization on Floods of Different Recurrence Interval." *Water Resources Research*, Vol. 11, No. 3, pp. 431–435, DOI: 10.1029/WR011i003p00431.

Homer, C., C. Huang, L. Yang, B. Wylie, and M. Coan. 2004. "Development of a 2001 National Land-Cover Database for the United States." *Photogrammetric Engineering and Remote Sensing*, Vol. 70, No. 7, pp. 829–840.

Homer, C.G., J.A. Dewitz, L. Yang, S. Jin, P. Danielson, G. Xian, J. Coulston, N.D. Herold, J.D. Wickham, and K. Megown. 2015. "Completion of the 2011 National Land Cover Database for the Conterminous United States – Representing a Decade of Land Cover Change Information." *Photogrammetric Engineering & Remote Sensing*, Vol. 81, No. 5, pp. 345–354.

Hotchkiss, R.H., and C.M. Frei. 2007. "Design for Fish Passage at Roadway-stream Crossings: Synthesis Report." *Publication No. FHWA-HIF-07-033*, U.S. Department of Transportation, Federal Highway Administration, McLean, VA, 280 p., URL: http://www.fhwa.dot.gov/engineering/hydraulics/pubs/07033/07033.pdf.

Inglis, C.C. 1947. "Meanders and Their Bearing on River Training. Maritime and Waterways Engineering Division." *Institution of Civil Engineers* (ICE) *Engineering Division Paper*, Vol. 5, No. 17, pp. 3–24, DOI: 10.1680/idivp.1947.13075.

Jennings, M.E., W.O. Thomas Jr., and H.C. Riggs. 1994. "Nationwide Summary of U.S. Geological Survey Regional Regression Equations for Estimating Magnitude and Frequency of Floods for Ungaged Sites, 1993," *Water-Resources Investigations Report 94-4002*, U.S. Geological Survey, Reston, VA, 196 p., URL: http://pubs.usgs.gov/wri/1994/4002/report.pdf.

Johnson, P.A., G.L. Gleason, and R.D. Hey. 1999. "Rapid Assessment of Channel Stability in Vicinity of Road Crossings." *Journal of Hydraulic Engineering*, Vol. 125, No. 6, pp. 645–651, DOI: 10.1061/(ASCE)0733-9429(1999)125:6(645).

Jones, M.L., and H.R. Seitz. 1980. "Sediment Transport in the Snake and Clearwater Rivers in the Vicinity of Lewiston, Idaho." *U.S. Geological Survey Open File Report 80-690*, 179 p.

Kahya, E., and S. Kalayci. 2004. "Trend Analysis of Streamflow in Turkey." *Journal of Hydrology*, Vol. 289, Nos. 1–4, pp. 128–144, DOI: 10.1016/j.jhydrol.2003.11.006.

Kendall, M.G. 1975. *Rank Correlation Methods*. Fourth Edition, Charles Griffin, London, UK.

King, J.G., W.W. Emmett, P.J. Whiting, R.P. Kenworthy, and J.J. Barry. 2004. "Sediment Transport Data and Related Information for Selected Coarse-Bed Streams and Rivers in Idaho." *General Technical Report RMRS-GTR-131*, U.S. Department of Agriculture, Forest Service, Rocky Mountain Research Station, 26 p., URL: http://www.fs.fed.us/rm/pubs/rmrs_gtr131.pdf\.

Klonsky, L., and R.M. Vogel (2011). "Effective Measures of "Effective" Discharge." *The Journal of Geology*, Vol. 119, No. 1, pp. 1–14, URL: http://www.jstor.org/stable/10.1086/657258.

Koenker, R., and G. Bassett. 1978. "Regression Quantiles." *Econometrics*, Vol. 46, No. 1, pp. 33–50.

Konrad, C.P. and D.B. Booth. 2002. "Hydrologic Trends Associated with Urban Development for Selected Streams in the Puget Sound Basin, Western Washington." *Water-Resources Investigations Report 02-4040*, U.S. Department of the Interior, U.S. Geological Survey, Tacoma, WA, 40 p.

Konrad, C.P., D.B. Booth, and S.J. Burges. 2005. "Effects of Urban Development in the Puget Lowland, Washington, on Interannual Streamflow Patterns: Consequences for Channel Form and Streambed Disturbance." *Water Resources Research*, Vol. 41, No. 7, W07009, DOI: 10.1029/2005WR004097.

Kruckeberg, A.R. 1991. *The Natural History of Puget Sound Country*. University of Washington Press, Seattle, WA.

Kumar, S., V. Merwade, J. Kam, and K. Thurner. 2009. "Streamflow Trends in Indiana: Effects of Long Term Persistence, Precipitation and Subsurface Drains." *Journal of Hydrology*, Vol. 374, Nos. 1–2, pp. 171–183, DOI: 10.1016/j.jhydrol.2009.06.012.

Lagasse, P.F., L.W. Zevenbergen, W.J. Spitz, and L.A. Arneson. 2012. "Stream Stability at Highway Structures." *Publication No. FHWA-HIF-12-004*, Fourth Edition, Department of Transportation, Federal Highway Administration, April, 328 p., URL: http://www.fhwa.dot.gov/engineering/hydraulics/pubs/hif12004.pdf.

Ley, R., M.C. Casper, H. Hellebrand, and R. Merz. 2011. "Catchment Classification by Runoff Behavior with Self-organizing Maps (SOM)." *Hydrology and Earth System Sciences*, Vol. 15, No. 9, pp. 2947–2962, DOI: 10.5194/hess-15-2947-2011.

Li, J., and A.D. Heap. 2011. "A Review of Comparative Studies of Spatial Interpolation Methods in Environmental Sciences: Performance and Impact Factors." *Ecological Informatics*, Vol. 6, Nos. 3–4, pp. 228–241, DOI: 10.1016/j.ecoinf.2010.12.003.

Lim, K.J., B.A. Engel, Z. Tang, J. Choi, K.S. Kim, S. Muthukrishnan, and D. Tripathy. 2005. "Automated Web GIS Based Hydrograph Analysis Tool, WHAT." *Journal of the American Water Resources Association*, Vol. 41, No. 6, pp. 1407–1416, DOI: 10.1111/j.1752-1688.2005.tb03808.x.

Limerinos, J.T. 1970. "Determination of the Manning Coefficient from Measured Bed Roughness in Natural Channels." *U.S. Geological Survey Water-Supply Paper 1898-B*, 47 p., U.S. Government Printing Office, Washington, DC, URL: http://pubs.usgs.gov/wsp/1898b/report.pdf.

Lu, G.Y., and D.W. Wong. 2008. "An Adaptive Inverse-distance Weighting Spatial Interpolation Technique." *Computers & Geosciences*, Vol. 34, No. 9, pp. 1044–1055, DOI: 10.1016/j.cageo.2007.07.010.

Mann, H.B. 1945. "Non-parametric Tests against Trend." *Econometricia*, Vol. 13, No. 3, pp. 245–259, DOI: 10.2307/1907187.

Martin, Y., and M. Church. 2000. "Re-examination of Bagnold's Empirical Bedload Formulae." *Earth Surface Processes and Landforms*, Vol. 25, No. 9, pp. 1011–1024, DOI: 10.1002/1096-9837(200008)25:9<1011::AID-ESP114>3.0.CO;2-H.

Meyer, S.C. 2005. "Analysis of Base Flow Trends in Urban Streams, Northeastern Illinois, USA." *Hydrogeology Journal*, Vol. 13, Nos. 5–6, pp. 871–885, DOI: 10.1007/s10040-004-0383-8.

Meyer-Peter, E., and R. Müller. 1948. "Formulas for Bed-load Transport." In: Proceedings 2nd Meeting International Association for Hydraulic Research (IAHR), TU Delft, Stockholm, pp. 39–64.

Milly, P.C.D. 2007. "Stationarity is Dead." *Ground Water News & Views*, Vol. 4, No. 1, pp. 6–8.

Minnesota Population Center. 2011. "National Historical Geographic Information System: Version 2.0." University of Minnesota, Minneapolis, MN.

Montgomery, D.R., and J.M. Buffington. 1997. "Channel-reach Morphology in Mountain Drainage Basins." *Geological Society of America Bulletin*, Vol. 109, No. 5, pp. 596–611, DOI: 10.1130/0016-7606(1997)109<0596: CRMIMD>2.3.CO;2.

Mueller, E.R., and J. Pitlick. 2013. "Sediment Supply and Channel Morphology in Mountain River Systems: 1. Relative Importance of Lithology, Topography, and Climate." *Journal of Geophysical Research: Earth Surface*, Vol. 118, No. 4, pp. 2325–2342, DOI: 10.1002/2013JF002843.

Musiake, K., S. Inokuti, and Y. Takahasi. 1975. "Dependence of Low Flow Characteristics on Basin Geology in Mountainous Areas of Japan." *IAHS Publication No. 117*, International Association of Hydrologic Sciences, Wallingford, Oxfordshire, UK, pp. 147–156.

Nanson, G.C., and J.C. Croke. 1992. "A Genetic Classification of Floodplains." *Geomorphology*, Vol. 4, No. 6, pp. 459–486, DOI: 10.1016/0169-555X(92)90039-Q.

Nash, D.B. 1994. "Effective Sediment-transporting Discharge from Magnitude-frequency Analysis." *The Journal of Geology*, Vol. 102, No. 1, pp. 79–95, URL: http://www.jstor.org/stable/30065712.

Natural Resources Conservation Service (NRCS). 1986. "Urban Hydrology for Small Watersheds." *Technical Release 55*, U.S. Department of Agriculture, NRCS, 164 p., URL: http://www.nrcs.usda.gov/Internet/FSE_DOCUMENTS /stelprdb1044171.pdf.

Natural Resources Conservation Service (NRCS). 2007. "Chapter 4: Stream Restoration Design Process." In: *Part 654 National Engineering Handbook,* U.S. Department of Agriculture, NRCS, Washington, DC.

Natural Resources Conservation Service (NRCS). 2010. "Chapter 15: Time of Concentration." In: *Part 630 National Engineering Handbook*, U.S. Department of Agriculture, NRCS, Washington, DC.

Niraula, R., T. Meixner, and L.M. Norman. 2015. "Determining the Importance of Model Calibration for Forecasting Absolute/Relative Changes in Streamflow from LULC and Climate Changes." *Journal of Hydrology,* Vol. 522, pp. 439–451, DOI: 10.1016/j.jhydrol.2015.01.007.

Nolan, K.M., T.M. Lisle, and H.M. Kelsey. 1987. "Bankfull discharge and sediment transport in northwestern California." Pages 439–450 in R.L. Beschta (Ed.): *Erosion and Sedimentation in the Pacific Rim*, IAHS Publications, Wallingford, Oxfordshire, UK.

Orndorff, R.L., and P.J. Whiting. 1999. "Computing Effective Discharge with S-PLUS." *Computers & Geosciences*, Vol. 25, No. 5, pp. 559–565, DOI: 10.1016/S0098-3004(98)00127-7.

Parker, G. 1979. "Hydraulic Geometry of Active Gravel Rivers." *Journal of the Hydraulics Division*, *Proceedings of the American Society of Civil Engineers*, Vol. 105, pp. 1185–1201.

Parker, G. 1990a. "Surface-based Bedload Transport Relation for Gravel Rivers." *Journal of Hydraulic Research*, Vol. 28, No. 4, pp. 417–436, DOI: 10.1080/00221689009499058.

Parker, G. 1990b. "The "acronym" Series of Pascal Programs for Computing Bedload Transport in Gravel Rivers." *External Memorandum M-220*, St. Anthony Falls Hydraulic Laboratory, University of Minnesota, Minneapolis, MN, 24 p.

Pickup, G., and R.F. Warner. 1976. "Effects of Hydrologic Regime on Magnitude and Frequency of Dominant Discharge." *Journal of Hydrology*, Vol. 29, Nos. 1–2, pp. 51–75, DOI: 10.1016/0022-1694(76)90005-6.

Poff, N. 1996. "A Hydrogeography of Unregulated Streams in the United States and an Examination of Scale-Dependence in Some Hydrological Descriptors." *Freshwater Biology*, Vol. 36, No. 1, pp. 71–91, DOI: 10.1046/j.1365-2427.1996.00073.x.

Poff, N.L., B.P. Bledsoe, and C.O. Cuhaciyan. 2006. "Hydrologic Variation with Land Use across the Contiguous United States: Geomorphic and Ecological Consequences for Stream Ecosystems." *Geomorphology*, Vol. 79, Nos. 3–4, pp. 264–285, DOI: 10.1016/j.geomorph.2006.06.032.

Praskievicz, S., and H. Chang. 2009. "A Review of Hydrological Modelling of Basin-scale Climate Change and Urban Development Impacts." *Progress in Physical Geography*, Vol. 33, No. 5, pp. 650–671, DOI: 10.1177/0309133309348098.

Price, K. 2011. "Effects of Watershed Topography, Soils, Land Use, and Climate on Baseflow Hydrology in Humid Regions: A Review." *Progress in Physical Geography*, Vol. 35, No. 4, pp. 465–492, DOI: 10.1177/0309133311402714.

Quader, A., and Y. Guo. 2009. "Relative Importance of Hydrological and Sediment-transport Characteristics Affecting Effective Discharge of Small Urban Streams in Southern Ontario." *Journal of Hydrologic Engineering*, Vol. 14, No. 7, pp. 698–710, DOI: 10.1061/(ASCE)HE.1943-5584.0000042).

Quader, A., Y. Guo, and J.R. Stedinger. 2008. "Analytical Estimation of Effective Discharge for Small Southern Ontario Streams." *Canadian Journal of Civil Engineering*, Vol. 35, No. 12, pp. 1414–1426, DOI: 10.1139/L08-088.

R CORE Team. 2014a. "Package 'MASS' – Support Functions and Datasets for Venables and Ripley's MASS." The Comprehensive R Archive Network (CRAN) Repository, URL: https://cran.r-project.org/web/packages/MASS/MASS.pdf.

R CORE Team. 2014b. "Package 'pracma' – Practical Numerical Math Functions." The Comprehensive R Archive Network (CRAN) Repository, URL: https://cran.r-project.org/web/packages/pracma/pracma.pdf.

R CORE Team. 2014c. "Package 'leaps' – Regression Subset Selection." The Comprehensive R Archive Network (CRAN) Repository, URL: https://cran.r-project.org/web/packages/leaps/leaps.pdf.

Rankl, J., and M. Smalley. 1992. "Transport of Sediment by Streams in the Sierra Madre, Southern Wyoming." *U.S. Geological Survey Open-File Report WRIR 92-4091*, Cheyenne, WY.

Reid, L.M., and T. Dunne. 1996. *Rapid Evaluation of Sediment Budgets*. Vol. 29, Geo-Ecology Texts, Catena Verlag, Reiskirchen, Germany, 164 p.

Reidy Liermann, C.A., J.D. Olden, T.J. Beechie, M.J. Kennard, P.B. Skidmore, C.P. Konrad, and H. Imaki. 2012. "Hydrogeomorphic Classification of Washington State Rivers to Support Emerging Environmental Flow Management Strategies." *River Research and Applications*, Vol. 28, No. 9, pp. 1340–1358, DOI: 10.1002/rra.1541.

Rosburg T. 2015. "Flow Duration Curves and Sediment Yield Estimation for Urbanizing Watersheds." M.S. Thesis, Colorado State University, Department of Civil and Environmental Engineering, Fort Collins, CO.

Rosgen, D.L. 1994. "A Classification of Natural Rivers." *Catena*, Vol. 22, No. 3, pp. 169–199, DOI: 10.1016/0341-8162(94)90001-9.

Sawicz, K.A., C. Kelleher, T. Wagener, P. Troch, M. Sivapalan, and G. Carrillo. 2014. "Characterizing Hydrologic Change through Catchment Classification." *Hydrology and Earth System Sciences*, Vol. 18, No. 1, pp. 273–285, DOI: 10.5194/hess-18-273-2014.

Schmelter, M.L., S.O. Erwin, and P.R. Wilcock. 2012. "Accounting for Uncertainty in Cumulative Sediment Transport Using Bayesian Statistics." *Geomorphology*, Vols. 175–176, pp. 1–13, DOI: 10.1016/j.geomorph.2012.06.012.

Schumm, S.A., M.D. Harvey, and C.C. Watson. 1984. *Incised Channels: Morphology, Dynamics, and Control*. Water Resources Publications LLC, Littleton, CO.

Searcy, J. K. 1959. "Flow-duration Curves (Manual of Hydrology: Part 2. Low-Flow Techniques)." *Geological Survey Water-Supply Paper 1542-A*, Geological Survey, U.S. Government Printing Office, Washington, DC, 33 p.

Sheng, J., and J.P. Wilson. 2009. "Watershed Urbanization and Changing Flood Behavior across the Los Angeles Metropolitan Region." *Natural Hazards*, Vol. 48, No. 1, pp. 41–57, DOI: 10.1007/s11069-008-9241-7.

Sherwood, J.M., and C.A. Huitger. 2005. "Bankfull Characteristics of Ohio Streams and their Relation to Peak Streamflows." *Scientific Investigations Report 2005-5153*, U.S. Department of the Interior, U.S. Geological Survey, Reston, VA, 52 p., URL: http://pubs.usgs.gov/sir/2005/5153/pdf/Bankfull_book.pdf.

Shields Jr., F.D., R.R. Copeland, P.C. Klingeman, M.W. Doyle, and A. Simon. 2003. "Design for Stream Restoration." *Journal of Hydraulic Engineering*, Vol. 129, No. 8, pp. 575–584, DOI: 10.1061/(ASCE)0733-9429(2003)129:8(575).

Shields Jr., F.D., R.R. Copeland, P.C. Klingeman, M.W. Doyle, and A. Simon. 2008. "Stream Restoration." Pages 461–503, Chapter 9, DOI: 10.1061/9780784408148.ch09, M. Garcia (Ed.): *Sedimentation Engineering: Processes, Measurements, Modeling, and Practice*, Manual of Practice (MOP) 110.

Sholtes, J. 2005. "On the Magnitude and Frequency of Sediment Transport in River." PhD Dissertation, Department of Civil and Environmental Engineering, Colorado State University, Fort Collins, CO.

Sichingabula, H.M. (1999). "Magnitude-frequency characteristics of effective discharge for suspended sediment transport, Fraser River, British Columbia, Canada." *Hydrological Processes*, Vol. 13, No. 9, pp. 1361–1380, DOI: 10.1002/(SICI)1099-1085(19990630)13:9<1361::AID-HYP808>3.0.CO;2-H.

Simmons, D.L., and R.J. Reynolds. 1982. "Effects of Urbanization on Base Flow of Selected South-shore Streams, Long Island, New York." *Journal of the American Water Resources Association*, Vol. 18, No. 5, pp. 797–805, DOI: 10.1111/j.1752-1688.1982.tb00075.x.

Simon, A. 1989. "A Model of Channel Response in Disturbed Alluvial Channels." *Earth Surface Processes and Landforms*, Vol. 14, No. 1, pp. 11–26, DOI: 10.1002/esp.3290140103.

Simon, A. 1995. "Adjustment and Recovery of Unstable Alluvial Channels: Identification and Approaches for Engineering Management." *Earth Surface Processes and Landforms*, Vol. 20, No. 7, pp. 611–628, DOI: 10.1002/esp.3290200705.

Simon, A., and P.W. Downs. 1995. "An Interdisciplinary Approach to Evaluation of Potential Instability in Alluvial Channels." *Geomorphology*, Vol. 12, No. 3, pp. 215–232, DOI: 10.1016/0169-555X(95)00005-P.

Simon, A., W. Dickerson, and A. Heins. 2004. "Suspended-sediment Transport Rates at the 1.5-year Recurrence Interval for Ecoregions of the United States: Transport Conditions at the Bankfull and Effective Discharge?" *Geomorphology*, Vol. 58, Nos. 1–4, pp. 243–262, DOI: 10.1016/j.geomorph.2003.07.003.

Smakhtin, V.Y. 1997. "Regional Low-flow Studies in South Africa." Pages 125–132 in: FRIEND '97, *Regional Hydrology: Concepts and Models for Sustainable Water Resource Management* (Eds. A. Gustard, S. Blazkova, M. Brilly, S. Demuth, J. Dixon, H. van Lanen, C. Llasat, S. Mkhandi, and E. Servat); *IAHS Publication No. 246*, International Association of Hydrologic Sciences, Wallingford, Oxfordshire, UK.

Smalley, M.L., W.W. Emmett, and A.M. Wacker. 1994. "Annual Replenishment of Bed Material by Sediment Transport in the Wind River near Riverton, Wyoming." *U.S. Geological Survey Water-Resources Investigations Report 94-4007*, Cheyenne, WY, 23 p.

Smith, J.A., M.L. Baeck, J.E. Morrison, P. Sturdevant-Rees, D.F. Turner-Gillespie, and P.D. Bates. 2002. "The Regional Hydrology of Extreme Floods in an Urbanizing Drainage Basin." *Journal of Hydrometeorology*, Vol. 3, No. 3, pp. 267–282, DOI: 10.1175/1525-7541(2002)003<0267:TRHOEF>2.0.CO;2.

Smith, R.F., R.J. Hawley, M.W. Neale, G.J. Vietz, E. Diaz-Pascacio, J. Herrmann, A.C. Lovell, C. Prescott, B. Rios-Touma, B. Smith, and R.M. Utz. 2016. "Urban Stream Renovation: Incorporating Societal Objectives to Achieve Ecological Improvements." *Freshwater Science*, Vol. 35, No. 1, DOI: 10.1086/685096.

Smith, S.M., and K.L. Prestegaard. 2005. "Hydraulic Performance of a Morphology-based Stream Channel Design." *Water Resources Research*, Vol. 41, No. 11, W11413, DOI: 10.1029/2004WR003926.

Snyder & Associates, Inc. 2013. "Fourmile Creek Watershed Study." Final Report, Snyder & Associates, Inc., Ankeny, IA, URL: www.fourmilecreekwatershed.org/FourmileCreek/FMCW_1_Report_Final-Web.pdf, accessed June 30, 2015.

Soar, P.J., and C.R. Thorne. 2001. "Channel Restoration Design for Meandering Rivers." *Technical Report No. ERDC/CHL CR-01-1*, Coastal and Hydraulics Laboratory, U.S. Army, Engineer Research and Development Center, Vicksburg, MS, URL: http://www.nrcs.usda.gov/Internet/FSE_DOCUMENTS/stelprdb1043218.pdf.

Soar, P.J., and C.R. Thorne. 2011. "Design Discharge for River Restoration." Pages 123–150 in A. Simon, S.J. Bennett, and J.M. Castro (Eds.): *Stream Restoration in Dynamic Fluvial Systems: Scientific Approaches, Analyses, and Tools*, Geophysical Monograph Series, Volume 194, American Geophysical Union, Geopress, Washington, DC.

Sophocleous, M. 2002. "Interactions between Groundwater and Surface Water: The State of the Science." *Hydrogeology Journal*, Vol. 10, No. 1, pp. 52–67, DOI: 10.1007/s10040-001-0170-8.

Stankowski, S.J. 1972. "Population Density as an Indirect Indicator of Urban and Suburban Land-surface Modifications." *U.S. Geological Survey Professional Paper 800-B*, pp. B219–B224.

Strahler, A.N. 1952. "Hypsometric (area-altitude) Analysis of Erosional Topography." *Bulletin of the Geological Society of America*, Vol. 63, No. 11, pp. 1117–1142, DOI: 10.1130/0016-7606(1952)63[1117:HAAOET]2.0.CO;2.

Syvitski, J.P., M.D. Morehead, D.B. Bahr, and T. Mulder. 2000. "Estimating Fluvial Sediment Transport: The Rating Parameters." *Water Resources Research*, Vol. 36, No. 9, pp. 2747–2760, DOI: 10.1029/2000WR900133.

Theil, H. 1958. *Economic Forecasts and Policy*. North Holland Publishing Company, Amsterdam.

Thomas, W.A., R.R. Copeland, and D.N. McComas. 2002. "SAM Hydraulic Design Package for Channels." Coastal and Hydraulics Laboratory, U.S. Army Engineer Research and Development Center, Vicksburg, MS, URL: http://www.stream.fs.fed.us/fishxing/fplibrary/ACOE_2002_SAM_Hydraulic_Design_Package_for_Channels.pdf.

Torizzo, M., and J. Pitlick. 2004. "Magnitude-frequency of bed-load transport in mountain streams in Colorado." *Journal of Hydrology*, Vol. 290, Nos. 1–2, pp. 137–151, DOI: 10.1016/j.jhydrol.2003.12.001.

U.S. Department of Agriculture, U.S. Forest Service (USDA USFS). 2014. "Sediment Transport in Colorado and Wyoming." Website URL: http://www.fs.fed.us/rm/boise/AWAE/projects/sediment_transport/sediment_transport_COWY.html, accessed May 15, 2014.

U.S. Forest Service (USFS). 2008. "Stream Simulation: An Ecological Approach to Providing Passage for Aquatic Organisms at Road-Stream Crossings." *Report 0877 1801—SDTDC* (San Dimas Technology and Development Center), U.S. Department of Agriculture, Forest Service, National Technology and Development Program, San Dimas, CA, May, 646 p., URL: http://www.stream.fs.fed.us/fishxing/aop_pdfs.html.

U.S. Forest Service (USFS), Boise Adjudication Team (BAT). 2014a. "Sediment Transport in Idaho and Nevada." U.S. Forest Service, Website URL: http://www.fs.fed.us/rm/boise/AWAE/projects/sediment_transport/sediment_transport_BAT.shtml, accessed May 18, 2014.

U.S. Forest Service (USFS). 2014b. "Sediment Transport in Colorado and Wyoming."

U.S. Geological Survey (USGS). 2012. "The StreamStats program." Website URL: http://streamstats.usgs.gov.

U.S. Geological Survey (USGS), Sediment Data Portal. 2014. "USGS Sediment Data Portal." Website URL: http://cida.usgs.gov/sediment/, accessed March 14, 2014.

U.S. Geological Service, National Water Information System (USGS NWIS). 2014. "USGS National Water Information System." Website URL: http://waterdata.usgs.gov/nwis/, accessed June 16, 2014.

Utz, R.M., K.G. Hopkins, L. Beesley, D.B. Booth, R.J. Hawley, M.E. Baker, M.C. Freeman, and K.L. Jones. 2016. "Ecological Resistance in Urban Streams: The Role of Natural and Legacy Attributes." *Freshwater Science*, Vol. 35, No. 1, pp. 380–397, DOI: 10.1086/684839.

van den Berg, J.H. 1995. "Prediction of Alluvial Channel Pattern of Perennial Rivers." *Geomorphology*, Vol. 12, No. 4, pp. 259–279, DOI: 10.1016/0169-555X(95)00014-V.

Vigil, J.F., R.J. Pike, and D.G. Howell. 2000. "A Tapestry of Time and Terrain." *Geologic Investigations Series 2720*, U.S. Geological Survey, 1 plate scale 1:2,500,000, 1 pamphlet, URL: http://pubs.usgs.gov/imap/i2720/.

Villarini, G., F. Serinaldi, J.A. Smith, and W.F. Krajewski. 2009. "On the Stationarity of Annual Flood Peaks in the Continental United States during the 20th Century." *Water Resources Research*, Vol. 45, No. 8, DOI: 10.1029/2008WR007645.

Vogel, R.M., J.R. Stedinger, and R.P. Hooper. 2003. "Discharge Indices for Water Quality Loads." *Water Resources Research*, Vol. 39, No. 10, DOI: 10.1029/2002WR001872.

Vogel, R.M., C. Yaindl, and M. Walter. 2011. "Nonstationarity: Flood Magnification and Recurrence Reduction Factors in the United States." *Journal of the American Water Resources Association*, Vol. 47, No. 3, pp. 464–474, DOI: 10.1111/j.1752-1688.2011.00541.x.

Walling, D.E. 1977. "Limitations of the Rating Curve Technique for Estimating Suspended Sediment Loads, with Particular Reference to British Rivers." *Journal of the International Association of Hydrological Sciences*, Vol. 122, pp. 34–48.

Walsh, C.J., A.H. Roy, J.W. Feminella, P.D. Cottingham, P.M. Groffman, and R.P. Morgan. 2005. "The Urban Stream Syndrome: Current Knowledge and the Search for a Cure." *Journal of the North American Benthological Society*, Vol. 24, No. 3, pp. 706–723, DOI: 10.1899/04-028.1.

Washington State. 2012. "Historical Data Set: Decennial Population Counts for the State, Counties, Cities and Towns." Office of Financial Management, URL: http://www.ofm.wa.gov/pop/april1/hseries/default.asp, accessed March 2015.

Watson, C.C, D. Dubler, and S.R. Abt. 1997. "Design Hydrology Investigations." Demonstration Erosion Control Project Report, Colorado State University, Fort Collins, CO, submitted to the U.S. Army Corps of Engineers, Waterways Experiment Station, Vicksburg, MS, 72 p.

Watson, C.C., D.S. Biedenharn, and B.P. Bledsoe. 2002. "Use of Incised Channel Evolution Models in Understanding Rehabilitation Alternatives." *Journal of the American Water Resources Association*, Vol. 38, No. 1, pp. 151–160, DOI: 10.1111/j.1752-1688.2002.tb01542.x.

Webb, B.W., and D.E. Walling. 1982. "The Magnitude and Frequency Characteristics of Fluvial Transport in a Devon Drainage Basin and Some Geomorphological Implications." *Catena*, Vol. 9, Nos. 1–2, pp. 9–23, DOI: 10.1016/S0341-8162(82)80002-7.

Western Washington Hydrology Model (WWHM). 2012. "Western Washington Continuous Simulation Hydrology Model 2012, User Manual." Prepared by Clear Creek Solutions, Inc. for Department of Ecology, State of Washington, Bellevue, WA, May 2014, URL: http://www.ecy.wa.gov/programs/wq/stormwater/wwhmtraining/ WWHM2012UserMnul2014May.pdf.

Whiting, P.J., and J.B. Bradley. 1993. "A Process-based Classification System for Headwater Streams." *Earth Surface Processes and Landforms*, Vol. 18, No. 7, pp. 603–612, DOI: 10.1002/esp.3290180704.

Whiting, P.J., J.F. Stamm, D.B. Moog, and R.L. Orndorff. 1999. "Sediment-transporting Flows in Headwater Streams." *The Geological Society of America Bulletin*, Vol. 111, No. 3, pp. 450–466, DOI: 10.1130/0016-7606(1999)111<0450:STFIHS>2.3.CO;2.

Wilcock, P.R. 2001. "Toward a Practical Method for Estimating Sediment-transport Rates in Gravel-bed Rivers." *Earth Surface Processes and Landforms*, Vol. 26, No. 13, pp. 1395–1408, DOI: 10.1002/esp.301.

Wilcock, P.R., and S.T. Kenworthy. 2002. "A Two-Fraction Model for the Transport of Sand/Gravel Mixtures." *Water Resources Research*, Vol. 38, No. 10, pp. 12-1–12-12, DOI: 10.1029/2001WR000684.

Wilcock, P.R., and J.C. Crowe. 2003. "Surface-based Transport Model for Mixed-size Sediment." *Journal of Hydraulic Engineering*, Vol. 129, No. 2, pp. 120–128, DOI: 10.1061/(ASCE)0733-9429(2003)129:2(120).

Williams, R.P., and J.P. Krupkin. 1984. "Erosion, Channel Change, and Sediment Transport in the Big Lost River, Idaho." *U.S. Geological Survey Water-Resources Investigations Report 84-414*, Boise, ID, 87 p.

Wohl, E., B.P. Bledsoe, R.B. Jacobson, N.L. Poff, S.L. Rathburn, D.M. Walters, and A.C. Wilcox. 2015. "The Natural Sediment Regime in Rivers: Broadening the Foundation for Ecosystem Management." *Bioscience*, Vol. 65, No. 4, pp. 358–371, DOI: 10.1093/biosci/biv002.

Wolman, M.G., and L.B. Leopold. 1957. "River Flood Plains: Some Observations on Their Formation." *Geological Survey Professional Paper 282-C*, U.S. Government Printing Office, Washington, DC, 30 p., URL: http://pubs.usgs.gov/pp/0282c/report.pdf.

Wolman, M.G., and J.P. Miller. 1960. "Magnitude and Frequency of Forces in Geomorphic Processes." *Journal of Geology*, Vol. 68, No. 1, pp. 54–74, DOI: 10.1086/626637.

Wong, M., and G. Parker. 2006. "Reanalysis and Correction of Bed-load Relation of Meyer-Peter and Müller using their Own Database." *Journal of Hydraulic Engineering*, Vol. 132, No. 11, pp. 1159–1168, DOI: 10.1061/(ASCE)0733-9429(2006)132:11(1159).

Yang, C.T. 1973. "Incipient Motion and Sediment Transport." *Journal of the Hydraulics Division*, Vol. 99, No. 10, pp. 1679–1704.

Yang, C.T. 1979. "Unit Stream Power Equations for Total Load." *Journal of Hydrology*, Vol. 40, Nos. 1–2, pp. 123–138, DOI: 10.1016/0022-1694(79)90092-1.

Yang, C.T. 1996. *Sediment Transport: Theory and Practice*. McGraw-Hill, New York, NY, 396 p.

LIST OF ABBREVIATIONS, ACRONYMS, INITIALISMS, AND SYMBOLS

Units of Measure

cfs	cubic feet per second
cms, m^3/s	cubic meter(s) per second
ft	foot or feet
H:V	horizontal:vertical
in.	inch(es)
kg/m^3	kilogram(s) per cubic meter
kg/s	kilogram(s) per second
$kg/s/m^3/s$	(kilogram(s) per second) per cubic meter / second
km	kilometer(s)
km^2	square kilometer(s)
L^3/T	volume per time
m	meter(s)
m/m	meter(s) per meter
m/s^2	meter(s) per second squared
m^2	square meter(s)
m^2/s	square meter(s) per second
m^3	cubic meter(s)
mm	millimeter(s)
%	percent
Pa	Pascal(s)
ppm	parts per million
W/m^2	Watt(s) per square meter
yr(s)	year(s)

Statistical Terms

a	best-fit sediment rating curve coefficient
b	best-fit sediment rating curve exponent
C_v	coefficient of variation
CDF	cumulative distribution function
CI	confidence interval
OLS	ordinary least squares
p-value	probability
PDF	probability density function
R^2	coefficient of determination

RMSD	root mean square deviation
RMSE	root mean square error
SD	standard error of the estimate
SE	standard error
U	measure of association
Var(KDF)	kernel density function
α	coefficient
β	sediment rating curve exponent
τ	Mann-Kendall test statistic

<u>Acronyms</u>

ARS	Agricultural Research Service
ASCE	American Society of Civil Engineers
BAT	Boise Adjudication Team
CEM	Channel Evolution Model
CSR	Capacity-Supply Ratio
CSU	Colorado State University
CSV	comma separated value
DEM	Digital Elevation Models
DOT	Department of Transportation
eRAMS	Environmental Risk Assessment & Management System
GOF	goodness-of-fit
EPA	U.S. Environmental Protection Agency
ESRI	Environmental Systems Research Institute
FDC	flow duration curve
GHCND	Global Historical Climatology Network – Daily
GIS	Geographical Information System
GOF	goodness-of -fit
HEC	Hydraulic Engineering Circular
HEC-20	*Hydraulic Engineering Circular No. 20*
HEC-HMS	Hydrologic Engineering Center Hydrologic Modeling System
HEC-RAS	Hydrologic Engineering Center River Analysis System
HG	at-a-station hydraulic geometry relation
HRU	Hydrologic Response Unit
HSPF	Hydrologic Simulation Program Fortran
HUC	Hydrologic Unit Code
HydroDEM	hydrologically conditioned DEM
Hydro-NHD	Hydro National Hydrography Dataset
IC	Indian Creek near Wyoming, Illinois, study site
IDA	Instantaneous Data Archive
IQR	interquartile range
LiDAR	Light Detection and Ranging
LOESS	local regression scatterplot smoothing
MASS	Modern Applied Statistics with S

MFA	magnitude-frequency analysis
MRLC	Multi-Resolution Land Characteristics Consortium
NASS	National Agricultural Statistics Service
NCDC	National Climatic Data Center
NCHRP	National Cooperative Highway Research Program
NHDPlus	National Hydrography Dataset Plus
NLCD	National Land Cover Database
NRCS	Natural Resources Conservation Service
NSF	National Science Foundation
NWIS	National Water Information System
O	on the order of
R-B Index	Richards-Baker Flashiness Index
RGA	rapid geomorphic assessment
RLM	robust linear model
SAM	Hydraulic Design Package for Channels
SR	South Fork of the Salmon River, Idaho, study site
SRP	Stream Response Potential
SSURGO	Soil Survey Geographic Database
STORET	STOrage and RETrieval
SWAT	Soil and Water Assessment Tool
SWAT-DEG	channel DEGradation portion of SWAT
SWMM	Storm Water Management Model
TC	Trapper Creek, Idaho, study site
U.S.	United States
USACE	U.S. Army Corps of Engineers
USDA-ARS	U.S. Department of Agriculture – Agricultural Research Service
USFS	U.S. Forest Service
USGS	U.S. Geological Survey
VBA	Visual Basic for Applications
WHAT	Web-based Hydrograph Analysis Tool
WK	Wilcock and Kenworthy two-fraction bedload model
WRAP	Watershed Rapid Assessment Program
WWHM	Western Washington Hydrology Model
XS	cross section
YR	Yampa River at Deerlodge, Colorado, study site

Flow Metrics

cv	coefficient of variation of daily flow ($s / \bar{x}$)
flash.RB	daily flow Richards-Baker flashiness metric
mean	mean of daily discharge [m^3/s]
skewness	skewness of daily flow
spread	(75th percentile flow – 25th percentile flow) / median flow
Q1.5	1.5-yr return interval flood [m^3/s]
Q1.5.mean	$Q_{1.5}$ normalized by the mean of the daily flows

Qeff	effective discharge [L^3/T]
T_{Qmean}	represents the fraction of the time that mean discharge was exceeded
yrs	number of years on flow record [yrs]

Physical Metrics

d50	average median diameter of the bed sediment [mm]
d84	84th percentile diameter of the bed sediment [mm]
da.km2	drainage area [km^2]
Qbf	bankfull discharge [m^3/s]
tau.star	dimensionless bed grain shear stress
w.d	bankfull width-to-depth ratio

Yield Metrics

beta, β	sediment rating curve exponent
f.plus, f+	percent of cumulative sediment transport above Q_{eff} [%]
Qs50.RI	return interval of half-yield discharge (Q_{s50}) [yrs]
Qs50.Q1.5	half-yield discharge normalized by $Q_{1.5}$
Qeff.Q1.5	Q_{eff} normalized by the $Q_{1.5}$
Qeff.RI	return interval of Q_{eff} [yrs]
Qeff.spread	similar to *yield.spread*, but centered on and normalized by Q_{eff}
Qeff.yield	percent of cumulative sediment transport below Q_{eff} [%]
yield.spread	$(Q_{s75} - Q_{s25}) / Q_{s50}$

Symbols

A	cross-sectional area [m^2]
b	bottom width [m]
b_{fp}	floodplain exponent for at-a-station hydraulic geometry relation
BPL	broken power law for at-a-station hydraulic geometry
C_{ppm}	sediment transport concentration [ppm]
d_{16} D_{16}	16th percentile diameter of the bed sediment [m]
d_{50}, D_{50}	median grain size of the bed material [m]
d_{84}, D_{84}	84th percentile diameter of the bed sediment [m]
d_i	distance from rainfall station *i* to the centroid of the watershed of interest [km]
D	grain size [m]
$D_{b,i}$	grain size representing each size class of the (active) layer of the bed [m]
D_g	geometric mean grain diameter [m]
D_i	characteristic grain size for each size class [m]
D_{sg}	geometric mean grain size [m]
DA	drainage area [km^2]
f+	fraction of sediment transported above the effective discharge
F_g	grain-related Froude number
F_i	fraction of grain size in surface layer
F_s	approximate fraction of sand in bed sediments
g	gravitational acceleration [m/s^2] and/or gravitational constant

G	specific gravity of sediment (2.65 is typically assumed)
h	depth [m]
i	day
KDF	kernel density function
$Max\ Q$	maximum discharge in flow record [m^3/s]
$Min\ Q$	minimum discharge in flow record [m^3/s]
n	Manning's roughness coefficient
n	number of samples, sites, total number of data points, and/or total number of days in the flow record
n_{bank}	Manning's roughness coefficient of bank partition
n_{sed}	number of sediment load measurements
N	number of rainfall stations
N	grain size ranges from $i = 1$ to $N + 1$
$P_{<,i}$	non-exceedance probability of each bin
P_{bank}	wetted perimeter of bank partition [m]
P_{bed}	bottom width = wetted perimeter of bed partition [m]
q	discharge per unit width [m^2/s]
q	daily-averaged discharge [m^2/s]
q_1	unit discharge rate at one point in time [m^2/s]
q_2	unit discharge rate at a second point in time [m^2/s]
q_{bi}	volume gravel bedload transport per unit width of grains in the ith size range [m^2/s]
q_{bT}	total volume gravel bedload transport rate per unit width over all sizes [m^2/s]
q_{Daily}	discharge per unit width generated from average daily flow records [m^2/s]
q_s	unit sediment transport rate [m^2/s]
q_{s1}	unit sediment transport rate at one point in time [m^2/s]
q_{s2}	unit sediment transport rate at a second point in time [m^2/s]
$q_{s-Daily}$	unit sediment transport rate generated from average daily flow records [m^2/s]
q_{s-Sub}	unit sediment transport rate generated from sub-daily flow records [m^2/s]
q_{Sub}	discharge per unit width generated from sub-daily flow records [m^2/s]
Q	discharge [m^3/s], median annual peak flow (Q_2), and/or water discharge rate
$Q_{1.5}, Q_2, Q_{25}, Q_{75}$	1.5-yr, 2-yr, 25-yr, and 75-yr return interval discharges, respectively [m^3/s]
$Q_{10}, Q_{90}, Q_{95}, Q_{98},$	
Q_{99}	10th, 90th, 95th, 98th, and 99th percentile discharges, respectively [m^3/s]
Q_{bf}, Q_{BF}	bankfull discharge [m^3/s]
Q_c	critical discharge for incipient motion [m^3/s]
Q_{c2}	critical discharge for incipient motion standardized by 2-yr peak discharge [m^3/s]
Q_{eff}	effective discharge [m^3/s]
Q_{eff}	single discharge that moves the most total sediment road (percentile) [m^3/s]
$Q_{eff\text{-}15}$	effective discharge generated from 15-minute flow records [m^3/s]
$Q_{eff.c}$	effective discharge for coarse-bed site [m^3/s]
$Q_{eff\text{-}Daily}$	effective discharge generated from average daily flow records [m^3/s]
$Q_{eff.f}$	effective discharge for fine-bed site [m^3/s]
Q_s	sediment transport rate and/or discharge rate [kg/s]

$Q_{s25}, Q_{s50}, Q_{s75}, Q_{s90}$	discharge associated with 25%, 50%, 75%, and 90% of cumulative sediment transport over the sorted flow record, respectively [m³/s]
$Q_{s25.c}, Q_{s50.c}, Q_{s75.c}$	discharge associated with 25%, 50%, and 75% of cumulative sediment transport over coarse-bed site, respectively [m³/s]
$Q_{s25.f}, Q_{s50.f}, Q_{s75.f}$	discharge associated with 25%, 50%, and 75% of cumulative sediment transport over fine-bed site, respectively [m³/s]
Q_{s50-15}	discharge associated with 50% cumulative sediment transport over 15-minute flow records [m³/s]
$Q_{s50-Daily}$	discharge associated with 50% cumulative sediment transport over average daily flow records [m³/s]
$Q_{s50,low}$	lower confidence interval on Q_{s50} [m³/s]
$Q_{s50,upp}$	upper confidence interval on Q_{s50} [m³/s]
$Q_{s50-Sub}$	discharge associated with 50% cumulative sediment transport over sub-daily flow records [m³/s]
R	hydraulic radius [m]
R	$(\rho_s / \rho) - 1$ = submerged specific density of sediment
R_{bank}	hydraulic radius of bank partition [m]
R_{bed}	hydraulic radius of bed partition [m]
R_i	rainfall at station i [mm]
R_p	unknown rainfall at the watershed of interest [mm]
RB	Richards-Baker Flashiness Index
RI	return interval [yrs]
$Range\ Q$	range of discharge in flow record [m³/s]
S	streambed slope, channel slope [m/m]
S	gradient [m/m]
S_1	channel slope at one point in time [m/m]
S_2	new channel slope at a second point in time [m/m]
S_{Daily}	channel slope generated from average daily flow records [m/m]
S_f	friction slope [m/m]
S_{Sub}	channel slope generated from sub-daily flow records [m/m]
SPL	single power law for at-a-station hydraulic geometry
S_v	valley slope [m/m]
SY	sediment yield [m³]
SY_{15}	sediment yield generated from 15-minute flow records [m³]
SY_{Daily}	sediment yield generated from average daily flow records [m³]
SY_{Sub}	sediment yield generated from sub-daily flow records [m³]
u_*	$\sqrt{\dfrac{\tau_b}{\rho}}$ = shear velocity on the bed [Pa]
V	cross-section averaged velocity [m/s]
V_c	critical velocity [m/s]
w	width, channel top width [m]
w/h	width/depth ratio
w_i	weighting of rainfall station i

z	bank angle, horizontal to vertical [H:V]
v	kinematic viscosity [m^2/s]
ρ	density of the fluid mixture [kg/m^3]
ρ_s	density of sediment [kg/m^3]
σ_g	geometric standard deviation of particles sizes and/or gradation coefficient
σ_s	arithmetic standard deviation
σ_{sg}	geometric standard deviation
τ^*	dimensionless bed grain shear stress
τ_b	boundary shear stress on the bed [Pa]
τ_c^*	critical dimensionless shear stress
τ_{sg}^*	Shields' stress
τ_{ssrg}^*	reference Shields' stress
Ψ_i	each grain size on the base 2 logarithmic ψ scale
ω	specific stream power [W/m^2] ($\omega = \rho gQS/w$)
ω^*	dimensionless specific stream power

Site-specific Information for Study Sites

APPENDIX A CONTENTS

LIST OF FIGURE(S)

LIST OF TABLES

A dataset was collected of 60 bedload sites (coarse-bed) and 93 suspended-load sites (fine-bed) (Figure A-1). These sites are tabulated by states in Table A-1 (bedload) and Table A-2 (suspended-load). Site-specific information for all sites used in this portion of the study is provided in Table A-3 (coarse-bed sites) and Table A-4 (fine-bed sites).
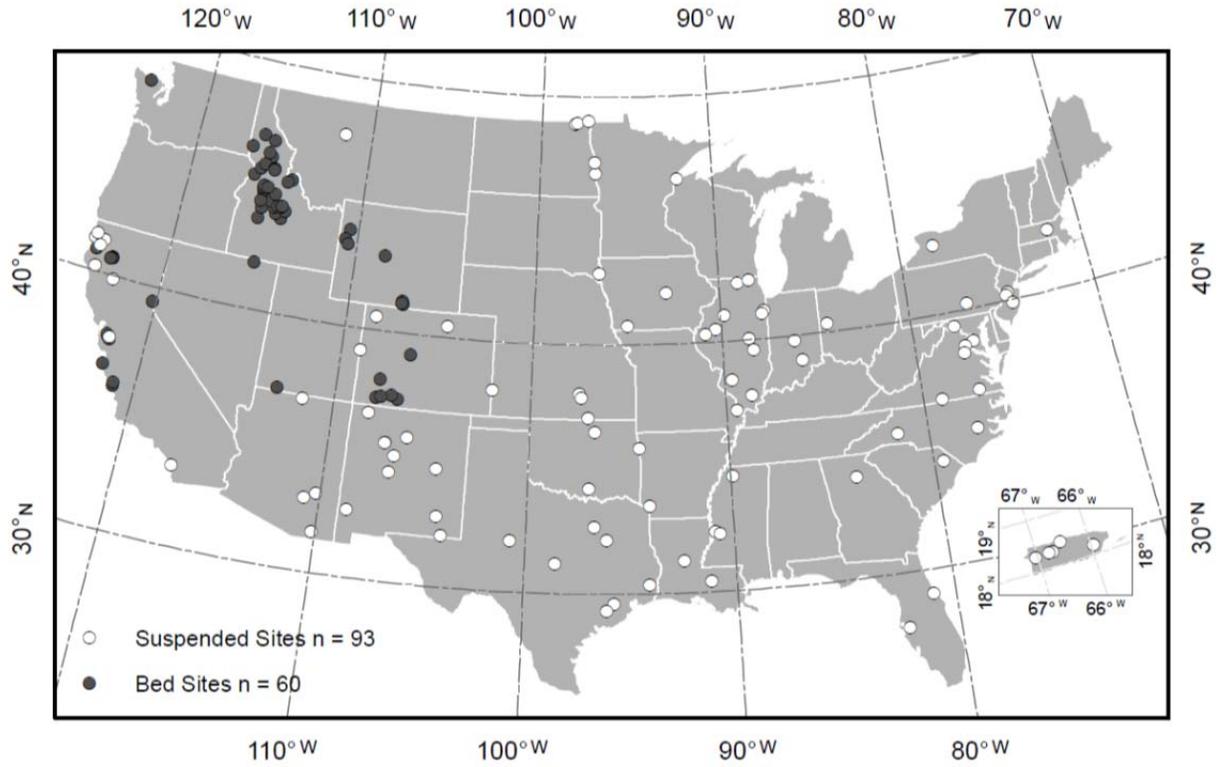
Figure A-1. Map of suspended-load (white circles) and bedload (black circles) study sites.

Table A-1. Sixty bedload sites (coarse-bed) by state.

	State	Site Name	Site Identification
1	California (CA)	Alameda near Sunol	11173575
2		Alameda Creek near Niles	11179000
3		Carmel River near Carmel	11143250
4		Cull Creek Above Reservoir near Castro Valley	11180960
5		Grass Valley near Lewiston	11525600
6		Indian Creek near Douglas City	11525670
7		Nacimiento River near Bryson	11148900
8		Redwood Creek at Orick	11482500
9		Redwood Creek near Blue Lake	11481500
10		Rush Creek near Lewiston	11525530
11		Sagehen Creek near Truckee	10343500
12		San Antonio River near Lockwood	11149900
13		Trinity River at Douglas City	11525854
14	Colorado (CO)	East Dallas Creek near Ridgeway	0914650A
15		East Fork San Juan River	09339900
16		Florida River near Lemon Reservoir	09362900
17		Halfmoon Creek near Malta	07083000
18		Junction Creek near Durango	09361400
19		Middle Fork Piedra River	09347200
20	Idaho (ID)	Big Wood River near Ketchum	13135500
21		Blackmare Creek near Cascade	13310565
22		Boise River near Twin Springs	13185000
23		Cat Spur Creek	1241490A
24		Clearwater River at Spalding	13342500
25		Dollar Creek near Cascade	13310520
26		Eggers Creek	M332AEC
27		Herd Creek	1329500B
28		Johns Creek	1333850A
29		Johnson Creek at Yellow Pine	13313000
30		Little Buckhorn Creek near Krassel Ranger Station	13310660
31		Little Slate Creek	1331650A
32		Lochsa River near Lowell	13337000
33		Lolo Creek	1333850B
34		Main Fork Red River	1333850C
35		Marsh Creek	1329500C
36		Middle Fork Salmon River near Yellow Pine	13309220
37		North Fork Clearwater River near Canyon Ranger Station	13340600
38		Rapid River	1331070A
39		Salmon River below Yankee Fork near Clayton	13296500
40		Salmon River near Obsidian	13292500
41		Salmon River near Shoup	13307000
42		South Fork Red River	1333850D
43		South Fork Salmon River	13310700
44		South Fork Payette River at Lowman	13235000
45		Squaw Creek near North Fork (USFS)	1329735A
46		Squaw Creek below Bruno Creek Near Clayton	13297355
47		Thompson Creek	13297330
48		Trapper Creek	1333850F
49		Valley Creek at Stanley	13295000

	State	Site Name	Site Identification
50		West Fork Buckhorn Creek near Krassel Ranger Station	13310670
51	Nevada (NV)	Jarbidge River below Jarbidge	13162225
52	Utah (UT)	East Fork Virgin River near Springdale	09404900
53	Washington (WA)	Elwha River above Lake Mills	12044900
54	Wyoming (WY)	Battle Creek near Encampment	09253400
55		Big Sandstone Creek near Savery	09255900
56		Cache Creek near Jackson	13018300
57		East Fork Savery Creek near Encampment	09255400
58		Little Granite Creek at Mouth near Bondurant	13019438
59		Pacific Creek at Moran	13011500
60		Wind River at Riverton	06228000

Table A-2. Ninety-three suspended-load sites (fine-bed) by state.

	State	Site Name	Site Identification
1	Arizona (AZ)	Gila River at Calva	09466500
2		Paria River at Lees Ferry	09382000
3		San Pedro River at Winkelman	09473500
4		San Pedro River at Charleston	09471000
5	Arkansas (AR)	Baron Fork at Dutch Mills	07196900
6		Red River at Index	07337000
7	California (CA)	Arroyo de la Laguna at Verona	11176900
8		Eel River at Fort Seward	11475000
9		Klamath River at Orleans	11523000
10		Klamath River near Klamath	11530500
11		Redwood Creek at Orick	11482500
12		San Luis Rey R. at Oceanside	11042000
13		Thomes Creek at Paskenta	11382000
14		Trinity River at Hoopa	11530000
15	Canada	Red River of the North at Emerson, Manitoba	05102500
16	Colorado (CO)	Colorado River near State Line	09163500
17		Little Snake River near Lily	09260000
18		Lonetree Creek near Greeley	06753990
19	Florida (FL)	Bullfrog Creek near Wimauma	02300700
20		Spruce Creek near Samsula	02248000
21	Georgia (GA)	Wheeler Creek near Auburn	02217274
22	Illinois (IL)	Brushy Creek near Harco	03382170
23		Indian Creek near Wyoming	05568800
24		Iroquois River near Chebanse	05526000
25		Kankakee River at Momence	05520500
26		Kaskaskia River at Cooks Mills	05591200
27		Kaskaskia River near Venedy Station	05594100
28		La Moine River at Colmar	05584500
29		Mississippi River at Thebes	07022000
30		Nippersink Creek above Wonder Lake	05548105
31		Sangamon River at Monticello	05572000
32		Spoon River at Seville	05570000
33		Spring Creek at Rockford	05437632
34	Indiana (IN)	East Fork White River at Seymour	03365500

	State	Site Name	Site Identification
35		Little Eagle Creek at Speedway	03353600
36	Iowa (IA)	Big Sioux River at Akron	06485500
37		Iowa River at Marshalltown	05451500
38		Nodaway River at Clarinda	06817000
39	Kansas (KS)	Arkansas River at Arkansas City	07146500
40		Arkansas River near Coolidge	07137500
41		Little Arkansas River 50 near Halstead	07143672
42		Little Arkansas River near Sedgwick	07144100
43	Louisiana (LA)	Mississippi River at Baton Rouge	07374000
44		Red River at Alexandria	07355500
45	Maine (MA)	Stillwater River near Sterling	01095220
46	Maryland (MD)	Piscataway Creek at Piscataway	01653600
47	Minnesota (MN)	Red River of the North at Halstad	05064500
48	Mississippi (MS)	Big Black River near Bovina	07290000
49		Hickahala Creek near Senatobia	07277700
50		Yazoo River below Steele Bayou	07288955
51	Montana (MT)	Muddy Creek near Vaughn	06088300
52	New Jersey (NJ)	Delaware River at Trenton	01463500
53		McDonalds Branch in Byrne State Forest	01466500
54		Stony Brook at Princeton	01401000
55	New Mexico (NM)	Animas River at Farmington	09364500
56		Arroyo Chico near Guadalupe	08340500
57		Gila River near Redrock	09431500
58		Pecos River at Red Bluff	08407500
59		Pecos River near Artesia	08396500
60		Pecos River near Puerto de Luna	08383500
61		Rio Grande at Albuquerque	08330000
62		Rio Grande at Otowi Bridge	08313000
63		Rio Puerco near Bernardo	08353000
64		Rio Puerco near Guadalupe	08334000
65	New York (NY)	Oatka Creek at Warsaw	04230380
66	North Carolina (NC)	Jacob Fork at Ramsey	02143040
67		Neuse River at Kinston	02089500
68	North Dakota (ND)	Little S. Pembina River near Walhalla	05099400
69		Pembina River at Walhalla	05099600
70		Red River of the North at Fargo	05054000
71	Ohio (OH)	Loramie Creek near Newport	03261950
72	Oklahoma (OK)	Arkansas River at Ralston	07152500
73		Washita River near Dickson	07331000
74	Pennsylvania (PA)	Susquehanna River at Harrisburg	01570500
75	Puerto Rico (PR)	Rio Grande de Arecibo below Utuado	50024950
76		Rio Grande de Manati near Manati	50038100
77		Rio Grande de Anasco near San Sebastian	50144000
78		Rio Grande de Loiza at San Lorenzo	50051800
79		Rio Tanama near Utuado	50028000
80	South Carolina (SC)	Pee Dee River at Peedee	02131000
81	Texas (TX)	Brazos River at Richmond	08114000
82		Colorado River above Silver	08123850
83		Colorado River at Wharton	08162000
84		Colorado River near San Saba	08147000

	State	Site Name	Site Identification
85		Neches River at Evadale	08041000
86		Trinity River at Trinidad	08062700
87		Trinity River below Dallas	08057410
88	Virginia (VA)	Dan River at Paces	02075500
89		Nottoway River near Sebrell	02047000
90		Rappahannock River near Fredericksburg	01668000
91		South Fork Quantico Creek near Ind. Hill	01658500
92	West Virginia (WV)	Potomac River at Shepherdstown	01618000
93	Wisconsin (WI)	Nemadji River near South Superior	04024430

Table A-3. Coarse-bed site information.

Site Identi-fication	Site Name	Sediment Source[a]	Record Ext.	Record Length [yrs]	α	β	R^2	C_v	Q_{bf} [m³/s]	$Q_{1.5}$ [m³/s]	Q_{eff} [m³/s]	Q_{s50} [m³/s]	D_{50} [mm]	DA [km²]	Latitude	Longitude
11173575	Alameda nr Sunol, CA	1		14	1.29E-04	1.40	0.54	3.48	5.7	44	9.1	12	15	386	37.54049080	-121.85634500
11179000	Alameda Ck nr Niles, CA	1		113	2.15E-05	1.95	0.71	4.31	-	67	57	141	5	1,639	37.58715679	-121.96079300
09253400	Battle Ck nr Encampment, WY	3		10	6.05E-05	3.32	0.69	2.13	-	7.4	10	10	80	34	41.13222220	-107.06916670
09255900	Big Sandstone Ck nr Savery, WY	3		5	2.35E-04	2.42	0.76	2.35	3.7	5.6	7.0	5.0	60	26	41.19996287	-107.17561070
13135500	Big Wood River nr Ketchum, ID	2		25	3.59E-06	3.64	0.87	1.31	-	21	43	29	116	355	43.78629677	-114.42505470
13310565	Blackmare Ck nr Cascade, ID	2	√	47	1.19E-03	1.89	0.59	1.33	4.7	4.1	3.9	4.6	98	46	44.82184460	-115.70484000
13185000	Boise River nr Twin Springs, ID	2		102	4.37E-06	2.64	0.85	1.22	167	162	163	151	70	2,155	43.66805556	-115.72527780
13018300	Cache Creek nr Jackson, WY	4		51	6.21E-04	2.65	0.75	1.28	3.9	1.7	1.5	2.0	46	27	43.45215258	-110.70409130
11143250	Carmel River nr Carmel, CA	1		51	7.32E-04	1.58	0.70	3.22	-	41	11	42	8	640	36.53912780	-121.88050840
1241490A	Cat Spur Creek, ID	2	√	48	3.06E-03	2.05	0.42	1.21	2.4	2.4	1.3	1.5	27	28	46.96380200	-116.25256400
13342500	Clearwater River at Spalding, ID	11		91	2.80E-07	2.20	0.72	1.09	-	1,880	1,277	1,424	74	24,043	46.44849828	-116.82737490
11180960	Cull Ck abv Res nr Castro Valley, CA	1		35	1.63E-02	1.63	0.75	4.75	-	6.7	0.4	3.2	4	15	37.71770737	-122.05440670
13310520	Dollar Creek nr Cascade, ID	2	√	47	1.06E-03	2.19	0.69	1.70	6.4	5.3	6.5	7.6	88	43	44.72017740	-115.69567230
0914650A	East Dallas Creek nr Ridgeway, CO	5	√	23	5.14E-03	2.84	0.76	1.21	3.7	3.3	3.5	3.4	58	44	38.09332490	-107.81367270
09339900	East Fork San Juan River, CO	4		45	3.77E-06	5.14	0.92	1.58	-	14	26	22	49	166	37.38972959	-106.84115090
09255400	East Fork Savery Ck nr Encampment, WY	3		4	8.71E-03	2.83	0.75	2.10	2.4	1.7	2.0	1.7	45	14	41.27218410	-107.15894320
09404900	East Fork Virgin River nr Springdale, UT	1		22	2.38E-03	0.97	0.46	0.87	-	14	1.1	1.6	25	888	37.16414955	-112.95854990
M332AEC	Eggers Creek, ID	2		32	9.16E-02	1.55	0.63	1.53	0.1	6.2	0.3	5.8	23	1	44.36780400	-115.77089300
12044900	Elwha R abv Lake Mills, WA	1	√	95	6.85E-04	2.34	0.70	0.81	-	312	55	91	-	513	47.97008900	-123.59074530
09362900	Florida River nr Lemon Reservoir, CO	4	√	79	1.14E-07	4.62	0.97	1.68	-	21	25	23	210	115	37.37916870	-107.66172700
11525600	Grass Valley nr Lewiston, CA	1		29	2.38E-03	0.59	0.09	1.69	-	11	0.3	1.6	19	80	40.67625718	-122.83057830
07083000	Halfmoon Creek nr Malta, CO	5		91	1.77E-04	3.33	0.66	1.56	6.2	6.0	5.6	5.8	49	61	39.17221259	-106.38919260
1329500B	Herd Creek, ID	2	√	92	3.10E-03	2.35	0.83	0.87	5.5	3.5	3.5	3.1	67	285	44.13274300	-114.27690100
11525670	Indian Ck nr Douglas City, CA	1	√	37	5.12E-06	2.87	0.87	2.14	-	12	18	33	-	87	40.65181225	-122.91446890
13162225	Jarbidge Rv bl Jarbidge, NV	2		14	1.97E-04	3.07	0.59	1.94	-	9.4	8.2	10	91	79	41.89046140	-115.42868160
1333850A	Johns Creek, ID	2	√	49	3.55E-06	2.48	0.50	1.20	49	20	23	19	197	293	45.82214900	-115.88850700
13313000	Johnson Creek at Yellow Pine, ID	2		85	4.56E-07	2.90	0.87	1.67	40	71	65	69	190	565	44.96166667	-115.50000000
09361400	Junction Ck nr Durango, CO	4	√	60	3.93E-07	4.80	0.79	1.85	-	4.9	7.6	7.4	64	68	37.33416764	-107.90951260
13310660	Little Buckhorn Ck nr Krassel Rngr Sta, ID	2	√	47	2.40E-02	2.13	0.49	1.08	-	0.5	0.8	0.7	66	16	44.91267746	-115.75067590
13019438	Little Granite Ck at Mth nr Bondurant, WY	4		10	2.41E-04	2.94	0.69	1.75	6.4	5.7	5.3	9.0	155	55	43.29861110	-110.51777780
1331650A	Little Slate Creek, ID	2		46	3.31E-04	1.45	0.44	1.02	12	12	1.1	7.7	125	162	45.61848200	-116.06672500

Table A-3 (cont.). Coarse-bed site information.

Site Identification	Site Name	Sediment Source[a]	Record Ext.	Record Length [yrs]	α	β	R^2	C_v	Q_{bf} [m³/s]	$Q_{1.5}$ [m³/s]	Q_{eff} [m³/s]	Q_{s50} [m³/s]	D_{50} [mm]	DA [km²]	Latitude	Longitude
13337000 Lochsa River nr Lowell, ID		2		86	1.83E-11	3.99	0.78	1.36	446	456	451	496	131	3,051	46.15083330	-115.58722220
1333850B Lolo Creek, ID		2		35	4.25E-04	1.61	0.37	1.22	12	11	7.0	8.4	74	106	46.31322900	-115.74887800
1333850C Main Fork Red River, ID		2		36	1.77E-03	1.79	0.62	1.39	9.3	11	10	8.9	55	129	45.70963100	-115.34096900
1329500C Marsh Creek, ID		2	√	92	2.43E-04	2.29	0.68	1.64	21	17	20	30	62	206	44.39677300	-115.16927000
09347200 Middle Fork Piedra River, CO		4	√	51	7.08E-06	4.59	0.91	1.58	-	5.5	25	15	79	83	37.48667027	-107.16338130
13309220 MF Salmon River nr Yellow Pine, ID		2		22	4.97E-16	6.39	0.82	1.37	-	209	586	498	134	2,699	44.72166667	-115.01638890
11148900 Nacimiento R nr Bryson, CA		1		42	1.36E-06	2.49	0.78	4.42	11	100	231	278	78	420	35.78857918	-121.09380480
13340600 NF Clearwater R nr Canyon Rngr Sta, ID		2		46	3.44E-11	3.92	0.88	1.15	453	430	454	513	86	3,357	46.84055556	-115.62111100
13011500 Pacific Creek at Moran, WY		6		65	1.71E-04	2.39	0.52	1.87	29	56	54	55	79	438	43.85027778	-110.51777780
1331070A Rapid River, ID		2		87	9.97E-05	2.30	0.58	1.20	-	20	18	22	72	280	45.35128100	-116.39857700
11482500 Redwood Creek at Orick, CA		1		62	1.73E-04	1.34	0.77	1.91	127	456	48	115	7.0	717	41.29928960	-124.05118250
11481500 Redwood Ck nr Blue Lake, CA		1		42	9.21E-06	2.46	0.75	1.80	28	113	29	68	22	175	40.90596479	-123.81533500
11525530 Rush Ck nr Lewiston, CA		1	√	37	3.27E-06	3.11	0.74	1.44	3.5	8.7	6.3	7.1	-	58	40.72458990	-122.83474580
10343500 Sagehen Creek nr Truckee, CA		7		60	6.29E-03	1.57	0.29	1.84	2	1.8	0.1	1.8	58	27	39.43157246	-120.23797930
13296500 Salmon River bl Yankee Fork nr Clayton, ID		2		79	3.68E-09	3.87	0.72	1.16	-	110	175	162	104	2,090	44.26833330	-114.73277780
13292500 Salmon River nr Obsidian, ID		2	√	92	1.99E-05	3.43	0.61	1.49	-	12	16	15	60	245	43.96574038	-114.80118190
13307000 Salmon River nr Shoup, ID		2		48	3.01E-10	3.87	0.71	0.97	-	325	402	408	96	16,159	45.32250000	-114.44000000
11149900 San Antonio R nr Lockwood, CA		1		48	4.47E-03	0.82	0.70	3.90	-	67	0.0	14	5.0	562	35.89663404	-121.08824910
1333850D SF Red River, ID		2		35	1.25E-03	1.52	0.41	1.51	7.2	6.7	3.5	6	104	99	45.70764000	-115.34381700
13310700 SF Salmon River, ID		2		41	2.29E-06	3.01	0.74	1.41	71	77	90	90	14	855	44.98694440	-115.72500000
13235000 SF Payette River at Lowman, ID		2		72	1.13E-04	2.13	0.70	1.14	86	99	82	90	95	1,155	44.08527778	-115.62222220
1329735A Squaw Ck nr North Fork, ID (USFS)		2	√	41	1.20E-02	2.30	0.49	1.16	0.6	0.5	0.4	0.5	27	37	45.41082800	-114.20056600
13297355 Squaw Ck bl Bruno Creek Nr Clayton, ID		2		41	1.32E-03	2.40	0.79	1.67	5.1	5.1	7.9	7.6	46	185	44.29083330	-114.47166670
13297330 Thompson Creek, ID		2		41	3.02E-03	2.99	0.87	1.74	2.5	2.4	3.5	4.8	63	75	44.27027778	-114.51666670
1333850F Trapper Creek, ID		2	√	49	5.84E-03	1.35	0.44	1.28	2.6	1.5	1.6	1.1	79	21	45.67160200	-115.32670800
11525854 Trinity R at Douglas City, CA		1		11	5.50E-09	2.98	0.71	1.20	113	177	191	184	-	2,411	40.64527778	-122.95666670
13295000 Valley Creek at Stanley, ID		2		73	9.08E-05	2.66	0.59	1.12	24	25	24	23	63	381	44.22250000	-114.93111100
13310670 WF Buckhorn Creek nr Krassel Rngr Sta, ID		2	√	47	1.59E-03	1.75	0.39	1.51	5.7	4.1	5.9	5.3	180	59	44.91684430	-115.74345350
06228000 Wind River at Riverton, WY		9		98	8.30E-03	1.18	0.22	1.51	142	131	10	68	22	5,980	43.01051478	-108.37677010

[a]Sediment Data Sources: 1 = USGS (2014), 2 = USFS, BAT (2014a), 3 = Rankl and Smalley (1992), 4 = USFS (2014b), Bunte and Abt (2009), 6 = Erwin et al. (2011), 7 = Andrews (1994), 8 = Andrews (2000), 9 = Smalley et al. (1994), 10 = Williams and Krupkin (1984), 11 = Jones and Seitz (1980).

Table A-4. Fine-bed site information.

Site Identification	Site Name	Record Length [yrs]	α	β	R^2	C_v	Q_{bf} [m³/s]	$Q_{1.5}$ [m³/s]	Q_{eff} [m³/s]	Q_{s50} [m³/s]	D_{50} [mm]	DA [km²]	Latitude	Longitude
09364500	Animas River at Farmington, NM	91	1.69E-03	2.23	0.62	1.37	-	129	111	124	0.29	3,522	36.72250000	-108.20175000
07146500	Arkansas R. at Arkansas City, KS	96	8.02E-04	1.96	0.78	1.90	481	429	40	545	0.43	113,216	37.05641799	-97.05809390
07137500	Arkansas R. nr Coolidge, KS	64	1.12E-02	1.89	0.77	4.60	31	34	12	1,678	0.53	65,812	38.02751290	-102.01157060
07152500	Arkansas River at Ralston, OK	89	1.12E-03	1.63	0.7	1.81	1,444	1,019	244	835	-	140,398	36.50421677	-96.72836720
08340500	Arroyo Chico nr Guadalupe, NM	51	1.86E+00	1.74	0.93	6.05	-	79	11	33	5	3,600	35.59225000	-107.18944440
11176900	Arroyo de la Laguna at Verona, CA	58	3.44E-03	1.99	0.77	4.16	26	90	77	70	2.91	1,044	37.62659915	-121.88301260
07196900	Baron Fork at Dutch Mills, AR	56	2.06E-03	0.97	0.72	3.55	-	1,465	0.9	4.2	-	105	35.88000000	-94.48638890
07290000	Big Black River nr Bovina, MS	78	3.52E-03	1.18	0.75	1.57	425	525	244	3,314	0.38	7,283	32.34777778	-90.69694440
06485500	Big Sioux R. at Akron, IA	86	4.50E-03	1.35	0.75	2.12	197	197	45	1,977	0.59	20,407	42.83752049	-96.56192190
08114000	Brazos River at Richmond, TX	94	3.67E-06	2.72	0.86	1.61	2,124	1,240	1,789	1,691	0.21	116,827	29.58245890	-95.75772750
03382170	Brushy Creek nr Harco, IL	47	3.28E-02	1.80	0.95	3.74	-	27	4	8.2	-	34	37.77504850	-88.65227890
02300700	Bullfrog Creek nr Wimauma, FL	36	2.15E-03	0.95	0.58	2.78	4.3	20	0.5	2.8	-	75	27.79197208	-82.35203690
08123850	Colorado River abv Silver, TX	47	2.40E-03	1.42	0.79	6.12	37	57	0.6	77	-	38,617	32.05374399	-100.76205200
08162000	Colorado River at Wharton, TX	75	7.64E-05	2.28	0.71	1.89	1,529	575	876	974	-	108,787	29.30913668	-96.10384820
08147000	Colorado River nr San Saba, TX	95	2.23E-03	1.09	0.53	4.33	283	504	5.1	292	-	80,852	31.21794515	-98.56448400
09163500	Colorado River nr State Line, CO	63	4.28E-05	2.32	0.7	1.07	1,246	5,292	481	7,391	-	46,229	39.13276047	-109.02705460
02075500	Dan River at Paces, VA	63	7.66E-05	2.05	0.62	1.19	680	586	77	399	-	6,700	36.64236056	-79.08945900
01463500	Delaware River at Trenton, NJ	101	1.95E-06	2.27	0.77	1.02	-	2,303	776	1,192	-	17,560	40.22166667	-74.77805560
03365500	E.F. White River at Seymour, IN	87	1.42E-02	0.99	0.69	1.67	313	7,831	46	1,541	1.63	6,063	38.98255300	-85.89914440
11475000	Eel River at Fort Seward, CA	59	1.26E-05	2.50	0.88	2.65	6,260	1,895	1,177	3,382	2.93	5,457	40.21820000	-123.63253000
09466500	Gila River at Calva, AZ	85	2.77E-02	1.95	0.87	4.42	-	95	69	1,026	-	29,707	33.18561278	-110.22009030
09431500	Gila River nr Redrock, NM	77	2.58E-03	2.09	0.65	2.75	-	1,151	26	262	-	7,327	32.72694444	-108.67555560
07277700	Hickahala Creek nr Senatobia, MS	24	8.16E-05	2.50	0.85	3.38	255	280	64	205	0.43	313	34.63194444	-89.92444440
05568800	Indian Creek nr Wyoming, IL	54	2.40E-02	1.36	0.64	2.36	18	36	1.5	6.9	1	162	41.01888889	-89.83555560
05451500	Iowa River at Marshalltown, IA	96	1.50E-03	1.77	0.82	1.61	282	183	59	139	0.47	3,968	42.06582096	-92.90769970
05526000	Iroquois River nr Chebanse, IL	91	1.88E-03	1.14	0.76	1.52	340	316	36	149	-	5,416	41.00892150	-87.82337190
02143040	Jacob Fork at Ramsey, NC	53	8.20E-04	1.75	0.73	1.57	-	41	1.2	7.4	-	67	35.59055556	-81.56694440
05520500	Kankakee River at Momence, IL	99	3.05E-04	1.76	0.63	0.73	34	174	110	113	-	5,941	41.16003338	-87.66864830
05591200	Kaskaskia River at Cooks Mills, IL	44	5.54E-03	0.99	0.67	1.77	20	120	7.1	35	0.91	1,225	39.58336660	-88.41338420
05594100	Kaskaskia River nr Venedy Sta., IL	45	2.14E-03	1.20	0.61	1.24	269	493	115	2,677	0.32	11,378	38.45060486	-89.62759260
11523000	Klamath River at Orleans, CA	87	3.49E-06	2.50	0.83	1.23	566	1,356	597	1,642	3.58	21,950	41.30345990	-123.53450360

Table A-4 (cont.). Fine-bed site information.

Site Identi-fication	Site Name	Record Length [yrs]	α	β	R^2	C_v	Q_{bf} [m³/s]	$Q_{1.5}$ [m³/s]	Q_{eff} [m³/s]	Q_{s50} [m³/s]	D_{50} [mm]	DA (km²)	Latitude	Longitude
11530500	Klamath River nr Klamath, CA	77	1.02E-06	2.61	0.88	1.28	1,841	27,691	1,003	33,131	-	31,339	41.51095430	-123.97951640
07143672	L. Arkansas R. 50 nr Halstead, KS	18	4.22E-03	1.45	0.89	3.71	170	95	0.6	110	-	1,966	38.02862230	-97.54059700
07144100	L. Arkansas R. nr Sedgwick, KS	20	1.48E-03	1.57	0.92	3.59	85	188	1.7	209	0.86	3,209	37.88306739	-97.42448640
05584500	La Moine River at Colmar, IL	69	3.25E-03	1.41	0.83	2.64	170	180	11	121	0.38	1,696	40.33032166	-90.89624510
03353600	Little Eagle Creek at Speedway, IN	54	1.27E-02	1.05	0.74	2.62	-	34	0.3	2.8	-	63	39.78754310	-86.22860010
05099400	Little S. Pembina River nr Walhalla, ND	39	1.47E-02	2.05	0.81	5.22	-	19	42	52	2.4	471	48.86527259	-98.00593170
09260000	Little Snake River nr Lily, CO	92	8.39E-02	1.48	0.62	1.82	-	107	79	85	0.63	10,448	40.54901667	-108.42432220
06753990	Lonetree Creek nr Greeley, CO	5	4.61E-02	1.52	0.72	2.30	-	4.6	0.2	1.6	-	1,487	40.44248080	-104.58884870
03261950	Loramie Creek nr Newport, OH	50	5.92E-04	1.74	0.89	2.49	8.5	67	38	44	0.38	394	40.30699246	-84.38383830
01466500	McDonalds Br in Byrne St. For., NJ	61	2.27E-03	1.26	0.22	0.53	0.2	0.2	0.04	0.1	-	6	39.88500000	-74.50527778
07374000	Mississippi R. at Baton Rouge, LA	9	1.30E-12	3.43	0.87	0.49	16,990	27,146	25,224	25,222	-	2,915,537	30.44566667	-91.19155560
07022000	Mississippi River at Thebes, IL	79	7.10E-05	1.73	0.49	0.67	16,424	13,459	6,651	6,651	0.44	1,847,181	37.22160000	-89.46297500
06088300	Muddy Creek nr Vaughn, MT	27	3.22E-03	2.51	0.85	1.03	-	15	8	9.7	-	580	47.62502220	-111.63540560
08041000	Neches River at Evadale, TX	95	5.63E-03	0.99	0.33	1.23	220	548	85	368	0.23	20,593	30.35576378	-94.09323730
04024430	Nemadji River nr South Superior, WI	40	4.93E-04	2.03	0.89	1.89	122	127	47	101	0.45	1,088	46.63327388	-92.09408030
02089500	Neuse River at Kinston, NC	83	7.94E-04	1.28	0.54	1.04	135	278	51	167	0.57	6,972	35.25777778	-77.58555560
05548105	Nippersink Ck. abv. Wonder Lake, IL	10	2.00E-02	0.93	0.61	1.63	-	19	0.7	2.6	-	219	42.38529819	-88.36953550
06817000	Nodaway River at Clarinda, IA	81	8.07E-04	2.22	0.92	2.90	-	2,581	111	3,681	0.48	1,974	40.74327778	-95.01419440
02047000	Nottoway River nr Sebrell, VA	73	7.66E-04	1.10	0.62	1.35	75	187	35	85	1.28	3,732	36.77042760	-77.16607780
04230380	Oatka Creek at Warsaw, NY	49	2.74E-04	3.08	0.92	1.65	-	39	14	24	-	101	42.74416667	-78.13750000
09382000	Paria River at Lees Ferry, AZ	91	9.81E-01	2.47	0.9	3.96	-	61	191	86	0.29	3,652	36.87220977	-111.59460520
08407500	Pecos River at Red Bluff, NM	77	4.76E-03	1.39	0.48	5.83	312	31	1.7	2,111	-	50,608	32.07519167	-104.03943610
08396500	Pecos River nr Artesia, NM	108	1.36E-02	1.84	0.85	3.10	99	63	23	293	-	39,627	32.84086110	-104.32383330
08383500	Pecos River nr Puerto de Luna, NM	76	6.39E-03	2.37	0.61	2.25	-	1,401	35	277	-	10,282	34.73008330	-104.52491110
02131000	Pee Dee River at Peedee, SC	74	1.68E-03	1.00	0.36	0.89	691	897	176	371	0.62	22,870	34.20432518	-79.54838960
05099600	Pembina River at Walhalla, ND	66	1.50E-02	1.53	0.78	2.85	113	40	19	97	1.47	8,676	48.91332840	-97.91703690
01653600	Piscataway Creek at Piscataway, MD	48	4.47E-03	1.98	0.76	2.62	17	24	1.7	36	-	102	38.70577778	-76.96619440
01618000	Potomac River at Shepherdstown, WV	70	4.55E-05	1.69	0.65	1.49	1,133	1,776	300	728	-	15,382	39.43472220	-77.80138889
01668000	Rappahannock R nr Fredericksburg, VA	107	1.94E-05	2.26	0.84	1.74	-	701	87	654	-	4,131	38.30846178	-77.52915268
05102500	Red R. of the N. at Emerson, Manitoba	101	5.92E-04	1.28	0.58	1.93	-	476	61	620	-	104,118	49.00832097	-97.21145070
07355500	Red River at Alexandria, LA	55	4.48E-05	2.15	0.76	1.08	-	2,486	2,375	2,795	-	174,824	31.31296019	-92.44291480

Table A-4 (cont.). Fine-bed site information.

Site Identi-fication	Site Name	Record Length [yrs]	α	β	R^2	C_v	Q_{bf} [m³/s]	$Q_{1.5}$ [m³/s]	Q_{eff} [m³/s]	Q_{s50} [m³/s]	D_{50} [mm]	DA [km²]	Latitude	Longitude
07337000	Red River at Index, AR	78	1.13E-05	2.42	0.76	1.39	1,352	1,727	1,604	1,846	0.26	124,320	33.55194444	-94.04111110
05054000	Red River of the North at Fargo, ND	112	7.35E-04	1.24	0.63	1.99	136	72	13	82	-	17,612	46.86107500	-96.78369240
05064500	Red River of the North at Halstad, MN	52	2.23E-03	0.98	0.5	1.89	623	265	26	189	0.62	56,462	47.35191800	-96.84369100
11482500	Redwood Ck. at Orick, CA	62	3.40E-04	2.29	0.86	1.91	105	456	108	300	5	717	41.29928960	-124.05118250
08330000	Rio Grande at Albuquerque, NM	72	3.25E-03	2.16	0.68	1.20	-	136	1,215	135	0.46	45,169	35.08916667	-106.68069440
08313000	Rio Grande at Otowi Bridge, NM	111	2.18E-02	1.70	0.44	1.25	-	151	21	153	0.84	37,037	35.87450000	-106.14244440
50024950	Rio Grande de Arecibo blw Utuado, PR	15	3.31E-02	2.12	0.73	1.95	-	195	5.6	133	-	170	18.29995229	-66.70378539
50038100	Rio Grnd de Manati nr Manati, PR	42	4.04E-03	1.56	0.94	3.77	170	447	5.1	391	-	510	18.42911367	-66.52656080
50144000	Rio Grnd. de Anasco nr Sn. Sebastian, PR	51	7.51E-04	2.31	0.82	2.13	-	332	838	18	-	244	20.91600000	-67.05129009
50051800	Rio Grnd. de Loiza at Sn. Lorenzo, PR	23	5.77E-03	2.05	0.83	2.04	-	215	2.7	69	-	106	18.18368835	-65.96095530
08353000	Rio Puerco nr Bernardo, NM	74	1.06E+00	1.76	0.85	5.37	43	40	27	57	2.64	19,036	34.41027778	-106.85444440
08334000	Rio Puerco nr Guadalupe, NM	62	4.00E+00	1.89	0.9	3.79	7.1	30	2	11	-	1,088	35.60088889	-107.16661110
50028000	Rio Tanama nr Utuado, PR	53	1.05E-02	2.38	0.84	1.29	-	118	1.8	22	1.5	48	18.29873289	-66.78263360
01658500	S.F. Quantico Ck nr Ind. Hill, VA	63	1.08E-02	1.70	0.96	2.86	1.4	13	0.2	3.5	-	20	38.58734270	-77.42859580
11042000	San Luis Rey R. at Oceanside, CA	80	2.49E-02	1.69	0.77	6.32	-	4	1.4	91	0.4	1,443	33.21809119	-117.36031620
09473500	San Pedro R. at Winkelman, AZ	12	5.85E-01	1.59	0.93	6.51	-	140	0.6	83	0.62	11,533	32.97728817	-110.77038300
09471000	San Pedro River at Charleston, AZ	99	9.87E-03	2.03	0.85	6.19	20	113	88	225	0.48	3,196	31.62592644	-110.17452260
05572000	Sangamon River at Monticello, IL	104	8.38E-03	1.02	0.6	1.85	60	110	7	35	0.49	1,424	40.03086735	-88.58895419
05570000	Spoon River at Seville, IL	99	7.79E-03	1.32	0.86	1.80	193	285	27	131	0.46	4,237	40.49004077	-90.34040250
05437632	Spring Cr. at Rockford, IL	63	2.25E-02	2.90	0.68	2.60	-	-	1.5	2.2	-	7	42.30972220	-88.98944440
02248000	Spruce Creek nr Samsula, FL	62	5.91E-03	1.34	0.79	2.33	5.7	13	0.8	6.2	-	87	29.05081845	-81.04644550
01095220	Stillwater River nr Sterling, MA	20	1.43E-03	1.28	0.87	1.46	15	23	2.3	4.2	-	82	42.41092507	-71.79118290
01401000	Stony Brook at Princeton, NJ	60	2.05E-04	2.08	0.67	2.54	37	87	18	36	-	115	40.33305556	-74.68194440
01570500	Susquehanna River at Harrisburg, PA	124	8.61E-06	1.86	0.82	1.20	-	6,569	1,575	3,341	-	62,419	40.25481164	-76.88608460
11382000	Thomes Ck. at Paskenta, CA	76	2.47E-03	2.25	0.91	2.37	71	129	30	181	5.43	526	39.88765496	-122.52916550
11530000	Trinity River at Hoopa, CA	87	1.28E-03	1.89	0.9	1.49	3,404	1,048	280	7,021	2	7,389	41.04985200	-123.67366800
08062700	Trinity River at Trinidad, TX	50	1.56E-04	1.90	0.67	1.62	623	718	413	649	-	22,113	32.14765255	-96.10247080
08057410	Trinity River blw Dallas, TX	54	4.87E-05	2.04	0.71	1.65	312	396	193	388	0.34	16,260	32.70763139	-96.73583190
07331000	Washita River nr Dickson, OK	85	3.76E-03	1.96	0.77	2.25	464	549	176	623	0.16	18,575	34.23342725	-96.97584470
02217274	Wheeler Ck nr Auburn, GA	13	1.27E-01	1.89	0.87	2.11	-	3.6	0.1	0.9	-	3	34.08232720	-83.85462170
07288955	Yazoo River blw Steele Bayou, MS	14	2.46E-03	1.14	0.35	0.78	-	1,729	374	875	0.06	34,589	32.44416667	-90.91416670

A.1   References

Andrews, E.D. 1994. "Marginal Bed Load Transport in a Gravel Bed Stream, Sagehen Creek, California." *Water Resources Research*, Vol. 30, No. 7, pp. 2241–2250, DOI: 10.1029/94WR00553.

Andrews, E.D. 2000. "Bed Material Transport in the Virgin River Utah." *Water Resources Research*, Vol. 36, No. 7, pp. 585–596, DOI: 10.1029/1999WR900257.

Bunte, K. and S.R. Abt. 2009. "Transport Relationships between Bedload Traps and 3-inch Helley-Smith Sampler in Coarse Gravel-bed Streams and Development of Adjustment Functions." U.S. Army Corps of Engineers, Federal Interagency Sedimentation Project, Vicksburg, MS, December, 138 p., URL: http://water.usgs.gov/fisp/docs/091221_Bunte_and_Abt_Trap_HS_comparison_and_adjustment_functions_final.pdf.

Erwin, S., J. Schmidt, and N. Nelson. 2011. "Downstream Effects of Impounding a Natural Lake: The Snake River Downstream from Jackson Lake Dam, Wyoming, USA." *Earth Surface Processes and Landforms*, Vol. 36, No. 11, pp. 1421–1434, DOI: 10.1002/esp.2159.

Jones, M.L., and H.R. Seitz. 1980. "Sediment Transport in the Snake and Clearwater Rivers in the Vicinity of Lewiston, Idaho." *U.S. Geological Survey Open File Report 80-690*, 179 p.

Rankl, J., and M. Smalley. 1992. "Transport of Sediment by Streams in the Sierra Madre, Southern Wyoming." *U.S. Geological Survey Open-File Report WRIR 92-4091*, Cheyenne, WY.

Smalley, M.L., W.W. Emmett, and A.M. Wacker. 1994. "Annual Replenishment of Bed Material by Sediment Transport in the Wind River near Riverton, Wyoming." *U.S. Geological Survey Water-Resources Investigations Report 94-4007*, Cheyenne, WY, 23 p.

U.S. Forest Service (USFS). 2014a. "Sediment Transport in Colorado and Wyoming."

U.S. Forest Service (USFS), Boise Adjudication Team (BAT). 2014b. "Sediment Transport in Idaho and Nevada." U.S. Forest Service, Website URL: http://www.fs.fed.us/rm/boise/AWAE/projects/sediment_transport/sediment_transport_BAT.shtml, accessed May 18, 2014.

U.S. Geological Survey (USGS), Sediment Data Portal. 2014. "USGS Sediment Data Portal." Website URL: http://cida.usgs.gov/sediment/, accessed March 14, 2014.

Williams, R.P., and J.P. Krupkin. 1984. "Erosion, Channel Change, and Sediment Transport in the Big Lost River, Idaho." *U.S. Geological Survey Water-Resources Investigations Report 84-414*, Boise, ID, 87 p.

A.2   Abbreviations

Units of Measure

km^2	square kilometer(s)
cms, m^3/s	cubic meter(s) per second
mm	millimeter(s)
yr(s)	year(s)

Statistical Terms

C_v	coefficient of variation
R^2	coefficient of determination
α	coefficient
β	sediment rating curve exponent

Acronyms

USFS	U.S. Forest Service
USFS BAT	U.S. Forest Service Boise Adjudication Team
USGS	U.S. Geological Survey

<u>Symbols</u>

D_{50}	median grain size [mm]
DA	drainage area [km^2]
$Q_{1.5}$	1.5-yr return interval discharge [m^3/s]
Q_{bf}	bankfull discharge [m^3/s]
Q_{eff}	effective discharge [m^3/s]
Q_{s50}	half-yield discharge [m^3/s]

eRAMS Tutorials

APPENDIX B CONTENTS

LIST OF FIGURES

LIST OF TABLE(S)

B.1 Tutorial: Accessing eRAMS

Many of the tools for this project are developed in the eRAMS (the environmental Resource Analysis and Management System) platform (https://erams.com/). eRAMS is an on-line service for collaboration in analyzing land, water, and energy-related concerns and opportunities to assist strategic and tactical decision-making at multiple scales. eRAMS also provides a web platform for developing information systems and applications tailored to specific business objectives not necessarily constrained to the natural resource domain, integrating geospatial analysis, content management, collaboration, and simple to complex modeling technologies.

B.2 Tutorial: Flow Statistics from Gage Data

Step 1: **Access the Flow Analysis tool.**

This can be done by either: (1) log-in to https://.erams.com and create a 'Flow Analysis' project or (2) directly visit the eRAMS Flow Analysis website https://erams.com/flowanalysis/ (no log-in required). Note that use of the non-log-in version does prevent you from saving any data within eRAMS (however, it can still be saved on your local computer).

> To learn more about eRAMS, including how to create a free user account, visit https://erams.com/documentation/.

Step 2: **Select site.**

You can use keyword search or map region search and filter both by attribute. By selecting a site in the "Station Search Results," a summary balloon will pop-up on the map allowing you to review both the location of each site and also the data availability (Figure B-1). Finally, select "Flow Analysis Model" link in the summary balloon for your chosen site.

> Full documentation for this tool can be found at https://erams.com/documentation/flow-analysis/.
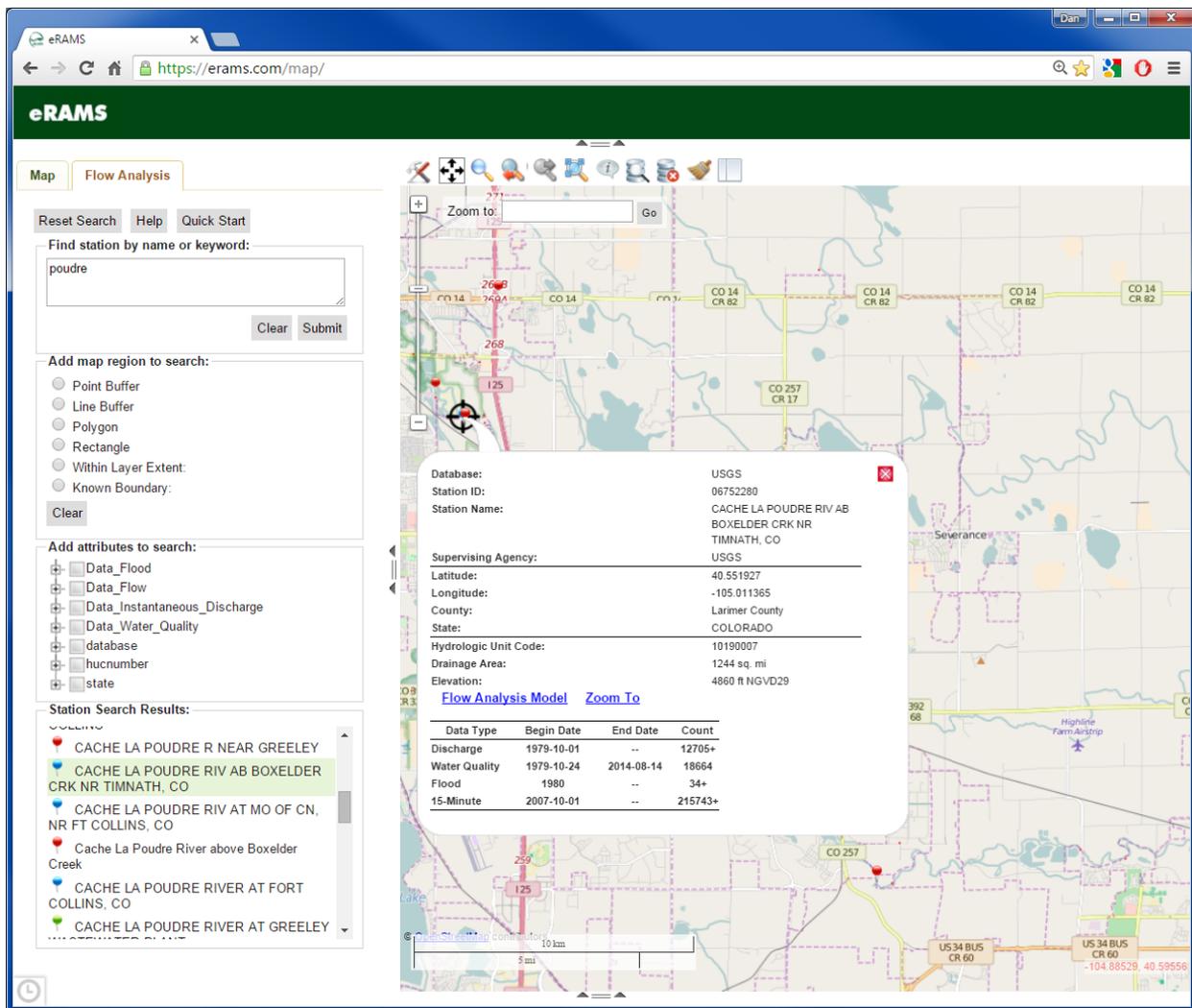
Figure B-1. Screenshot of "Station Search Results" menu.

Step 3:   Navigating to the Data summary tool.

- Select the "Data" tab (Figure B-2).
- Select the Analysis period (defaults to the oldest available through the newest available data).
- Flow Statistics are not dependent on the graph type.
- Under Advanced Options you have the option of:
  o viewing the data by calendar year (default) or water year (if option is selected);
  o specifying a specific period of the year (season) for additional metrics in the statistics summary to evaluate; and
  o selecting multiple periods for analysis (as opposed to the full analysis period).
- When inputs are finalized, click "Run Model."
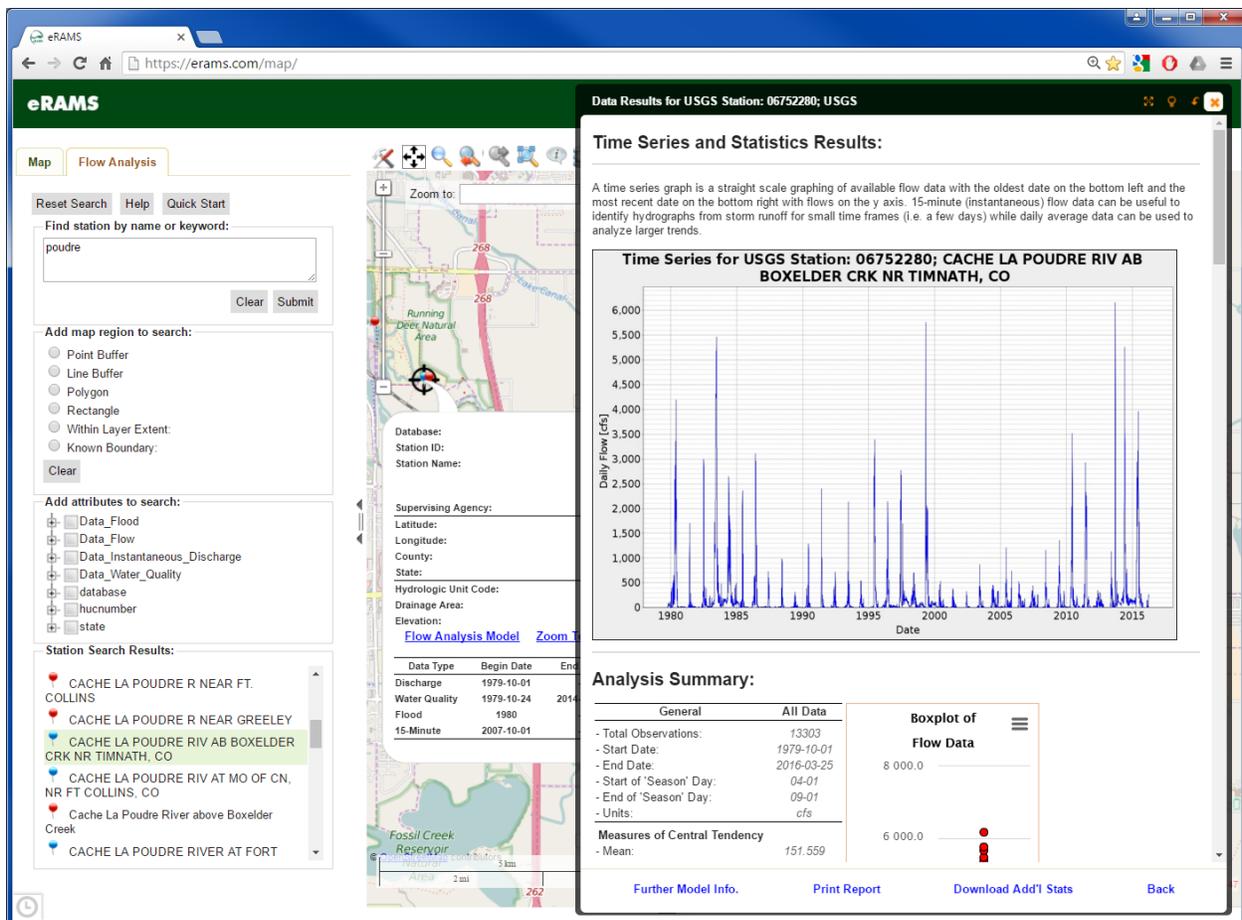
Figure B-2. Screenshot of "Time Series and Statistics Results" from "Data" tab.

Step 4:   Review Report.

This report provides an overview of the data for the gage including a:
- time series plot,
- analysis summary,
- envelope graph,
- raster plot,
- monthly average graph,
- histogram graph, and
- cumulative distribution graph.

Step 5:   Download Flow Additional Statistics.

In the bottom bar of the results report click on the **Download Add'l Stats** link. This will download a comma separated values (CSV) file of flow statistics for the overall period of analysis and each year (or water year if selected). Of particular importance to this project is the metric "Richards-Baker Flow 'Flashiness' Index" as in the decision tree supporting Q_{s50} calculations.

B.3   Tutorial: Rapid Watershed Assessment

Step 1:   Visit the eRAMS Watershed Rapid Assessment Program (WRAP) website (https://erams.com/wrap/).

Step 2:   Navigate map to area of interest.

This is the area that you believe contains the watershed upstream of the point of interest.

Step 3:   Define a watershed boundary using one of the tools listed below.

- **Point Buffer** – with user-defined radius in miles.
- **Line Buffer** – with user-defined radius in miles.
- **Polygon** – the corners of which are specified by the user on the map.
- **Rectangle** – the corners of which are specified by the user on the map.
- **Upload a Boundary** – a shapefile can be uploaded (what forms?).
- **Within Layer Extent** – shapefile layers (including watershed delineations) previously created on eRAMs can be selected and used.
- **Known Boundary** – State, county, Hydrologic Unit Code (HUC) (HUC 8–digit, HUC 10–digit, and HUC 12–digit) watersheds are available. The program pre-filters the available boundaries to those which intersect the map view.

Step 4:   Extract data.

A wide array of data is available (Figure B-3). This list will expand as more data layers are uploaded into eRAMS over time. Click on the data type you require. Some general data categories (e.g., Water Quality) will allow you to pick more specific data for your report.

▼ 2. Extract Data

Select the types of data to be included in the assessment.

Climate and Snowpack
☐ Climate Projection
☐ Historical/Current Climate
☐ PRISM   Data Info.

Environmental Resources
☐ Wetlands and Riparian Zones   Data Info.

Hydrology and Streams
☐ Historical/Current Stream Discharge
☐ Historical/Current Water Quality
☐ Hydrography
☐ Impaired and Use-Limited Waterbodies (U.S. EPA 303d)
☐ Waterbody Classification (U.S. EPA 305b)
☐ Water Quality Standards
☐ Water Rights   Data Info.

Geology and Soils
☐ Soils   Data Info.

Groundwater
☐ Historical/Current Groundwater   Data Info.

Land Surface
☐ Land Use:
☐ Land Use Trends:
☐ Population
☐ Topography   Data Info.

Other
☐ Atmospheric Deposition
☐ Confined Animal Feeding Operations (CAFOs)
☐ Wastewater Treatment Plants   Data Info.

Figure B-3. Screenshot of "Extract Data" menu.

Step 5:   Generate report.

The report will contain the data you requested. Note that larger geographic areas and the selection of some data types will significantly increase the run time of report generation.

B.4   Tutorial: Single-gage Flow Duration Curve (FDC) Computation within eRAMS

Step 1:   Access the Flow Analysis tool.

This can be done by either: (1) log-in to https://.erams.com and create a 'Flow Analysis' project or (2) directly visit the eRAMS Flow Analysis website https://erams.com/flowanalysis/ (no log-in required). Note that use of the non-log-in version does prevent you from saving any data within eRAMS (however, it can still be saved on your local computer).

> Full documentation for this tool can be found at https://erams.com/documentation/flow-analysis/.

Step 2:   Select site.

You can use keyword search or map region search and filter both by attribute. By selecting a site in the "Station Search Results," a summary balloon will pop-up on the map allowing you to review both the location of each site and also the data availability (Figure B-4). Finally, select the "Flow Analysis Model" link in the summary balloon for your chosen site.
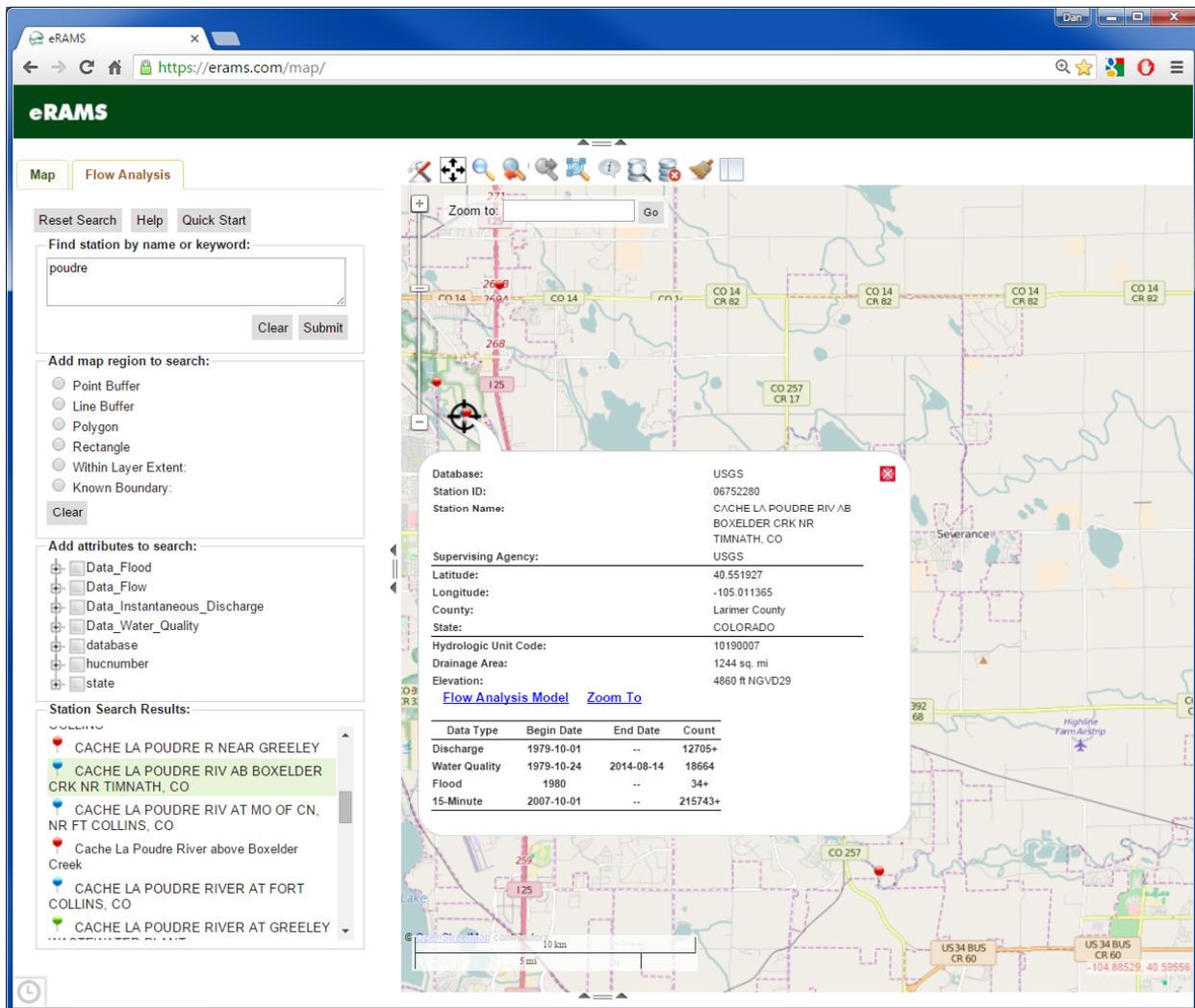
Figure B-4. Screenshot of "Station Search Results" tab.

Step 3: **Navigating to the FDC tool.**

- Select the "Duration Curves" tab (Figure B-5).
- Make sure the FDC radio button is selected.
- Select the Analysis period (defaults to the oldest available through the newest available data).
- Interactive graphs are available for smaller datasets. They will load with +20 yrs of daily data, but could take a few minutes for large datasets.
- There are advanced options related to seasonal analysis or computation of separate FDCs for multiple time periods.
- When inputs are finalized, click "Run Model."
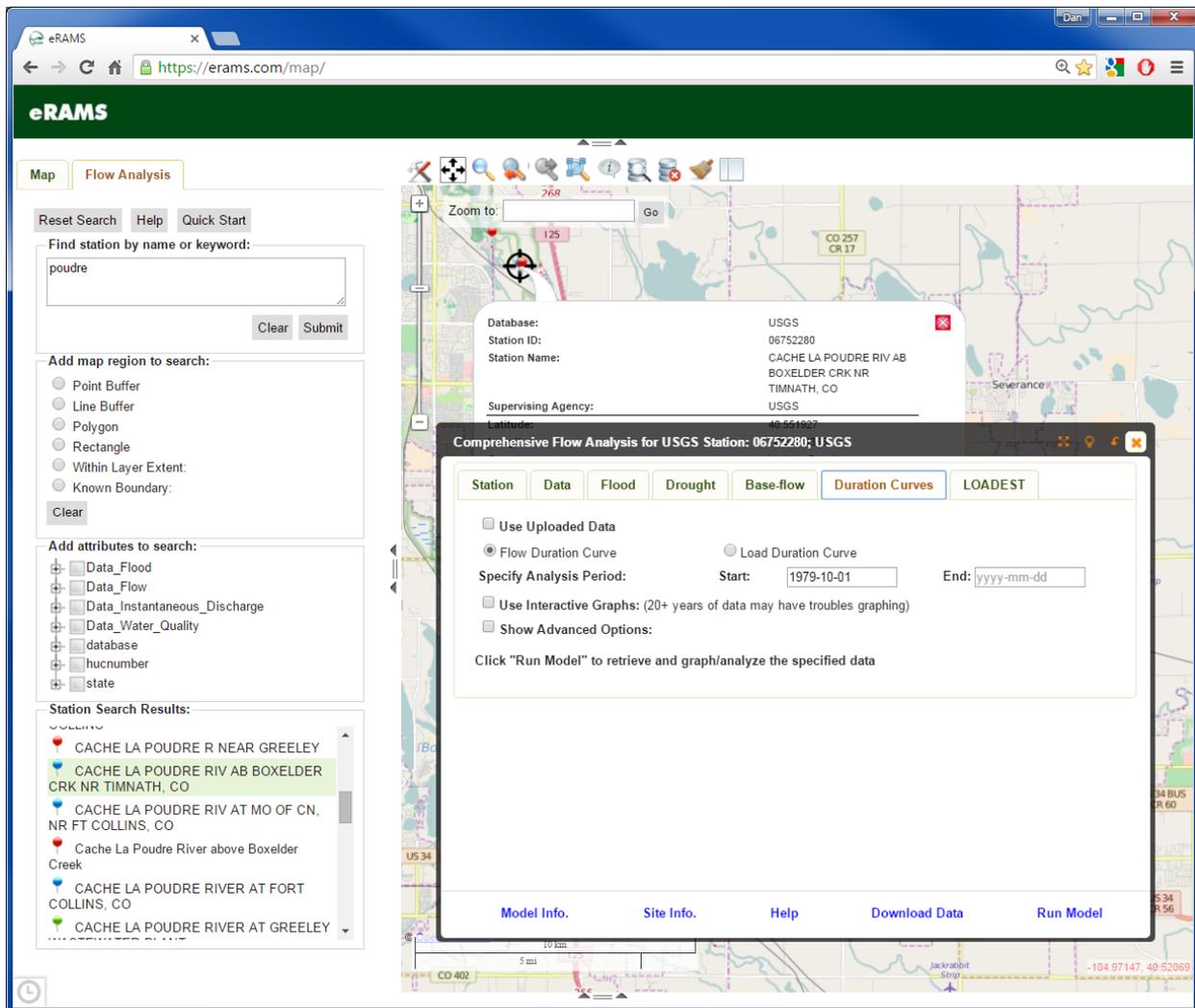
Figure B-5. Screenshot of "Flow Duration Curve" tab.

Step 4: **A FDC report will then be generated (Figure B-6). This report can be printed ("Print Report") or the FDC data can be saved ("Download Results").**
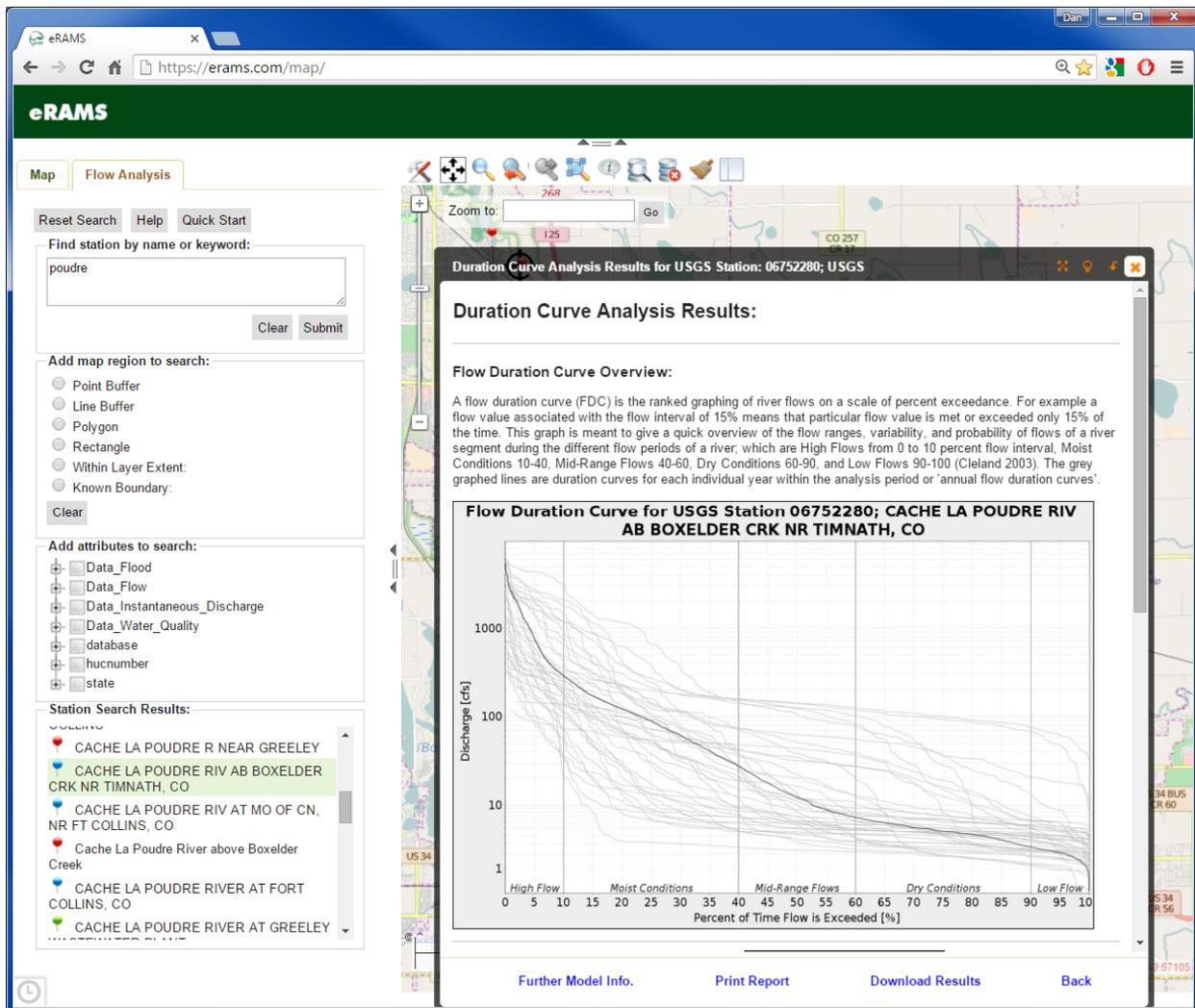
Figure B-6. Screenshot of "Flow Duration Curve" report.

B.5   Tutorial: Regional FDC Estimation within eRAMS

Step 1:   Access the Flow Analysis tool.

This can be done by either: (1) log-in to www.erams.com and create a flow analysis project or (2) visit the eRAMS Flow Analysis website https://erams.com/flowanalysis/ (no log-in required). Note that use of the non-log-in version does prevent you from saving any data within eRAMS (however, it can still be saved on your local computer).

Step 2:   Select Multiple Representative Gages.

Sites should be in the same geographic area and have complementary hydrology to your ungaged location. In the left bar of the Flow Analysis tool, use a keyword search or map region search to find gages. After you have developed a list in the "Station Search Results," select your desired gages from this list of stations by holding 'Ctrl' and left-clicking (Windows) each stations name. As you select each site, a summary balloon will pop-up on the map allowing you to review both the location of each site and also

the data availability. Finally, once all sites are selected, click the `Multiple Site Comparison` button in the lower left corner of the page which will bring up the Multi-Site Flow Analysis toolbox. In the example below, we have selected three sites in the "Station Search Results" list and clicked `Multiple Site Comparison` (Figure B-7).
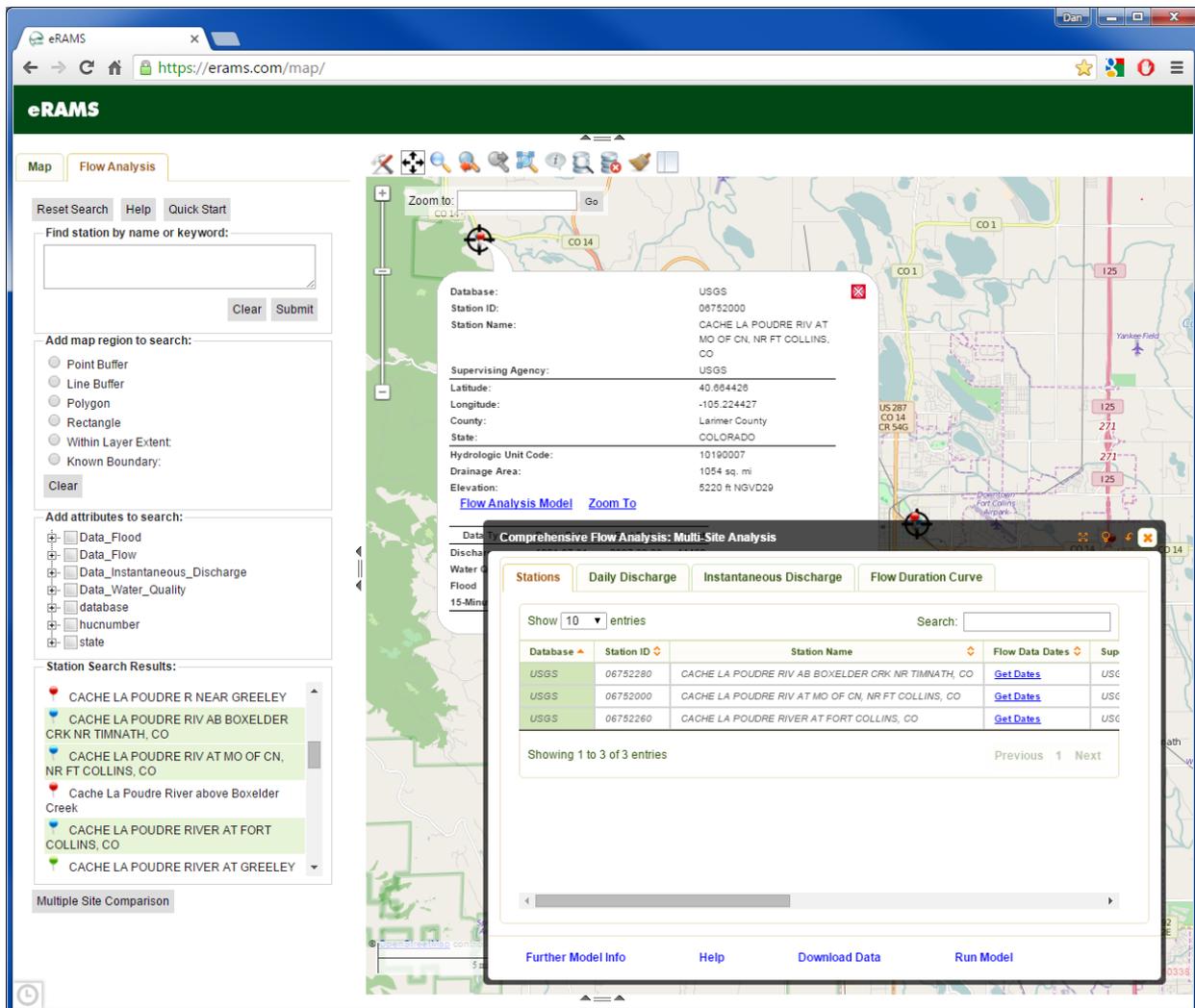

Figure B-7. Screenshot of "Multiple Site Comparison" button.

Step 3:   Navigate to the FDC tool.

- Select the "Flow Duration Curve" tab in the Multi-Site Analysis tool (Figure B-8).
- Make sure the "Regional Flow Duration Curve" radio button is selected.
- Select the Analysis period (tool defaults to the oldest available through the newest available data).
- Select the normalizing metric to collapse all FDCs into a single curve:
  - Drainage area in square miles (*recommended*). eRAMS will extract the watershed area for each of the gages selected and ask you to confirm these areas. If you have not computed the drainage area for your ungaged location, you are welcome to use one of the watershed delineation tools in eRAMS (see additional tutorial on this topic).

o   Flow statistics are computed from gage data (average flow, median flow, or various flood flows derived from the single-station analysis) which make them easy to use for creating a normalized FDC curve, but you must also have data for the ungaged location to scale the FDC back up to a dimensional curve.
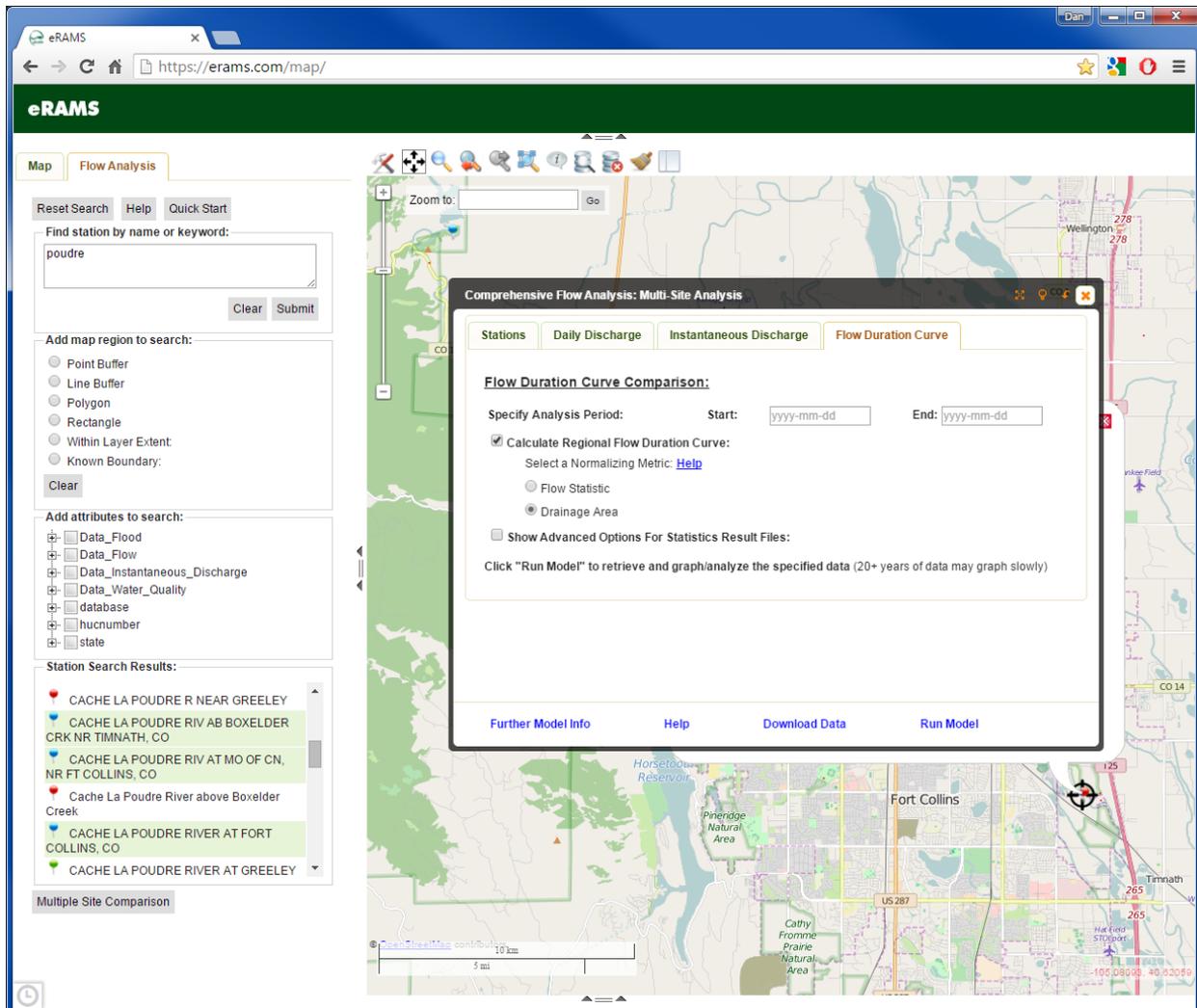

Figure B-8. Screenshot of "Flow Duration Curve" tab on the "Comprehensive Flow Analysis: Multi-Site Analysis" menu.

Step 4:   Examine the resultant regional curve, if a station does not fit the regional trends, uncheck the box next to its name on the results page, and re-run the regional curve calculation.

B.6 Tutorial: Watershed Delineation

Step 1: **Access any www.erams.com project type in a web browser.**

The watershed delineation tools are available in the Map Tools ⚒ > Hydrology > Watershed Delineation from any eRAMS project type. As of March 2016, watershed delineation in eRAMS is based upon 30-m Digital Elevation Models (DEMs) in the U.S. (for more information see http://www.horizon-systems.com/nhdplus/NHDPlusV2_home.php) and 90-m DEMs in the rest of the world. The eRAMS delineation tools have been tested and validated using USGS StreamStats.

Step 2: **Change Base Layer to Hydro-NHD.**

This will enable you to view HUC watersheds and see stream locations. Click on the main "Map" tab, then on "Base Layers," finally click on the "Hydro-NHD" (Hydro National Hydrography Dataset) under the U.S. Geological Survey (USGS) National Map heading.
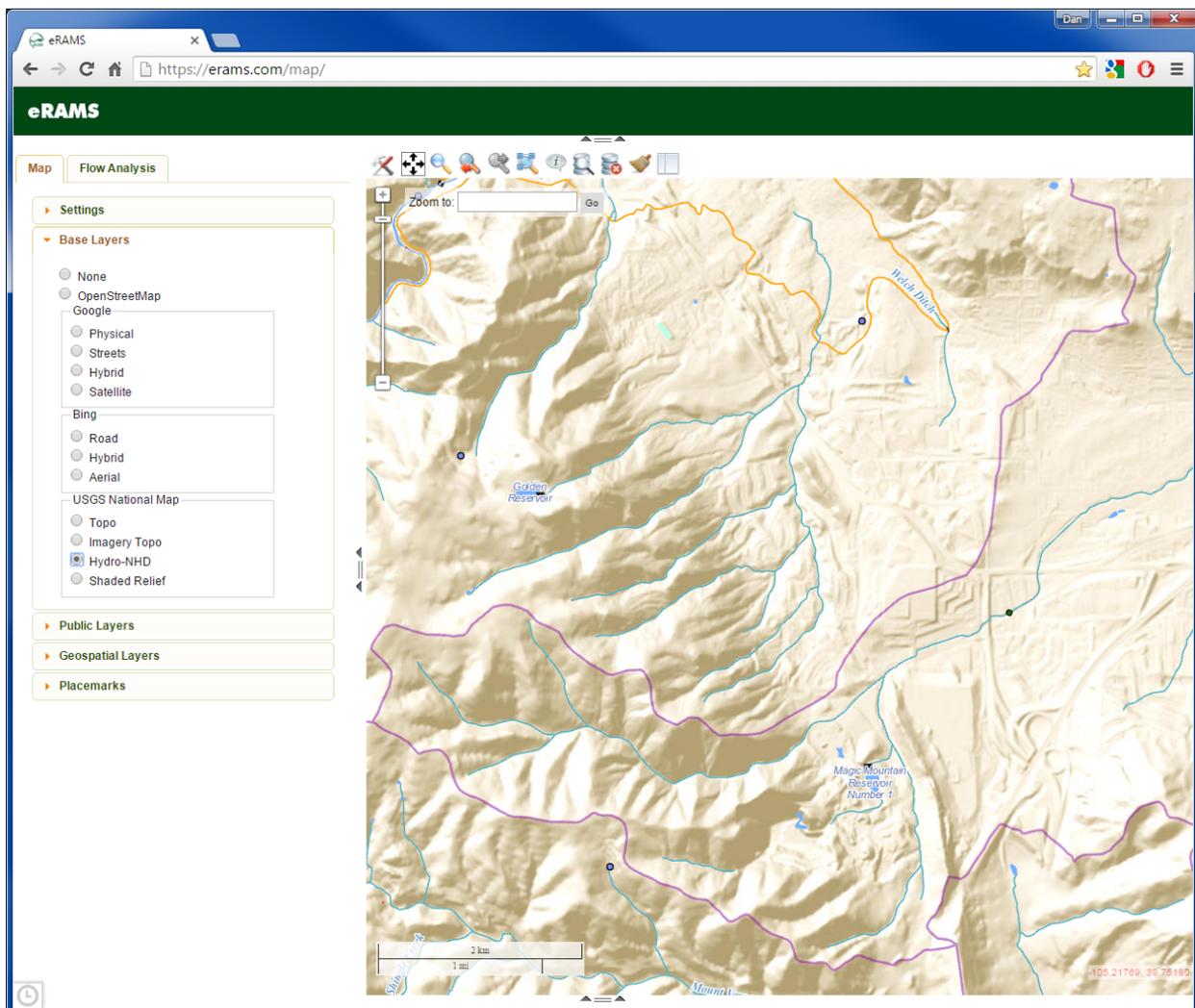

Figure B-9. Screenshot of "Map" tab.

Step 3:   Navigate map to area of interest.

This is the area that you believe contains the watershed upstream of the point of interest (Figure B-10). You'll be asked to highlight an analysis area so it is easiest to have it visible on the screen.
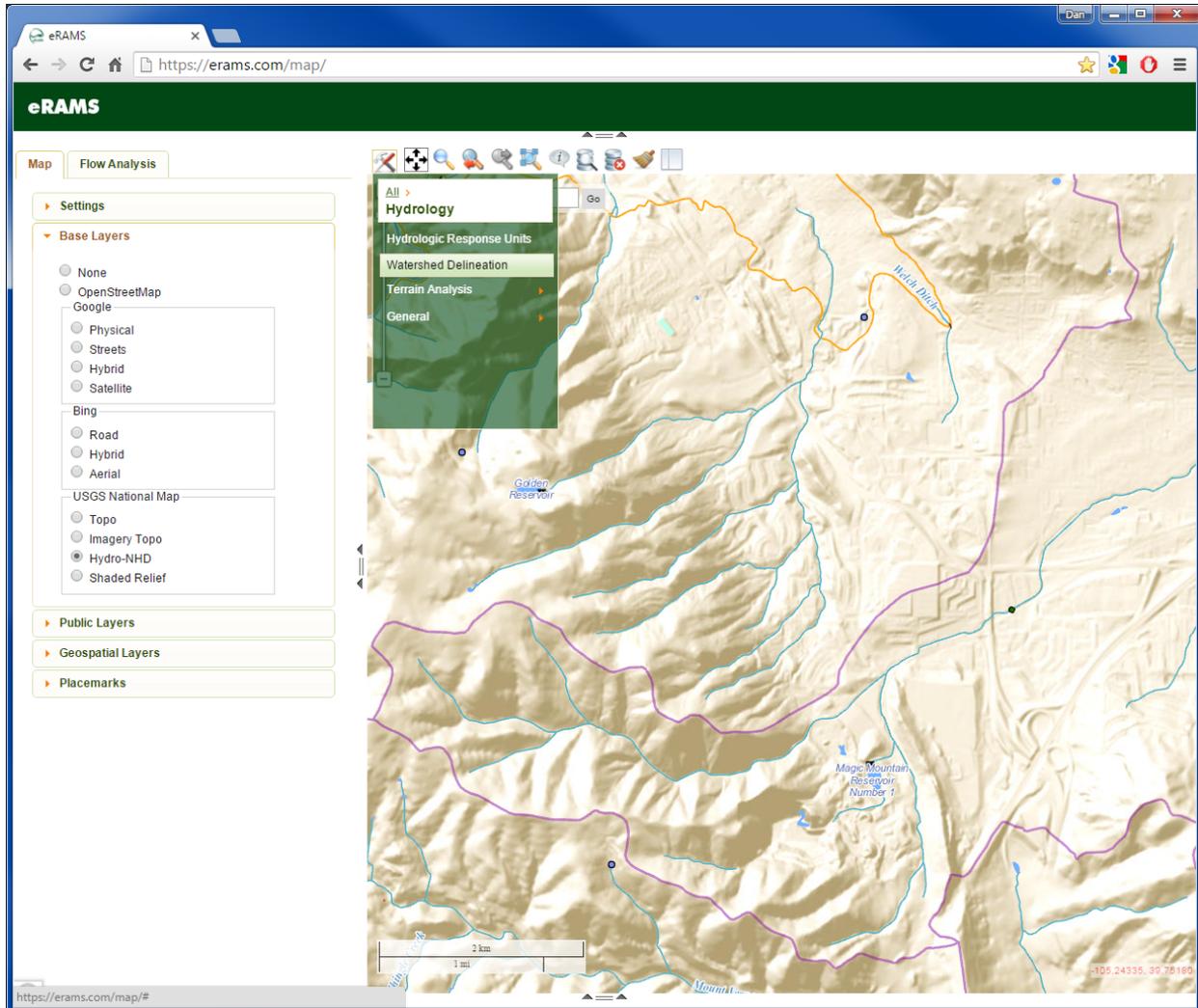

Figure B-10. Screenshot of "Map" tab for Hydro-NHD map.

Step 4:   Choose "Watershed Delineation" option.

This tutorial will cover the Watershed Extraction option, hence, select the radio button next to "Watershed Extraction" (Figure B-11). This tool runs only the steps required to create a final watershed shapefile and defaults to clip a DEM from the 30-m resolution National Hydrography Dataset Plus (NHDPlus) hydrologically conditioned DEM (HydroDEM).

Other Watershed Delineation tool options (not included in this tutorial) include:

- **Basic** – This mode automates several of the steps in the 'Advanced' watershed delineation process and produces a number of rasters (filled DEM, slope, and flow direction) in addition to

the final watershed shapefile. This tool can use either a user-uploaded DEM or can clip from the 30-m resolution NHDPlus HydroDEM.

- **Advanced** – Essentially the same steps as if you were using the Hydrology toolset in Environmental Systems Research Institute (ESRI) ArcGIS. This requires you to clip and fill the DEM, compute flow direction and accumulation, and further allows you to modify the stream network (i.e., weighted accumulation or stream accumulation threshold analysis) before finally extracting the watershed.
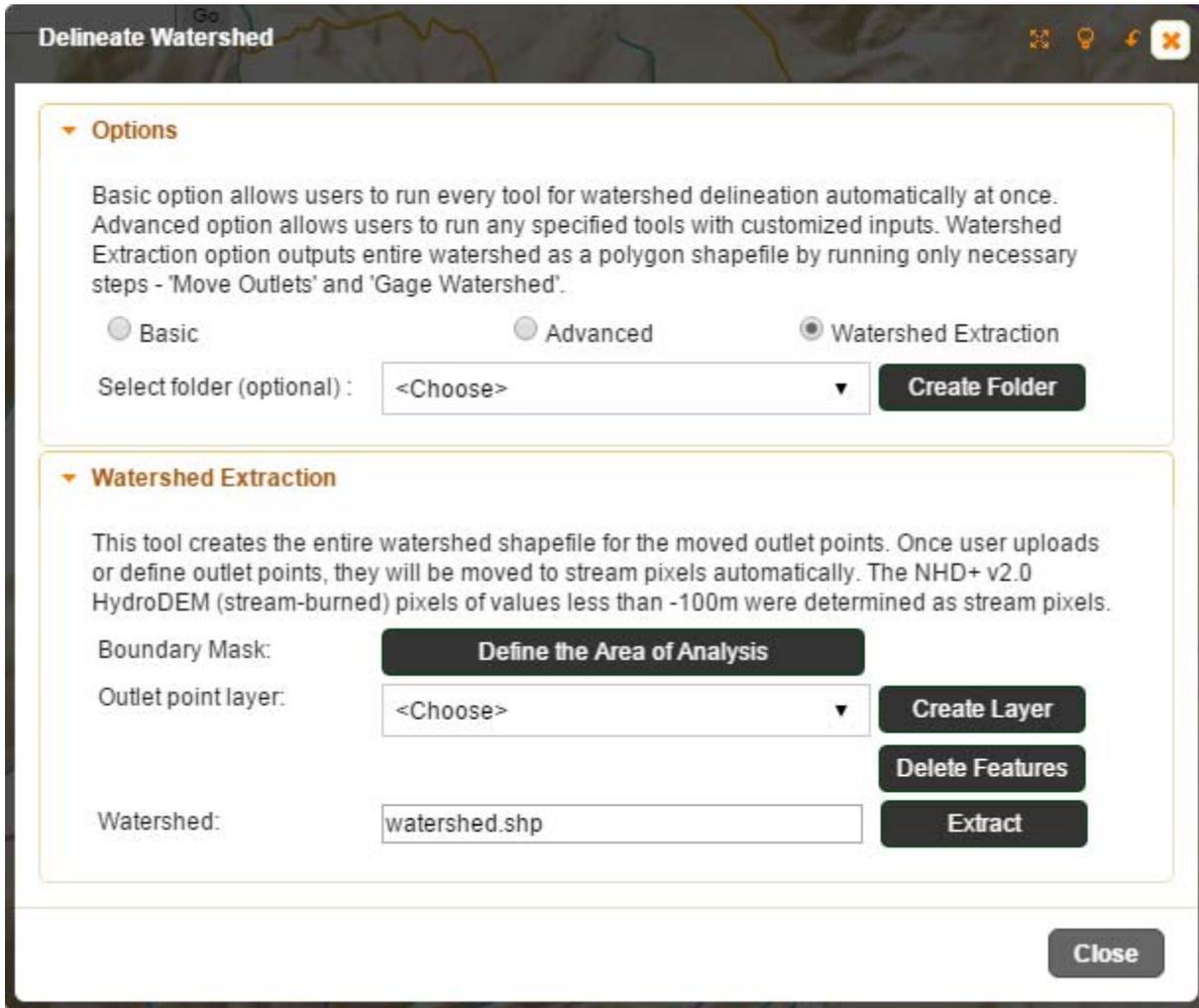

Figure B-11. Screenshot of "Watershed Extraction" on the "Delineate Watershed" menu.

Step 5:   Define the area of analysis.

This tells the Watershed Delineation tool the extent of DEM data which needs to be downloaded (Figure B-12). This is done by left-clicking (holding) and dragging a box across the mapping window.
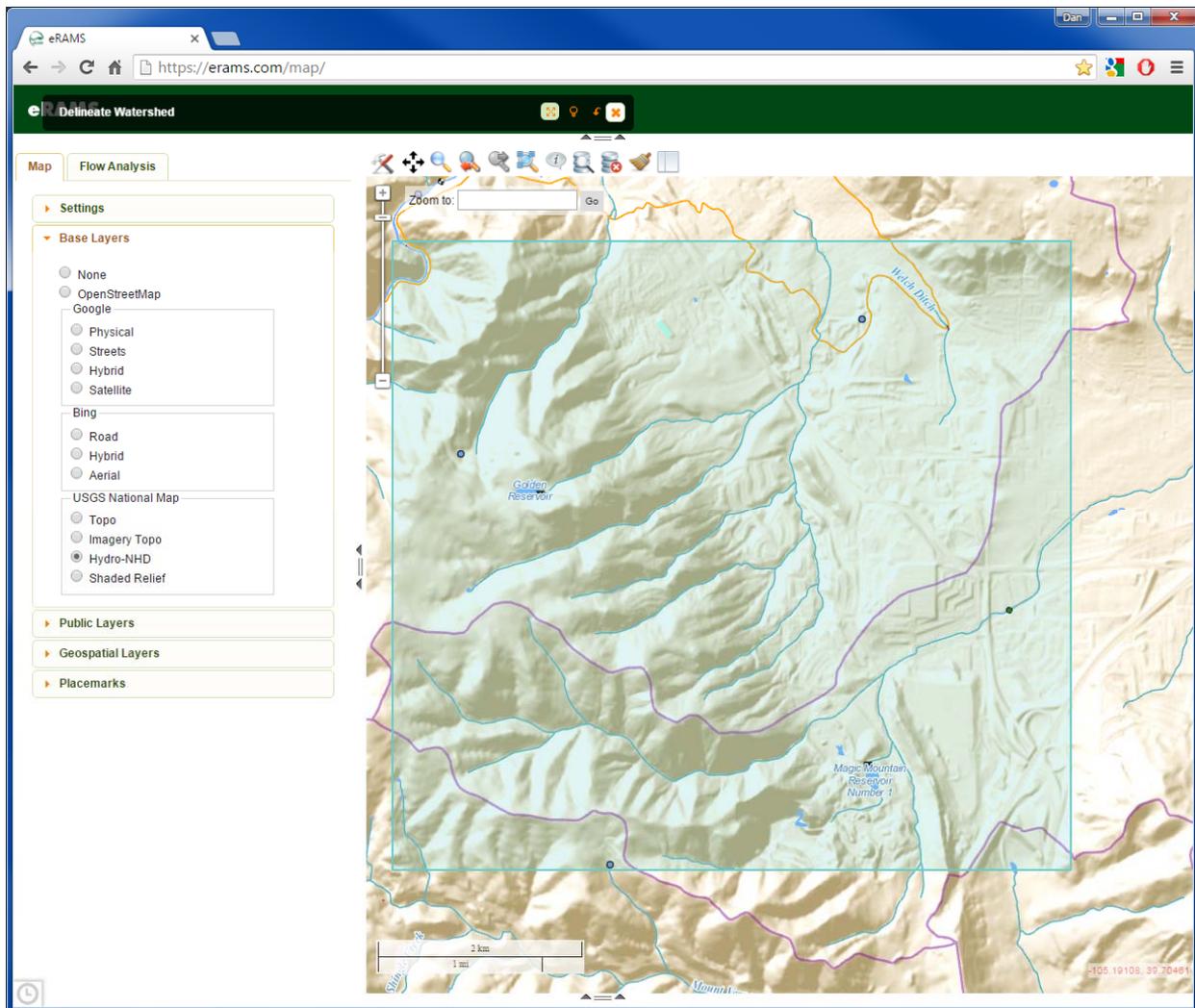
Figure B-12. Screenshot showing defined area of interest.

Step 6:   Create an outlet (pour) point.

First select [Create Layer] (if you had not done so previously), then [Add Outlet] by clicking on the map closest to your point of interest (Figure B-13). A red circle will appear where you have clicked.
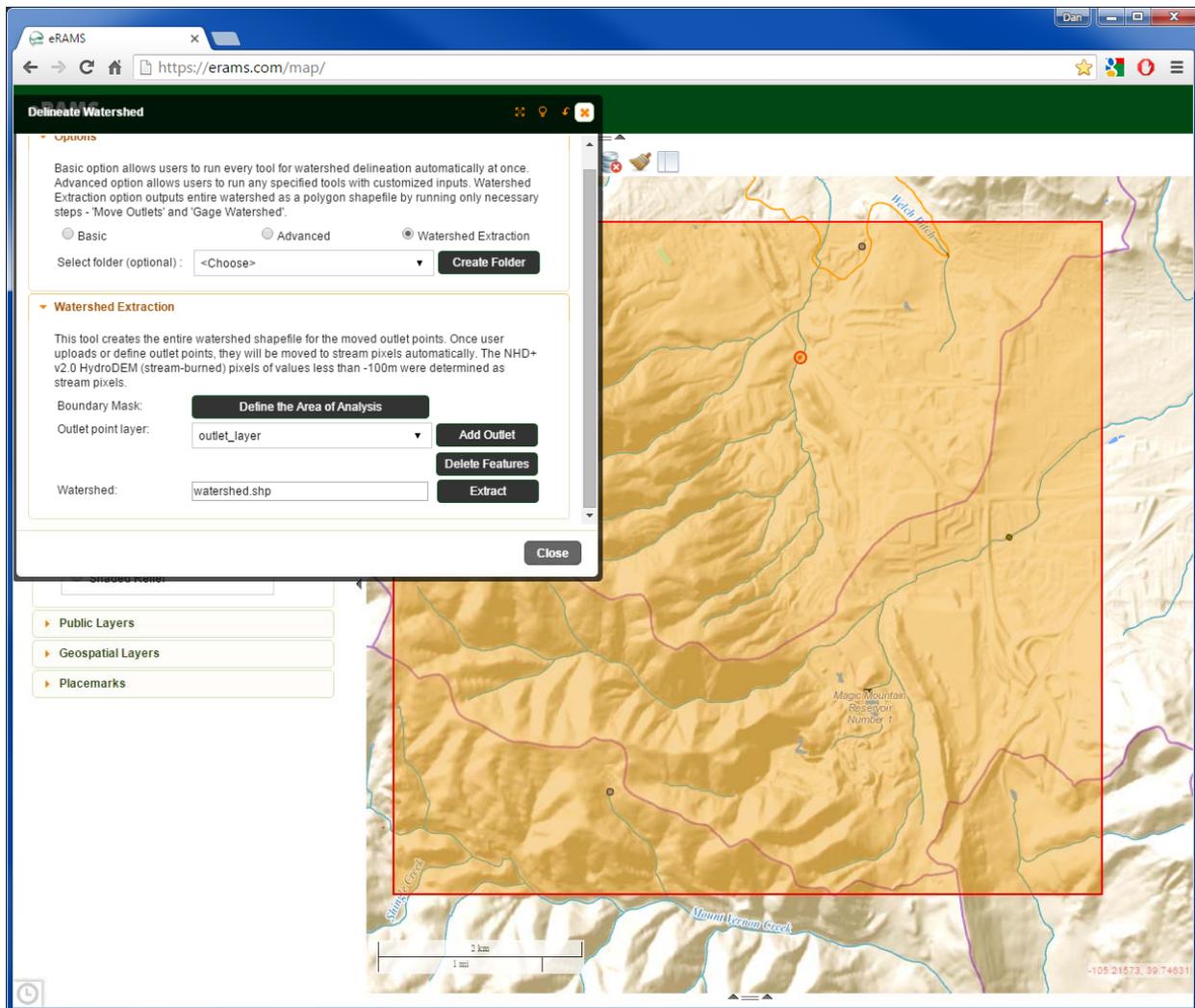
Figure B-13. Screenshot showing creation of an outlet (pour) point layer.

Step 7:   Extract your watershed.

Click on the [Extract] button (Figure B-14). A red watershed shapefile should soon appear. In Figure B-14 the opacity of the watershed has been changed to 70% by editing the Properties (Map tab > Geospatial Layers > right-click on watershed). This watershed is now saved within eRAMS for this session (if you have not logged in) or can be saved permanently in your eRAMS file storage space (if you have logged in).
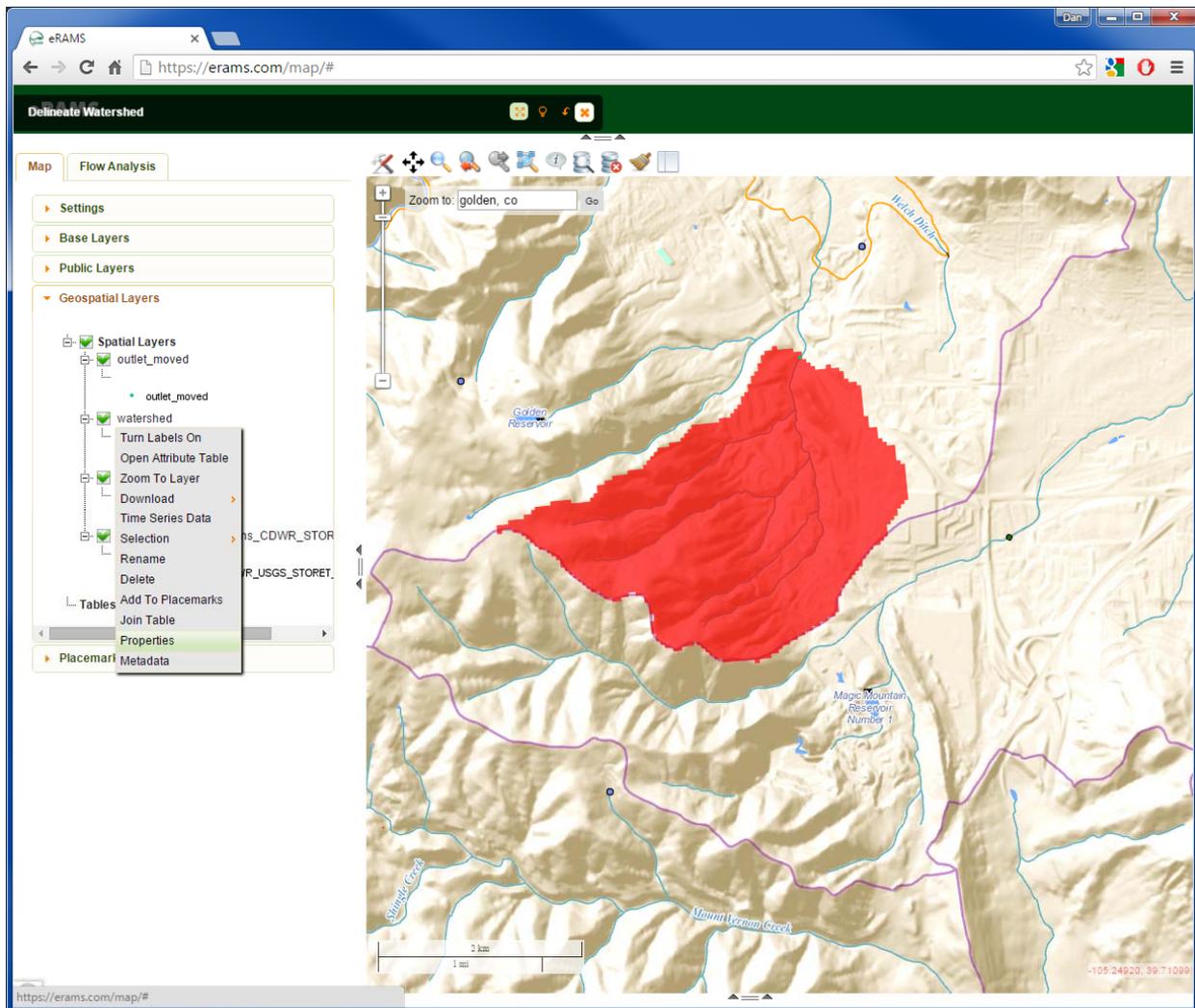
Figure B-14. Screenshot showing extraction of watershed.

B.7 Tutorial: FDC Estimation with the eRAMS Soil and Water Assessment Tool – channel DEGgradation (SWAT-DEG)

Disclaimer: Keep in mind that the SWAT-DEG model is a distributed hydrologic model which provides an estimated FDC given the model inputs. However, it is not currently calibrated to any existing flow data for a modeled watershed. As such, it should be treated as a relative comparison tool where results from SWAT-DEG are only compared to other scenarios from SWAT-DEG and not against gage-based hydrologic data.

Step 1: **Access the SWAT-DEG tool.**

The SWAT-DEG tool requires the use of the log-in version of eRAMS. Log into https://beta.erams.com and create a SWAT-DEG project.

Step 2:   Identify your watershed.

Use the Watershed Delineation tool (Map Tools ⚒ > Hydrology > Watershed Delineation) or another source to identify your basin of interest (Figure B-15). You will need to have this defined prior to starting the SWAT-DEG analysis.
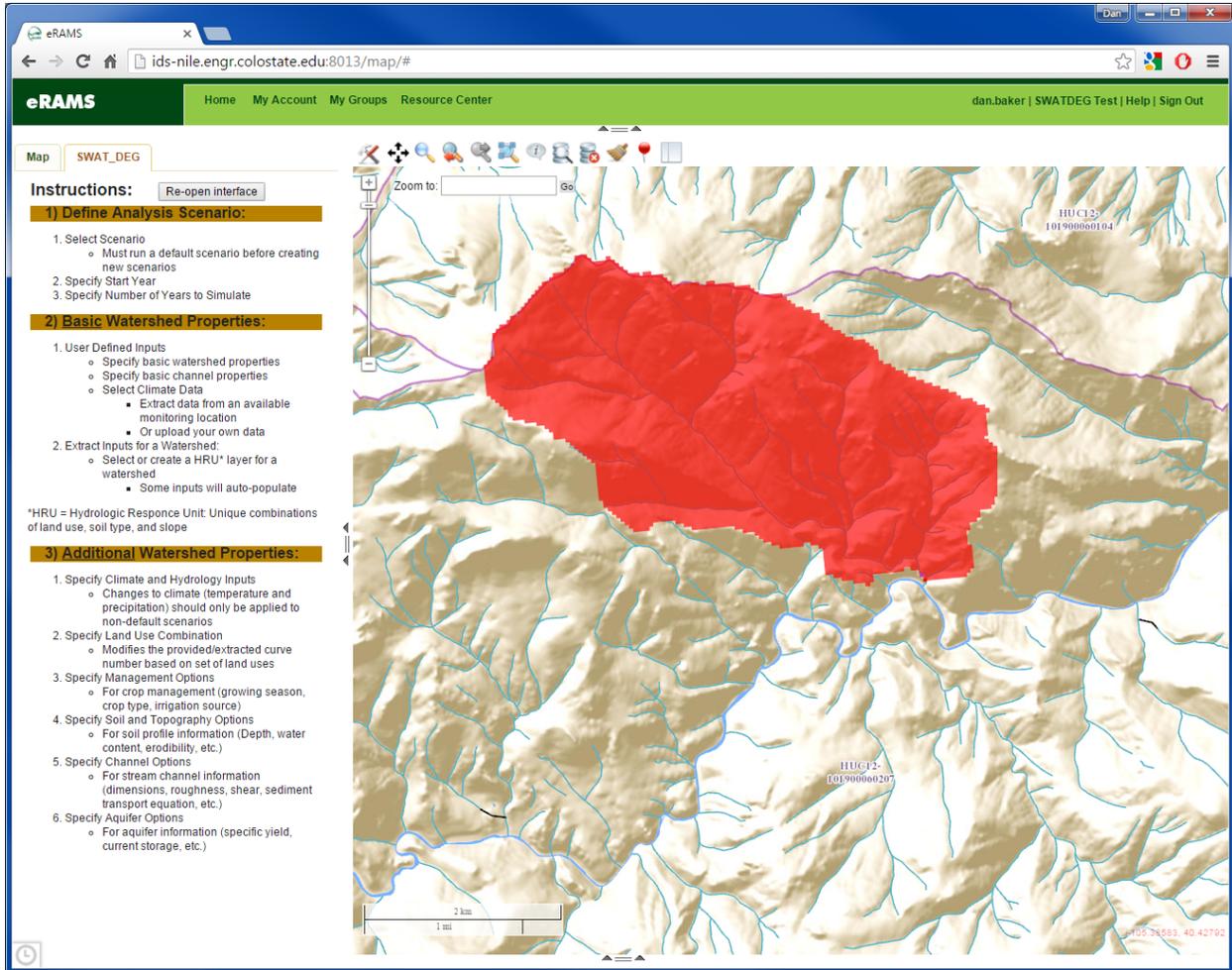
Figure B-15. Screenshot showing identification of watershed.

Step 3:   Establish a 'default' Scenario.

This should be your baseline (often present day) scenario prior to assigning any changes in land use or other changes to the model. In the example, we are looking at a 15-yr scenario starting in 2000. The date range determines the date range of the climate data and land use which is sampled to create the Hydrologic Response Units (HRUs). Click `Create` to create the Scenario (Figure B-16).
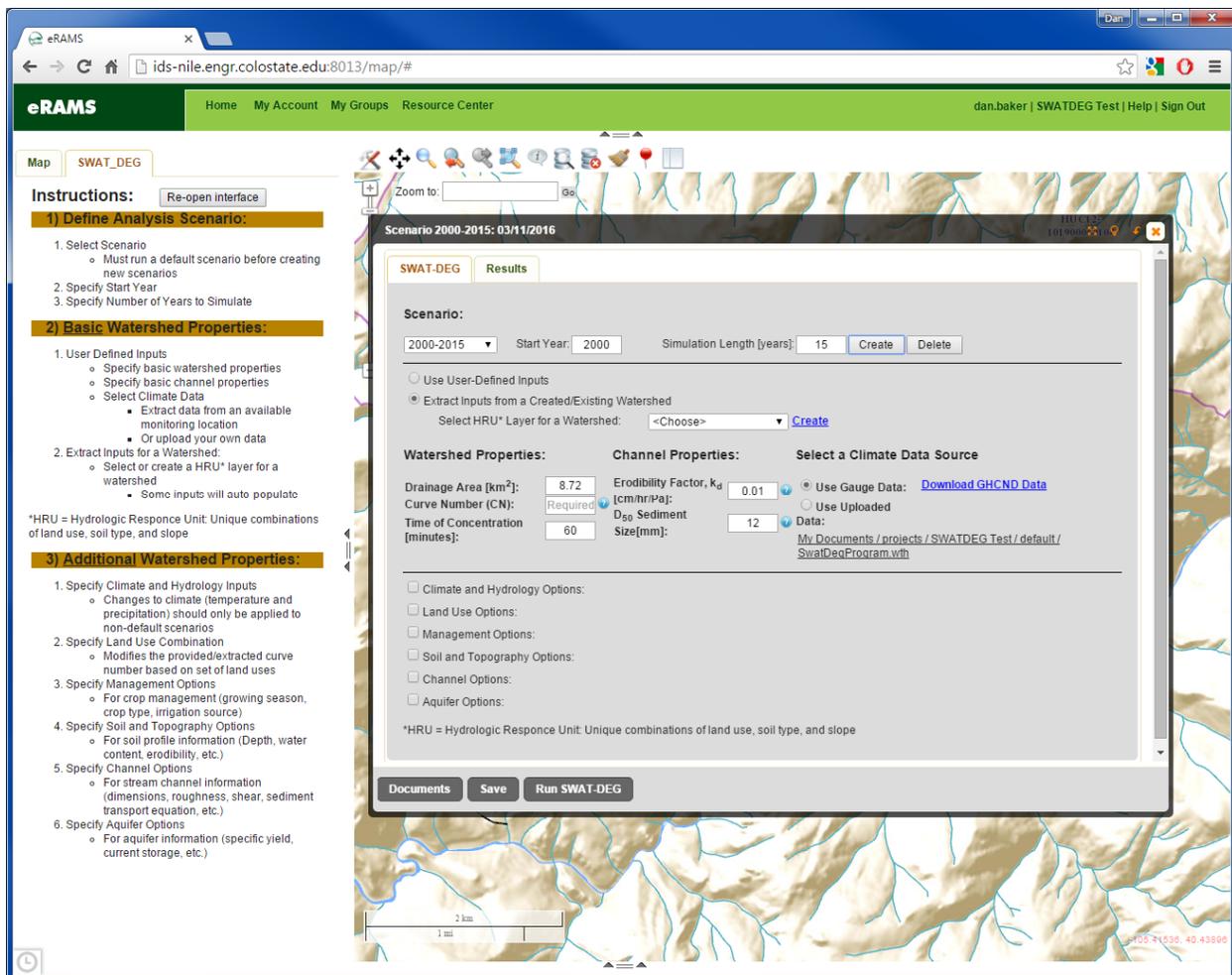
Figure B-16. Screenshot of created Scenario.

Step 4: **Extract Basic Watershed Properties from your watershed shapefile. This includes multiple sub-steps.**

- Below we have chosen to "Extract Inputs from a Created/Existing Watershed" and then click **Create** (if you have not done this step previously) (Figure B-17).

- Pick an existing folder or create a **New Folder**.

- Watersheds can be either the one which you previously created in eRAMS, drawn on the map, or pre-defined as a HUC 8–digit, HUC 10–digit, or HUC 12–digit boundary. We are using one previously delineated by the Watershed Delineation tool called 'watershed.' Note that you may want to use an explicit name instead of 'watershed' as SWAT-DEG includes this name in the names of the land use, soil, and slope layers.

- **Build** (or select previously created) land use layer. Two options are available for land use NLCD (National Land Cover Data) and NASS (National Agricultural Statistics Service). We recommend the NASS only for agricultural areas and the NLCD for mixed-use or non-agricultural areas. Click **Create**.

- **Build** (or select previously created) soil layer. Only one option is available (Soil Survey Geographic Database (SSURGO)). Click **Create**.
- **Build** (or select previously created) slope layer. Only one option is available (NHD+ elev_cm). Click **Create**.
- Finally, select **Create** at the bottom of this dialog to create a "HRU Layer" and close this dialog box.
- Back in the main SWAT-DEG window select your recently created "HRU Layer" under the dropdown next to Select HRU* Layer for a Watershed: .
- The Drainage Area and Curve Number will automatically update given the information from this HRU.
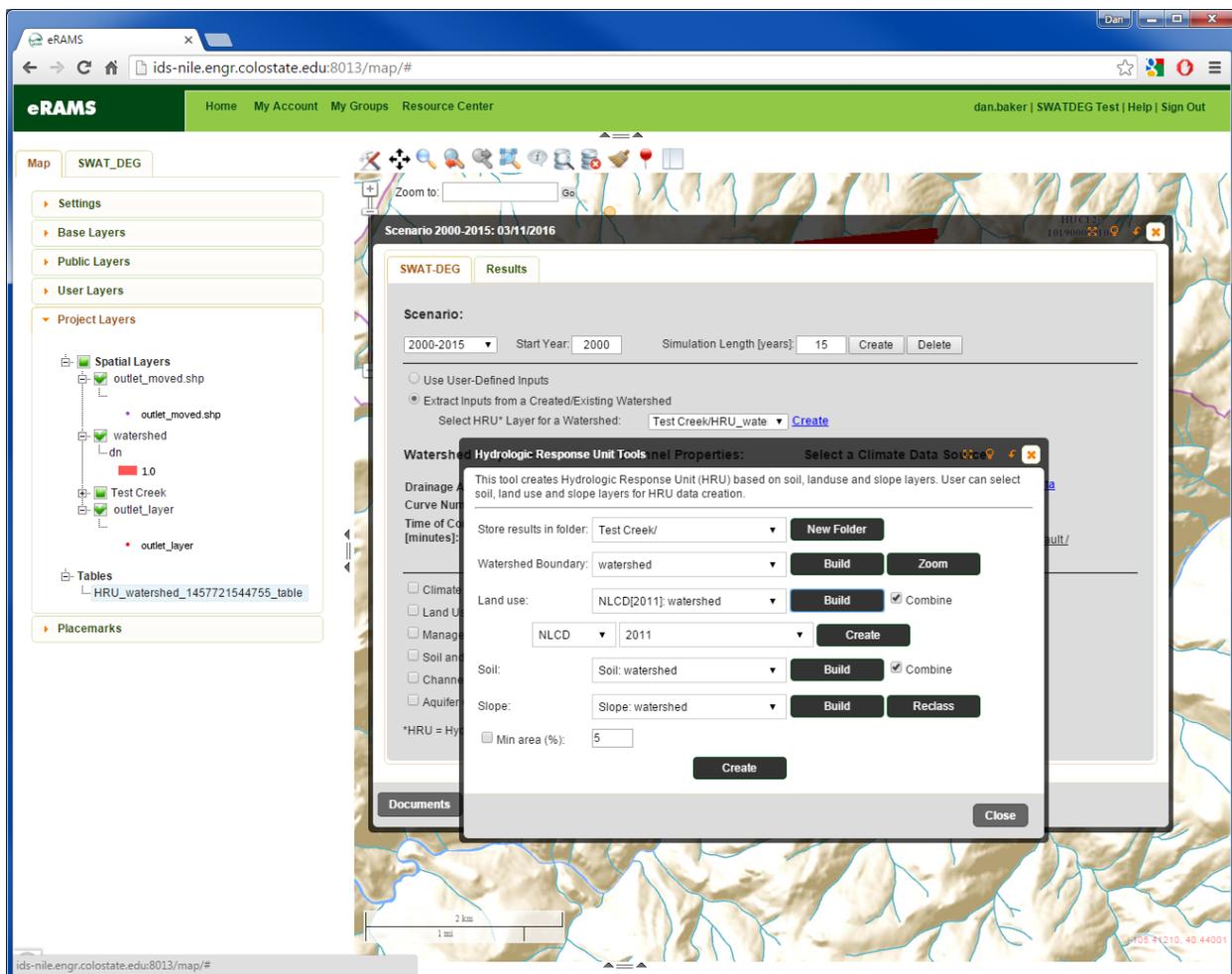
Figure B-17. Screenshot showing extraction of basic watershed properties.

Step 5:   Assign a time of concentration.

Currently there is not an automatic way to compute time of concentration in eRAMS. In future editions of the tool, this will be one of the parameters which is auto-calibrated, but that functionality does not exist at the time of this report.

Note that you can ignore the Channel Properties portion of SWAT-DEG as the computation of a FDC does not include these variables.

> For more information related to time of concentration please visit: Natural Resources Conservation Service (NRCS 2010; Chapter 15: Time of Concentration in: Part 630 National Engineering Handbook, U.S. Department of Agriculture (USDA), NRCS, Washington, DC).

Step 6:   Select and download climate data.

The interface will locate climate stations within the designated map region. In this walkthrough, we selected a 'Point Buffer' of 5 miles from the "GHCND" (Global Historical Climatology Network – Daily) menu (Figure B-18).
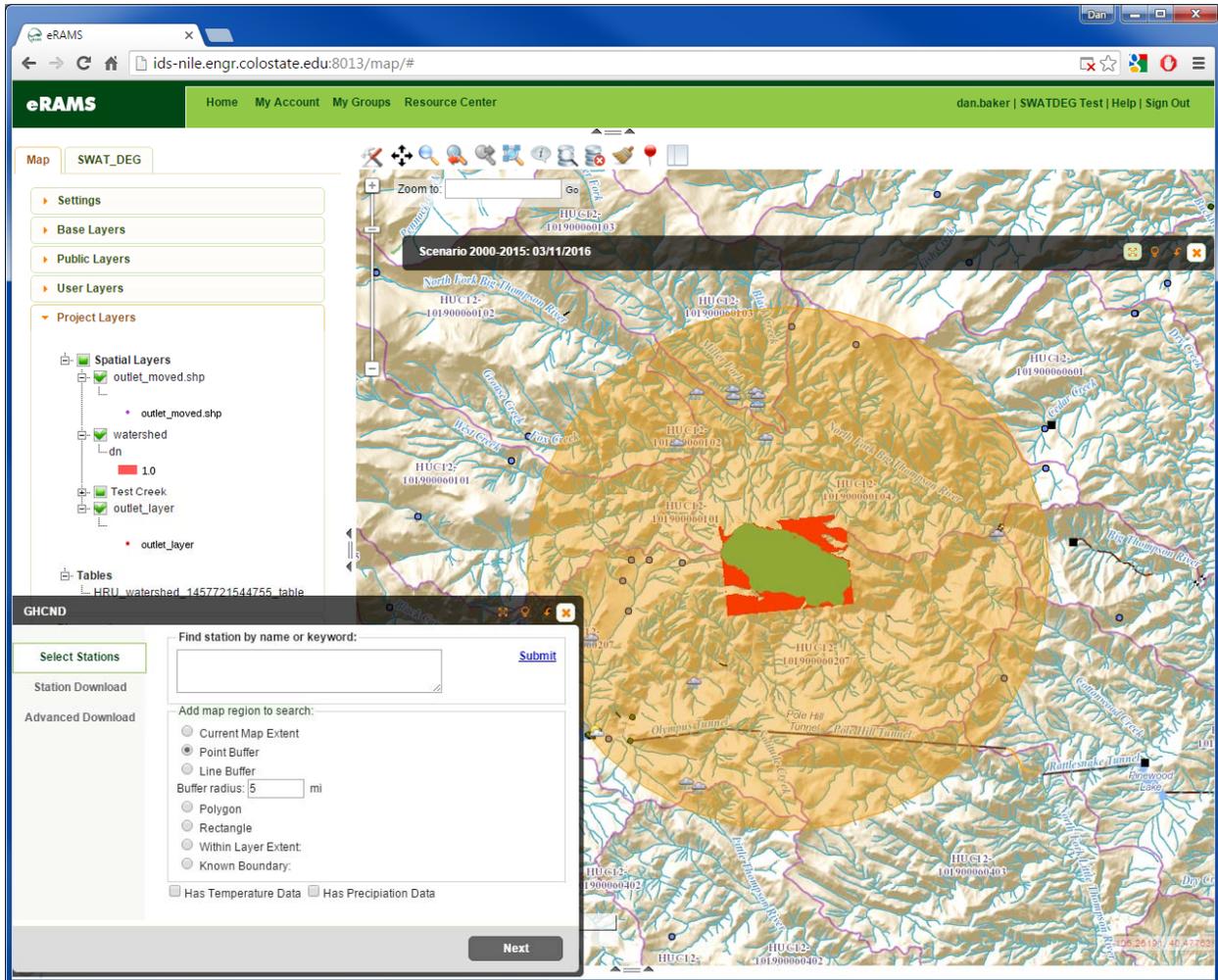
Figure B-18. Screenshot of "Point Buffer" button on "GHCND" menu.

After clicking **Next**, you will see a list of the sites which have also been highlighted on the map (Figure B-19). Select one of these sites, click **Next** and then **Download** the data to eRAMS. You can then close the GHCND interface by clicking on the ❌ in the upper right corner of the window.
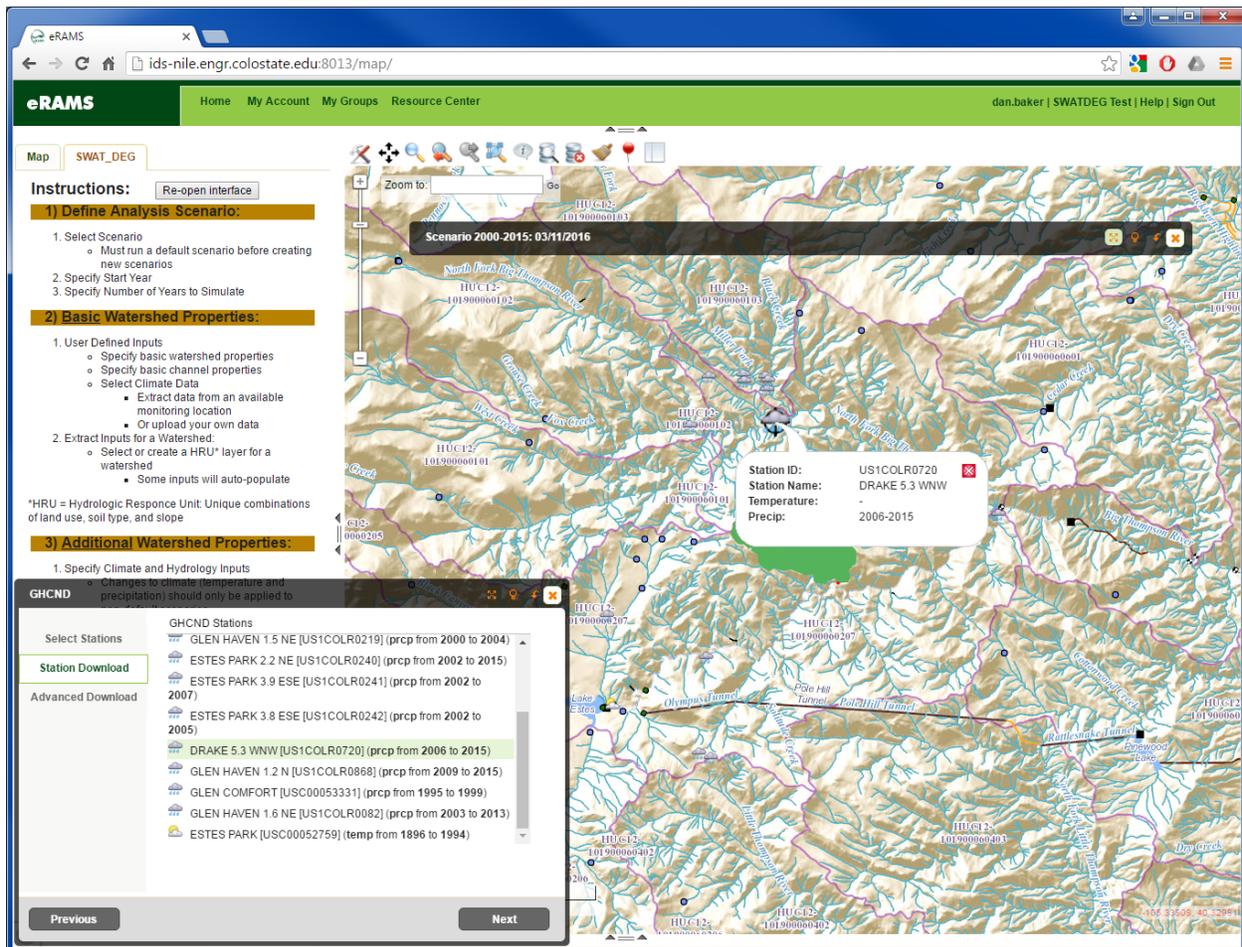
Figure B-19. Screenshot of "Station Download" on "GHCND" menu.

Step 7: **Run SWAT-DEG for your current conditions.**

- Click **Run SWAT-DEG** and the results window will open up (Figure B-20).
- By selecting your chosen scenario and type of output (most applicable for this project is the FDC) you can then either **Graph Output** or **Download Data**:
  - note that the FDC is developed for the pour point (most-downstream point) of your watershed.
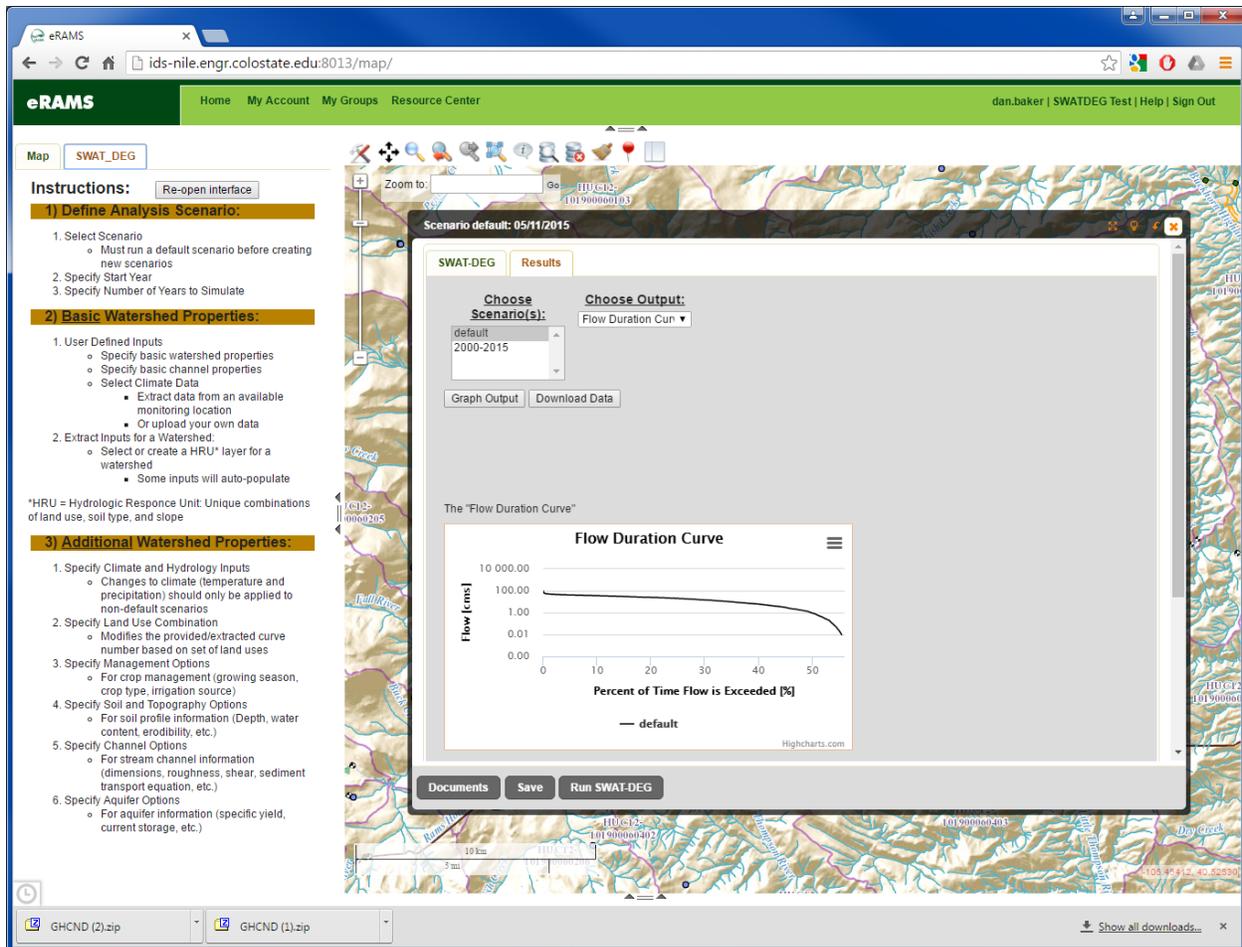
Figure B-20. Screenshot of resulting FDC.

Step 8: **Vary land use to observe changes in.**

- Change the land use percentages (Figure B-21):
  - you will need to define the appropriate curve numbers for non-current land uses,
  - make sure they add up to 100%, and
  - click on **Update CN** .
- Rerun the SWAT-DEG model and compare results to those of baseline conditions.
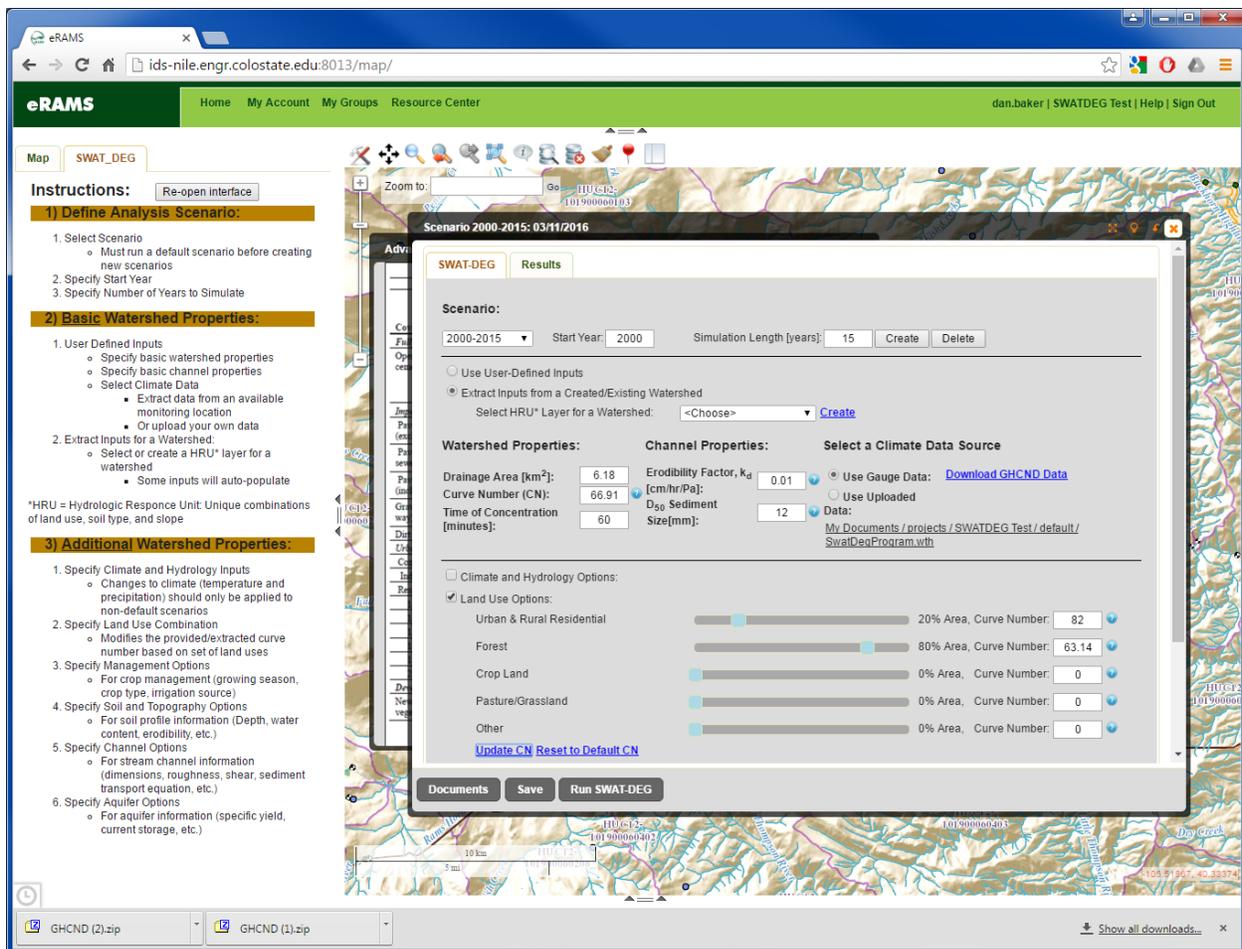
Figure B-21. Screenshot of changed land use percentages for comparison.

B.8 Tutorial: Sediment Yield Computations with eRAMS Cross Section Tool

Step 1:   Access the Cross Section tool.

This can be done by either: (1) log-in to www.erams.com and create a flow analysis project or (2) visit the eRAMS Flow Analysis website https://erams.com/crosssection/ (no log-in required). Note that use of the non-log-in version does prevent you from saving any data within eRAMS (however, it can still be saved on your local computer).

Step 2:   Navigate map to area of interest.

This is the location of the stream cross section which you wish to model.

Step 3:   Change Base Layer to one which allows you to view satellite/aerial imagery at a high enough resolution to see local features at your stream cross section.

Click on the main "Map" tab, then on "Base Layers," finally select either Google Earth Satellite or Bing Maps Aerial (Figure B-22).
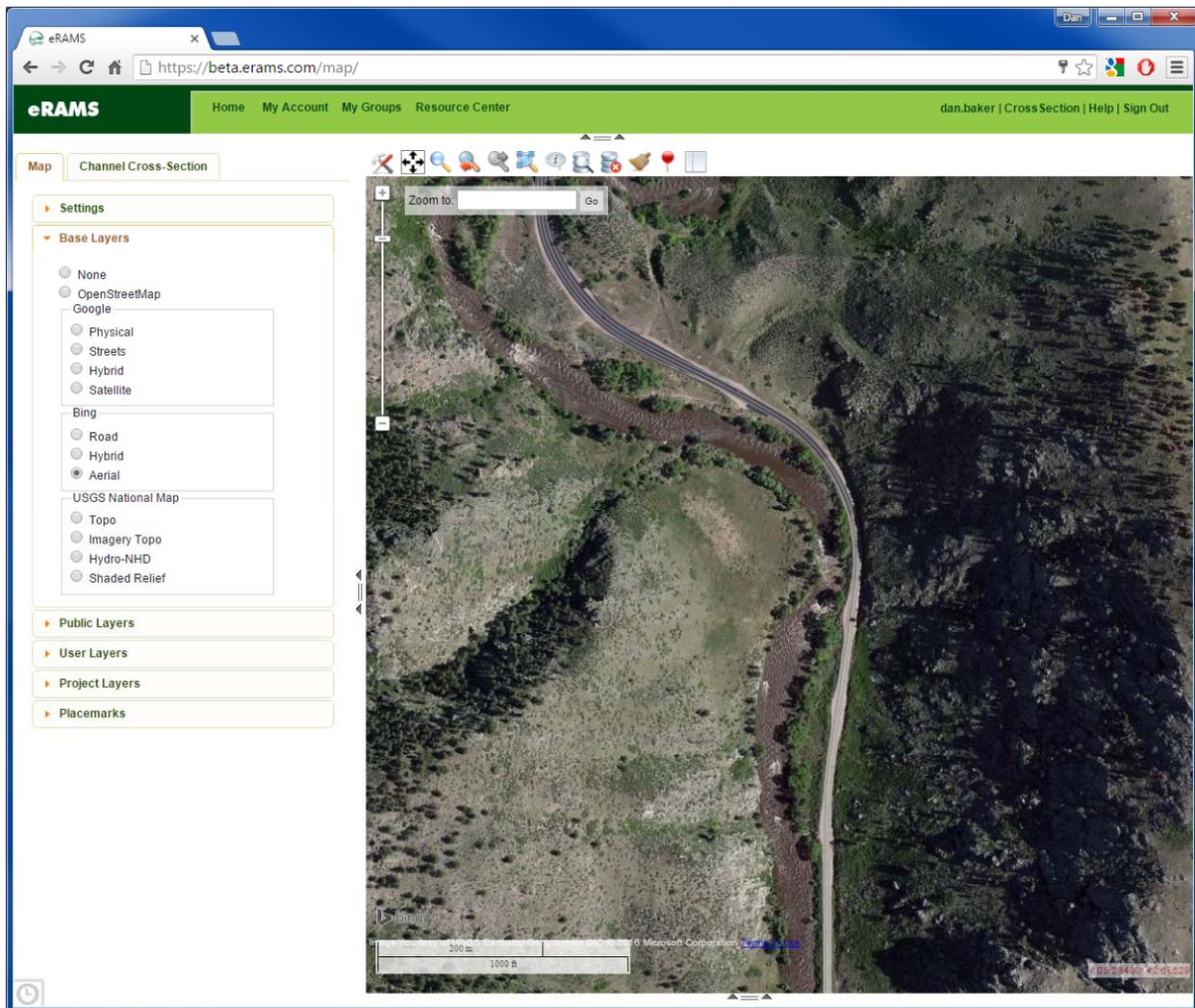
Figure B-22. Screenshot of "Map" tab and resulting Bing Maps Aerial photograph.

Step 4:   Create and refine cross section.

Click on the "Channel Cross-Section" tab and follow the instructions to create a channel cross section (Figure B-23). Note that the "Create on Map" tool only has access to 30-m DEM data, thus you are recommended to either upload survey data using "Create from Spreadsheet" or adapt the DEM-based cross section to reflect the actual channel dimensions. Finally save changes to your cross section by selecting the "Save Changes" link below the graph.
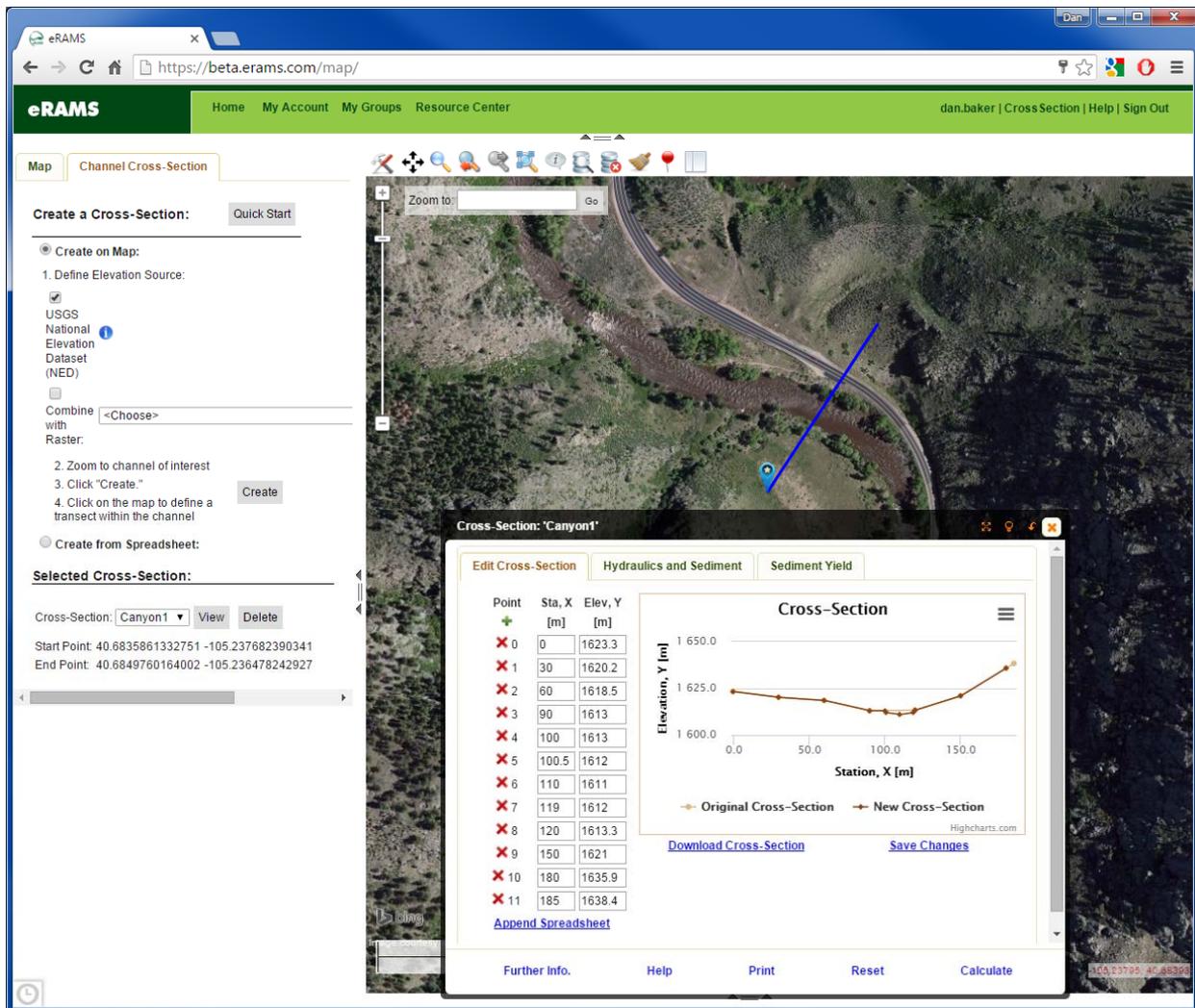
Figure B-23. Screenshot of "Channel Cross-Section" tab.

Step 5: **Select Sediment Yield tab. Now that your cross section is set, it is now time to begin the hydrologic and sediment calculations.**

Step 6: **Select a FDC Source.**

This list includes:
- single-gage FDC generation,
- regional (multi-site) FDC generation,
- upload an FDC (previously computed or external of eRAMS), and
- (soon to be included) the computation of a FDC from SWAT.

> Please see other tutorials for computations of any of the eRAMS-based FDCs.

Step 7:   Select appropriate Sediment Transport Equation.

Clicking on the question mark ⓘ next to the dropdown menu of "Sediment Transport Equations" provides the information in Figure B-24.
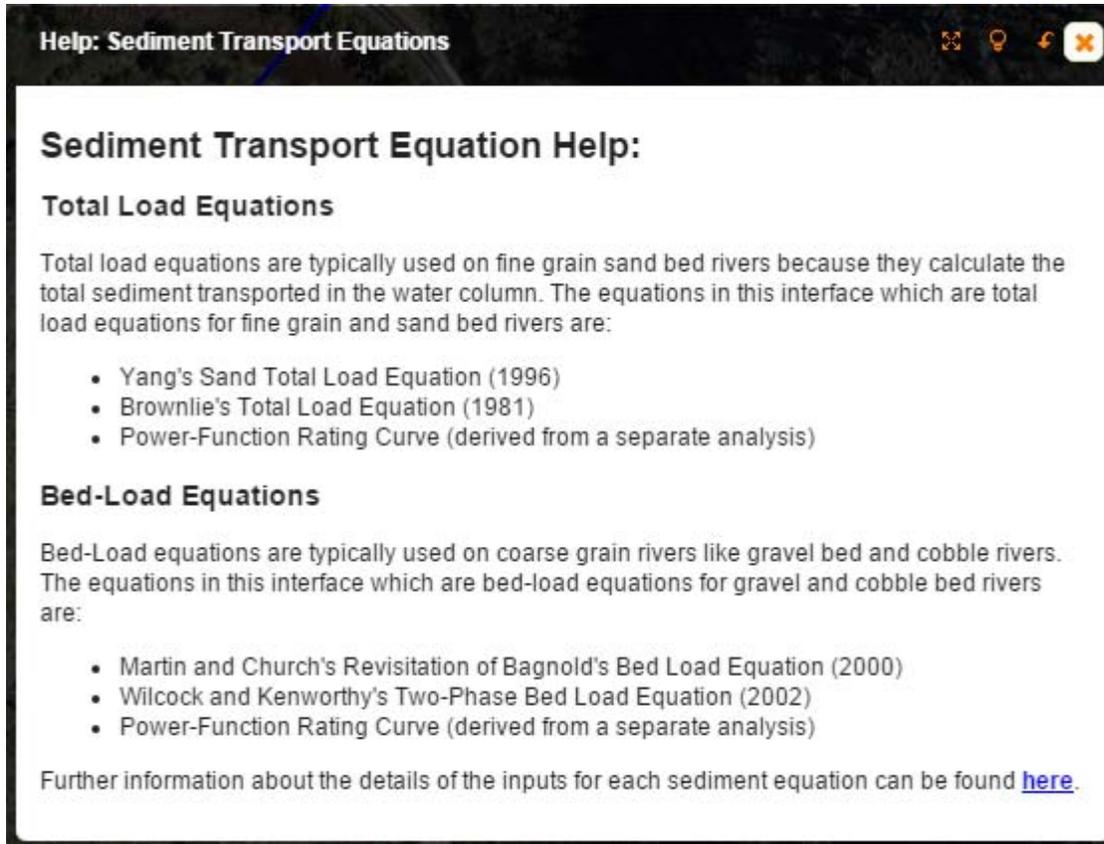
Figure B-24. Screenshot of "Sediment Transport Equation Help" menu.

It is critical at this step to select a sediment transport equation which is appropriate for your system. As general guidance, select:
- Yang or Brownlie if the bed of the river is largely sand,
- Bagnold if the bed is gravel and cobble and does not contain large amounts (>15% sand), and
- Wilcock and Kenworth if the bed is a mix of sand and gravel/cobble.

Step 8:   Input measured (or estimated) sediment properties.

Each sediment transport equation requires its own unique set of parameters (Table B-1).

Table B-1. Input parameters required for sediment transport equations.

Parameter	Yang (1996)	Brownlie (1981)	Bagnold as modified by Martin and Church (2000)	Wilcock-Kenworthy (2002)	Power Function
Transported Sediment Diameter [mm]	√	√	√		
Gravel Sediment Diameter [mm]				√	
Sand Sediment Diameter [mm]				√	
Percent Sand [%]				√	
Bed Sediment d_{50} [mm]		√			
Bed Sediment d_{84} [mm]		√			
Bed Sediment d_{16} [mm]		√			
Manning's n	√	√	√	√	√
Bottom Width [m]			√	√	
Bed Slope [m/m]	√		√	√	
Energy Grade Line Slope [m/m]	√				
Friction Slope [m/m]		√			
Power-function Coefficient					√
Power-function Exponent					√
Power-function Units					√

Step 9:   Calculate the sediment yield curve and report.

Select "Calculate" in the bottom menu and the sediment transport will be calculated for each bin of flows in the FDC resulting in a graph of sediment yield density versus discharge. The maximum value of sediment yield density on this curve corresponds to the effective discharge (red dot) and the discharge at which half of the total sediment load has been transported is the half-load discharge (blue dot).

Combining the information provided in the FDC (magnitude and frequency) with the sediment transport at each flow results in an effectiveness curve of sediment production over the period of analysis. Figure B-25 shows the sediment yield results.
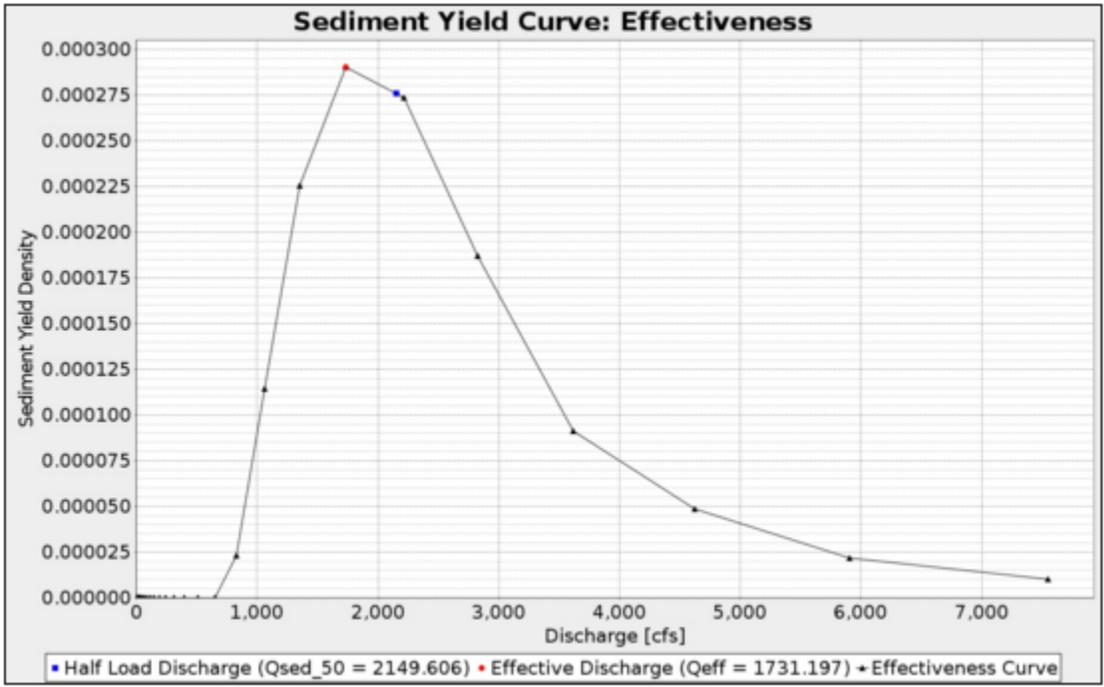
Figure B-25. Sediment yield results.

B.9 References

Brownlie, W.R. 1981. "Prediction of Flow Depth and Sediment Discharge in Open-channels." *Report No. KH-R-43A*, California Institute of Technology, W.M. Keck Laboratory, Pasadena, CA.

Martin, Y., and M. Church. 2000. "Re-examination of Bagnold's Empirical Bedload Formulae." *Earth Surface Processes and Landforms*, Vol. 25, No. 9, pp. 1011–1024, DOI: 10.1002/1096-9837(200008)25:9<1011::AID-ESP114>3.0.CO;2-H.

Wilcock, P.R., and S.T. Kenworthy. 2002. "A Two-Fraction Model for the Transport of Sand/Gravel Mixtures." *Water Resources Research*, Vol. 38, No. 10, pp. 12-1–12-12, DOI: 10.1029/2001WR000684.

Yang, C.T. 1996. *Sediment Transport: Theory and Practice*. McGraw-Hill, New York, NY, 396 p.

B.10 Abbreviations

Units of Measure

m	meter(s)
m/m	meter(s) per meter
mm	millimeter(s)
%	percent
yr(s)	year(s)

Acronyms

CSV	comma separated values
DEM	Digital Elevation Models
eRAMS	Environmental Risk Assessment & Management System
ESRI	Environmental Systems Research Institute

FDC   flow duration curve
GHCND   Global Historical Climatology Network – Daily
HRU   Hydrologic Response Unit
HUC   Hydrologic Unit Code
HydroDEM   hydrologically conditioned DEM
Hydro-NHD   Hydro National Hydrography Dataset
NASS   National Agricultural Statistics Service
NHDPlus   National Hydrography Dataset
NLCD   National Land Cover Database
NRCS   Natural Resources Conservation Service
SSURGO   Soil Survey Geographic Database
SWAT   Soil and Water Assessment Tool
SWAT-DEG   channel DEGradation portion of SWAT
U.S.   United States
USDA   U.S. Department of Agriculture
USGS   U.S. Geological Survey
WRAP   Watershed Rapid Assessment Program

Symbols

d_{16} 16th percentile diameter of the bed sediment [mm]
d_{50} median grain size of the bed material [mm]
d_{84} 84th percentile diameter of the bed sediment [mm]
n Manning's roughness coefficient
Q_{s50} half-yield discharge [m^3/s]

Reference Manual: CSR Tool

APPENDIX D CONTENTS

LIST OF FIGURES

LIST OF TABLES

This reference manual summarizes the theoretical background and methodology used to develop the CSR Stable Channel Design Tool (CSR Tool) based in Excel® Visual Basic for Applications (VBA). It provides background information, the theoretical basis of the tool's functionalities, the code structure methodology, and how the tool was tested for accuracy.

D.1 Analytical Channel Design using Sediment Continuity

The underlying methodology of the CSR Tool uses an analytical channel design procedure to produce stable channel configurations for a reach of interest. This is achieved by estimating sediment continuity within the reach by using empirically derived equations to estimate the sediment transport capacity or potential ability of the reach to transport sediment versus the incoming sediment load delivered from an upstream supply reach. Two approaches to analytical channel design were the main focus in the development of this tool: (1) the Copeland Method from the Stable Channel Design section of HEC-RAS (Copeland 1994), and (2) the CSR method presented by Soar and Thorne (2001). This tool was developed to provide a user friendly means to use the CSR method for stable channel design. The coding scheme for the tool follows the Copeland method as closely as possible in order to compare between the two approaches. The following sections will give an overview of these methods, the fundamental relationships and equations used, and how they apply to the development of the CSR Tool.

D.1.1 Basic Hydraulic Equations

The continuity equation for 1-D cross-section averaged, steady flow is used in the calculations as follows:

$$Q = VA \tag{D-1}$$

and the Manning's equation:

$$V = c\frac{R^{2/3}S_f^{1/2}}{n} \tag{D-2}$$

where:
Q = discharge [m³/s, ft³/s];
V = cross-section averaged velocity [m/s, ft/s];
A = cross-sectional area [m², ft²];
R = hydraulic radius [m, ft];
S_f = friction slope [m/m, ft/ft];
n = Manning's roughness coefficient; and
c = constant, conversion factor (1.0 for SI units and 1.486 for English units).

D.1.2 Copeland Method

The Copeland Method was developed by Dr. Ronald Copeland at the Waterways Experiment Station for use in the SAM software package (Copeland 1994). It is an analytical channel design approach that is based on the use of empirically derived equations. The method was developed solely to design sand-bed channels by estimating sediment continuity in a design reach using the total load sediment transport equation created by Brownlie (1981). For a given design discharge, the model solves for stable depth and

slope for a range of bottom widths for trapezoidal cross sections. The Brownlie (1981) relationship used to calculate transport concentration is as follows:

$$C_{ppm} = 9022 \left(\frac{V - V_c}{\sqrt{(G - 1)gD_{50}}} \right)^{1.978} S_f^{0.6601} \left(\frac{R}{D_{50}} \right)^{-0.3301}$$ **(D-3)**

where:
C_{ppm} = sediment transport concentration [ppm];
V = cross-section averaged velocity [m/s, ft/s];
V_c = critical velocity [m/s, ft/s];
G = specific gravity of sediment particles;
g = gravitational constant;
D_{50} = median grain size [m, ft];
S_f = friction slope [m/m, ft/ft]; and
R = hydraulic radius [m, ft].

This method calculates a critical velocity to determine how much sediment will be transported. If the cross-section averaged velocity, V is less than the critical velocity (V_c), then no sediment transport is assumed. The critical velocity is calculated by using the following equations:

$$V_c = 4.596 \, \tau_{*c}^{0.529} \, S_f^{-0.1405} \, \sigma_g^{-0.1606}$$ **(D-4a)**

$$\sigma_g = \sqrt{\frac{D_{84}}{D_{16}}}$$ **(D-4b)**

$$\tau_{*c} = 0.22Y + 0.06(10^{-7.7Y})$$ **(D-4c)**

$$Y = \left(\frac{\sqrt{(G - 1)gD_{50}^3}}{v} \right)^{-0.6}$$ **(D-4d)**

where:
τ_{*c} = dimensionless critical shear stress;
S_f = friction slope [m/m, ft/ft];
σ_g = gradation coefficient;
D_{84} = particle size for which 84% of all sediments is smaller [m, ft];
D_{16} = particle size for which 16% of all sediments is smaller [m, ft];
G = specific gravity of sediment particles;
g = gravitational constant; and
v = kinematic viscosity [m²/s, ft²/s].

The critical shear stress is calculated using regression equations of the original Shields diagram. Next, Brownlie developed the following depth predictor equations that take into account the effects of sand-bed forms for lower and upper regimes.

$$R_{bank} = 0.05761(G-1)^{0.9447} F_g^{1.889} S^{-0.7345} \sigma_g^{0.3034} (D_{50}) \tag{D-5a}$$

$$R_{bank} = 0.03478(G-1)^{0.8326} F_g^{1.665} S^{-0.7668} \sigma_g^{0.2136} (D_{50}) \tag{D-5b}$$

$$F_g = \frac{Q}{A\sqrt{(G-1)gD_{50}}} \tag{D-5c}$$

where:

R_{bank}	=	hydraulic radius of bank partition [m, ft];
G	=	specific gravity of sediment particles;
F_g	=	grain-related Froude number;
S	=	gradient [m/m, ft/ft];
σ_g	=	gradation coefficient;
D_{50}	=	median grain size [m, ft]);
Q	=	discharge [m³/s, ft³/s];
A	=	cross-sectional area [m², ft²];
G	=	specific gravity of sediment particles; and
g	=	gravitational constant.

These equations are used in conjunction with the previous equation to find the total estimated sediment transport for different design combinations. The lower and upper regime is determined by regression equations presented by (Brownlie 1981) of the relationship of grain Froude number versus slope. If the slope of the channel is greater than 0.006 then only upper regime is expected. When the slope is less than 0.006, the maximum velocity of the lower regime can be determined by solving for velocity from the following equation:

$$F_g = 1.25 F_g' \tag{D-6a}$$

with:

$$F_g' = 1.74 S^{1/3} \tag{D-6b}$$

The channel is partitioned into bed and bank components and sediment transport is assumed to occur only on the bed. The Einstein (1950) equation is utilized to partition the hydraulic parameters of the channel.

$$A = R_{bed}P_{bed} + R_{bank}P_{bank} \tag{D-7}$$

where:
A = cross-sectional area [m^2, ft^2];
R_{bed} = hydraulic radius of bed partition [m, ft];
P_{bed} = bottom width = wetted perimeter of bed partition [m, ft];
R_{bank} = hydraulic radius of bank partition [m, ft]; and
P_{bank} = wetted perimeter of bank partition [m, ft].

This method assumes that the average velocity for the bank and the bed partitions are both equal to the cross-section averaged velocity for the whole channel. Thus, the channel banks can be described by rearranging the Manning's equation as the following:

$$R_{bank} = \left(\frac{Vn_{bank}}{S^{1/2}}\right) \tag{D-8}$$

where:
R_{bank} = hydraulic radius of bank partition [m, ft];
V = cross-section averaged velocity [m/s, ft/s];
n_{bank} = Manning's roughness coefficient of bank partition; and
S = slope [m/m, ft/ft].

The Manning's n of the banks are required inputs, but the roughness of the bed partition is calculated within the program with the Brownlie (1983) roughness equations:

$$n = \left[1.6940\left(\frac{R}{D_{50}}\right)^{0.1374} S^{0.1112}\sigma^{0.1605}\right] 0.034(D_{50})^{0.167} \text{ (lower regime)} \tag{D-9a}$$

$$n = \left[1.0213\left(\frac{R}{D_{50}}\right)^{0.0662} S^{0.0395}\sigma^{0.1282}\right] 0.034(D_{50})^{0.167} \text{ (upper regime)} \tag{D-9b}$$

where:
n = Manning's roughness coefficient;
R = hydraulic radius [m, ft];
D_{50} = median grain size [m, ft]; and
S = slope [m/m, ft/ft].

In order to run the model, an incoming sediment load must be defined. There are two options to define the sediment supply in HEC-RAS. The user can simply enter an incoming sediment concentration, or the user can have the program estimate the concentration for them using a user-defined trapezoidal cross section that represents an upstream supply reach that will produce the incoming sediment load.

The user must then define the desired characteristics of the design reach and enter a single design discharge that will be used in the equations presented above. This discharge will be assumed to represent the most channel-forming flow that can be seen in the flow record for the channel. "To date, no generally accepted discharge for stable channel design is agreed upon, therefore, the use of a range of discharges is recommended" (Copeland 1994). The HEC-RAS reference manual further suggests the use of a 2-yr

frequency flood (perennial streams), 10-yr frequency flood (ephemeral streams), bankfull discharge, or effective discharge for the design discharge. The program can then solve for depth, slope, and width combinations that will successfully pass the incoming sediment load through the design channel based on its estimated sediment transport potential using Brownlie (1981). The results of the model produce a family of stable channel designs similar to Figure D-1.
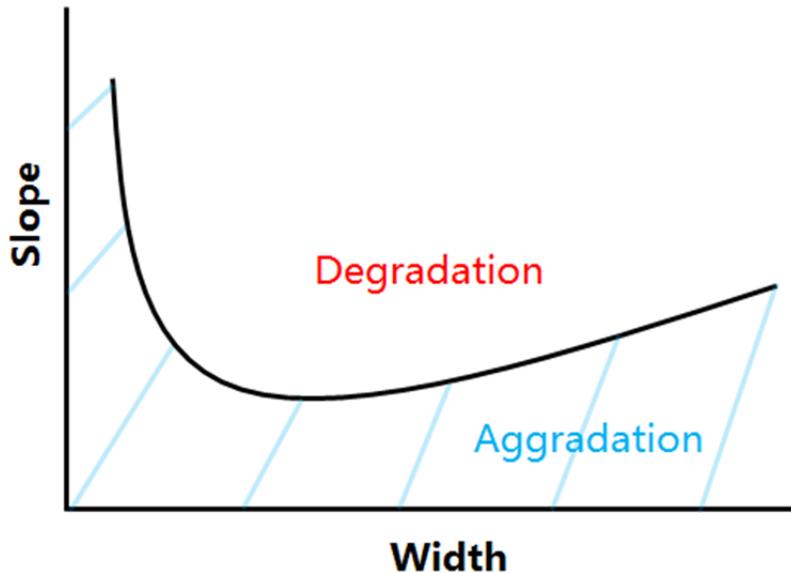
Figure D-1. Slope-width combinations that provide continuity of water and sediment based on the Copeland Method.

This curve represents the stable slope and width combinations that provide continuity of water and sediment for the design channel. If slope and width combinations for the design channel fall above this curve then one can expect degradation because the channel is estimated to have to a higher sediment transport capacity than supply. Alternatively, if the design falls below the curve, aggradation is expected since supply exceeds capacity.

D.1.3   CSR Method

The Capacity/Supply Ratio (CSR) concept was first introduced by (Soar and Thorne 2001). They used this concept to analyze the faults in a design that led to a failed river restoration project at White Marsh Run, Maryland. The CSR is a simple balance between the ability of a given river reach to transport sediment (capacity), to the sediment that is being transported into the reach of interest (supply). This is the same sediment balance concept as used in the Copeland Method; however, the difference comes from the discharge(s) the sediment transport capacity is calculated with. More specifically, the CSR can be described with the following equation:

$$CSR = \frac{\int_{time} transport\,capacity\,of\,Design\,Reach}{\int_{time} transport\,capacity\,of\,Supply\,Reach}$$

(D-10)

This equation describes the CSR as the time integrated ratio of sediment transport capacity of a design reach to the incoming sediment supply. In other words, "*The CSR is defined as the bed-material load transported through the river reach by a sequence of flows over an extended time period divided by the bed-material load transported into the reach by the same sequence of flows over the same time period*" (Wohl et al. 2015). Ultimately, the CSR method balances the total average sediment yield over the entire flow record rather than just for a single representative discharge as in the Copeland Method.

If the capacity of the reach to transport sediment exceeds the sediment entering the reach from upstream, then degradation or erosion can be expected in the reach with a CSR > 1. On the other hand, if the sediment entering the reach exceeds the capacity of the reach to transport it, then aggradation or sediment accumulation is expected with a CSR < 1. A CSR within 10% of unity will be the most likely to have sediment balance with minimal aggradation or degradation in the channel (Soar and Thorne 2001):

- CSR > 1 (degradation);
- CSR ≈ 1 (equilibrium); and
- CSR < 1 (aggradation).

D.1.4 Effectiveness Analysis

In order to find the time integrated sediment transport, a magnitude/frequency analysis (MFA) needs to be performed to find the total 'effectiveness' for each reach. In the context of this tool, the sequence of flows over an extended time period is derived from a user-defined flow record, or a flow duration curve (FDC) from another source for the river reach of interest. These flows are used to calculate the probability that a given flow will occur on average in the associated reach in a given day. Then, the potential that the given flow has to move sediment is estimated with an appropriate sediment transport equation. The effectiveness or the sediment transported on average over a period of time is calculated by multiplying the probability of the given flow by the potential sediment that can be transported by that flow. The effectiveness for each flow in the record is summed to get the total effectiveness or time integrated sediment transport capacity of the reach.

D.1.5 Hydrology

A more extensive hydrologic analysis is required by the CSR Tool in order to estimate the time integrated sediment transport capacity of the reaches over the entire FDC rather than a single discharge. The CSR Tool can use a flow gage record, or a pre-derived flow duration curve. These flow characteristics are assumed to be the same and representative of the flows seen by the supply and design reach.

If a gage record is chosen for the hydrology data, then the program will sort the discharges using an arithmetic binning procedure. This method splits the flows into a specified number of equal interval bins. A total number of bins must be defined by the user or the program defaults to 25 bins as recommended by Biedenharn et al. (2000). Each bin represents a range of discharges that the flows of the record could fall into. This is defined by the following equation:

$$Range\,Q = \frac{Max\,Q - Min\,Q}{\#\,of\,bins}$$

(D-11)

where:
$Range\,Q$ = range of discharge in flow record [m^3/s, ft^3/s];
$Max\,Q$ = maximum discharge in flow record [m^3/s, ft^3/s]; and
$Min\,Q$ = minimum discharge in flow record [m^3/s, ft^3/s].

The program then counts how many flows from the flow record falls into each range of discharges. The process starts at 25 arithmetic discharge bins and reduces the amount of bins until there are no bins with zero frequency. In cases where there is still zero frequency at 10 bins then the process starts again at 25 bins and combines the discharges above the zero frequency bin into one. The geometric mean of the range of discharges in each bin is calculated to be used later in the sediment transport estimations for that bin. The probability of occurrence for flows in each bin can be calculated by the simple equation also known as the relative frequency:

$$probability = \frac{frequency\ of\ flows\ in\ bin}{total\ \#\ of\ flows\ in\ record} \qquad \textbf{(D-12)}$$

Finally, this can be converted to a probability density for each bin by dividing by the discharge range of each bin:

$$probability\ density = \frac{frequency\ of\ flows\ in\ bin}{total\ \#\ of\ discharges\ in\ record * Range\ Q} \qquad \textbf{(D-13)}$$

The most common method to perform a MFA is using a flow record when possible, however, it is rare in practice to have a sufficiently long and representative flow record for a stable reach upstream of the design reach. There has been research that has developed ways to help this by extrapolating FDC's at un-gaged sites and factoring in effects such as land use into the FDC. So, to strengthen and broaden the applicability of this tool a feature was added to allow the user to enter their own FDC rather use a flow record. The program that was focused on for this feature, that is made to produce specialized FDC curves, is SWAT-DEG (channel DEGradation portion of SWAT) in eRams (environmental Risk Assessment & Management System). Instead of entering the flows for a gage record, the user simply enters the values of the FDC. For example, the SWAT-DEG program creates a very detailed FDC and outputs a table of exceedance probabilities versus discharges that can be directly pasted into the CSR Tool. This FDC is very detailed and often thousands of cells long so the user is required to define a lower number of bins to consolidate the FDC for use in sediment calculations. The default is set to 25 bins but the user can choose up to 50 bins. The user can then run the associated tab to consolidate the original FDC. The larger FDC is sampled logarithmically for the user-defined number of bins. To perform this sampling, the range of discharges for the FDC is converted to log space to find a logarithmic interval to sample the data:

$$Min\ Q_{log} = \frac{\log(Min\ Q)}{\log(10)} \qquad \textbf{(D-14a)}$$

$$Max\ Q_{log} = \frac{\log(Max\ Q)}{\log(10)} \qquad \textbf{(D-14b)}$$

$$sampling\ interval = \frac{Max\ Q_{log} - Min\ Q_{log}}{\#\ of\ bins} \qquad \textbf{(D-14c)}$$

This sampling interval is added to the minimum Q in log space for the given number of bins. These discharges are then converted back from log space to represent the new consolidated range of discharges. The match function of Excel® is then used to search for the exceedance probabilities that are associated with each sampled discharge. The exceedance probabilities of the new consolidated FDC are then converted to non-exceedance probabilities with:

$$\text{non-exceedance probability} = 1 - \text{exceedance probability} \qquad \textbf{(D-15)}$$

Finally, the non-exceedance probabilities and their associated discharges represent the cumulative distribution function (CDF). This CDF can be differentiated to find the associated probability density function (PDF). The differentiation or the slope of the CDF at each discharge point, can be approximated using the central difference method:

$$f'(\text{CDF}) = \frac{P_{<,i+1} - P_{<,i}}{Q_{i+1} - Q_{i+1}} \qquad \textbf{(D-16)}$$

where:
$P_{<,i}$ = non-exceedance probability of each bin.

This PDF can then be used in the sediment transport calculations for the tool.

D.1.6 Using the CSR/Effectiveness in the Context of the Tool

The CSR Stable Channel Design Tool requires the input of hydrology information and the dimensions and hydraulic characteristics of a supply reach to perform the CSR analysis. The information is used to perform a MFA for the supply reach to estimate the total effectiveness or sediment supply entering the design reach of interest downstream. The hydrologic information for the supply reach is assumed to be the same for the design reach, and the sediment transported by the supply reach is assumed to be the value that is entering the design reach. The program also requires dimensions and hydraulic characteristics for a potential design reach except a width and slope. Then, the program loops through width and slope combinations that produce an effectiveness that balances with the calculated incoming sediment from the supply reach giving a CSR = 1. This curve is analogous to the stable channel design curve produced by Copeland's method is HEC-RAS. The curve shown in (Figure D-2) represents a family of channel slope and width combinations with a CSR = 1. Any design with a slope/width above this line can expect degradation or erosion, while any below could expect aggradation or sediment accumulation.
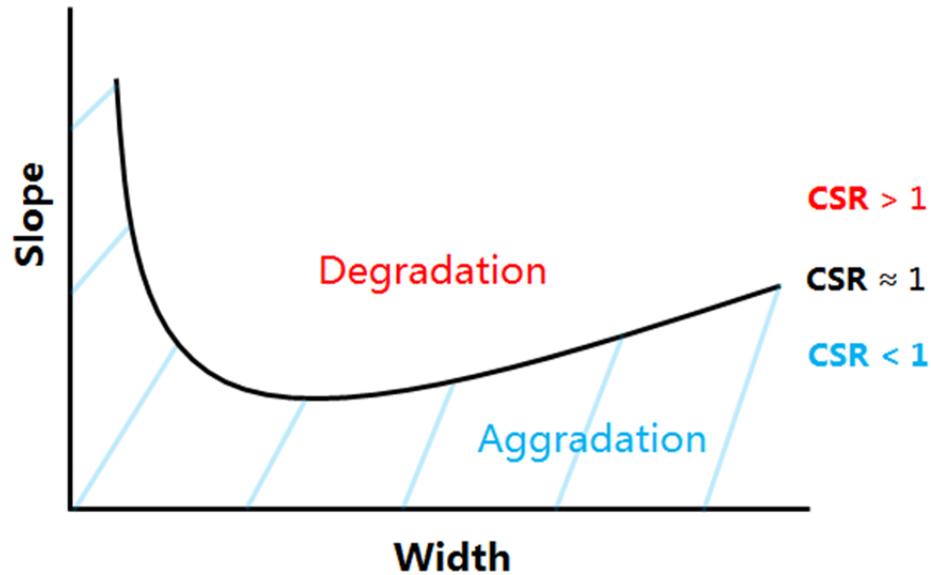
Figure D-2. Family of width and slope combinations which provide continuity of water and sediment.

Figure D-3 shows a visual representation of the methodology behind the tool using a CSR analysis. The figure shows a delineated upstream supply reach and downstream design reach. Each reach shows an idealized flow frequency/ probability distribution (A), an idealized sediment discharge curve (B), and the resulting product of (A) and (B) which gives the effectiveness curve (C). The area under the effectiveness curve represents the total sediment moved on average by each reach and is used to find the sediment balance of the design reach using the CSR. The curves are colored coded to correspond with the CSR equation shown at the top of Figure D-3.

$$\text{Capacity/Supply Ratio(CSR)} = \frac{\int_{time} \text{Sediment transport capacity of Design Reach}}{\int_{time} \text{Sediment transport capacity of Supply Reach}}$$
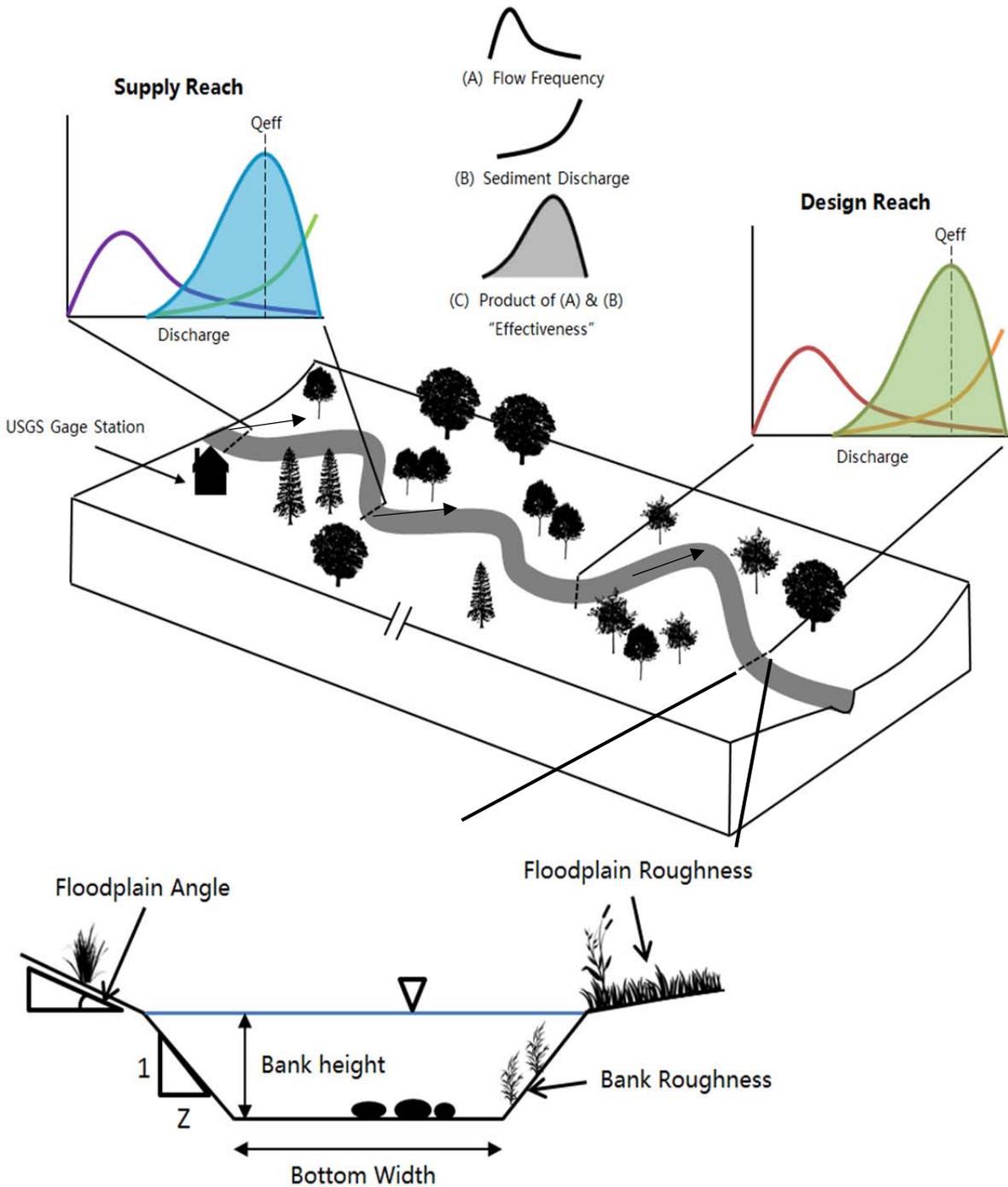
Figure D-3. Visual representation of CSR analysis in tool and simplified trapezoidal features.

D.1.7 Simplified Trapezoidal Channel

The tool uses a simplified trapezoidal channel to represent the supply reach and design reach as shown at the bottom of Figure D-3. All of the trapezoidal dimensions (bank height, bottom width, bank/floodplain angle) and roughness characteristics (bank/floodplain Manning's *n*) are required inputs for the supply reach of the tool. As opposed to the Copeland method in HEC-RAS, The CSR Tool models overbank flow thus requires inputs for floodplain angle and roughness. The bed Manning's *n* is calculated in conjunction with the sediment transport equations. The design reach requires the same inputs except bottom width and slope because these variables are varied by the program to find new channel dimensions that will produce a CSR = 1. The equations used to model the trapezoid channel are shown below:

$$A_{channel} = (b + zh)h \qquad \qquad \textbf{(D-17a)}$$

$$P_{Bank} = h(\sqrt{1 + z^2}) \qquad \qquad \textbf{(D-17b)}$$

$$P_{Bank} = b \qquad \qquad \textbf{(D-17c)}$$

$$R_{Bank} = h(\sqrt{1 + z^2}) \qquad \qquad \textbf{(D-17d)}$$

where:
$A_{channel}$ = cross-sectional area of channel [m^2, ft^2];
b = bottom width [m, ft];
z = bank angle, horizontal to vertical [H:V];
h = depth [m, ft];
P_{bank} = wetted perimeter of bank partition [m, ft]; and
R_{bank} = hydraulic radius of bank partition [m, ft].

D.1.8 Channel Partitioning

The in-channel partitioning approach for the CSR Tool follows the method used by Copeland in HEC-RAS, which breaks the channel into bed and bank components with separate roughness characteristics (Figure D-4a). The bank roughness is specified by the user and the bed roughness is calculated in conjunction with the sediment transport analysis. The Einstein (1950) equation is utilized to partition the components.

Unlike the Copeland method, the CSR Tool also models overbank flow. Once the flow in the channel breaks into overbank flow, the partition approach is altered because the Einstein (1950) method is no longer valid. In contrast to the in-channel method, the partitions are simply delineated by vertical lines as shown in Figure D-4b. The bed partition is centered over the bed, the bank components over both banks, and the floodplain components over each floodplain (Figure D-4):

(a)

1

Z

Bank Height

Bottom Width

Bed Partition

Bank Partition

(b)

1

Z

Bank Height

Bottom Width

Bed Partition

Bank Partition

Floodplain Partition
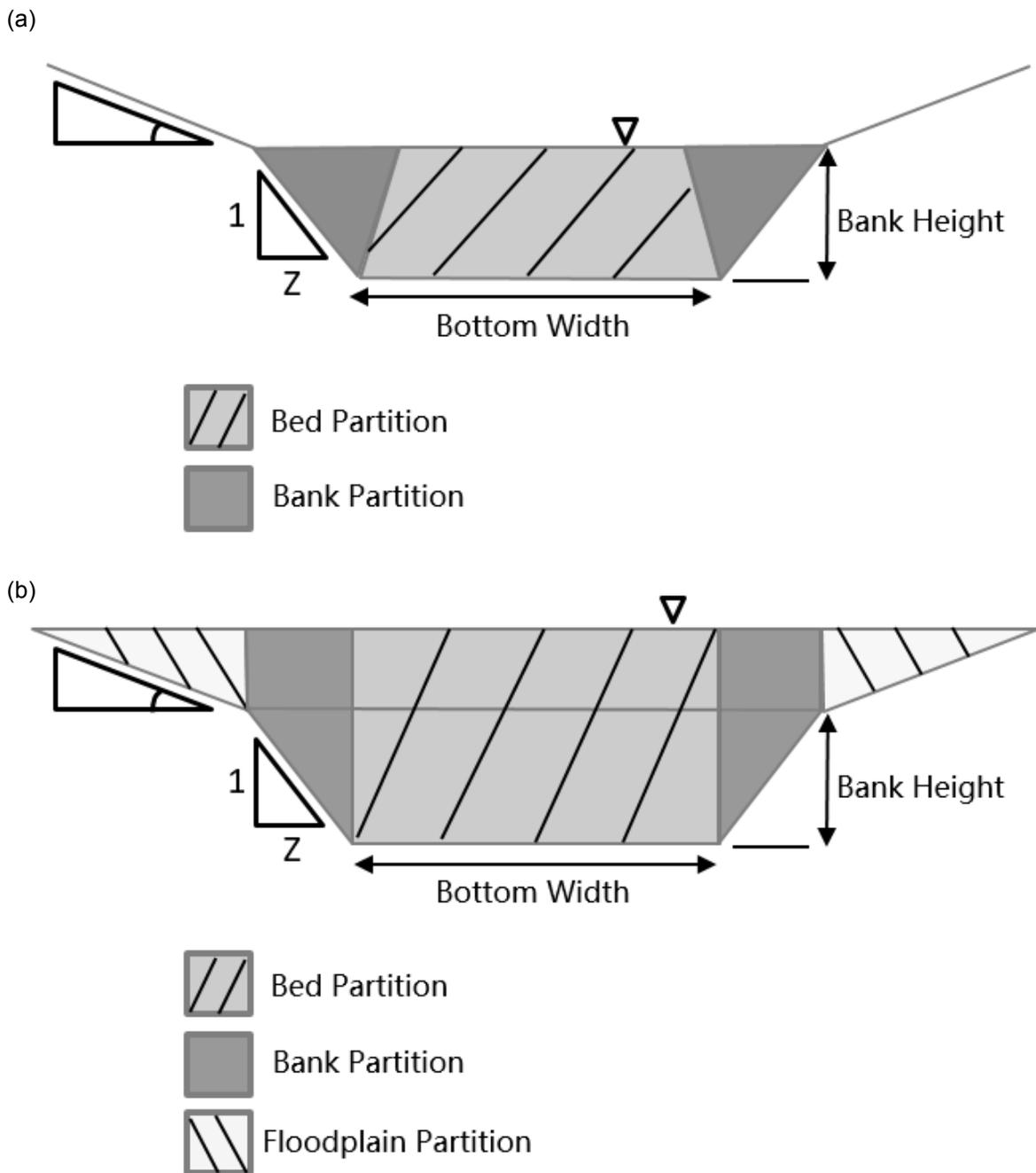
Figure D-4. Visual representation of channel partitioning methodology for the (a) in-channel flow partitioning approach and (b) overbank flow partitioning approach.

Instead, a conveyance method that is used by HEC-RAS (USACE) is utilized to help converge on a depth solution. The conveyance (K) of the floodplain partition is calculated with the following:

$$K_{OB} = \frac{1}{n_{floodplain}} A_{OB} R_{OB}^{2/3}$$

(D-18)

where:

K_{OB}	=	conveyance of bed partition;
$n_{floodplain}$	=	Manning's roughness of floodplain partition;
A_{OB}	=	area of floodplain partition [m^2, ft^2]; and
R_{OB}	=	hydraulic radius of floodplain partition [m, ft].

This variable is used in solving the system of equations to converge on a depth solution.

D.2 Gravel- / Cobble-Bed Analysis

The CSR Tool, as opposed to the Copeland method, can run the CSR analysis to find stable channel design solutions for both sand-bed *and* gravel- / cobble-bed streams.

The sand-bed portion of the tool uses the Brownlie (1981) total load sediment transport equation to estimate transport rate similar to the Copeland method in HEC-RAS except with the full CSR approach. Two bedload sediment transport equations, the Parker (1990) and Wilcock-Crowe (2003) equations are available to estimate sediment transport rates in gravel- / cobble-bed streams. Pre-existing code from Gary Parker was obtained for these equations and implemented/adapted for use in the tool. This includes the addition of an extra tab for the input and sorting of the grain size distribution for calculations. The Parker (1990) bedload equation is appropriate for use with rivers of gravel size (>2 mm diameter) and larger substrate. The Wilcock-Crowe (2003) bedload equation can be used with gravel- / cobble-bed streams that include a sand fraction (<2 mm diameter). Refer to the CSR Tool Guidance Document (Appendix B of this document) for further selection guidance on stream type.

The code methodology for the gravel- / cobble-bed portion was matched as closely as possible to the sand-bed structure. The biggest difference between the methodologies for the calculation of hydraulic parameters is with the hydraulic roughness. The sand-bed portion of the tool uses the Manning's equation and the roughness predictor with bedforms from (Brownlie 1983). It was chosen to use the Manning's and Limerinos (1970) equations to calculate the roughness in the channel for the gravel-bed portion of the tool. The Limerinos (1970) equation was calibrated to account for mostly grain roughness of larger particles from gravels to boulders:

$$n = \frac{(\beta)R^{1/6}}{1.16 + 2.0\log_{10}\left(\frac{R}{D_{84}}\right)} \tag{D-19}$$

where:

n	=	Manning's roughness coefficient;
β	=	conversion factor (0.1129 for SI units and 0.0926 for English units);
R	=	hydraulic radius (m, ft); and
D_{84}	=	particle size for which 84% of all sediments is smaller (m, ft).

D.2.1 Grain Size Distribution Calculations

To run the CSR analysis for a gravel- / cobble-bed stream the user is required to enter a grain size distribution as the percent finer (%) versus grain size class (mm). The grain size classes are defined by the following for N grain size ranges from $i = 1$ to $N + 1$:

$$(D_{b,i} * D_{b,i+1}) \tag{D-20}$$

The characteristic grain size (D_i) and fraction of the surface layer (F_i) is then:

$$D_i = \sqrt{D_{b,i}(D_{b,i+1})} \qquad \textbf{(D-21a)}$$

$$F_i = \frac{F_{f,i} - F_{f,i+1}}{100} \qquad \textbf{(D-21b)}$$

where:
$D_{b,i}$ = grain size representing each size class of the (active) layer of the bed [m, ft].

Each grain size on the base-2 logarithmic ψ scale is computed by the following:

$$\psi_i = \ln(D_i) = \frac{\log_{10}(D_i)}{\log_{10}(2)} \qquad \textbf{(D-22)}$$

where:
Ψ_i = each grain size on the base 2 logarithmic ψ scale; and
D_i = characteristic grain size for each size class [m, ft].

Then the geometric mean grain size (D_{sg}) can be calculated with:

$$D_{sg} = 2^{\overline{\psi_s}} \qquad \textbf{(D-23a)}$$

$$\overline{\psi_s} = \sum_{i=1}^{N} \psi_i F_i \qquad \textbf{(D-23b)}$$

where:
N = grain size ranges from i = 1 to N + 1;
Ψ_i = each grain size on the base 2 logarithmic ψ scale; and
F_i = fraction of grain size in surface layer.

The geometric and arithmetic standard deviations σ_{sg} and σ_s, respectively:

$$\sigma_{sg} = 2^{\sigma} \qquad \textbf{(D-24a)}$$

$$\sigma_s^2 = \sum_{i=1}^{N} (\psi_i - \overline{\psi_s})^2 F_i \qquad \textbf{(D-24b)}$$

where:

σ_{sg} = geometric standard deviation;
σ_s = arithmetic standard deviation;
N = grain size ranges from $i = 1$ to $N + 1$;
Ψ_i = each grain size on the base 2 logarithmic ψ scale; and
F_i = fraction of grain size in surface layer.

D.2.2 Bedload Sediment Transport Relationships

The gravel- / cobble-bed portion of the tool has two options for running the CSR analysis. The user can choose the Parker (1990) or Wilcock-Crowe (2003) bedload equation. Both of these equations estimate the total bedload transport rate per unit width. This amount is then converted into an effectiveness for each discharge. The Parker (1990) bedload transport relation can be expressed as the following:

$$W_i^* = 0.00218 \mathrm{G}(\phi_i) = \frac{Rgq_{bi}}{F_i u_*^3} \tag{D-25}$$

where:

$$\phi_i = \omega \phi_{sgo} \left(\frac{D_i}{D_{sg}} \right)^{-0.0951}$$

$$\phi_{sgo} = \frac{\tau_{sg}^*}{\tau_{ssrg}^*}$$

$$\tau_{sg}^* = \frac{u_*^2}{RgD_{sg}}$$

$$\tau_{ssrg}^* = 0.0386$$

$$G(\phi) = \begin{cases} 5474 \left(1 - \frac{0.853}{\phi}\right)^{4.5} & \text{for } \phi > 1.59 \\ \exp\left[14.2(\phi - 1) - 9.28(\phi - 1)^2\right] & \text{for } 1 \leq \phi \leq 1.59 \\ \phi^{14.2} & \text{for } \phi < 1 \end{cases}$$

$$\omega = 1 + \frac{\sigma_s}{\sigma_{O(\phi_{sgo})}} \left[\omega_O \left(\phi_{sgo} \right) - 1 \right]$$

where:

G = specific gravity of sediment particles;

R = $(\rho_s / \rho) - 1$ = submerged specific density of sediment; where ρ_s = density of sediment [kg/m^3];

g = gravitational constant;

q_{bi} = volume gravel bedload transport per unit width of grains in the ith size range [m^2/s, ft^2/s];

F_i = fraction of grain size in surface layer;

u_* = $\sqrt{\dfrac{\tau_b}{\rho}}$ = shear velocity on the bed [m/s]; where τ_b = boundary shear stress on the bed [Pa], and ρ
    = density of water [kg/m^3];

ω = strain function for the Parker (1990) bedload equation

D_i = characteristic grain size for each size class [m, ft];

D_{sg} = geometric mean grain size [m, ft];

τ^*_{sg} = Shields' stress;

τ^*_{ssrg} = reference Shields' stress; and

σ_s = arithmetic standard deviation.

The functions $\sigma_O(\phi_{sgo})$ and $\omega_O(\phi_{sgo})$ are found from a lookup table representing the strain functions (Figure D-5).
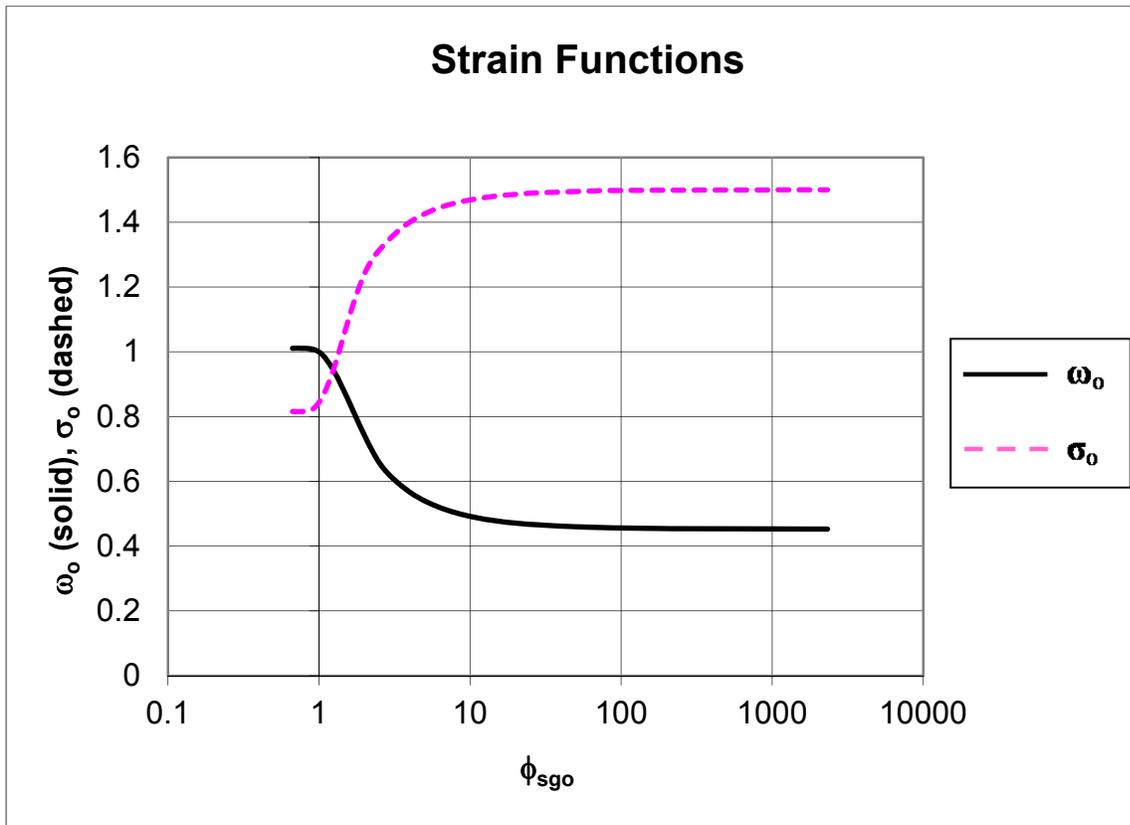
Figure D-5. Strain functions for the Parker (1990) gravel bedload transport relation.

Finally, the total volume bedload transport rate per unit width (q_{bT}) is calculated with:

$$q_{bT} = \sum_{i=1}^{N} q_{bi} \qquad \textbf{(D-26)}$$

where:

q_{bT} = total volume gravel bedload transport rate per unit width over all sizes [m²/s, ft²/s];
N = grain size ranges from $i = 1$ to $N + 1$; and
q_{bi} = volume gravel bedload transport per unit width of grains in the ith size range [m²/s, ft²/s].

The Wilcock-Crowe (2003) bedload transport equation is similar to the Parker (1990) equation except it adds the effects of the sand fraction in the mixture on the estimated transport rate. This equation can be expressed as the following:

$$W_i^* = G(\phi_i) = \frac{Rgq_{bi}}{F_i u_*^3} \qquad \textbf{(D-27)}$$

where:

$$\phi_i = \phi_{sgo} \left(\frac{D_i}{D_{sg}} \right)^{-b}$$

$$\phi_{sgo} = \frac{\tau_{sg}^*}{\tau_{ssrg}^*}$$

$$\tau_{sg}^* = \frac{u_*^2}{RgD_{sg}}$$

$$\tau_{ssrg}^* = 0.021 + 0.015 \exp(-20F_s)$$

$$b = \frac{0.67}{1 + \exp\left(1.5 - \frac{D_i}{D_{sg}}\right)}$$

and

$$G(\phi) = \begin{cases} 0.002\phi^{7.5} & \text{for } \phi < 1.35 \\ 14\left(1 - \frac{0.894}{\phi^{0.5}}\right)^{4.5} & \text{for } \phi \geq 1.35 \end{cases}$$

where:

G = specific gravity of sediment particles;

R = $(\rho_s / \rho) - 1$ = submerged specific density of sediment; where ρ_s = density of sediment [kg/m³];

g = gravitational constant;

q_{bi} = volume gravel bedload transport per unit width of grains in the ith size range [m²/s, ft²/s];

F_i = fraction of grain size in surface layer;

u_* = $\sqrt{\dfrac{\tau_b}{\rho}}$ = shear velocity on the bed [m/s]; where τ_b = boundary shear stress on the bed [Pa], and ρ = density of water [kg/m³];

D_i = characteristic grain size for each size class [m, ft];

D_{sg} = geometric mean grain size [m, ft];

τ_{sg}^* = Shields' stress;

τ_{ssrg}^* = reference Shields' stress; and

F_s = fraction of sand on the bed surface.

Finally, just as for the Parker (1990), the total volume bedload transport rate per unit width q_{bT} is calculated with:

$$q_{bT} = \sum_{i=1}^{N} q_{bi} \qquad\qquad \textbf{(D-28)}$$

where:

q_{bT} = total volume gravel bedload transport rate per unit width over all sizes [m²/s, ft²/s];

N = grain size ranges from $i = 1$ to $N + 1$; and

q_{bi} = volume gravel bedload transport per unit width of grains in the ith size range [m²/s, ft²/s].

This amount is converted into a total transport load by multiplying by the bottom width (transport assumed to only occur on the bed) and the density of the sediment.

D.3   Sediment Transport Equation Selection

Table D-1 summarizes the grain size class delineations of sediment, and Table D-2 lists the boundaries published by the authors, of the associated sediment transport equations, for the development of the relationships. These tables can be referenced to help select the proper 'Stream Type' and 'Transport Relationship' for the CSR Tool analysis. This can also give insight to when these sediment transport equations are more or less appropriate for the analysis of interest. For further guidance on the selection of 'Stream Type' and 'Transport Relationship' for the tool see the CSR Tool Guidance Document (Appendix B of this document).

Table D-1. Grain size class delineations sediment transport equations.

	Class Name	Particle Diameter [mm]	Particle Diameter [ft]
Boulder	Very Large	>2,048	>6.719
	Large	>1,024	>3.360
	Medium	>512	>1.680
	Small	>256	>0.840
Cobble	Large	>128	>0.420
	Small	>64	>0.210
Gravel	Very Coarse	>32	>0.105
	Coarse	>16	>0.0525
	Medium	>8	>0.0262
	Fine	>4	>0.0131
	Very Fine	>2	>0.0066
Sand	Very Coarse	>1	>0.0033
	Coarse	>0.5	>0.0016
	Medium	>0.25	>0.00082
	Fine	>0.125	>0.00041
	Very Fine	>0.0625	>0.00021
Silt	Coarse	>0.031	>0.00010
	Medium	>0.016	>5.25E-05
	Fine	>0.008	>2.62E-05
	Very Fine	>0.004	>1.31E-05
Clay	Coarse	>0.002	>6.56E-06
	Medium	>0.001	>3.28E-06
	Fine	>0.0005	>1.64E-06
	Very Fine	>0.00024	>7.87E-07

Table D-2. Boundaries of sediment transport equations used in tool.

	Variable	Minimum	Maximum
Brownlie (1981)	D_{50}, mm (ft)	0.088 (0.0029)	2.8 (0.0092)
	Unit discharge, m^3/s/m (ft^2/s/ft)	0.012 (0.129)	40 (430)
	Discharge, m^3/s (ft^3/s)	0.0032 (0.113)	22,000 (776,900)
	Slope	0.000003	0.037
	Hydraulic radius, m (ft)	0.025 (0.082)	17 (56)
	Temperature, °C (°F)	0 (32)	63 (145)
	Width/depth ratio		≥ 4
	Geometric standard deviation of particles sizes, σ_g		≤ 5
Parker (1990)	Gravel-sized particles, mm (ft)	2 (0.0066)	203 (0.666)
	Sand-sized particles, mm (ft)	sand removed	
	(%) of sand in mixture	3.3% surface	13% subsurface
Wilcock-Crowe (2003)	Gravel-sized particles, mm (ft)	2 (0.0066)	64 (0.210)
	Sand-sized particles, mm (ft)	0.5 (0.0016)	2 (0.0066)
	(%) of sand in mixture	6.2	34.3
	Depth, m (ft)	0.09 (0.295)	0.12 (0.394)

D.4   CSR Analysis Code Structure

The main routine performed by the CSR Tool is running the design reach to perform the CSR analysis and search for stable channel designs. This part of the tool is run after the incoming sediment load is calculated for the supply reach using the given hydrologic information. The CSR Tool code structure went through many iterations to find the most reliable and efficient configuration. The final code methodology for calculating stable channel design solutions is outlined in Figure D-6.
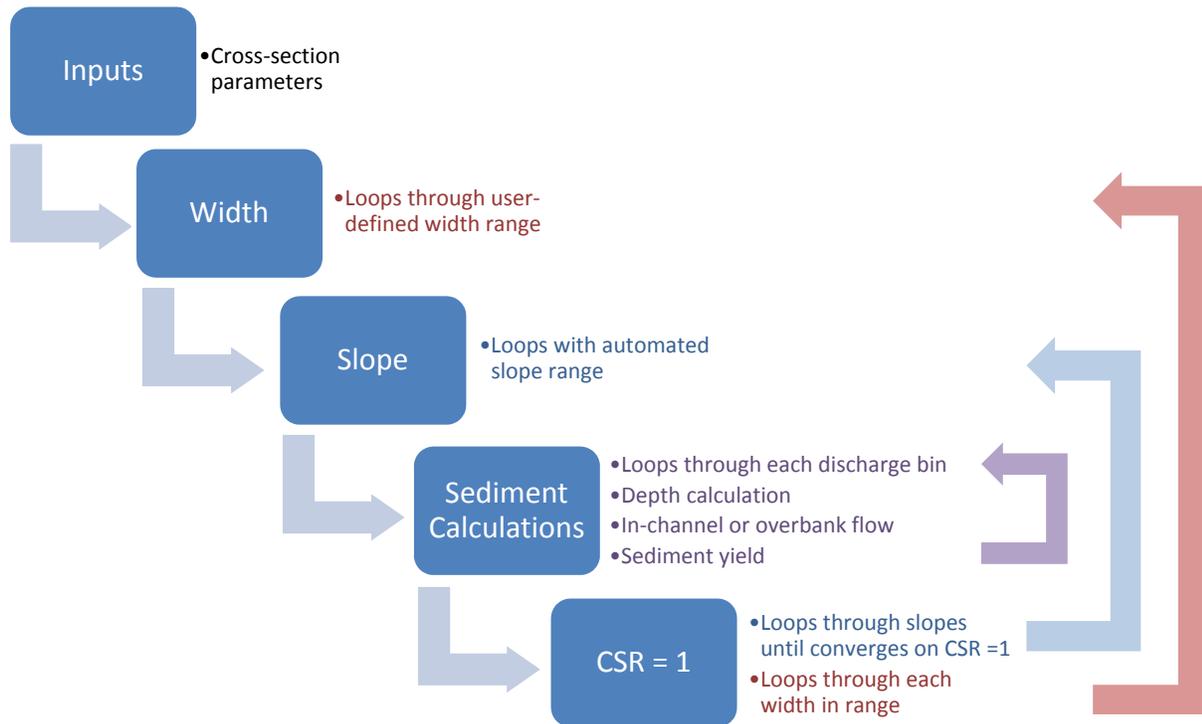
Figure D-6. Schematic of design reach code methodology.

Firstly, the program reads the cross-sectional information entered by the user. Screenshots of the required inputs for the supply and design reaches are shown in (Figure D-7). Next, an outer loop initiates that goes through each width in the user-defined range. The loop proceeds for every other meter in the width range (i.e., 1, 3, 5, 7 m, etc.) if the supply reach bottom width is above 15 m and every meter (i.e., 1, 2, 3, 4 m, etc.) if the supply reach bottom width is below 15 m. This was chosen to be the most efficient set up while still retaining enough resolution of the outputs. The default for the minimum width in the range is 1 m to produce all possible results and the entire family of stable channel design solutions curve. The program guesses an initial slope and calculates the depth, in channel or overbank flow, and upper and lower regime to calculate sediment yield for each average discharge in the binned FDC. The sediment yield summed over all discharges is compared with the supply reach total sediment yield to calculate the CSR for that slope estimate. The slope is then updated using a bisection method until it converges on the slope that will give a CSR = 1 within a tolerance of 0.025 for each width in the defined range.

Design Reach:

Supply Reach:

Inputs For Supply Reach		
Main Channel		
Bottom Width	*	m
Bank Height	*	m
Bank Angle	*	H:V
Slope	*	m/m
Right Bank (n)	*	
Left Bank (n)	*	
Grain Size		
D16	*	mm
D50	*	mm
D84	*	mm
Floodplain		
Floodplain Angle	*	H:V
Floodplain (n)	*	

Run Supply Reach

Tab Guidance

Required Inputs
(-) *Auto-updated values*

Inputs for Design Reach		
Main Channel		
Bank Height	*	m
Bank Angle	*	H:V
Right Bank (n)	*	
Left Bank (n)	*	
Grain Size		
D16	-	mm
D50	-	mm
D84	-	mm
Floodplain		
Floodplain Angle	*	H:V
Floodplain (n)	*	
Planform/ Valley (Optional)		
Valley Slope, Sv	*	m/m
Max Meander Beltwidth	*	m
Beltwidth Buffer	*	m
Program Constraints		
Min Bottom Width	1	m (default)
Max Bottom Width	*	m

Run CSR Tool

Tab Guidance

Required Inputs
Optional Inputs
(-) *Auto-updated values*

Figure D-7. Required inputs for the Supply Reach and the Design Reach of the Stable Channel Design tool.

D.5   CSR Tool Validation

When the CSR tool is given a single discharge rather than a full FDC, its results can be directly compared to the implementation of the Copeland method in the HEC-RAS stable channel design tool. Many examples have shown very similar results between HEC-RAS output and single-discharge calculations from the CSR Tool, which fosters confidence in the validity of the tool's output. Figure D-8 is an example of the CSR Tool's output with a single discharge for Big Raccoon Creek in Indiana compared to HEC-RAS's stable channel design using the Copeland method.
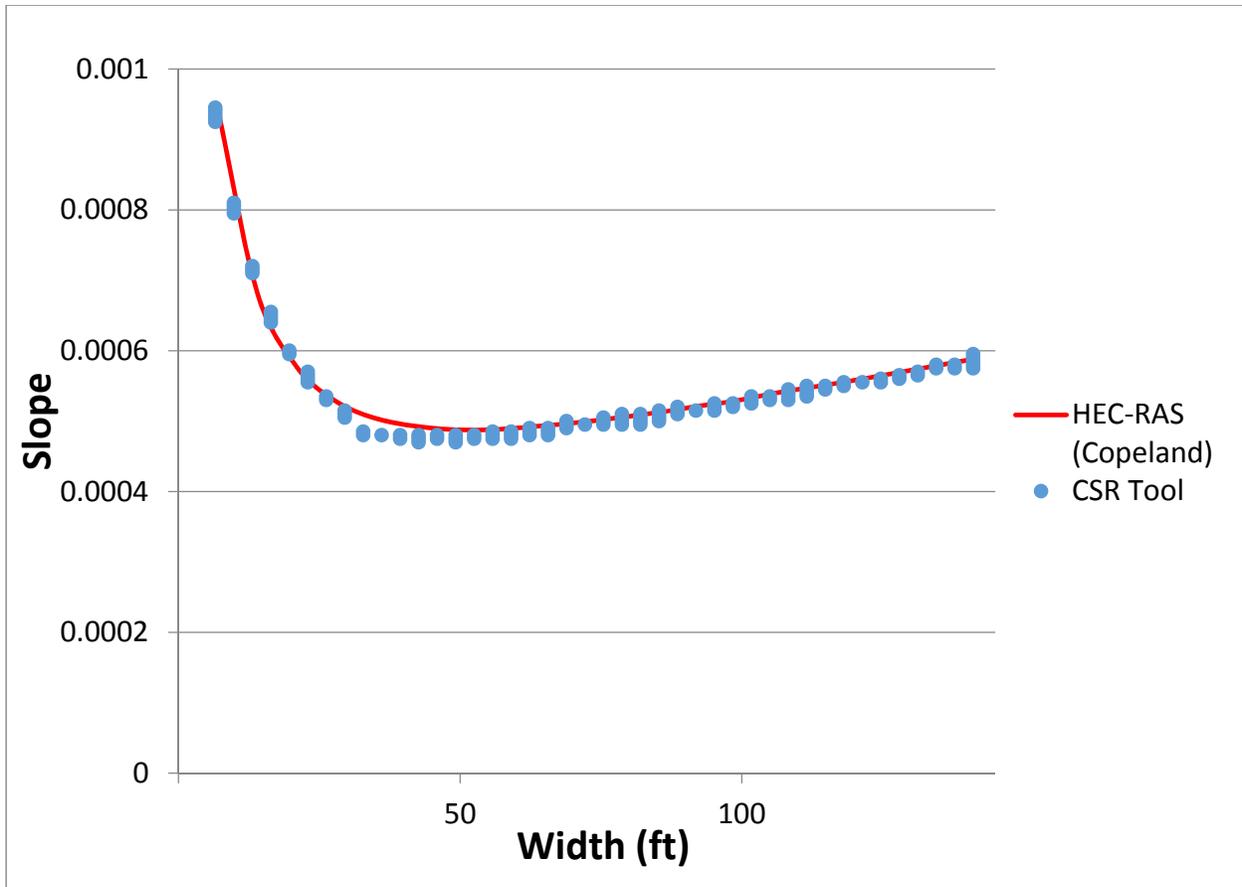
Figure D-8. Comparison of CSR Tool with HEC-RAS stable channel design using the Copeland method with the same channel dimensions, grain size distribution and single discharge.

The CSR Tool estimated a total sediment concentration of 279 ppm at 1,246 cfs and HEC-RAS estimated a total sediment concentration of 286 ppm at 1,246 cfs. The data for this example were taken from Soar and Thorne (2001).

D.6 Planform Characteristics

An optional addition to the tool is to include planform characteristics to the design reach output. If a valley slope is entered then the sinuosity, meander belt width, and braiding risk can be calculated for each slope/width solution. The following simple equation is used to calculate the sinuosity for each slope/width combination:

$$\text{sinuosity} = P = \frac{\text{valley slope}}{\text{bed slope}} = \frac{S_v}{S_o} \qquad \textbf{(D-29)}$$

This is an estimate but gives a good indication of what a single-thread channel of the corresponding dimensions would tend toward for meandering. This result can then be used to find the meander belt width and wavelength based off an idealized sine-generated curve, shown in Figure D-9. The sinuosity

output could also give indication on the limits a design can have to allow for sediment continuity but also have enough sinuosity for aesthetic appeal that may be desired in a restoration project. The wavelength can be estimated by the following equation. The meander wavelength range represents the 95% confidence interval derived from a data set for 438 streams ranging from nearly straight to tortuous meanders (Soar and Thorne 2001):

$$\text{meander wavelength} = \lambda \approx (11.26 \text{ to } 12.47) * \text{width} \approx 12(W) \qquad \textbf{(D-30)}$$

The minimum meander belt width produced by the corresponding sinuosity and channel width can be estimated with the following (Hagerman and Williams 2000):

$$\text{minimum belt width} = \lambda(6.0625\varphi^3 - 5.1279\varphi^2 + 2.509\varphi + 0.0005) + \text{width} + \text{buffer} \textbf{ (D-31a)}$$

with:

$$\varphi = \frac{P-1}{P} \qquad \textbf{(D-31b)}$$
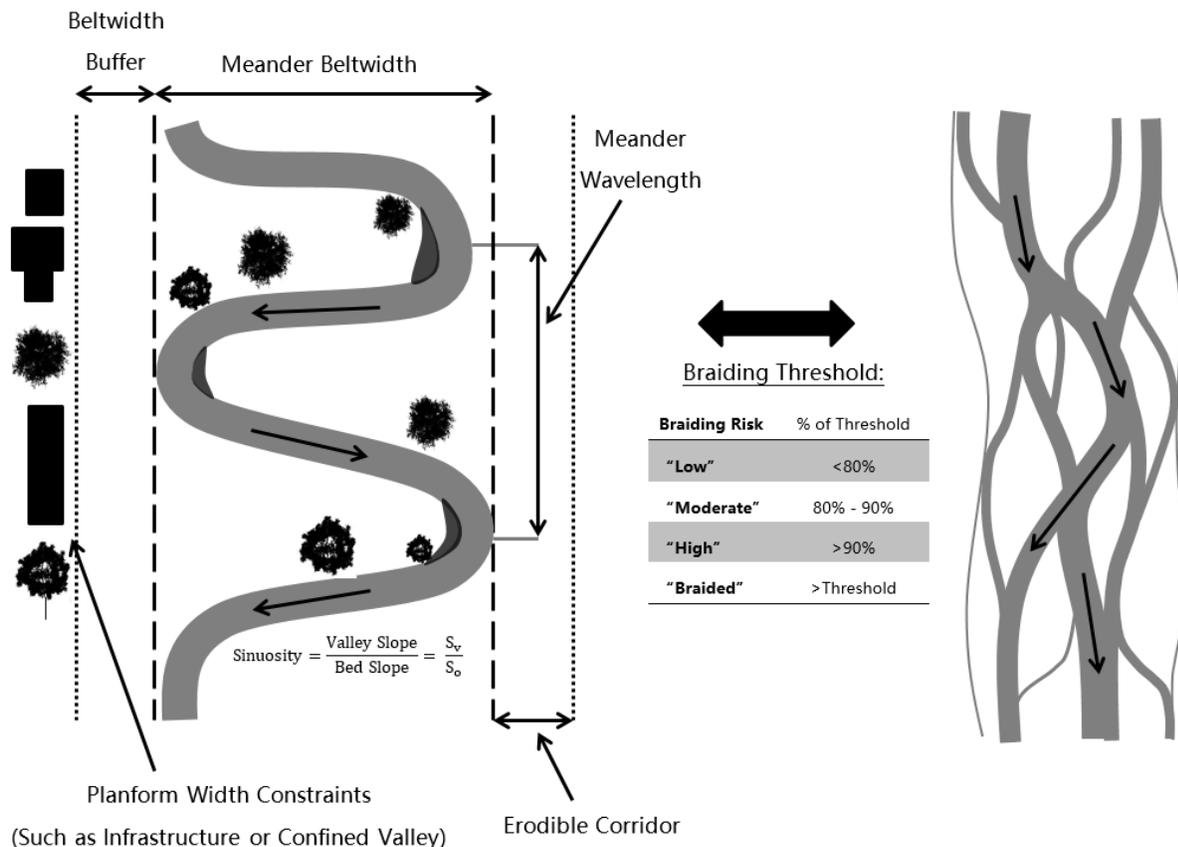
Figure D-9. Visual representation of the planform characteristics included in the tool.

The meander belt width is an estimation of the total planform width the river will span to support the projected dimensions and sinuosity of the design (Hagerman and Williams 2000). This can be useful for visualizing the size of the design and determining whether planform width constraints exist in the design area (Figure D-9). Following this concept, the tool allows the user to specify a maximum allowable meander belt width between the edge of the river and any planform constraint such as infrastructure. If any solution is over this amount then it will be highlighted in red in the outputs, so the user can know which solutions might conflict with this lateral restriction. Additionally, has the equation above suggests, the tool allows the user to enter a buffer to be included in the belt width calculations. The buffer will be added to the calculated belt width and considered in the maximum belt width determination. This buffer aligns with the "room for the river" or "erodible corridor" concept that sets aside extra space around the river to allow for natural movement and adjustments of the channel without compromising the surrounding infrastructure (Piégay et al. 2005; Kondolf 2011).

Lastly, the valley slope can be used to estimate the braiding risk for the channel with the addition of a bankfull discharge (Q_{bf}) and a median grain size (D_{50}) of the design reach. The tool automatically extracts these values to calculate a risk for the design single thread channel to cross the geomorphic threshold to a braided or multi-thread channel, shown in Figure D-9. This is an important consideration in design because channels near the threshold and braided channels are characteristically unstable (Schumm 1977; Bledsoe and Watson 2001). The tool uses the channel braiding relationships developed in van den Berg (1995). Van den Berg analyzed 228 data sets from 192 rivers for their relationships between channel type, channel pattern, and graphed them based on D_{50} grain size and ω unit stream power (Figure D-10).
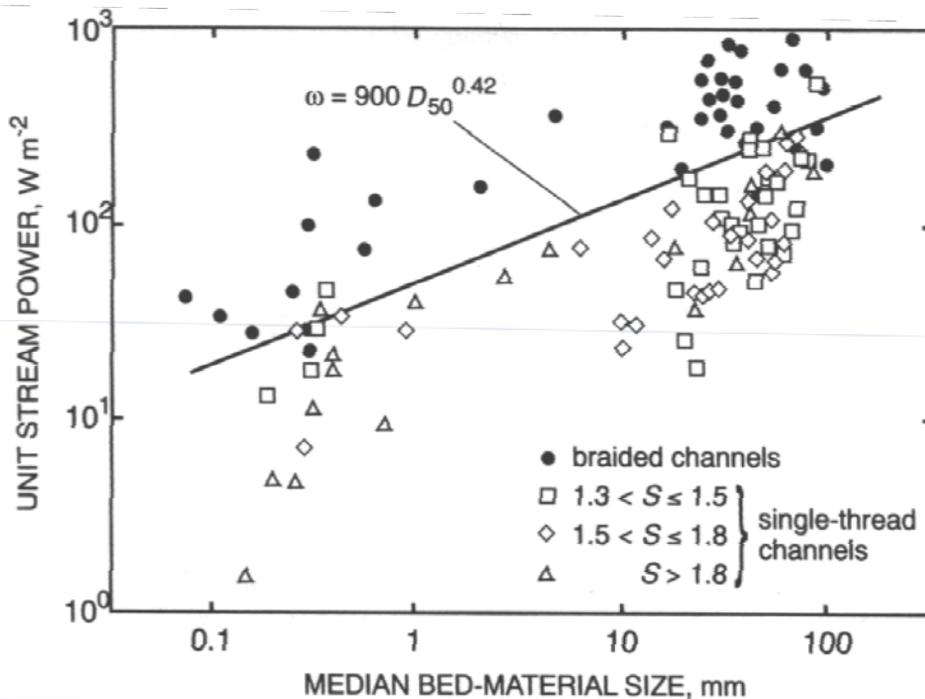
Figure D-10. Braiding threshold on plot of channel pattern in relation to median grain size and potential specific stream power (van den Berg 1995).

Potential specific stream power is calculated with the given reach characteristics with the following equations:

$$\omega_v = 2100\, S_v \sqrt{Q_{bf}} \quad \text{(sand channels)} \qquad \textbf{(D-32a)}$$

$$\omega_v = 3300\, S_v \sqrt{Q_{bf}} \quad \text{(gravel channels)} \qquad \textbf{(D-32b)}$$

where:
ω_v = potential specific stream power [W/m^2];
S_v = valley slope [m/m, ft/ft]; and
Q_{bf} = bankfull discharge [m^3/s];

These values are then compared to the value calculated using the following equation representing the threshold in Figure D-10:

$$\omega = 900\, D_{50}^{0.42} \qquad \textbf{(D-33)}$$

where:
D_{50} = median grain size [m].

The risk for braiding is then denoted by the following categories listed in Table D-3.

Table D-3. The categories for braiding risk in terms of percent from van den Berg (1995) braiding threshold.

Braiding Risk	% of Threshold
"Low"	<80%
"Moderate"	80 – 90%
"High"	>90%
"Braided"	>Threshold

D.7   Sediment Yield Percentiles

Additional outputs of sediment yield percentiles are included on the "Detailed Results" tab of the CSR Tool. These percentiles are defined as follows:
- Q_{s50} = discharge associated with 50% of the cumulative sediment yield;
- Q_{s75} = discharge associated with 75% of the cumulative sediment yield;
- Q_{s90} = discharge associated with 90% of the cumulative sediment yield; and
- Q_{eff} = single discharge that moves the most total sediment load.

These percentiles are calculated for the supply reach and each stable slope and width combination for the design reach. An example output of these variables from the tool can be seen in Figure D-12.

D.8 Key Differences between CSR and Copeland Stable Channel Design Tools

The CSR Tool is very similar to the Copeland method in HEC-RAS (Copeland 1994), although there are some key differences:

- Sediment transport is calculated using the entire FDC associated with the design reach rather than just a single representative discharge and, therefore, accounts for the morphological influence of the other flows.
- Overbank flow is modeled and considered in transport calculations unlike the Copeland method. This can help avoid overestimating the effectiveness of overbank flows.
- The tool is capable of performing the CSR analysis for not only sand-bed streams but also gravel-/ cobble-bed streams using the Wilcock-Crowe (2003) and Parker (1990) equations.
- Additional planform outputs and sediment percentiles are listed for each stable solution.

D.9 CSR Tool Outputs

The following shows examples of the output solutions produced by the CSR Tool for a sand-bed stream (Figure D-11) and a gravel-bed stream (Figure D-13). Figure D-11a shows the plot of the family of channel slope and width combinations which provide continuity of water and sediment (i.e., CSR = 1) for the associated design. Figure D-11b shows the associated table of solutions with the planform characteristics listed for each design. These outputs are shown on the 'Results' tab of the CSR Tool. This example was developed using data retrieved from Soar and Thorne (2001) for a reach on Big Raccoon Creek in Indiana.

Figure D-12 shows an example output from the 'Detailed Results' tab of the CSR Tool. This is a summary of the 'effectiveness' in tons/day for each average bin discharge for the supply reach. Below the 'effectiveness' table shows the associated sediment percentiles summary (see Sediment Yield Percentiles). The 'Detailed Results' tab of the CSR Tool also displays this same output for each stable slope and width combinations as well.

Figure D-13a shows the plot of the family of channel slope and width combinations which provide continuity of water and sediment (i.e., CSR = 1) for the associated design. Figure D-13b shows the associated table of solutions with the planform characteristics listed for each design. This example was developed using data retrieved from (King et al. 2004) for a reach on the Red River in Idaho.

(a)
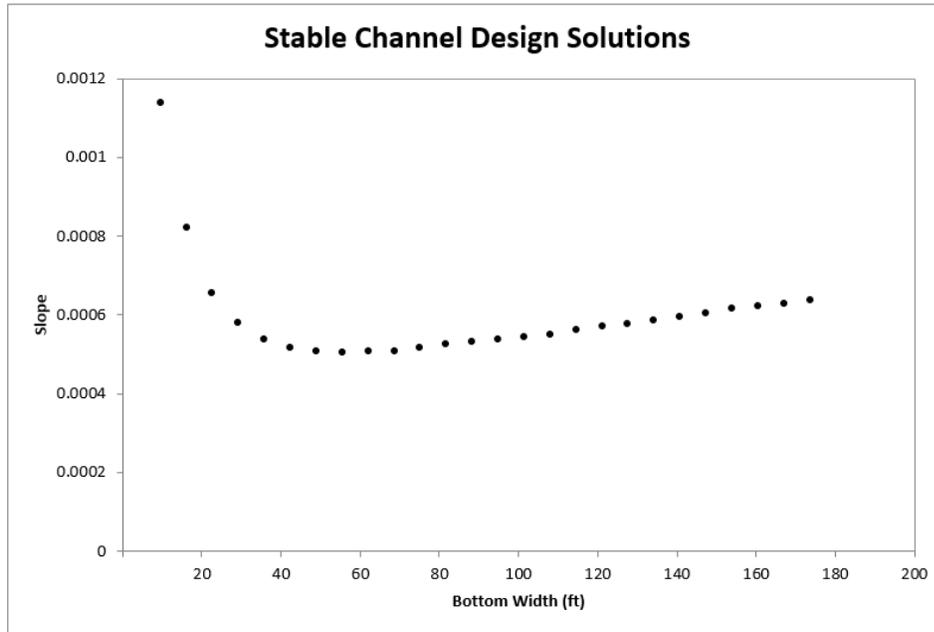
Stable Channel Design Solutions

(b)

Stable Geometries				Planform Characteristics					
Width (ft)	Width (m)	Slope	CSR	w/h Ratio	Sinuosity	Braiding Risk	Belt Width(ft)	Min Wavelength(ft)	Max Wavelength(ft)
10	3	0.00114	1.000	1	< 1	Low	-	33	36
16	5	0.00082	1.001	2	< 1	Low	-	55	61
23	7	0.00066	0.999	3	< 1	Low	-	78	86
29	9	0.00058	1.000	3	1.12	Low	79	100	111
36	11	0.00054	0.998	4	1.20	Low	106	123	136
42	13	0.00052	0.999	5	1.25	Low	126	145	161
49	15	0.00051	1.001	6	1.27	Low	140	168	186
55	17	0.00051	1.001	6	1.28	Low	152	190	211
62	19	0.00051	1.000	7	1.28	Low	162	213	236
69	21	0.00051	0.999	8	1.27	Low	172	235	261
75	23	0.00052	1.002	9	1.25	Low	178	258	286
82	25	0.00052	1.002	10	1.24	Low	183	281	311
88	27	0.00053	0.999	10	1.22	Low	188	303	336
95	29	0.00054	0.999	11	1.21	Low	192	326	361
101	31	0.00055	1.000	12	1.19	Low	194	348	386
108	33	0.00055	0.999	13	1.18	Low	197	371	410
115	35	0.00056	1.000	13	1.15	Low	192	393	435
121	37	0.00057	0.999	14	1.14	Low	192	416	460
128	39	0.00058	1.001	15	1.12	Low	189	438	485
134	41	0.00059	0.999	16	1.11	Low	183	461	510
141	43	0.00059	1.000	16	1.09	Low	177	483	535
147	45	0.0006	0.999	17	1.07	Low	165	506	560
154	47	0.00062	0.998	18	1.05	Low	144	528	585
160	49	0.00062	0.998	19	1.04	Low	137	551	610
167	51	0.00063	1.002	20	1.03	Low	129	573	635
174	53	0.00064	1.001	20	1.02	Low	107	596	660

Figure D-11. (a) Plot of family of width and slope combinations which provide continuity of water and sediment, and (b) output table of stable geometries and planform characteristics for each solution. Example: Big Raccoon Creek, Indiana.

Supply Reach Summary

Discharge (cfs)	Supply Effectiveness
169.64	16.12
432.92	35.47
696.20	44.43
959.48	33.16
1222.76	36.22
1486.04	29.42
1749.32	46.79
2012.60	33.65
2275.88	34.82
2539.16	8.28
2802.44	9.61
3065.72	7.28
3329.00	6.11
3592.28	6.92
3855.56	5.03
4118.84	8.35
4382.12	6.12
4645.40	6.62
4908.68	3.56
5171.96	15.36
5435.24	4.12
5698.52	4.40
5961.80	14.02
6225.08	4.98
6488.36	5.30

Qs Percentiles	Discharge (cfs)
Qs50	1588.71
Qs75	2573.10
Qs90	5004.06
Qeff	1749.32

Figure D-12. Example output on 'Detailed Results' tab. Example: Big Raccoon Creek, Indiana.

(a)

(b)

Stable Geometries   **Planform Characteristics**

Width (ft)	Width (m)	Slope	CSR	w/h Ratio	Sinuosity	Braiding Risk	Belt Width(m)	Min Wavelength(m)	Max Wavelength(m)
3	1	0.00737	1.002	1	1.03	Low	13	11	12
7	2	0.00603	0.999	2	1.26	Low	33	23	25
10	3	0.00582	0.999	4	1.31	Low	41	34	37
13	4	0.00578	0.998	5	1.31	Low	47	45	50
16	5	0.00582	0.998	6	1.30	Low	52	56	62
20	6	0.00586	1.001	7	1.30	Low	57	68	75
23	7	0.00593	0.998	8	1.28	Low	61	79	87
26	8	0.00616	1.000	10	1.23	Low	62	90	100
30	9	0.00621	0.999	11	1.22	Low	66	101	112
33	10	0.00636	0.999	12	1.20	Low	67	113	125
36	11	0.00646	1.001	13	1.18	Low	68	124	137
39	12	0.00659	0.999	14	1.15	Low	68	135	150
43	13	0.00663	1.001	15	1.15	Low	70	146	162
46	14	0.00682	1.000	17	1.11	Low	66	158	175
49	15	0.00698	0.999	18	1.09	Low	62	169	187
52	16	0.00704	1.002	19	1.08	Low	62	180	200
56	17	0.00715	1.000	20	1.06	Low	58	191	212
59	18	0.00728	1.000	21	1.04	Low	51	203	224
62	19	0.00734	1.002	23	1.04	Low	49	214	237
66	20	0.00756	1.002	24	1.01	Low	32	225	249

Figure D-13. (a) Plot of family of width and slope combinations which provide continuity of water and sediment, and (b) output table of stable geometries and planform characteristics for each solution. Example: Red River, Idaho.

D.10 References

Biedenharn, D.S., R.R. Copeland, C.R. Thorne, P.J. Soar, R.D. Hey, and C.C. Watson. 2000. "Effective Discharge Calculation: A Practical Guide." *Technical Report No. ERDC/CHL TR-00-15*, U.S. Army Corps of Engineers, Engineer Research and Development Center, Vicksburg, MS.

Bledsoe, B.P., and C.C. Watson. 2001. "Logistic Analysis of Channel Pattern Thresholds: Meandering, Braiding, and Incising." *Geomorphology*, Vol. 38, No. 3, pp. 281–300, DOI: 10.1016/S0169-555X(00)00099-4.

Brownlie, W.R. 1981. "Prediction of Flow Depth and Sediment Discharge in Open-channels." *Report No. KH-R-43A*, California Institute of Technology, W.M. Keck Laboratory, Pasadena, CA.

Brownlie, W.R. 1983. "Flow Depth in Sand-bed Channels." *Journal of Hydraulic Engineering*, Vol. 109, No. 7, pp. 959–990, DOI: 10.1061/(ASCE)0733-9429(1983)109:7(959).

Copeland, R.R. 1994. "Application of Channel Stability Methods – Case Studies." *Technical Report HL-94-11*, U.S. Army Corps of Engineers, Waterways Experiment Station, Vicksburg, MS, September, 60 p., URL: http://www.dtic.mil/dtic/tr/fulltext/u2/a285625.pdf.

Einstein, H.A. 1950. "The Bed Load Function for Sediment Transport in Open Channel Flows." *Technical Bulletin No. 1026*, U.S. Department of Agriculture, Soil Conservation Service, Washington, DC.

Hagerman, J.R., and J.D. Williams. 2000. "Meander Shape and the Design of Stable Meanders." In: Proceedings of the American Water Resources Association, Spring Specialty Conference: *Riparian Ecology and Management in Multi-land Use Watersheds*, Anchorage, AK, April 30 - May 4, pp. 563–568.

King, J.G., W.W. Emmett, P.J. Whiting, R.P. Kenworthy, and J.J. Barry. 2004. "Sediment Transport Data and Related Information for Selected Coarse-Bed Streams and Rivers in Idaho." *General Technical Report RMRS-GTR-131*, U.S. Department of Agriculture, Forest Service, Rocky Mountain Research Station, 26 p., URL: http://www.fs.fed.us/rm/pubs/rmrs_gtr131.pdf\.

Kondolf, G.M. 2011. "Setting Goals in River Restoration: When and Where Can the River 'Heal Itself'?" Pages 29–43 in: *Stream Restoration in Dynamic Fluvial Systems: Scientific Approaches, Analyses, and Tools*, Geophysical Monograph Series 194, American Geophysical Union, URL: https://institutbeaumont.files.wordpress.com/2007/09/kondolf2011-settinggoals.pdf.

Limerinos, J.T. 1970. "Determination of the Manning Coefficient from Measured Bed Roughness in Natural Channels." *U.S. Geological Survey Water-Supply Paper 1898-B*, 47 p., U.S. Government Printing Office, Washington, DC, URL: http://pubs.usgs.gov/wsp/1898b/report.pdf.

Parker, G. 1990. "Surface-based Bedload Transport Relation for Gravel Rivers." *Journal of Hydraulic Research*, Vol. 28, No. 4, pp. 417–436, DOI: 10.1080/00221689009499058.

Piégay, H., S.E. Darby, E. Mosselman, and N. Surian. 2005. "A Review of Techniques Available for Delimiting the Erodible River Corridor: A Sustainable Approach to Managing Bank Erosion." *River Research and Applications*, Vol. 21, No. 7, pp. 773–789, DOI: 10.1002/rra.881.

Schumm, S.A. 1977. *The Fluvial System*. Vol. 338, Wiley, New York, NY.

Soar, P.J., and C.R. Thorne. 2001. "Channel Restoration Design for Meandering Rivers." *Technical Report No. ERDC/CHL CR-01-1*, Coastal and Hydraulics Laboratory, U.S. Army, Engineer Research and Development Center, Vicksburg, MS, URL: http://www.nrcs.usda.gov/Internet/FSE_DOCUMENTS/stelprdb1043218.pdf.

van den Berg, J.H. 1995. "Prediction of Alluvial Channel Pattern of Perennial Rivers." *Geomorphology*, Vol. 12, No. 4, pp. 259–279, DOI: 10.1016/0169-555X(95)00014-V.

Wilcock, P.R., and J.C. Crowe. 2003. "Surface-based Transport Model for Mixed-size Sediment." *Journal of Hydraulic Engineering*, Vol. 129, No. 2, pp. 120–128, DOI: 10.1061/(ASCE)0733-9429(2003)129:2(120).

Wohl, E., B.P. Bledsoe, R.B. Jacobson, N.L. Poff, S.L. Rathburn, D.M. Walters, and A.C. Wilcox. 2015. "The Natural Sediment Regime in Rivers: Broadening the Foundation for Ecosystem Management." *Bioscience*, Vol. 65, No. 4, pp. 358–371, DOI: 10.1093/biosci/biv002.

D.11 Abbreviations

<u>Units of Measure</u>

°C	degree(s) Celsius
°F	degree(s) Fahrenheit
cfs, ft^3/s	cubic feet per second
cms, m^3/s	cubic meter(s) per second
ft	foot or feet
ft/ft	feet per foot
ft/s	feet per second
ft^2	square feet
ft^2/s	square feet per second
$ft^2/s/ft$	square feet per second per foot
H:V	horizontal:vertical
kg/m^3	kilogram(s) per cubic meter
m	meter(s)
m/m	meter(s) per meter
m/s	meter(s) per second
m^2	square meter(s)
m^2/s	square meter(s) per second
$m^3/s/m$	cubic meter(s) per second per meter
mm	millimeter(s)
Pa	Pascal(s)
ppm	part(s) per million
%	percent
W/m^2	Watt(s) per square meter
yr(s)	year(s)

<u>Acronyms</u>

CDF	cumulative distribution function
CSR	Capacity-Supply Ratio
CSR Tool	CSR Stable Channel Design Tool
eRAMS	Environmental Risk Assessment & Management System
FDC	flow duration curve
HEC-RAS	Hydrologic Engineering Centers River Analysis System
NCHRP	National Cooperative Highway Research Program
MFA	magnitude-frequency analysis
PDF	probability density function
SWAT	Soil and Water Assessment Tool
SWAT-DEG	channel DEGradation portion of SWAT
VBA	Visual Basic for Applications

<u>Symbols</u>[5]

A	cross-sectional area [m^2, ft^2]
$A_{channel}$	cross-sectional area of channel [m^2, ft^2]
A_{OB}	area of floodplain partition [m^2, ft^2]
b	bottom width [m, ft]
c	constant, conversion factor (1.0 for SI units and 1.486 for English units)
C_{ppm}	sediment transport concentration [ppm]
D_{50}	median grain size [m, ft]
D_{16}, D_{84}	particle size for which 16% and 84% of all sediments is smaller, respectively [m, ft]
$D_{b,i}$	grain size representing each size class of the (active) layer of the bed [m, ft]
D_i	characteristic grain size for each size class [m, ft]
D_{sg}	geometric mean grain size [m, ft]
F_g	grain-related Froude number
F_i	fraction of grain size in surface layer
F_s	fraction of sand on the bed surface
g	gravitational constant
G	specific gravity of sediment particles
h	depth [m, ft]
K	conveyance
K_{OB}	conveyance of bed partition
$Max\ Q$	maximum discharge in flow record [m^3/s, ft^3/s]
$Min\ Q$	minimum discharge in flow record [m^3/s, ft^3/s]
n	Manning's roughness coefficient
n_{bank}	Manning's roughness coefficient of bank partition
$n_{floodplain}$	Manning's roughness of floodplain partition
N	grain size ranges from $i = 1$ to $N + 1$
$P_{<,i}$	non-exceedance probability of each bin
P_{bank}	wetted perimeter of bank partition [m, ft]
P_{bed}	bottom width = wetted perimeter of bed partition [m, ft]
q_{bi}	volume gravel bedload transport per unit width of grains in the ith size range [m^2/s, ft^2/s]
q_{bT}	total volume gravel bedload transport rate per unit width over all sizes [m^2/s, ft^2/s]
Q	discharge [m^3/s, ft^3/s]
Q_{bf}	bankfull discharge [m^3/s]
Q_{eff}	single discharge that moves the most total sediment road (percentile) [m^3/s, ft^3/s]
Q_{s50}	discharge that moves the 50% of the total estimated sediment load (percentile) [m^3/s, ft^3/s]
Q_{s75}	discharge that moves the 75% of the total estimated sediment load (percentile) [m^3/s, ft^3/s]
Q_{s90}	the discharge that moves the 90% of the total estimated sediment load (percentile) [m^3/s, ft^3/s]
R	hydraulic radius [m, ft]
R	$(\rho_s / \rho) - 1$ = submerged specific density of sediment
R_{bank}	hydraulic radius of bank partition [m, ft]
R_{bed}	hydraulic radius of bed partition [m, ft]
R_{OB}	hydraulic radius of floodplain partition [m, ft]
$Range\ Q$	range of discharge in flow record [m^3/s, ft^3/s]
S	slope [m/m, ft/ft]

---

[5] Variables are reported with SI units or English units or both to accommodate equation and/or software input. The software works in both SI and English units.

S_f	friction slope [m/m, ft/ft]
S_o	bed slope [m/m, ft/ft]
S_v	valley slope [m/m, ft/ft]
u_*	$\sqrt{\dfrac{\tau_b}{\rho}}$ = shear velocity on the bed [m/s, ft/s]
V	cross-section averaged velocity [m/s, ft/s]
V_c	critical velocity [m/s, ft/s]
w/h	width-to-depth ratio
z	bank angle, horizontal to vertical [H:V]
v	kinematic viscosity [m²/s, ft²/s]
ρ	density of water [kg/m³]
ρ_s	density of sediment [kg/m³]
σ_g	gradation coefficient
σ_s	arithmetic standard deviation
σ_{sg}	geometric standard deviation
τ_b	boundary shear stress on the bed [Pa]
τ_{*c}	dimensionless critical shear stress
τ_{sg}^*	Shields' stress
τ_{ssrg}^*	reference Shields' stress
Ψ_i	each grain size on the base 2 logarithmic ψ scale
ω	strain function for the Parker (1990) bedload equation
ω_v	potential specific stream power [W/m²]